

Characterisation of OmcA From *Shewanella oneidensis* MR-1: Biophysical and Mineral Reduction Properties

Nanakow A. Baiden

PhD Thesis

University of East Anglia
School of Biological Sciences

September 2014

This copy of the thesis has been supplied on condition that anyone who consults it is understood to recognise that its copyright rests with the author and that use of any information derived there from must be in accordance with current UK Copyright Law. In addition, any quotation or extract must include full attribution.

Index

<u>Section</u>	<u>Page</u>
Index.....	ii
List of Abbreviations.....	vi
Acknowledgements.....	viii
Abstract.....	ix
Chapter 1: An Overview of the Dissimilatory Mineral Respiration Components in <i>Shewanella oneidensis</i> MR-1.	
1.1 Introduction.....	1
1.2 Anaerobic Respiration.....	4
1.3 Dissimilatory Mineral Respiration by <i>Shewanella oneidensis</i> MR-1.....	5
1.3.1 The Environmental Significance of Mineral Respiration.....	5
1.3.2 Electron transfer from the cytoplasmic membrane to the outer membrane.....	6
1.3.3 The outer membrane multihaem cytochromes (OMMCs).....	8
1.3.4 The role of haem chemistry in OMMC function.....	13
1.3.5 Electron transfer from the OMMCs to extracellular minerals.....	13
1.3.6 The extracellular environment of OMMCs.....	19
1.4 Biophysical Properties of the MtrCAB complex and OmcA.....	19
1.5 Thesis Aims.....	21
References.....	22
Chapter 2: Purification and Spectroscopic Characterisation of OmcA from <i>Shewanella oneidensis</i> MR-1.	
2.1 Introduction.....	29
2.2 Results.....	30
2.2.1 The Purification of OmcA _(wt) , and two recombinant forms of OmcA.....	30
2.2.2 UV-Vis spectroscopy of purified OmcA _(wt) , pOmcA and eOmcA.....	33
2.2.3 MCD spectroscopy of purified pOmcA.....	34
2.2.4 EPR spectroscopy of purified OmcA _(wt) , pOmcA and eOmcA.....	36
2.2.5 The Impact of pH on the Spectroscopic Properties of OmcA.....	36
2.3 Discussion.....	40
References.....	41
Chapter 3: Crystallographic Structural Studies of OmcA.	
3.1 Introduction.....	44
3.2 Results & Discussion.....	45
3.2.1 X-Ray Crystal Structure of eOmcA.....	47
3.2.2 The Effect of Y ³⁷⁴ F Mutation on the Putative Dimer-Interface.....	53
3.3 Conclusions.....	53

References.....	57
-----------------	----

Chapter 4: Solution-state Structural Studies of OmcA.

4.1	Introduction.....	60
4.2	Results.....	61
4.2.1	Analytical Gel Filtration Chromatography (AGFC).....	61
4.2.2	AGFC Column Performance.....	66
4.2.3	Blue Native PAGE.....	67
4.2.4	Analytical Ultracentrifugation (AUC).....	68
4.2.5	Small Angle X-Ray Scattering.....	70
4.2.6	Probing the Oligomeric State of eOmcA mutant Y ³⁷⁴ F.....	70
4.2.7	Solution studies of the Oligomeric state of MtrC.....	71
4.3	Discussion.....	73
References.....		77

Chapter 5: Spectropotentiometric Studies of OmcA using EPR.

5.1	Introduction.....	80
4.2.1	Paramagnetic Resolution of <i>c</i> -type Haems to Characterise OMMCs..	80
5.2	Results.....	85
5.2.1	An Overview of the EPR-monitored Potentiometric Titration of eOmcA.....	85
5.2.2	Simulation of eOmcA's EPR Signals.....	87
5.2.3	Spin Quantitation of eOmcA's EPR Redox Titre.....	94
5.3	Discussion.....	96
5.3.1	Correlating Spin Quantitation with eOmcA Haem Ligation.....	96
5.3.2	Exploring the Origin of Low Spin 3 Resonance.....	99
5.3.2	Fitting the Nernst Equation to eOmcA's Spin Quantitated Potentiometric Titre.....	102
5.3.4	Quantitative Analysis of eOmcA at different pHs.....	104
References.....		105

Chapter 6: Potentiometric Studies of UndA, a homologue of OmcA in several *Shewanella spp*

6.1	Introduction.....	108
6.2	Results.....	110
6.2.1	EPR-Monitored Redox Titre of eUndA.....	110
6.2.2	Simulation of eUndA's EPR Signals.....	110
6.2.3	Spin Quantitation of eUndA's EPR Redox Titre.....	116
6.3	Discussion.....	117
6.3.1	Correlating Spin Quantitation with eUndA Haem Ligation.....	117
6.3.2	Comparison of OMMC Spectropotentiometric Properties.....	121
References.....		128

Chapter 7: The Functional Consequences of Mutations near Haem 10 of OmcA

7.1	Introduction.....	130
-----	-------------------	-----

7.1.1	Current Knowledge of OmcA Function.....	130
7.1.2	Building on Current Knowledge of OmcA with Mutagenic Studies.....	131
7.2	Results.....	132
7.2.1	Crystallographic Confirmation of Successful Mutagenesis.....	132
7.2.2	Potentiometric Properties of eT ⁷²⁵ G	136
7.2.3	Localisation of mOmcA in <i>S. oneidensis</i> mutant cells.....	139
7.2.4	Whole Cell Mineral Reduction Assay of OmcA MIP mutants	141
7.3	Discussion.....	143
	References.....	146

Chapter 8: Discussion on the Role of OmcA in DMR & Future Perspectives.

8.1	Introduction.....	149
8.2	Electron Ingress/Egress Sites and OmcA Orientation at the Outer Membrane.....	149
8.2.1	Details of the OmcA:MtrC Interaction.....	150
8.3	The OmcA “Interactome” of the Outer Bacterial Membrane.....	152
8.4	The Role of the Biofilm State in DMR.....	153
8.4.1	Conductive Pili in Biofilms.....	154
8.4.2	Quorum Sensing and Multiple Roles for Flavin in <i>Shewanella</i> Biofilms.....	154
8.4.3	Spatiotemporal cellular differentiation and the porin-cytochrome module in <i>Shewanella</i> biofilms.....	155
	References.....	156

Materials & Methods

M.1	SDS-PAGE experiments.....	160
M.1.1	Gel Staining.....	160
M.2	Ultraviolet Absorption Spectroscopy.....	160
M.2.1	Oxidised and reduced protein spectra.....	161
M.2.2	Protein Quantitation.....	161
M.2.3	Pyridine Hemochrome Determination of Molar Extinction Coefficients, ϵ_{λ}	161
M.3	Protein Purification.....	162
M.3.1	OmcA _(wt) Purification.....	162
M.3.2	pOmcA Purification.....	163
M.3.3	eOmcA Purification.....	163
M.4	Electron Paramagnetic Resonance Spectroscopy.....	164
M.4.1	Potentiometric Titration.....	164
M.4.2.1	Data Processing.....	165
M.4.2.2	Spin-Integration & Fitting the Nernst Equation.....	166
M.4.4	Spin-Integration & Fitting the Nernst Equation.....	166
M.5	Magnetic Circular Dichroism (NIR-MCD).....	167
M.6	X-Ray Crystallography.....	167
M.6.1	Protein Crystallisation.....	167
M.6.2	X-ray Diffraction Experiments.....	168
M.6.2	X-ray Diffraction Experiments.....	168
M.7	Analytical Gel Filtration Chromatography.....	169
M.8	Analytical Ultracentrifugation (AUC).....	169

M.9	Small Angle X-ray Scattering (SAXS).....	170
M.10	Analytical Gel Filtration Chromatography (AGFC).....	170
M.11	Mineral Reduction Assay of nano-Hematite (α -Fe ₂ O ₃ , 30-43 nm diameter) via Ferrozine Assay determination of Ferrous Iron Concentration.....	171
	M.11.1 Site-Directed Mutagenesis and Cloning of <i>omcA</i>	172
	M.11.2 Recombinant-OmcA Localisation Assay.....	172
	M.11.2.1 Western Blotting.....	173
	References.....	173
	Appendices.....	184

List of Abbreviations

λ	Wavelength
\AA	Angstrom (10^{-10} m)
ADP	Adenosine Diphosphate
ADQS	9,10-Anthraquinone-2,6-disulfonic acid disodium salt
AFM	Atomic force microscopy
AGFC	Analytical gel filtration chromatography
AQS	Anthraquinone-2-sulphonic acid
A_s	Peak asymmetry
ATP	Adenosine Triphosphate
A.U.	Absorbance Units
AUC	Analytical Ultracentrifugation
AUC-SE	Analytical Ultracentrifugation Sedimentation Equilibrium
BICINE	2-(Bis(2-hydroxyethyl)amino)acetic acid
CHAPS	3-[(3-Cholamidopropyl)dimethylammonio]-1-propanesulfonate hydrate
CV	Column Volume
DAD	2,3,5,6-tetramethyl-p-phenylenediamine
DEAE	Diethylaminoethyl
DMR	Dissimilatory Mineral Respiration
EPR	Electron Paramagnetic Resonance
ETC	Electron Transfer Chain
FZ	Ferrozine
DMSO	Dimethylsulfoxide
DTT	Dithiothreitol
EDTA	Ethylenediaminetetraacetic acid
E_m	Mid-point reduction potential
EPS	Exopolysaccharide
FAD	Flavin Adenine Dinucleotide
FMN	Flavin Mononucleotide
FPLC	Fast Protein Liquid Chromatography
HBM	Hematite binding motif
HEPES	4-(2-Hydroxyethyl)piperazine-1-ethanesulfonic acid
IgG	Immunoglobulin G
kDa	Kilo Dalton
LB	Luria Bertani Media
LBB	Leucoberberlin blue assay
LGM	Large g_{\max}
LS	Low-spin
LPS	Lipopolysaccharide
MAD	Multiple wavelength anomalous diffraction
MES	2-(N-morpholino)ethanesulfonic acid
MIP	Mineral Interaction Peptide
MQ	Menaquinone
MQH	Menaquinol
mT	MilliTesla
MW	Molecular weight
MW_{app}	Apparent molecular weight
NAD⁺	Nicotinamide adenine dinucleotide (oxidised)
NADH	Nicotinamide adenine dinucleotide (reduced)

NIR-MCD	Near-Infrared Magnetic Circular Dichroism
nm	Nanometer (10^{-9} m)
NTA	Nitrilotriacetic acid
OMMC	Outer Membrane Multihaem Cytochromes
OGP	octyl-glucopyranoside
PDB	Protein Data Bank
PES	Phenazine ethosulphate
PEG	Polyethylene glycol
PIPES	1,4-Piperazinediethanesulfonic acid
PFV	Protein Film Voltammogram
PMS	Phenazine methosulphate
Q	Quinone
QH	Quinol
QS	Quorum sensing
rpm	Revolutions per minute
SAD	Single wavelength anomalous diffraction
SAXS	Small angle X-Ray Scattering
SDS-PAGE	Sodium dodecyl sulphate-polyacrylamide gel electrophoresis
S.H.E.	Standard Hydrogen Electrode
TEA	Terminal Electron Acceptor
TRIS	2-Amino-2-hydroxymethyl-propane-1,3-diol
UV-Vis	Ultraviolet-Visible
W_h	Peak width at half peak height

Acknowledgments

Firstly, I would like to thank the guidance and support of my supervisory team Professor David Richardson, Professor Julea Butt and Dr Tom Clarke. I would also like to thank Dr Andrew Gates and Dr Marcus Edwards for their guidance and experimental support.

I would like to thank Dr Jim Fredrickson and Dr John Zachara for their input to discussing my data and for working with Professor David Richardson to make this PhD available. Many thanks to Dr Liang Shi and Dr Dave Kennedy for their input to data analysis, experimental support and hosting my visit to their research facility.

I would like to thank Dr Myles Cheesman and Dr Dima Svitsunenko for access to their resources and collaborative discussions.

I would like to thank my friends, and especially my family for their belligerent support and helpful distractions.

Abstract

Several *Shewanella spp* are versatile in the respiratory substrates they use. A novel set of respiratory substrates implicated are insoluble Fe(III) and Mn(III,IV) oxides. OmcA from *Shewanella oneidensis* MR-1 plays a role in the terminal electron transfer during respiratory mineral reduction, but has minimal or contrasting properties in the literature. A suite of biophysical techniques confirmed the *bis*-histidine axial ligation of all OmcA's haem content in the crystal structure and in solution. The paramagnetic resonance feature designated "LS3" was identified to be unique to OmcA. However this resonance signal is modelled to be produced spin-coupling and not unique haem ligation. OmcA's electroactive coverage is comparable to UndA and the other major outer membrane multihem cytochrome (OMMC) clades MtrC and MtrF (i.e. +0.08 V to -0.47 V vs S.H.E.). The crystal structure of OmcA shows domain fold, domain organisation and haem orientation conservation with MtrF and UndA. Comprehensive solution-structure studies of OmcA provided contrasting experimental data on the oligomeric state of OmcA, such that it is unresolved whether OmcA forms an ion-sensitive dimer. The crystal structure shows a predicted mineral interaction peptide (i.e. T⁷²⁵P⁷²⁶S⁷²⁷) is solvent exposed and would putatively bind substrate within electron tunneling distance of a terminal haem. Site-directed mutagenesis indicates Thr⁷²⁵ is significant to maintenance of the molecular environment of haem 10. Although T⁷²⁵G mutation produces a ~80% decrease in whole cell reduction of synthesised hematite over 120 hours; secondary effects of change in haem reduction potentials or widespread conformational effects were ruled out. OmcA has thus been shown to share a common OMMC-fold and exist in *S. oneidensis* MR-1 outer membranes as a functioning mineral reductase cytochrome with unique paramagnetic resonance properties in this set of studies.

Chapter 1:

An Overview of the Dissimilatory Mineral Respiration

Components in *Shewanella oneidensis* MR-1.

1.1 – Introduction

Respiration, a defining process of living things, utilises electrons obtained from a relatively energy-rich molecule (highly saturated organic compounds for chemo-organotrophs) and delivers them to a suitable terminal electron acceptor through an “electron transfer chain” of oxido-reductase enzymes. This process is fundamental to all taxonomically ranked kingdoms of life, and in higher organisms such as plants and humans, respiration is performed by the cellular organelles called mitochondria. The mitochondrion loosely resembles a Gram-negative bacterium cell in the sense that it is a double-membrane bound structure of comparable size, and the electron transfer chain components are associated with the inner membrane of both mitochondria and (Gram-negative) bacterial cells.

At the molecular level, the oxidation of fuel molecules transfers electrons and protons to produce low redox potential electron carriers such as nicotinamide adenine dinucleotide (NADH) and succinate. These electron carriers reduce specific dehydrogenases of the membrane-associated respiratory chain, which in turn feed electrons to the quinone pool. Independent of the fuel molecule being oxidised, all electrons liberated from fuel sources feed into the electron transfer chain by reducing quinones (Q) that diffuse freely through the hydrophobic layer of the cytoplasmic membrane. The quinol dehydrogenase then feeds electrons via subsequent redox reaction(s) to a terminal oxidoreductase where the terminal oxidant is reduced (as observed in aerobic respiration; Fig. 1.1). The driving force for these electron transfers is the redox potential difference between the terminal oxidant and the electron sources. The free energy (i.e. Gibb’s free energy, G) available from electron transfer across the redox potential difference between reductant and oxidant (ΔE) can be quantified using the following equation:

$$\Delta G = -nF\Delta E \dots\dots\dots \text{(Eqn. 1.1)}$$

(n = moles of electrons transferred; F =Faraday’s constant, 96.485 kJ V⁻¹ mol⁻¹)

In Gram-negative bacteria, energy is transduced in the electron transfer chain every time electron transfer is coupled to proton translocation/quinone cycling across the cytoplasmic membrane into the periplasm. Several proton translocating enzymes function via a conformational pump mechanism, where redox-induced changes in the enzyme's proton affinity result in the binding of cytoplasmic proton(s) to reduced (proton-pumping) enzyme and subsequent periplasmic release of proton(s) by the oxidised enzyme. The thermodynamic advantage of the conformational pump mechanism is that whereas the reaction is stoichiometrically dependent on reductant, the reactants do not directly supply all the protons being pumped. Redox reactions can thus be coupled to translocation of multiple protons from the cytoplasm in a manner that is not limited by the protonation capacity of the reductant.

Quinone cycling, however, is the predominant form of proton translocation in respiratory enzymes such as cytochrome *bc*₁, formate dehydrogenase and nitrite reductase [1]. The entire process, in which a quinone cycling enzyme localises quinone within the lipid bi-layer according to its redox state, is also referred to as a redox loop. A quinone cycling enzyme reduces quinone at the cytoplasmic face of the inner bacterial membrane, and couples quinol oxidation at the periplasmic face of the inner membrane with release of protons into the periplasm. The protons are obtained from oxidation of the quinol molecule, and protons translocated during quinol cycling are dependent on the protonation capacity of quinone (i.e. 2 protons per fully reduced quinol molecule).

Reduction of proton-pumping electron transfer chain components result in charge separation of proton and electron, which in turn decreases cytoplasmic proton concentration and generates an electrochemical proton gradient. Periplasmic protons flow spontaneously back into the cytoplasm, through adenosine triphosphate (ATP) synthase and down the electrochemical proton gradient generated. This powers ATP synthesis (4 protons per ATP molecule). Since the electrochemical gradient is generated by the potential difference between fuel molecule oxidation and terminal oxidant reduction (i.e. ΔE), the process of terminal oxidant reduction (i.e. respiration) is coupled directly to the cell's capacity to power its own metabolism with ATP.

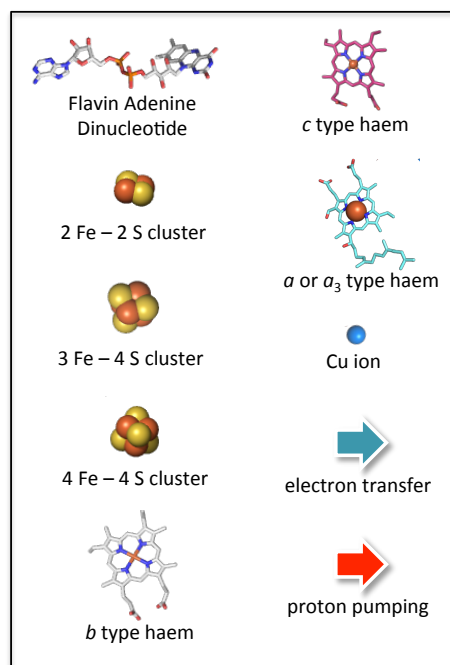
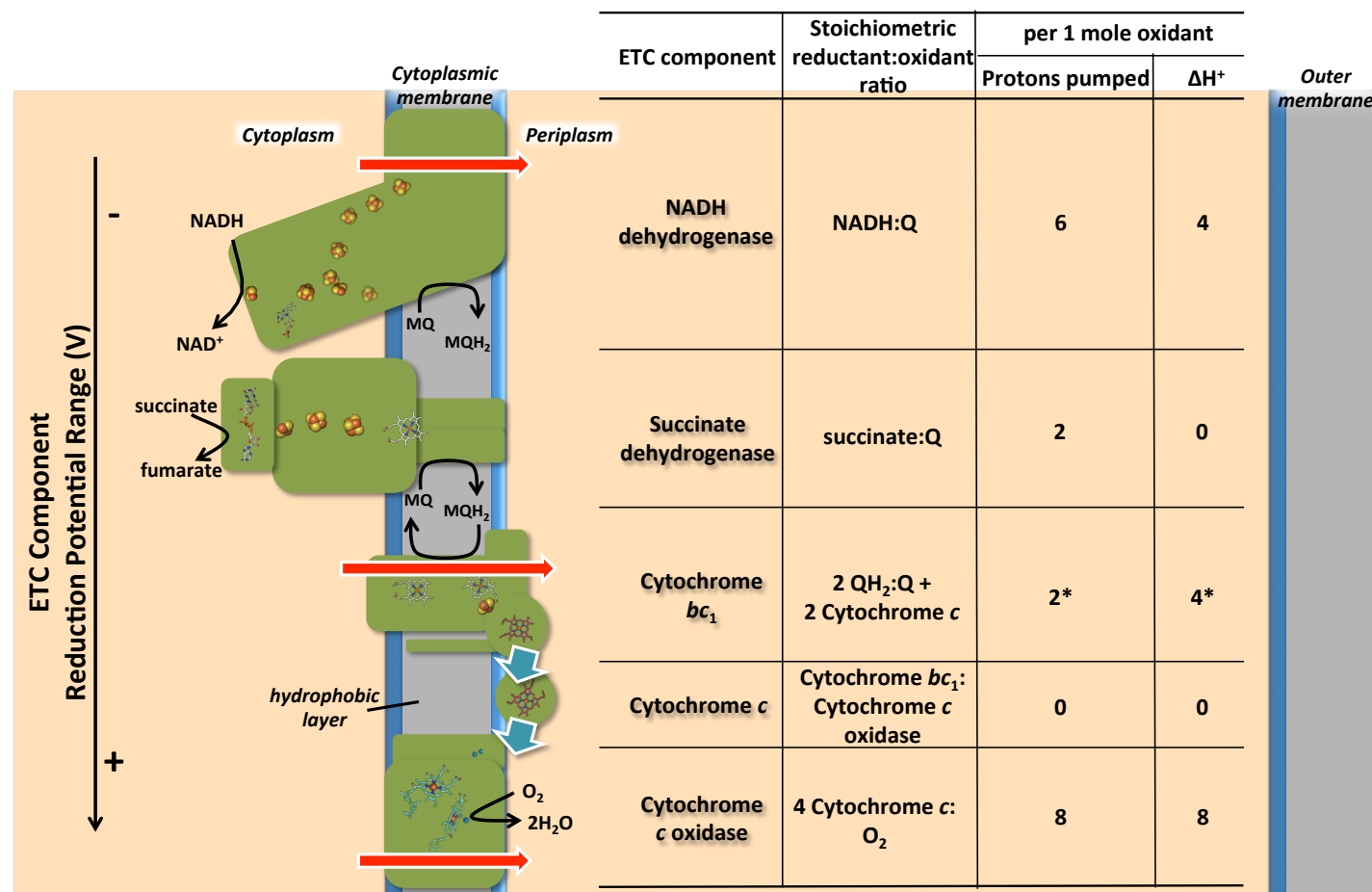


Figure 1.1. – A cartoon of the electron transfer chain (ETC) components in aerobic respiration in *Shewanella oneidensis* strain MR-1. “Protons

pumped” refers to protons translocated from the cytoplasm via conformational changes in membrane-spanning proteins. “ ΔH^+ ” denotes net proton loss from the cytoplasm that is translocated to the periplasm. The inner membrane phospholipid bi-layer has adjacent phospholipid fatty acid groups that form the hydrophobic layer that quinones diffuse through. Cartoons and depicted co-factors of the electron transfer chain (ETC) components are obtained from the respective references of NADH dehydrogenase (PDB code 4HEA, [2]), succinate dehydrogenase (PDB code 1NEK, [3]), cytochrome bc_1 (PDB code 1BE3, [4]) and cytochrome c oxidase (PDB code 1AR1, [5]). Note that the cytochrome bc_1 homodimer is not depicted. MQ = menaquinone, MQH₂ = menaquinol * = per net oxidation of 1 mol quinol.



Aerobic respiration utilises the large ΔE between the NAD^+/NADH couple ($E_{m,7} = -0.32 \text{ V}$ vs S.H.E.) and the $\text{O}_2/\text{H}_2\text{O}$ couple ($E_{m,7} = +0.82 \text{ V}$ vs S.H.E.). The O_2 reduction mechanism of cytochrome *c* oxidase results in proton translocation (Fig. 1.1). The resultant ΔG (i.e. -224 kJ mol^{-1}) makes O_2 the most efficient terminal oxidant utilised in respiration. There are 8 protons pumped by cytochrome *c* oxidase per O_2 molecule fully reduced. The ability of electroneutral O_2 molecules to diffuse through the outer-membrane lipid bi-layer to the periplasm negates the need for O_2 -specific transporters, subsequently decreasing the energetic cost in protein expression compared to respiration utilising other terminal oxidants.

1.2 – Anaerobic Respiration in *S. oneidensis* MR-1

Respiratory versatility is a common ability of bacteria that consistently adapt to changing environments, where compounds other than molecular oxygen are utilised as the terminal oxidant, i.e. anaerobic respiration. During anaerobic respiration the menaquinone pool is reduced via NADH dehydrogenase, succinate dehydrogenase, and other dehydrogenases in a similar manner to aerobic respiration (as in *S. oneidensis* MR-1, Fig. 1.2). The subsequent oxidation of the menaquinol pool, driven by the terminal electron acceptor (TEA), replenishes the inner membrane's menaquinone content for protonmotive reduction as described earlier.

Bacteria that occupy “metabolically unattractive” niches (that organisms with fastidious requirements, or simply inadequate pathways cannot colonise) employ respiratory versatility by using more than two TEAs. Many bacteria can utilise NO_3^- , SO_4^- or fumarate as their TEA [6]. The capacity to respire on more than 10 TEAs in the absence of O_2 [7, 8] makes *S. oneidensis* MR-1 a model organism for respiratory versatility. The majority of the TEAs utilised by bacteria are soluble compounds. These anaerobic TEAs utilised by bacteria such as *S. oneidensis* MR-1 are imported to the periplasm to their respective oxidoreductase enzymes (e.g. predicted transport of $\text{NO}_2^-/\text{NO}_3^-$ by NrtCD, *S. oneidensis* MR-1 gene locus SO0455-SO0456 [9]; formate transported by DcuB; gene locus SO4417 [10]). *S. oneidensis* MR-1 TEAs that are not imported to the periplasm have dedicated oxidoreductases that localise to the outer bacterial membrane. These TEAs include soluble substrates like DMSO (reduced by DmsABF [11]), soluble metals Cr(VI) [12] and U(VI) [13] and mineral oxides of Fe(III) and Mn(IV). In the case of extracellular TEA reduction, the electron transfer chain that

originates at the cytoplasmic membrane must span the periplasm and outer membrane to terminate at the extracellular TEA. This thesis describes studies of outer membrane cytochrome A (OmcA) and its associated with extracellular mineral reduction, a process that is described in the next section.

1.3 – Dissimilatory Mineral Respiration by *Shewanella oneidensis* MR-1

1.3.1 – The Environmental Significance of Mineral Respiration

Before widespread bioavailability of molecular oxygen in early Earth, there is evidence that Fe(III) oxides served as the first TEA coupled to organic matter oxidation [6, 14]. Fe(III) oxide reduction is the dominant driving force of organic matter oxidation in estuary sediments, and contributes significantly to organic molecule oxidation in a variety of aquatic and sedimentary environments that are redox stratified or anoxic [14]. The dominant flux of electrons from organic molecule oxidation to Fe(III) and Mn(III,IV) oxide reduction inhibits biogenic methanogenesis [15] and sulphate reduction [16]. Water-logged soil sediments are anaerobic and commonly have elevated Fe(II) content, a significant amount of this activity has been attributed to biogenic Fe(II) production [17]. Bioreductive dissolution of Fe(III) and Mn(III/IV) minerals leach soluble Fe(II) and Mn(II) that contaminates groundwater, and oxidative precipitation of these metals in aerobic groundwater zones [14]. The aforementioned metal oxides have the capacity to adsorb a variety of chemical species, linking biogenic mineral dissolution to the environmental availability of adsorbed phosphate and trace metals [14, 18, 19]. Within clay soils, Fe(III) has a structural role, and bioreduction has been implied to cause clay degradation [14].

Shewanella spp couple decomposition of a variety of organic molecules to reduction of Fe(III) and Mn(III/III,IV/IV) oxides/oxyhydroxides [20-22]. Combined with its ability to reach high biomass in rich, aerobic growth media [23] and the suite of genetic tools that have been developed [24, 25], *S. oneidensis* MR-1 is a model organism for studying DMR. Carbon cycling by *Shewanella spp* is linked to geochemical cycles of mineral-adsorbed metals by bioreductive dissolution in *Shewanella's* aquatic and sediment habitats. Wild-type and several *Shewanella sp.* ANA-3 mutants showed that deficiency in arsenate reduction inhibited reduction of ferrihydrite with arsenate adsorbed to its surface [26]. The mineral TEA in DMR also undergoes biomineralisation processes that are dependent on environmental conditions. The

redox cycling of U(VI) by *Shewanella putrefaciens* CN-32 to reduce Mn(III/IV) mineral before U(VI) is fully reduced affects UO₂ nanoparticle biogenesis [27]. The mineral phases produced during *S. oneidensis* MR-1 reduction of ferrihydrite are dependent on environmental Si and P abundance [28, 29]. This includes the ratio of organic matter and hydrous ferric oxide, which determines the biomineralisation product of ferrihydrite reduction by *S. putrefaciens* CN-32 [30]. As such, mechanistic understanding of DMR provides insights into biogeochemical cycles and may be used for bioremediation of metal environmental contaminants [31].

1.3.2 – Electron transfer from the cytoplasmic membrane to the outer membrane

The novelty of the dissimilatory mineral respiratory (DMR) process is the termination of the electron transfer chain, originating from the inner bacterial membrane, at an *insoluble extracellular* substrate. Key proteins in this process were identified by fractionation of *S. oneidensis* MR-1 cell membranes which indicated localisation of cytochromes to the cytoplasmic and outer bacterial membranes [24]. CymA of the NapC/NirT/NrfH family of tetrahaem quinol dehydrogenases is anchored to the periplasmic side of the cytoplasmic membrane [24, 32]. Transposon disruption of *cymA* inhibits respiration on Fe(III), Mn(IV), NO₃⁻ and fumarate; which is complemented by *in trans* expression of *cymA* [32]. At the cytoplasmic membrane, Δ *cymA* complementation functions to oxidise the menaquinol pool and relay electrons to the anaerobic oxidoreductases at the cytoplasmic membrane and periplasm of *S. oneidensis* MR-1 (Fig. 1.2) [33]. Recent work has shown CymA requires menaquinone-7 as a 5th bound co-factor and the electrochemical driving force of NADH reduction to function as a quinol dehydrogenase [34].

The decahaem cytochrome MtrA is localised to the outer bacterial membrane [24, 35], where it associates strongly with MtrB and the decahaem cytochrome MtrC (also referred to as OmcB) [35-37]. Electrons from CymA may traverse the periplasmic gap directly to MtrA [38]. The underlying question, is whether or not MtrA localises close enough to CymA for direct electron transfer between the two cytochromes during DMR [38]. In an attempt to gain more structural data on MtrA in the absence of a crystal structure, SAXS data permitted simulation of the dimensions and shape of MtrA in solution [38]. The study concluded that MtrA's axial dimension made it long enough to traverse the periplasmic space and position it's haem(s) within electron transfer of distance of CymA's haem(s) (i.e. ≤ 14 Å [39]).

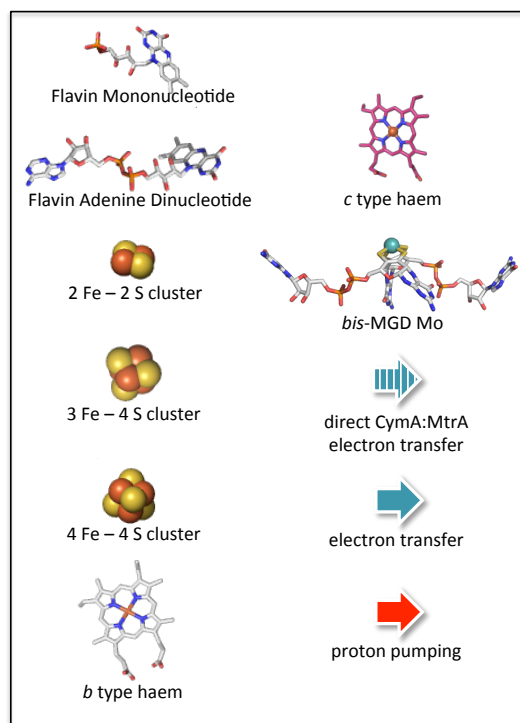
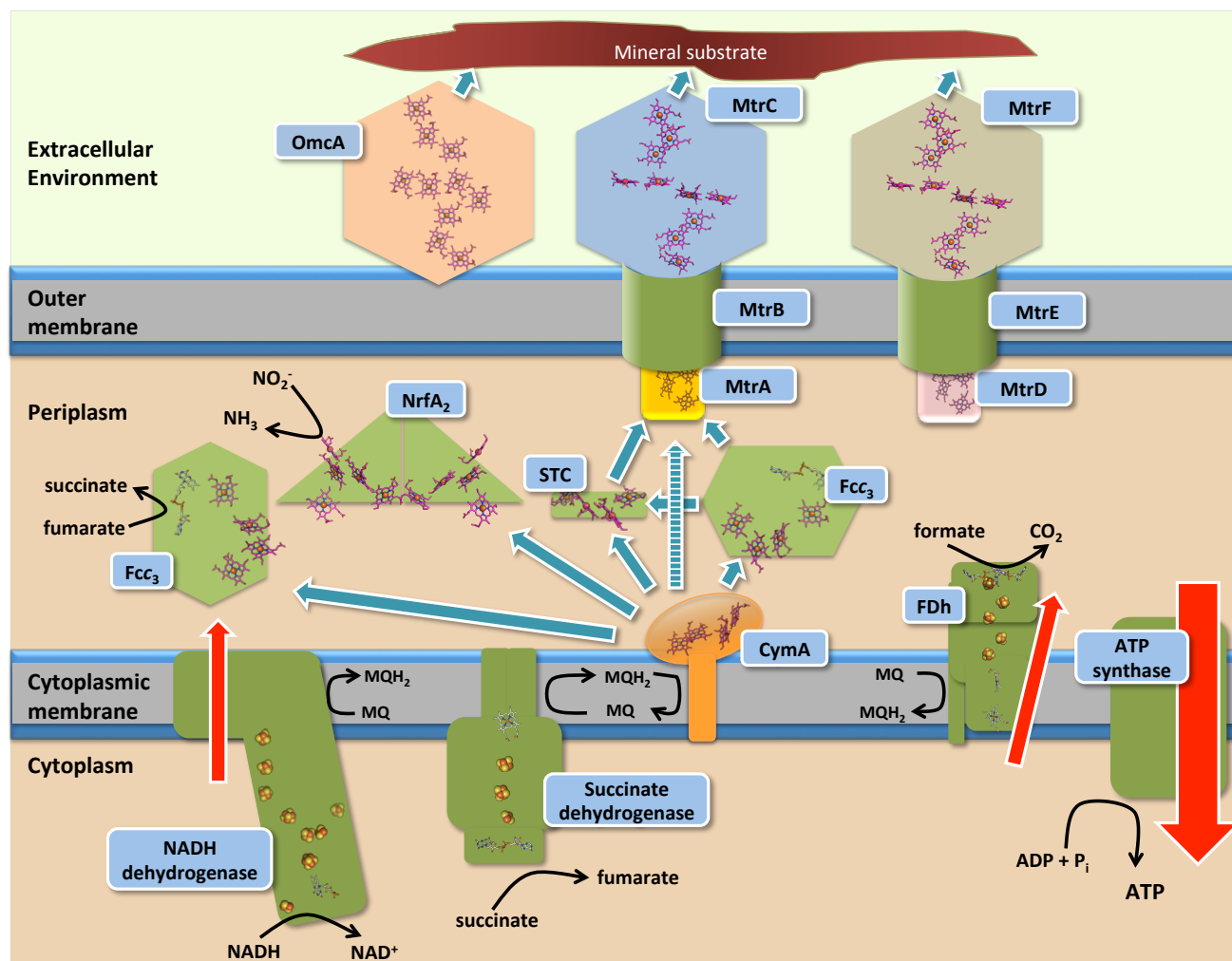


Figure 1.2. –A cartoon of anaerobic respiration components in *S. oneidensis* MR-1. The enzymes have been simplified here to highlight their associated redox cofactors, which are taken from [2, 40-42].

The functional homology of the MtrFDE complex with the more annotated MtrCAB hetero-trimer is shown here, as such MtrC has been depicted with the haem arrangement of MtrF (PDB code 3PMQ, [43]). The cofactors of decahaems MtrA and MtrD are hidden by the predicted β -barrels of MtrB and MtrE respectively [44]. FDh = formate dehydrogenase PDB code 1KQF [41]; STC = Small Tetrahaem Cytochrome PDB code 1M1Q [45]; Fcc₃ = fumarate reductase flavocytochrome c₃ PDB code 1D4C [46]; NrfA₂ = nitrite reductase dimer PDB code 2RDZ [47]; MQ = menaquinone; MQH₂ = menaquinol.



However, considering the size of the periplasmic gap between cytoplasmic and outer bacterial membranes (i.e. $235 \text{ \AA} \pm 37$ [48]), it is unlikely CymA (23 kDa) and MtrA (35 kDa) span this distance to enable electron tunnelling. Periplasmic cytochromes such as Small Tetrahaem Cytochrome (STC) [49] and fumarate reductase flavocytochrome c_3 (i.e. Fcc₃, also referred to as Cct and soluble fumarate reductase) [34, 49, 50] have been implicated in relaying electrons between the two membrane-associated cytochromes. A further complication in elucidating CymA:MtrA electron transfer route is that most gene knockout studies focus on membrane-associated cytochromes and attribute dominant mineral reduction activity to MtrA/MtrC/OmcA [51, 52]. Furthermore, although an Δfcc_3 mutant has been shown to maintain near-wild type hydrous ferric iron reduction activity [50], an Δstc mutant has been reported loses the capacity to reduce (water-soluble) ferric citrate [49], suggesting TEA-specific electron transfer routes. As such the necessity for an electron shuttle between CymA and MtrA, and the identity of such a periplasmic electron shuttle(s) has not been experimentally resolved.

1.3.3 – The outer membrane multihaem cytochromes (OMMCs)

Proteinase K digestion has shown the exposure of the cytochromes OmcA and MtrC to the extracellular surface of *S. oneidensis* cells [53, 54], and whole cell spectroscopy demonstrates accessibility of heterologously expressed OmcA to the reducing agent sodium dithionite (i.e. Na₂S₂O₄) [55]. Based on localisation to the extracellular surface of the outer membrane, these cytochromes are called outer-membrane multihaem cytochrome (OMMCs). Sequence analysis indicates that the OMMCs all contain the lipid anchor motif LXXC to which phospholipid is covalently bound, anchoring the OMMC lipoproteins to the outer membrane (Fig. 1.3) [56].

All OMMCs experimentally linked to the DMR process are encoded for in the “metal respiration” (i.e. *mtr*) gene cluster of *Shewanella spp* genomes (Fig. 1.4). Each *Shewanella spp* capable of DMR encodes a minimum of the *mtrCAB* operon and *omcA/undA* gene in its *mtr* gene cluster [8]. Many contain the *mtrDEF* operon, which encodes the putative analogue to the MtrCAB complex. Some *Shewanella spp* have several open reading frames with homology *omcA/mtrC* [8]. Corroborated by the absence of a dedicated MtrAB module encoded for OmcA in the *mtr* gene cluster, several studies indicate an OmcA:MtrCAB interaction through which OmcA receives electrons to reduce mineral TEA [36, 57, 58].

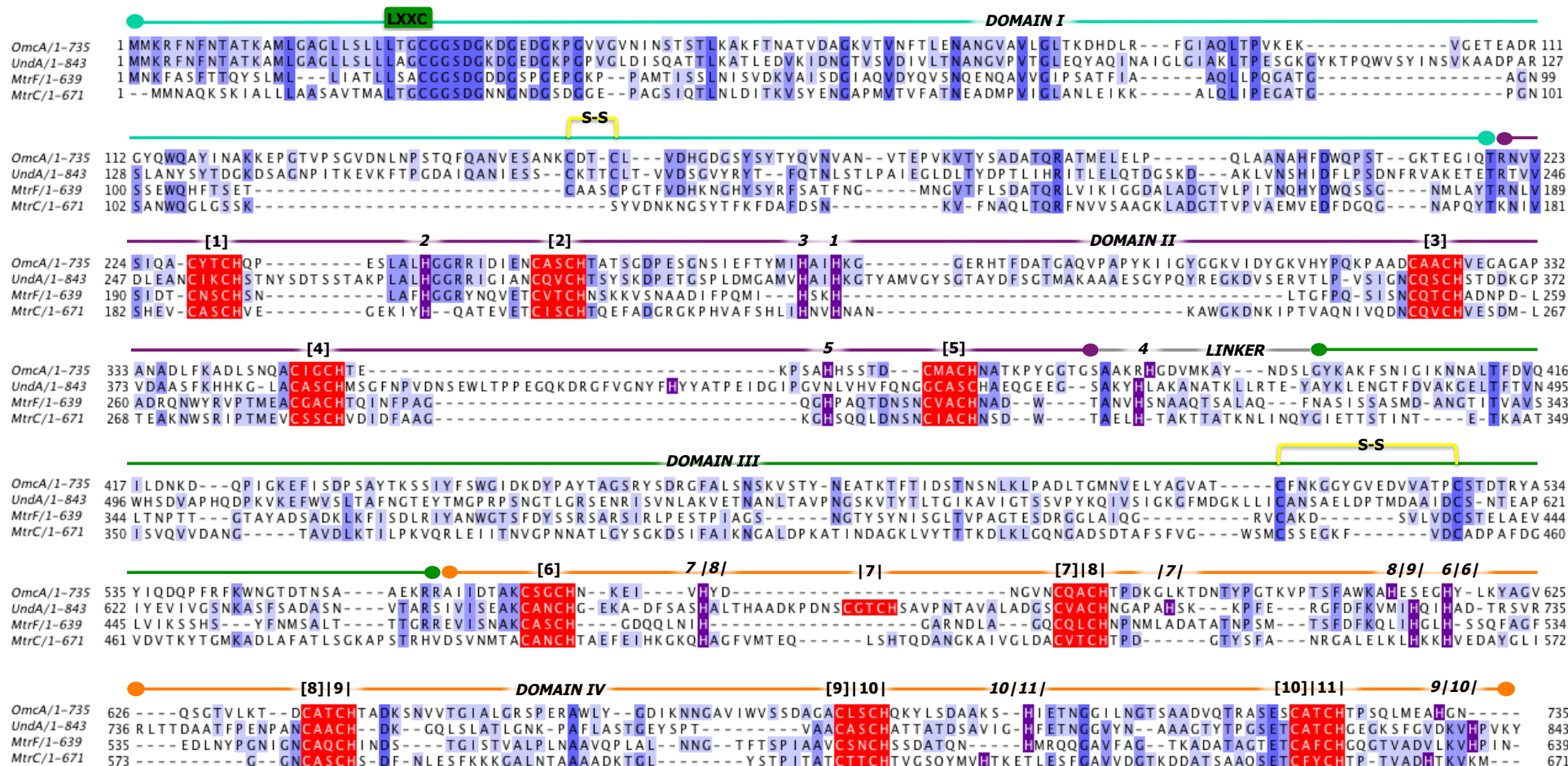


Figure 1.3. – **Primary Structure comparison of *Shewanella* spp major OMMC clades.** The primary amino acid sequences of OmcA, MtrF and MtrC from *S. oneidensis* MR-1 [59] and UndA from *Shewanella* sp. strain HRCR-6 [8, 60] were aligned using the CLUSTALW service and output made using Jalview. CXXCH motifs (red) are numbered in square brackets, || = different haems of UndA are numbered; green LXXC box = lipid binding motif; yellow S-S bridge = disulphide bridge; distal histidines (purple) and numbered with italics; amino acid conservation are in shades of blue where > 80% is the darkest blue.

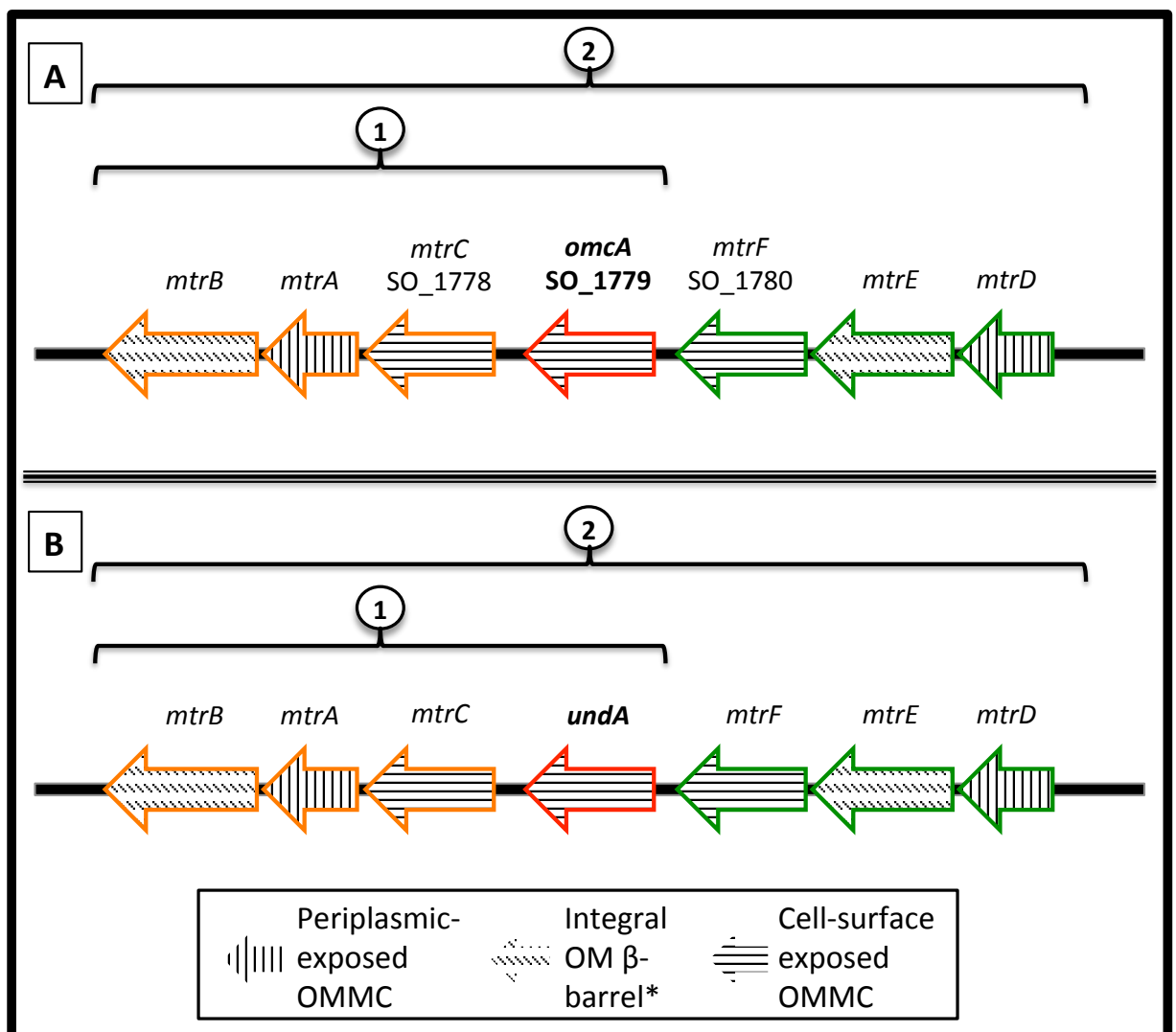


Figure 1.4 – **Cartoon of the “*mtr*” gene cluster amongst *Shewanella* spp.** Open reading frames are designated with arrows in 5’3’ direction [8, 59]. Cell-surface exposed OMMC genes are also labeled with their respective locus numbers in *S. oneidensis* MR-1. Heterotrimeric complexes are colour-code outlined. (A) *Shewanella* spp. containing *omcA* (1) *S. frigidimarina*, *S. woodyi*, *S. benthica* (2) *S. oneidensis* MR-1, *S. baltica* (strains OS155, OS185 and OS195), *Shewanella* spp. (strains ANA-3, MR-4 and MR-7). (B) *Shewanella* spp. containing *unda* (1) *S. putrefaciens* (strains CN-32, W3-18-1 and 200) (2) *S. baltica* OS223. Please note that the *mtr* gene clusters of the *Shewanella* spp. not listed here encode for other OMMCs (homologous with *omcA* and *mtrC*) [8]. * = modeled to have β-barrel structure.

Mn(IV) reduction by *S. oneidensis* MR-1 is decreased 75% and 45% by $\Delta mtrC$ and $\Delta omcA$ respectively [61]. This is corroborated by an $\Delta mtrF\Delta omcA$ *S. oneidensis* strain retaining 61% of MR-1 Mn(IV) reduction activity, compared to $\Delta mtrF$ having negligible effect on Mn(IV) reduction [62]. The effect of $\Delta omcA$ is less deleterious to *S. oneidensis* MR-1 Fe(III) reduction than to Mn(IV) reduction, although dependent on the ferric oxide mineral morphology (Table 1.1), suggesting substrate selectivity by OmcA and MtrC.

The question of functional overlap/redundancy is apparent when considering the paralogous *S. oneidensis* MtrFDE complex of the more annotated MtrCAB, and the OMMC OmcA. All the aforementioned OMMCs are upregulated in the presence of Fe(III) [63, 64]. OMMC upregulation is stimulated more by fumarate [63], most likely due to *Shewanella* cells adapting to couple organic matter oxidation to DMR in anaerobic environments [22]. Experimentally, only MtrD has been linked to differential expression within mature biofilm colonies [65]. In several *Shewanella* spp, *omcA* is replaced by what appears to be its undeca-haem functional analogue UndA [8]. Heterologous *undA* expression by *S. oneidensis* MR-1 shows that UndA is localised to the extracellular environment, and this localisation is inhibited by gene knockouts of the Type II Secretion System [60]. As documented in Table 1.1, *in trans* expression of *undA* partially complements $\Delta mtrC\Delta omcA$ mutant's ferrihydrite reduction activity.

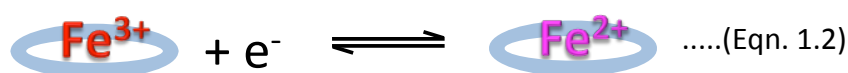
A comprehensive gene knockout study addresses the role of 3 *mtrA* paralogues (i.e. *mtrD*, SO4360, *dmsA*), 2 *mtrB* paralogues (i.e. *mtrE* and *dmsB*) and 2 of the 3 *mtrC* paralogues (i.e. *mtrF*, *omcA*, but not SO1659) by a series of single and combination deletion mutations [66]. Chelated metal reduction was shown to only require the presence of a single putative icosahaem porin-cytochrome module. DMR with an iron oxide mineral is shown to be dependent on more of the encoded cytochromes. Of the OMMCs encoded, $\Delta mtrC$ has a greater effect on DMR than $\Delta omcA$. Double mutations aid to clarify that cells expressing the OMMCs MtrC and/or OmcA show significant retention of wild-type DMR activity (Table 1.1).

Table 1.1 – **Review of OMMC involvement in *Shewanella spp* Mineral Respiration.** Compiled are anaerobic cell culture studies with mineral as the TEA. *FZ* = Turnover determined via Ferrozine assay [70]. *LBB* = Turnover determined via leucoberbelin blue assay [71].

Mineral Substrate	Experimental Design (Additional Details)	Phenotype			$\Delta mtrC/\Delta omcA$ Complementation Phenotype		Reference
		$\Delta mtrC$	$\Delta omcA$	$\Delta mtrC/\Delta omcA$	$mtrC^+$	$omcA^+$	
Hematite (α-Fe₂O₃) surface	Hematite-coated slides TEA. Turnover measured via soluble Fe (i.e. not specific to Fe ²⁺).	Negligible soluble Fe; negligible hematite surface coverage	Lowered soluble Fe; \approx MR-1 hematite surface coverage	Negligible soluble Fe; negligible hematite surface coverage	N/A	N/A	[67]
"Fe₂O₃"	Suspension of Fe ₂ O ₃ TEA. (α , β or γ -Fe ₂ O ₃ not specified). <i>FZ</i> .	\approx 50 % MR-1 [Fe ²⁺] at 24 hours	\approx 75 % MR-1 [Fe ²⁺] at 24 hours	Negligible [Fe ²⁺] production	N/A	N/A	[66]
Fe₂O₃ electrode	Cyclic voltammograms of adsorbed cells. (Electrode surface dissolution affects adsorbed cells).	Anodic peak height identical to OmcA protein film voltammogram	Anodic peak height identical to MtrC protein film voltammogram	Negligible electron exchange between cells and electrode	N/A	N/A	[68]
Birnessite (Mn⁴⁺/Mn³⁺ oxide)	Suspension of birnessite TEA. <i>LBB</i> .	N/A	N/A	\approx 8 % MR-1 Mn reduction at 48 hours	\approx 50 % MR-1 Mn reduction at 48 hours	\approx 25 % MR-1 Mn reduction at 48 hours	[69]
Ferrihydrite (Fe³⁺ oxide)	Suspension of ferrihydrite TEA. <i>FZ</i> .	\approx 75 % MR-1 [Fe ²⁺] at 24 hours	\approx 75 % MR-1 [Fe ²⁺] at 24 hours	\approx 20 % MR-1 [Fe ²⁺] at 24 hours	N/A	N/A	[29]
Mineral Substrate	Experimental Design (Additional Details)	$\Delta mtrC/\Delta omcA$ Phenotype			$\Delta mtrC/\Delta omcA$ Complementation Phenotype		Reference
					$mtrC^+/omcA^+$	$undA^+$	
Ferrihydrite (Fe³⁺ oxide)	Suspension of ferrihydrite TEA. <i>FZ</i> .	Up to \approx 8 % MR-1/HRCR-6 [Fe ²⁺] at 24 hours			\approx 50 % MR-1 [Fe ²⁺] at 24 hours	\approx 40 % MR-1 [Fe ²⁺] at 24 hours	[60]

1.3.4 – The role of haem chemistry in OMMC function

A unique element of the *Shewanella spp.* genome is the high number of c-type cytochromes it encodes for (i.e. 42 in *S. oneidensis* MR-1 [72]), many of which are implicated or proven to be involved in mineral respiration [73] (Figure 1.2, Table 1.1). A c-type haem molecule consists of an iron ion that is tetra-coordinated by a porphyrin macrocycle (Figure 1.5). The type of haem depends on how the constituent tetrapyrrole groups of the porphyrin are modified (Fig. 1.5). The electronic structure of an iron atom is $1s^2 2s^2 2p^6 3s^2 3p^6 3d^6 4s^2 = [\text{Ar}] 3d^6 4s^2$ (where s, p and d are the electronic orbitals). The haem molecule functions as a redox active co-factor by cycling its iron between oxidised and reduced states within metalloproteins known as cytochromes. The iron ion of an oxidised haem is ferric ($\text{Fe}^{3+} = [\text{Ar}] 3d^5 4s^0$), and a reduced haem contains a ferrous ($\text{Fe}^{2+} = [\text{Ar}] 3d^6 4s^0$) iron in the vast majority of known cytochromes [74] as in Eqn. 1.2.



(Where =  porphyrin)

The primary amino acid structure of a c-type cytochrome most commonly contains the haem-binding motif CXXCH (as in UndA; Fig. 1.6). The c-type haem co-factor(s) is covalently attached to the peptide by a thioether bond of the porphyrin to each of the cysteines of the motif [75] (see Fig. 1.6). The histidine of this motif is the *proximal* haem ligand. The *distal* ligand (of a hexa-coordinate c-type haem) can be located anywhere within the protein sequence (i.e. not part of a motif), and is typically histidine in the multihaem c-type cytochromes of *Shewanella spp.*

1.3.5 – Electron transfer from the OMMCs to extracellular minerals

There are four mechanisms proposed for the terminal electron transfer from OMMC(s) to mineral substrate: (1) direct haem contact, (2) flavin shuttling/chelation (3) semiflavoquinone-cofactor contact and (4) conductive pili (Fig. 1.7). Direct contact requires that mineral TEA localises within 14 Å of OMMC terminal haem(s) for electron tunnelling to occur from OMMC to mineral (Fig. 1.7A). This is feasible because OmcA and MtrC localise to the outer membrane [54], where the terminal haem(s) of the OMMCs can be within 14 Å of the mineral substrate for facile electron transfer [39].

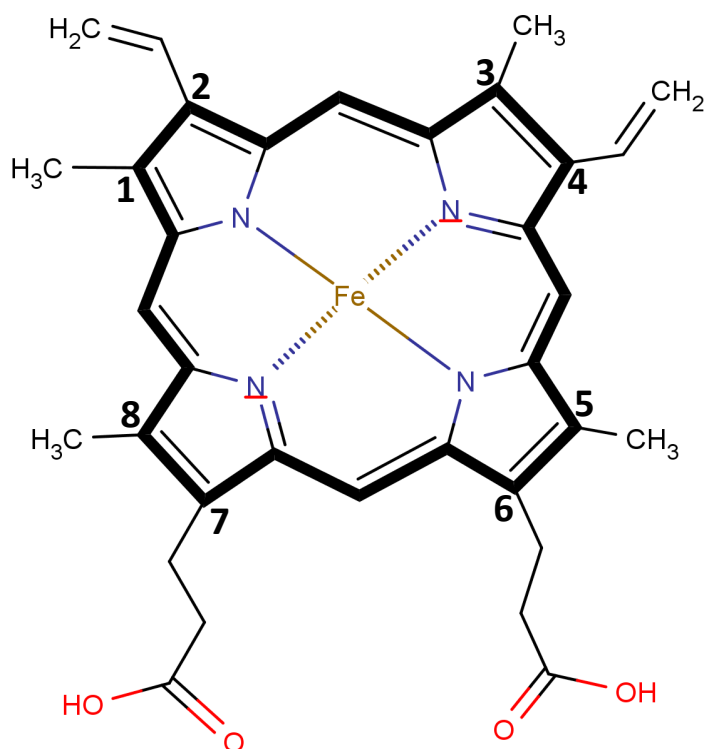
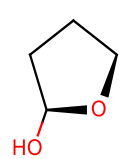


Figure 1.5 – **Ferric Porphyrin and its many variants.** All substitutions for the numbered carbons of the macrocycle (bold) are stated in the table below.

Haem type	Substitution at position 2	Substitution at position 4	Other Substitutions	References
<i>a</i>	-CH(OH)- $((\text{CH}_3)_2\text{CH}=\text{C}(\text{CH}_3))_3\text{-CH}_3$	None	8- -CH(=O)	[75]
<i>b</i>	None	None	None	
<i>c</i>	-CH(CH ₃)-S-Cys (where S is a component of cysteine residue)	-CH(CH ₃)-S-Cys (where S is a component of cysteine residue)	None	
<i>d</i>	None	None	 7- HO 8- -OH	[76]
<i>d</i>₁	-CH(CH ₃)CH ₂ COOH	-CH(CH ₃)CH ₂ COOH	1- =O 2- =O	[77]
<i>o</i>	-CH(OH)- $((\text{CH}_2)_2\text{-CH}=\text{CH})_2\text{-(CH}_2)_2\text{-CH}=\text{C}(\text{CH}_3)\text{-CH}(\text{CH}_3)$	None	None	[78]

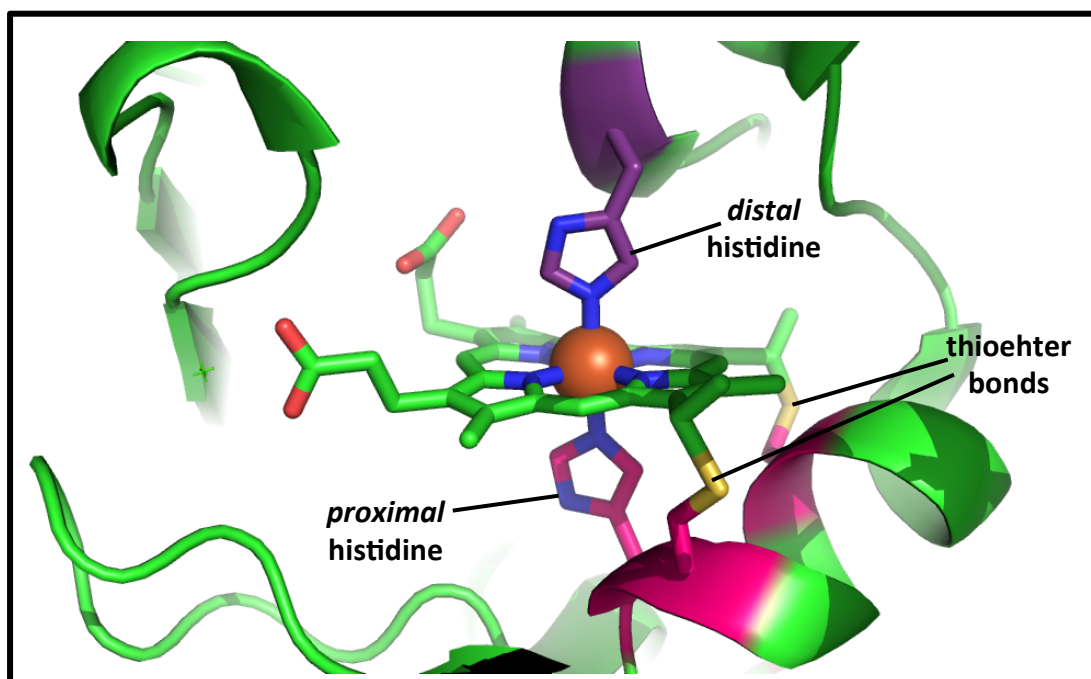


Figure 1.6 – **An example of c-type haem attachment to cytochromes.** Haem 2 of UndA is shown here with CXXCH motif in red/pink and distal histidine residue in purple.

MtrCAB-proteoliposomes driven by strong reductant have demonstrated that direct haem contact reduction of minerals can occur at electron transfer rates sufficient to support cellular metabolism [79]. The combination of “metabolic” redox poise (i.e. reduced methyl viologen) and correct orientation within a lipid bi-layer provides a representative experimental system to determine the maximum electron transfer rate possible through MtrCAB.

Several studies have indicated the capacity of *Shewanella* cells to secrete the flavin compounds riboflavin, flavin mononucleotide (FMN) and flavin adenine dinucleotide (FAD) [80-83]. Flavins are proposed to shuttle electrons from OMMCs to insoluble mineral TEA to overcome negligible substrate diffusion (Fig. 1.7B). Purified OmcA and MtrC samples were shown to have electron transfer rates enhanced with the addition of flavins [57, 84]. The conclusion drawn was that electron shuttling from cytochrome to mediator was fundamental for DMR (Fig. 1.7B). Electron transfer over a distance beyond 0.3 μm was shown [81], where steric occlusion of *Shewanella* cells from the majority of the ferric TEA substrate using an alginate bead system produced substrate turnover in excess of the iron content within 0.3 μm of the bead surfaces. The flavin content of *S. oneidensis* are compartmentalised such that FAD is retained within the cytoplasm and periplasm, whereas FMN and riboflavin are exported into

the extracellular environment [83]. UshA has been identified as a 5'-nucleotidase responsible for turning FAD to FMN within the periplasm of *S. oneidensis* MR-1 [85]. Flavin secretion has been experimentally linked with biofilm formation [81, 86]. Riboflavin content in the spent media of established *S. oneidensis* MR-1 biofilms adsorbs to an electrode surface poised to function as TEA during biofilm growth (identified by HPLC and voltammetry) [82]. Electric current from *Shewanella* cells to the poised electrode was depleted and complemented by respective replacement and re-introduction of the spent media.

Flavin compounds have documented redox activity [87], the intuitive cause of the increase in mineral reduction rate or electrode current [83, 88, 89]. A possible shuttling-chelator "shelator" mechanism was discussed by [82], whereby OMMCs reduce soluble extracellular flavins [43, 52] that are capable of both rapid diffusion to the insoluble substrate and mineral chelation via their metal-coordinating isoalloxazine rings. Understanding the extent that mineral-chelation by flavins contributes to DMR is experimentally challenging, especially considering the known redox activity of flavins.

Alternate mechanisms to overcome the negligible diffusion rate of insoluble mineral substrate include chelation strategies and mineral interaction sites of OMMCs. *Shewanella spp.* have been shown to produce siderophores, small organic compounds with high affinity for metallic ions as a trace nutrient-sequestration mechanism, namely putrebactin [90]. X-ray crystallography of Undecahem A (UndA) of *Shewanella sp.* HRCR-1 shows highly ordered orientation of $\text{Fe}^{3+}_2\text{-NTA}_2$ and $\text{Fe}^{3+}_3\text{-citrate}$ by residues Arg₅₂₈, Glu₆₅₉, Ser₇₁₀ and Lys₇₁₁ near haem 7 [91]. As a putative functional analogue of OmcA within the *Shewanella* genus, ligated metal-chelates could thus be part of the DMR mechanism. Studies have indicated OmcA and MtrC contain a mineral binding peptide [92-94]. However, where electron transfer over μm distances has been shown, only flavin-based compounds have been implicated experimentally [81]. Furthermore, nitrilotriacetic acid and citrate are not known to be naturally occurring chelates in *Shewanella's* environments at significant concentrations. As such putrebactin may simply function as siderophores do in many genera of bacteria; to chelate and scavenge metals solely for the trace mineral requirements of the cell [95, 96].

Recently, further clarification on the possible role of flavins in DMR has been provided by [97] which shows the discovery of a signature semiflavoquinone peak in differential pulse voltammograms of *Shewanella* whole cells. The peak was shown to be FMN in an MtrC-dependent semi-reduced state, and an OmcA-dependent semiflavoquinone peak of riboflavin was also observed. Identification of such an unstable and thus usually transient flavin state was tied to rapid electron transfer to cytochrome-bound flavin species from respective OMMCs where kinetics favour single-electron reduction of respective flavins. Specifically, the significantly enhanced electron transfer rate of the oxidised flavin:semiflavoquinone redox couple is dependent on the continuous supply of electrons from cellular metabolism. As such semiflavoquinone-cofactor contact provides better mechanistic improvement to DMR than the diffusion of flavin between OMMC haem and mineral TEA surface participating in the two-electron redox reactions according to this model (Fig. 1.7C).

Several studies have indicated that pili attributed atypical electrical conduction properties contribute to the mineral reduction capacities of the Gram positive bacterium *Geobacter sulfurreducens* [98] and *S. oneidensis* MR-1 [99] (Fig. 1.7D). The conductive properties attributed to pili from *Shewanella spp* is dependent on the presence of OMMCs [99]. *Geobacter spp* also produce several multihaem cytochromes that localize to the extracellular surface of its bacterial membrane [100]. One of these cytochromes, OmcS, has been detected to localize along the length of the *Geobacter* pili, but beyond electron transfer distance of each other (i.e. 28.6 ± 10.5 nm) [101]. However this may be a function of imaging resolution of the gold-linked antibodies used to visualise OmcS. In a similar manner, secretory membrane vesicles that align along the length of *S. oneidensis* pili have haem-staining protein content with molecular weights equivalent to OmcA, MtrC and MtrA [99, 102]. The effect of pili deletion mutations has a near-equivalent effect to OMMC deletion on whole cell cyclic voltammograms of *S. oneidensis*. In *Geobacter* biofilms formed on an anode, reductive current was shown to be directly proportional to both biomass and biofilm aggregate height [98]. This fits the model of insoluble substrate reduction powering metabolism and biofilm growth. Pili deletion and *in trans* expression was shown to respectively decrease and complement anode reduction.

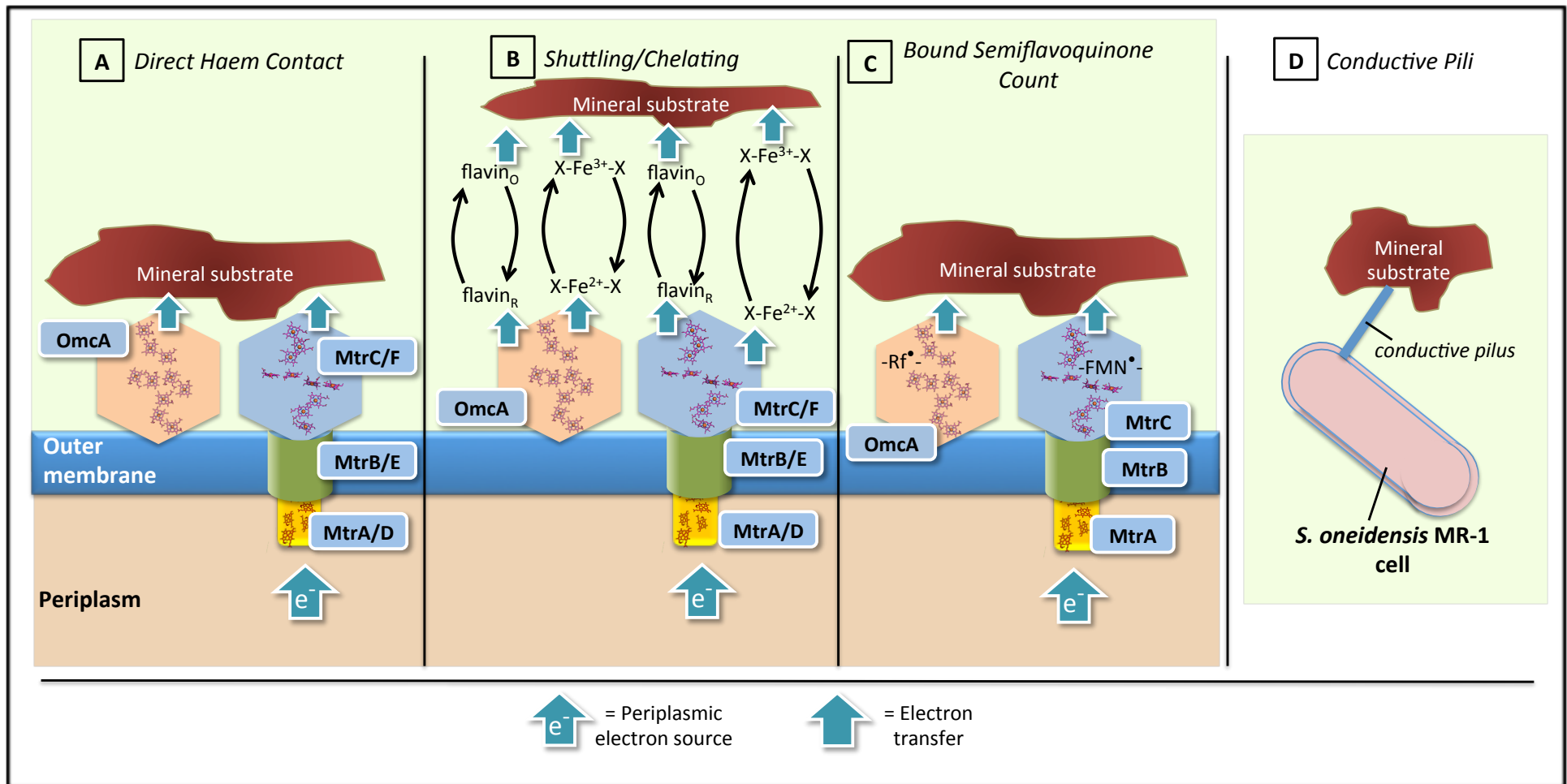


Figure 1.7 – **The proposed mechanisms of mineral substrate reduction by OMMCs.** Namely (A) direct haem contact [79], (B) either soluble electron shuttling [81] or substrate chelation [90], (C) direct contact OMMC-bound semiflavoquinone contact [97], and (D) conductive pili [99]. flavin_R = reduced flavin; flavin_S = semi-reduced flavin; flavin_O = oxidised flavin; X-Fe²⁺-X = chelated ferrous iron; X-Fe³⁺-X = chelated ferric iron.

Criticism for the conductive pili (also referred to as a “nanowire”) model in the literature is based on the metabolic expense of pili and cytochrome expression for DMR, the dependence of pili conduction on the presence of OMMCs, the unknown electron relay system between CymA/periplasmic electron sources and the conductive pili and/or OMMCs, and the lack of conventional redox-active pili constituents to tunnel electrons along length of the pili. However, solvent-exposed aromatic residues (Phe and Tyr) were recently postulated to contribute to electron shuttling between *Geobacter* cytochromes [103]. Furthermore, the pili deletion strain phenotype includes deficient auto-aggregation and biofilm formation capacity for both *S. oneidensis* [104] and *G. sulfurreducens* [105], with demonstrated impact on electrode reduction by *G. sulfurreducens*.

1.3.6 – The extracellular environment of OMMCs

The full context of the extracellular environment that these OMMCs are exposed to includes lipopolysaccharides (LPS). The lipid component embeds in the outer-membrane’s external lipid layer and the carbohydrate portion constitutes the bacterial capsule/slime layer [106]. Gram-negative bacteria also have an additional extracellular polysaccharide layer of varying chemical composition and quantity that envelops the outer-membrane [107]. Although the additional extracellular polysaccharide layer is loosely membrane-associating material, it can also adhere strongly to cells via non-covalent means [108]. As such extracellular polysaccharide (EPS) content can thus be sub-divided into tight and loosely associated EPS based on the presence of an EPS lipid anchor. A significant consideration to make of biofilms performing DMR is that the hydrated bacterial capsule of *Shewanella oneidensis* MR-4 extends over 0.5 μm from the bacterial outer membrane surface [109]. As such lipid-anchored OMMCs with longest dimension ≈ 9 nm [43, 91, 110] would putatively function whilst embedded deep within an EPS environment.

1.4 – Biophysical Properties of the MtrCAB complex and OmcA

The previous sections provide evidence of the importance of MtrCAB and OmcA to the DMR process. This has prompted subsequent characterisation of the biochemical and structural properties of these proteins implicated in relaying electrons across the outer bacterial membrane.

Several studies corroborate the orientation of MtrCAB in the *S. oneidensis* outer membrane. MtrA localises to the outer bacterial membrane [24, 35] and localises to the periplasm during heterologous in *Escherichia coli* [111]. MtrC has been consistently shown to localise to the extracellular surface of the outer bacterial membrane [53, 54, 62]. MtrB is a putative trans-membrane β -barrel [44], required for proper incorporation of MtrC and OmcA to the outer membrane that enables wild-type Mn^{4+} oxide reduction activity [62]. Cues to the orientation of MtrB in the outer bacterial membrane has been provided by proteinase K digestion of MtrCAB-proteoliposomes [79]. Contrary to convention, the predicted longer loops encoded are modelled to encompass MtrA at the periplasmic surface of the outer membrane.

The molecular weight of the MtrCAB complex was determined as 198 kDa in a Sedimentation Equilibrium experiment using Analytical Ultracentrifugation (AUC-SE [36]). A heterotrimer this size is large enough to be a trans-membrane protein that transfers electrons across the outer membrane (i.e. outer membrane width ≈ 70 Å [112]). AUC-SE provides a $k_D \approx 11$ μM for MtrA:MtrC interaction, and an estimated $k_D < 0.1$ μM for the MtrAB:MtrC interaction. The nature of the MtrCAB protein film voltammogram mentioned earlier is continuous (i.e. not composed of discrete, resolved redox active species) and is not a summative voltammogram of the purified MtrA and MtrC voltammograms [37]. As such the current working-model for the MtrCAB complex is a trans-membrane β -barrel spanning the outer-membrane. Electrons from CymA reach the outer-membrane at the decahaem cytochrome MtrA that is inserted into the MtrB channel but putatively exposed to the periplasm. MtrC, which is inserted into the MtrB lumen at the extracellular surface of the outer-membrane, receives electrons from MtrA. MtrB orients and modulates the mid-point potentials of MtrA and MtrC haems appropriately for electron transfer between the two cytochromes.

Strong anion exchange chromatography is required to disrupt the putative interaction between OmcA and MtrC [36], and whole cell *S. oneidensis* MR-1 cross-linking data using ≤ 11 Å cross-linker molecules confirms that OmcA localises within electron tunnelling distance of the MtrCAB complex via MtrC [36, 58]. Without a dedicated porin-cytochrome in an operon with *omcA*, the MtrAB module is thought to transfer electrons to OmcA via MtrC. Isolation of tagged OmcA from an *S. oneidensis* expression strain resulted in the co-purification of MtrC [57]. The isolated OmcA:MtrC

complex has a $K_D < 0.5 \mu\text{M}$ that is sensitive to KCl concentration, and a 1:1 OmcA:MtrC mixture from the same study showed $\approx 40\%$ increase in Fe^{3+} -NTA reductase activity per mg of protein compared to purified OmcA or MtrC. Since there is no known route of electron transfer from periplasm directly to OmcA (and *mtrC* deletion produces negligible Mn^{4+} reduction), the 45 % wild-type Mn^{4+} reduction phenotype of ΔomcA is indicative of OmcA:MtrCAB interaction.

Recent X-ray crystallography data is emerging to show the most divergent proteins of the four major OMMC clades (i.e. MtrF and UndA [110]) share significant tertiary structure and haem arrangement conservation. MtrF has four structural domains, two split β -barrel domains that flank the two pentahaem modules oriented such that all *c*-type haems bound are within 10 Å of its nearest haem neighbour [43]. Despite < 24% sequence identity the same domain arrangement is observed for UndA, and the “staggered haem cross” arrangement of MtrF is highly maintained in UndA, excluding 180° rotation of haem 5 and incorporation of an additional haem [91].

1.5 – Thesis Aims

Despite the key role that OmcA has been shown to play in DMR, its structural and biochemical properties are relatively unexplored compared to those of MtrCAB. This thesis attempts to address this knowledge gap by:

1. Developing systems to perform large-scale purification of OmcA with properties comparable to the wild-type protein, detailed in Chapter 2.
2. Structurally characterising OmcA and its haem environments using spectroscopy and X-ray crystallography, addressed in Chapters 3, 4 & 5.
3. Defining the redox properties of OmcA's haems and compare them to those of MtrC, MtrF and UndA. See Chapters 5 & 6.
4. Attempting to correlate OmcA structure to its function via the phenotypes of site-directed mutants. This is addressed in Chapter 7.

After the objectives listed are reported in the following five chapters, the implications of these studies to the role of OmcA in DMR are discussed in the concluding chapter (i.e. Chapter 8).

References.

- 1 Richardson, D. and Sawers, G. (2002) PMF through the redox loop. *Science*. **295**, 1842-1843
- 2 Baradaran, R., Berrisford, J. M., Minhas, G. S. and Sazanov, L. A. (2013) Crystal structure of the entire respiratory complex I. *Nature*. **494**, 443-448
- 3 Yankovskaya, V., Horsefield, R., Tornroth, S., Luna-Chavez, C., Miyoshi, H., Leger, C., Byrne, B., Cecchini, G. and Iwata, S. (2003) Architecture of succinate dehydrogenase and reactive oxygen species generation. *Science*. **299**, 700-704
- 4 Iwata, S., Lee, J. W., Okada, K., Lee, J. K., Iwata, M., Rasmussen, B., Link, T. A., Ramaswamy, S. and Jap, B. K. (1998) Complete structure of the 11-subunit bovine mitochondrial cytochrome bc(1) complex. *Science*. **281**, 64-71
- 5 Ostermeier, C., Harrenga, A., Ermler, U. and Michel, H. (1997) Structure at 2.7 angstrom resolution of the *Paracoccus denitrificans* two-subunit cytochrome c oxidase complexed with an antibody F-V fragment. *Proceedings of the National Academy of Sciences of the United States of America*. **94**, 10547-10553
- 6 Richardson, D. J. (2000) Bacterial respiration: a flexible process for a changing environment. *Microbiology-Sgm*. **146**, 551-571
- 7 Myers, C. R. and Nealson, K. H. (1988) Bacterial manganese reduction and growth with manganese oxide as the sole electron-acceptor. *Science*. **240**, 1319-1321
- 8 Fredrickson, J. K., Romine, M. F., Beliaev, A. S., Auchtung, J. M., Driscoll, M. E., Gardner, T. S., Nealson, K. H., Osterman, A. L., Pinchuk, G., Reed, J. L., Rodionov, D. A., Rodrigues, J. L. M., Saffarini, D. A., Serres, M. H., Spormann, A. M., Zhulin, I. B. and Tiedje, J. M. (2008) Towards environmental systems biology of *Shewanella*. *Nature Reviews Microbiology*. **6**, 592-603
- 9 Maeda, S. I. and Omata, T. (1997) Substrate-binding lipoprotein of the cyanobacterium *Synechococcus* sp strain PCC 7942 involved in the transport of nitrate and nitrite. *Journal of Biological Chemistry*. **272**, 3036-3041
- 10 Janausch, I. G., Zientz, E., Tran, Q. H., Kroger, A. and Unden, G. (2002) C-4-dicarboxylate carriers and sensors in bacteria. *Biochimica Et Biophysica Acta-Bioenergetics*. **1553**, 39-56
- 11 Gralnick, J. A., Vali, H., Lies, D. P. and Newman, D. K. (2006) Extracellular respiration of dimethyl sulfoxide by *Shewanella oneidensis* strain MR-1. *Proceedings of the National Academy of Sciences of the United States of America*. **103**, 4669-4674
- 12 Belchik, S. M., Kennedy, D. W., Dohnalkova, A. C., Wang, Y., Sevinc, P. C., Wu, H., Lin, Y., Lu, H. P., Fredrickson, J. K. and Shi, L. (2011) Extracellular Reduction of Hexavalent Chromium by Cytochromes MtrC and OmcA of *Shewanella oneidensis* MR-1. *Applied and Environmental Microbiology*. **77**, 4035-4041
- 13 Marshall, M. J., Beliaev, A. S., Dohnalkova, A. C., Kennedy, D. W., Shi, L., Wang, Z. M., Boyanov, M. I., Lai, B., Kemner, K. M., McLean, J. S., Reed, S. B., Culley, D. E., Bailey, V. L., Simonson, C. J., Saffarini, D. A., Romine, M. F., Zachara, J. M. and Fredrickson, J. K. (2006) c-Type cytochrome-dependent formation of U(IV) nanoparticles by *Shewanella oneidensis*. *Plos Biology*. **4**, 1324-1333
- 14 Lovley, D. R. (1991) Dissimilatory Fe(III) and Mn(IV) reduction. *Microbiological Reviews*. **55**, 259-287
- 15 Ponnampertuma, F. N. and Brady, N. C. (1972) The Chemistry of Submerged Soils. In *Advances in Agronomy*. pp. 29-96, Academic Press
- 16 Presley, B. J., Nissenba.A, Kaplan, I. R. and Kolodny, Y. (1972) Early diagenesis in a reducing fjord, Saanich inlet, British Columbia .2. Trace element distribution in interstitial water and sediment. *Geochimica Et Cosmochimica Acta*. **36**, 1073-+
- 17 Ottow, J. C. G. (1970) Bacterial mechanism of gley formation in artificially submerged soil. *Nature*. **225**, 103-&
- 18 Nealson, K. H., Belz, A. and McKee, B. (2002) Breathing metals as a way of life: geobiology in action. *Antonie Van Leeuwenhoek International Journal of General and Molecular Microbiology*. **81**, 215-222

- 19 Mortimer, C. H. (1941) The Exchange of Dissolved Substances Between Mud and Water in Lakes. *Journal of Ecology*. **29**, 280-329
- 20 Lovley, D. R., Phillips, E. J. P. and Lonergan, D. J. (1989) Hydrogen and formate oxidation coupled to dissimilatory reduction of iron or manganese by *Alteromonas putrefaciens*. *Applied and Environmental Microbiology*. **55**, 700-706
- 21 Nealson, K. H. and Myers, C. R. (1992) Microbial reduction of manganese and iron - new approaches to carbon cycling. *Applied and Environmental Microbiology*. **58**, 439-443
- 22 Lovley, D. R. and Phillips, E. J. P. (1988) Novel mode of microbial energy-metabolism - organic-carbon oxidation coupled to dissimilatory reduction of iron or manganese. *Applied and Environmental Microbiology*. **54**, 1472-1480
- 23 Croal, L. R., Gralnick, J. A., Malasarn, D. and Newman, D. K. (2004) The genetics of geochemistry. *Annual Review of Genetics*. **38**, 175-202
- 24 Myers, C. R. and Myers, J. M. (1992) Location of cytochromes to the outer-membrane of anaerobically grown *Shewanella putrefaciens* MR-1. *Journal of Bacteriology*. **174**, 3429-3438
- 25 Yang, H., Krumholz, E. W., Brutinel, E. D., Palani, N. P., Sadowsky, M. J., Odlyzko, A. M., Gralnick, J. A. and Libourel, I. G. L. (2014) Genome-Scale Metabolic Network Validation of *Shewanella oneidensis* Using Transposon Insertion Frequency Analysis. *Plos Computational Biology*. **10**
- 26 Reyes, C., Murphy, J. N. and Saltikov, C. W. (2010) Mutational and gene expression analysis of *mtrDEF*, *omcA* and *mtrCAB* during arsenate and iron reduction in *Shewanella* sp ANA-3. *Environmental Microbiology*. **12**, 1878-1888
- 27 Fredrickson, J. K., Zachara, J. M., Kennedy, D. W., Liu, C. X., Duff, M. C., Hunter, D. B. and Dohnalkova, A. (2002) Influence of Mn oxides on the reduction of uranium(VI) by the metal-reducing bacterium *Shewanella putrefaciens*. *Geochimica Et Cosmochimica Acta*. **66**, 3247-3262
- 28 Kukkadapu, R. K., Zachara, J. M., Fredrickson, J. K. and Kennedy, D. W. (2004) Biotransformation of two-line silica-ferrihydrite by a dissimilatory Fe(III)-reducing bacterium: Formation of carbonate green rust in the presence of phosphate. *Geochimica Et Cosmochimica Acta*. **68**, 2799-2814
- 29 Reardon, C. L., Dohnalkova, A. C., Nachimuthu, P., Kennedy, D. W., Saffarini, D. A., Arey, B. W., Shi, L., Wang, Z., Moore, D., McLean, J. S., Moyles, D., Marshall, M. J., Zachara, J. M., Fredrickson, J. K. and Beliaev, A. S. (2010) Role of outer-membrane cytochromes *MtrC* and *OmcA* in the biomineralization of ferrihydrite by *Shewanella oneidensis* MR-1. *Geobiology*. **8**, 56-68
- 30 Fredrickson, J. K., Kota, S., Kukkadapu, R. K., Liu, C. X. and Zachara, J. M. (2003) Influence of electron donor/acceptor concentrations on hydrous ferric oxide (HFO) bioreduction. *Biodegradation*. **14**, 91-103
- 31 Lovley, D. R. (1995) Bioremediation of organic and metal contaminants with dissimilatory metal reduction. *Journal of Industrial Microbiology*. **14**, 85-93
- 32 Myers, C. R. and Myers, J. M. (1997) Cloning and sequence of *cymA* a gene encoding a tetraheme cytochrome c required for reduction of iron(III), fumarate, and nitrate by *Shewanella putrefaciens* MR-1. *Journal of Bacteriology*. **179**, 1143-1152
- 33 Myers, J. M. and Myers, C. R. (2000) Role of the tetraheme cytochrome *CymA* in anaerobic electron transport in cells of *Shewanella putrefaciens* MR-1 with normal levels of menaquinone. *Journal of Bacteriology*. **182**, 67-75
- 34 Marritt, S. J., Lowe, T. G., Bye, J., McMillan, D. G. G., Shi, L., Fredrickson, J., Zachara, J., Richardson, D. J., Cheesman, M. R., Jeuken, L. J. C. and Butt, J. N. (2012) A functional description of *CymA*, an electron-transfer hub supporting anaerobic respiratory flexibility in *Shewanella*. *Biochemical Journal*. **444**, 465-474
- 35 Ruebush, S. S., Brantley, S. L. and Tien, M. (2006) Reduction of soluble and insoluble iron forms by membrane fractions of *Shewanella oneidensis* grown under aerobic and anaerobic conditions. *Applied and Environmental Microbiology*. **72**, 2925-2935
- 36 Ross, D. E., Ruebush, S. S., Brantley, S. L., Hartshorne, R. S., Clarke, T. A., Richardson, D. J. and Tien, M. (2007) Characterization of protein-protein interactions

involved in iron reduction by *Shewanella oneidensis* MR-1. *Applied and Environmental Microbiology*. **73**, 5797-5808

- 37 Hartshorne, R. S., Reardon, C. L., Ross, D., Nuester, J., Clarke, T. A., Gates, A. J., Mills, P. C., Fredrickson, J. K., Zachara, J. M., Shi, L., Beliaev, A. S., Marshall, M. J., Tien, M., Brantley, S., Butt, J. N. and Richardson, D. J. (2009) Characterization of an electron conduit between bacteria and the extracellular environment. *Proceedings of the National Academy of Sciences of the United States of America*. **106**, 22169-22174
- 38 Firer-Sherwood, M. A., Ando, N., Drennan, C. L. and Elliott, S. J. (2011) Solution-Based Structural Analysis of the Decaheme Cytochrome, MtrA, by Small-Angle X-ray Scattering and Analytical Ultracentrifugation. *Journal of Physical Chemistry B*. **115**, 11208-11214
- 39 Page, C. C., Moser, C. C., Chen, X. X. and Dutton, P. L. (1999) Natural engineering principles of electron tunnelling in biological oxidation-reduction. *Nature*. **402**, 47-52
- 40 Oyedotun, K. S. and Lemire, B. D. (2004) The quaternary structure of the *Saccharomyces cerevisiae* succinate dehydrogenase - Homology modeling, cofactor docking, and molecular dynamics simulation studies. *Journal of Biological Chemistry*. **279**, 9424-9431
- 41 Jormakka, M., Tornroth, S., Byrne, B. and Iwata, S. (2002) Molecular basis of proton motive force generation: Structure of formate dehydrogenase-N. *Science*. **295**, 1863-1868
- 42 Rodrigues, M. L., Oliveira, T. F., Pereira, I. A. C. and Archer, M. (2006) X-ray structure of the membrane-bound cytochrome c quinol dehydrogenase NrfH reveals novel haem coordination. *Embo Journal*. **25**, 5951-5960
- 43 Clarke, T. A., Edwards, M. J., Gates, A. J., Hall, A., White, G. F., Bradley, J., Reardon, C. L., Shi, L., Beliaev, A. S., Marshall, M. J., Wang, Z., Watmough, N. J., Fredrickson, J. K., Zachara, J. M., Butt, J. N. and Richardson, D. J. (2011) Structure of a bacterial cell surface decaheme electron conduit. *Proceedings of the National Academy of Sciences of the United States of America*. **108**, 9384-9389
- 44 Jiao, Y. and Newman, D. K. (2007) The pio operon is essential for phototrophic Fe(II) oxidation in *Rhodospseudomonas palustris* TIE-1. *Journal of Bacteriology*. **189**, 1765-1773
- 45 Leys, D., Meyer, T. E., Tsapin, A. S., Nealson, K. H., Cusanovich, M. A. and Van Beeumen, J. J. (2002) Crystal structures at atomic resolution reveal the novel concept of "electron-harvesting" as a role for the small tetraheme cytochrome c. *J Biol Chem*. **277**, 35703-35711
- 46 Leys, D., Tsapin, A. S., Nealson, K. H., Meyer, T. E., Cusanovich, M. A. and Van Beeumen, J. J. (1999) Structure and mechanism of the flavocytochrome c fumarate reductase of *Shewanella putrefaciens* MR-1. *Nat Struct Biol*. **6**, 1113-1117
- 47 Clarke, T. A., Holley, T., Hartshorne, R. S., Fredrickson, J. K., Zachara, J. M., Shi, L. and Richardson, D. J. (2008) The role of multihaem cytochromes in the respiration of nitrite in *Escherichia coli* and Fe(III) in *Shewanella oneidensis*. *Biochemical Society Transactions*. **36**, 1005-1010
- 48 Dohnalkova, A. C., Marshall, M. J., Arey, B. W., Williams, K. H., Buck, E. C. and Fredrickson, J. K. (2011) Imaging Hydrated Microbial Extracellular Polymers: Comparative Analysis by Electron Microscopy. *Applied and Environmental Microbiology*. **77**, 1254-1262
- 49 Gordon, E. H. J., Pike, A. D., Hill, A. E., Cuthbertson, P. M., Chapman, S. K. and Reid, G. A. (2000) Identification and characterization of a novel cytochrome c(3) from *Shewanella frigidimarina* that is involved in Fe(III) respiration. *Biochemical Journal*. **349**, 153-158
- 50 Schuetz, B., Schicklberger, M., Kuermann, J., Spormann, A. M. and Gescher, J. (2009) Periplasmic Electron Transfer via the c-Type Cytochromes MtrA and FccA of *Shewanella oneidensis* MR-1. *Applied and Environmental Microbiology*. **75**, 7789-7796
- 51 Beliaev, A. S., Saffarini, D. A., McLaughlin, J. L. and Hunnicutt, D. (2001) MtrC, an outer membrane decahaem c cytochrome required for metal reduction in *Shewanella putrefaciens* MR-1. *Molecular Microbiology*. **39**, 722-730

- 52 Coursole, D., Baron, D. B., Bond, D. R. and Gralnick, J. A. (2010) The Mtr Respiratory Pathway Is Essential for Reducing Flavins and Electrodes in *Shewanella oneidensis*. *Journal of Bacteriology*. **192**, 467-474
- 53 Myers, C. R. and Myers, J. M. (2003) Cell surface exposure of the outer membrane cytochromes of *Shewanella oneidensis* MR-1. *Letters in Applied Microbiology*. **37**, 254-258
- 54 Shi, L., Deng, S., Marshall, M. J., Wang, Z. M., Kennedy, D. W., Dohnalkova, A. C., Mottaz, H. M., Hill, E. A., Gorby, Y. A., Beliaev, A. S., Richardson, D. J., Zachara, J. M. and Fredrickson, J. K. (2008) Direct involvement of type II secretion system in extracellular translocation of *Shewanella oneidensis* outer membrane cytochromes MtrC and OmcA. *Journal of Bacteriology*. **190**, 5512-5516
- 55 Donald, J. W., Hicks, M. G., Richardson, D. J. and Palmer, T. (2008) The c-type cytochrome OmcA localizes to the outer membrane upon heterologous expression in *Escherichia coli*. *Journal of Bacteriology*. **190**, 5127-5131
- 56 Myers, J. M. and Myers, C. R. (1998) Isolation and sequence of *omcA*, a gene encoding a decaheme outer membrane cytochrome c of *Shewanella putrefaciens* MR-1, and detection of *omcA* homologs in other strains of *S. putrefaciens*. *Biochimica Et Biophysica Acta-Biomembranes*. **1373**, 237-251
- 57 Shi, L., Chen, B. W., Wang, Z. M., Elias, D. A., Mayer, M. U., Gorby, Y. A., Ni, S., Lower, B. H., Kennedy, D. W., Wunschel, D. S., Mottaz, H. M., Marshall, M. J., Hill, E. A., Beliaev, A. S., Zachara, J. M., Fredrickson, J. K. and Squier, T. C. (2006) Isolation of a high-affinity functional protein complex between OmcA and MtrC: Two outer membrane decaheme c-type cytochromes of *Shewanella oneidensis* MR-1. *Journal of Bacteriology*. **188**, 4705-4714
- 58 Zhang, H., Tang, X., Munske, G. R., Zakharova, N., Yang, L., Zheng, C., Wolff, M. A., Tolic, N., Anderson, G. A., Shi, L., Marshall, M. J., Fredrickson, J. K. and Bruce, J. E. (2008) In vivo identification of the outer membrane protein *omcA*-*mtrC* interaction network in *Shewanella oneidensis* MR-1 cells using novel hydrophobic chemical cross-linkers. *Journal of Proteome Research*. **7**, 1712-1720
- 59 Heidelberg, J. F., Paulsen, I. T., Nelson, K. E., Gaidos, E. J., Nelson, W. C., Read, T. D., Eisen, J. A., Seshadri, R., Ward, N., Methe, B., Clayton, R. A., Meyer, T., Tsapin, A., Scott, J., Beanan, M., Brinkac, L., Daugherty, S., DeBoy, R. T., Dodson, R. J., Durkin, A. S., Haft, D. H., Kolonay, J. F., Madupu, R., Peterson, J. D., Umayam, L. A., White, O., Wolf, A. M., Vamathevan, J., Weidman, J., Impraim, M., Lee, K., Berry, K., Lee, C., Mueller, J., Khouri, H., Gill, J., Utterback, T. R., McDonald, L. A., Feldblyum, T. V., Smith, H. O., Venter, J. C., Nealson, K. H. and Fraser, C. M. (2002) Genome sequence of the dissimilatory metal ion-reducing bacterium *Shewanella oneidensis*. *Nature Biotechnology*. **20**, 1118-1123
- 60 Shi, L., Belchik, S. M., Wang, Z., Kennedy, D. W., Dohnalkova, A. C., Marshall, M. J., Zachara, J. M. and Fredrickson, J. K. (2011) Identification and Characterization of UndA(HRCR-6), an Outer Membrane Endecaheme c-Type Cytochrome of *Shewanella* sp Strain HRCR-6. *Applied and Environmental Microbiology*. **77**, 5521-5523
- 61 Myers, J. M. and Myers, C. R. (2001) Role for outer membrane cytochromes OmcA and OmcB of *Shewanella putrefaciens* MR-1 in reduction of manganese dioxide. *Applied and Environmental Microbiology*. **67**, 260-269
- 62 Myers, C. R. and Myers, J. M. (2002) MtrB is required for proper incorporation of the cytochromes OmcA and OmcB into the outer membrane of *Shewanella putrefaciens* MR-1. *Applied and Environmental Microbiology*. **68**, 5585-5594
- 63 Beliaev, A. S., Thompson, D. K., Khare, T., Lim, H., Brandt, C. C., Li, G., Murray, A. E., Heidelberg, J. F., Giometti, C. S., Yates, J., 3rd, Nealson, K. H., Tiedje, J. M. and Zhou, J. (2002) Gene and protein expression profiles of *Shewanella oneidensis* during anaerobic growth with different electron acceptors. *Omics : a journal of integrative biology*. **6**, 39-60
- 64 Beliaev, A. S., Klingeman, D. M., Klappenbach, J. A., Wu, L., Romine, M. F., Tiedje, J. A., Nealson, K. H., Fredrickson, J. K. and Zhou, J. (2005) Global transcriptome analysis of *Shewanella oneidensis* MR-1 exposed to different terminal electron acceptors. *Journal of Bacteriology*. **187**, 7138-7145

- 65 McLean, J. S., Pinchuk, G. E., Geydebrekht, O. V., Bilskis, C. L., Zakrajsek, B. A., Hill, E. A., Saffarini, D. A., Romine, M. F., Gorby, Y. A., Fredrickson, J. K. and Beliaev, A. S. (2008) Oxygen-dependent autoaggregation in *Shewanella oneidensis* MR-1. *Environmental Microbiology*. **10**, 1861-1876
- 66 Coursolle, D. and Gralnick, J. A. (2010) Modularity of the Mtr respiratory pathway of *Shewanella oneidensis* strain MR-1. *Molecular Microbiology*. **77**, 995-1008
- 67 Mitchell, A. C., Peterson, L., Reardon, C. L., Reed, S. B., Culley, D. E., Romine, M. R. and Geesey, G. G. (2012) Role of outer membrane c-type cytochromes MtrC and OmcA in *Shewanella oneidensis* MR-1 cell production, accumulation, and detachment during respiration on hematite. *Geobiology*. **10**, 355-370
- 68 Meitl, L. A., Eggleston, C. M., Colberg, P. J. S., Khare, N., Reardon, C. L. and Shi, L. (2009) Electrochemical interaction of *Shewanella oneidensis* MR-1 and its outer membrane cytochromes OmcA and MtrC with hematite electrodes. *Geochimica Et Cosmochimica Acta*. **73**, 5292-5307
- 69 Bucking, C., Popp, F., Kerzenmacher, S. and Gescher, J. (2010) Involvement and specificity of *Shewanella oneidensis* outer membrane cytochromes in the reduction of soluble and solid-phase terminal electron acceptors. *Fems Microbiology Letters*. **306**, 144-151
- 70 Stookey, L. L. (1970) Ferrozine - A new spectrophotometric reagent for iron. *Analytical Chemistry*. **42**, 779-&
- 71 Booger, F. C. and Devrind, J. P. M. (1987) Manganese oxidation by *Leptothrix discophora*. *Journal of Bacteriology*. **169**, 489-494
- 72 Meyer, T. E., Tsapin, A. I., Vandenberghe, I., de Smet, L., Frishman, D., Neelson, K. H., Cusanovich, M. A. and van Beeumen, J. J. (2004) Identification of 42 possible cytochrome C genes in the *Shewanella oneidensis* genome and characterization of six soluble cytochromes. *OMICS*. **8**, 57-77
- 73 Richardson, D. J., Butt, J. N., Fredrickson, J. K., Zachara, J. M., Shi, L., Edwards, M. J., White, G., Baiden, N., Gates, A. J., Marritt, S. J. and Clarke, T. A. (2012) The 'porin-cytochrome' model for microbe-to-mineral electron transfer. *Molecular Microbiology*. **85**, 201-212
- 74 Moore, G. R. and Pettigrew, G. W. (1990) SPRINGER SERIES IN MOLECULAR BIOLOGY CYTOCHROMES C EVOLUTIONARY STRUCTURAL AND PHYSICOCHEMICAL ASPECTS. Moore, G. R. and G. W. Pettigrew. Springer Series in Molecular Biology: Cytochromes C: Evolutionary, Structural and Physicochemical Aspects. Xvi+478p. Springer-Verlag: Berlin, Germany; New York, New York, USA. Illus
- 75 Pettigrew, G. W. and Moore, G. R. (1987) SPRINGER SERIES IN MOLECULAR BIOLOGY CYTOCHROMES C BIOLOGICAL ASPECTS
- 76 Murshudov, G. N., Grebenko, A. I., Barynin, V., Dauter, Z., Wilson, K. S., Vainshtein, B. K., MelikAdamyanyan, W., Bravo, J., Ferran, J. M., Ferrer, J. C., Switala, J., Loewen, P. C. and Fita, I. (1996) Structure of the heme d of *Penicillium vitale* and *Escherichia coli* catalases. *Journal of Biological Chemistry*. **271**, 8863-8868
- 77 Chang, C. K. and Wu, W. (1986) The porphinedione structure of heme-d1 - Synthesis and spectral properties of model compounds of the prosthetic group of dissimilatory nitrite reductase. *Journal of Biological Chemistry*. **261**, 8593-8596
- 78 Abramson, J., Riistama, S., Larsson, G., Jasaitis, A., Svensson-Ek, M., Laakkonen, L., Puustinen, A., Iwata, S. and Wikstrom, M. (2000) The structure of the ubiquinol oxidase from *Escherichia coli* and its ubiquinone binding site. *Nature Structural Biology*. **7**, 910-917
- 79 White, G. F., Shi, Z., Shi, L., Wang, Z. M., Dohnalkova, A. C., Marshall, M. J., Fredrickson, J. K., Zachara, J. M., Butt, J. N., Richardson, D. J. and Clarke, T. A. (2013) Rapid electron exchange between surface-exposed bacterial cytochromes and Fe(III) minerals. *Proceedings of the National Academy of Sciences of the United States of America*. **110**, 6346-6351
- 80 Hernandez, M. E. and Newman, D. K. (2001) Extracellular electron transfer. *Cellular and Molecular Life Sciences*. **58**, 1562-1571

- 81 Lies, D. P., Hernandez, M. E., Kappler, A., Mielke, R. E., Gralnick, J. A. and Newman, D. K. (2005) *Shewanella oneidensis* MR-1 uses overlapping pathways for iron reduction at a distance and by direct contact under conditions relevant for biofilms. *Applied and Environmental Microbiology*. **71**, 4414-4426
- 82 Marsili, E., Baron, D. B., Shikhare, I. D., Coursolle, D., Gralnick, J. A. and Bond, D. R. (2008) *Shewanella* Secretes flavins that mediate extracellular electron transfer. *Proceedings of the National Academy of Sciences of the United States of America*. **105**, 3968-3973
- 83 von Canstein, H., Ogawa, J., Shimizu, S. and Lloyd, J. R. (2008) Secretion of flavins by *Shewanella* species and their role in extracellular electron transfer. *Applied and Environmental Microbiology*. **74**, 615-623
- 84 Ross, D. E., Brantley, S. L. and Tien, M. (2009) Kinetic Characterization of OmcA and MtrC, Terminal Reductases Involved in Respiratory Electron Transfer for Dissimilatory Iron Reduction in *Shewanella oneidensis* MR-1. *Applied and Environmental Microbiology*. **75**, 5218-5226
- 85 Covington, E. D., Gelbmann, C. B., Kotloski, N. J. and Gralnick, J. A. (2010) An essential role for UshA in processing of extracellular flavin electron shuttles by *Shewanella oneidensis*. *Molecular Microbiology*. **78**, 519-532
- 86 De Vriendt, K., Theunissen, S., Carpentier, W., De Smet, L., Devreese, B. and Van Beeumen, J. (2005) Proteomics of *Shewanella oneidensis* MR-1 biofilm reveals differentially expressed proteins, including AggA and RibB. *Proteomics*. **5**, 1308-1316
- 87 Kao, Y. T., Saxena, C., He, T. F., Guo, L. J., Wang, L. J., Sancar, A. and Zhong, D. P. (2008) Ultrafast dynamics of flavins in five redox states. *Journal of the American Chemical Society*. **130**, 13132-13139
- 88 Suzuki, Y., Kitatsuji, Y., Ohnuki, T. and Tsujimura, S. (2010) Flavin mononucleotide mediated electron pathway for microbial U(VI) reduction. *Phys Chem Chem Phys*. **12**, 10081-10087
- 89 Baron, D., LaBelle, E., Coursolle, D., Gralnick, J. A. and Bond, D. R. (2009) Electrochemical Measurement of Electron Transfer Kinetics by *Shewanella oneidensis* MR-1. *Journal of Biological Chemistry*. **284**, 28865-28873
- 90 Ledyard, K. M. and Butler, A. (1997) Structure of putrebactin, a new dihydroxamate siderophore produced by *Shewanella putrefaciens*. *Journal of Biological Inorganic Chemistry*. **2**, 93-97
- 91 Edwards, M. J., Hall, A., Shi, L., Fredrickson, J. K., Zachara, J. M., Butt, J. N., Richardson, D. J. and Clarke, T. A. (2012) The Crystal Structure of the Extracellular 11-heme Cytochrome UndA Reveals a Conserved 10-heme Motif and Defined Binding Site for Soluble Iron Chelates. *Structure*. **20**, 1275-1284
- 92 Lower, B. H., Shi, L., Yongsunthon, R., Droubay, T. C., McCready, D. E. and Lower, S. K. (2007) Specific bonds between an iron oxide surface and outer membrane cytochromes MtrC and OmcA from *Shewanella oneidensis* MR-1. *Journal of Bacteriology*. **189**, 4944-4952
- 93 Lower, B. H., Yongsunthon, R., Shi, L., Wildling, L., Gruber, H. J., Wigginton, N. S., Reardon, C. L., Pinchuk, G. E., Droubay, T. C., Boily, J.-F. and Lower, S. K. (2009) Antibody Recognition Force Microscopy Shows that Outer Membrane Cytochromes OmcA and MtrC Are Expressed on the Exterior Surface of *Shewanella oneidensis* MR-1. *Applied and Environmental Microbiology*. **75**, 2931-2935
- 94 Lower, B. H., Lins, R. D., Oestreich, Z., Straatsma, T. P., Hochella, M. F., Shi, L. A. and Lower, S. K. (2008) In vitro evolution of a peptide with a hematite binding motif that may constitute a natural metal-oxide binding archetype. *Environmental Science & Technology*. **42**, 3821-3827
- 95 Cornelis, P. (2010) Iron uptake and metabolism in pseudomonads. *Applied Microbiology and Biotechnology*. **86**, 1637-1645
- 96 Miethke, M. (2013) Molecular strategies of microbial iron assimilation: from high-affinity complexes to cofactor assembly systems. *Metallomics*. **5**, 15-28
- 97 Okamoto, A., Hashimoto, K., Nealson, K. H. and Nakamura, R. (2013) Rate enhancement of bacterial extracellular electron transport involves bound flavin

- semiquinones. Proceedings of the National Academy of Sciences of the United States of America. **110**, 7856-7861
- 98 Reguera, G., Nevin, K. P., Nicoll, J. S., Covalla, S. F., Woodard, T. L. and Lovley, D. R. (2006) Biofilm and nanowire production leads to increased current in *Geobacter sulfurreducens* fuel cells. Applied and Environmental Microbiology. **72**, 7345-7348
- 99 Gorby, Y. A., Yanina, S., McLean, J. S., Rosso, K. M., Moyles, D., Dohnalkova, A., Beveridge, T. J., Chang, I. S., Kim, B. H., Kim, K. S., Culley, D. E., Reed, S. B., Romine, M. F., Saffarini, D. A., Hill, E. A., Shi, L., Elias, D. A., Kennedy, D. W., Pinchuk, G., Watanabe, K., Ishii, S., Logan, B., Nealsen, K. H. and Fredrickson, J. K. (2006) Electrically conductive bacterial nanowires produced by *Shewanella oneidensis* strain MR-1 and other microorganisms. Proceedings of the National Academy of Sciences of the United States of America. **103**, 11358-11363
- 100 Shi, L., Squier, T. C., Zachara, J. M. and Fredrickson, J. K. (2007) Respiration of metal (hydr)oxides by *Shewanella* and *Geobacter*: a key role for multihaem c-type cytochromes. Molecular Microbiology. **65**, 12-20
- 101 Leang, C., Qian, X. L., Mester, T. and Lovley, D. R. (2010) Alignment of the c-Type Cytochrome OmcS along Pili of *Geobacter sulfurreducens*. Applied and Environmental Microbiology. **76**, 4080-4084
- 102 Gorby, Y., McLean, J., Korenevsky, A., Rosso, K. M., El-Naggar, M. Y. and Beveridge, T. J. (2008) Redox-reactive membrane vesicles produced by *Shewanella*. Geobiology. **6**, 232-241
- 103 Bonanni, P. S., Massazza, D. and Busalmen, J. P. (2013) Stepping stones in the electron transport from cells to electrodes in *Geobacter sulfurreducens* biofilms. Physical Chemistry Chemical Physics. **15**, 10300-10306
- 104 Thormann, K. M., Saville, R. M., Shukla, S., Pelletier, D. A. and Spormann, A. M. (2004) Initial phases of biofilm formation in *Shewanella oneidensis* MR-1. Journal of Bacteriology. **186**, 8096-8104
- 105 Reguera, G., Pollina, R. B., Nicoll, J. S. and Lovley, D. R. (2007) Possible nonconductive role of *Geobacter sulfurreducens* pilus nanowires in biofilm formation. Journal of Bacteriology. **189**, 2125-2127
- 106 Dirienzo, J. M. and Macleod, R. A. (1978) Composition of fractions separated by polyacrylamide-gel electrophoresis of lipopolysaccharide of a marine bacterium. Journal of Bacteriology. **136**, 158-167
- 107 Dirienzo, J. M., Nakamura, K. and Inouye, M. (1978) Outer membrane proteins of Gram-negative bacteria - biosynthesis, assembly, and functions. Annual Review of Biochemistry. **47**, 481-532
- 108 Roberts, I. S. (1996) The biochemistry and genetics of capsular polysaccharide production in bacteria. Annual Review of Microbiology. **50**, 285-315
- 109 Stukalov, O., Korenevsky, A., Beveridge, T. J. and Dutcher, J. R. (2008) Use of atomic force microscopy and transmission electron microscopy for correlative studies of bacterial capsules. Applied and Environmental Microbiology. **74**, 5457-5465
- 110 Edwards, M. J., Fredrickson, J. K., Zachara, J. M., Richardson, D. J. and Clarke, T. A. (2012) Analysis of structural MtrC models based on homology with the crystal structure of MtrF. Biochemical Society Transactions. **40**, 1181-1185
- 111 Pitts, K. E., Dobbin, P. S., Reyes-Ramirez, F., Thomson, A. J., Richardson, D. J. and Seward, H. E. (2003) Characterization of the *Shewanella oneidensis* MR-1 decaheme cytochrome MtrA. Journal of Biological Chemistry. **278**, 27758-27765
- 112 Matias, V. R. F., Al-Amoudi, A., Dubochet, J. and Beveridge, T. J. (2003) Cryo-transmission electron Microscopy of frozen-hydrated sections of *Escherichia coli* and *Pseudomonas aeruginosa*. Journal of Bacteriology. **185**, 6112-6118

Chapter 2: **Purification and Spectroscopic Characterisation of OmcA from** ***Shewanella oneidensis* MR-1.**

2.1 – Introduction

The Outer Membrane Multihaem Cytochromes (OMMCs) OmcA and MtrC from *S. oneidensis* MR-1 have been studied extensively for their role in Dissimilatory Mineral Respiration (DMR) [1-3]. This includes the analysis of the *Shewanella spp* genomes which revealed an “*mtr* gene cluster” [4-6] and identified functional paralogues to OmcA and MtrC within the genome of *S. oneidensis* MR-1 and other *Shewanella spp* [7]. Several experiments have confirmed the localisation of both OmcA and MtrC to the extracellular surface of the outer bacterial membrane [8, 9], where both proteins have been shown to contribute to the mineral reduction capacity of *Shewanella* cells [10-13]. However solution-state analysis of the purified proteins (and their bound haem cofactors) is central to thorough characterisation of OMMC function, which may provide novel insights considering the unique localisation and substrate of these respiratory cytochromes.

Despite a wealth of studies that have focused on the OMMCs OmcA and MtrC, a robust characterisation of OmcA from *Shewanella oneidensis* MR-1 is yet to be published. The molar extinction coefficients previously determined for OmcA and MtrC [14, 15] account adequately for their ten bound *c*-type haems (i.e. $\epsilon_{410\text{ nm}} > 106,000\text{ M}^{-1}\text{cm}^{-1}$ per *c*-type haem [16]). However, the aforementioned characterisations of OmcA have contrasting spin-state data. The biophysical study of OmcA from *Shewanella frigidimarina* NCIMB400 provided UV-Visible electronic absorbance (UV-Vis), Near Infrared Magnetic Circular Dichroism (NIR MCD) and Electron Paramagnetic Resonance (EPR) data that all the haems of OmcA detected are low-spin and *bis*-histidine coordinated [14]. EPR data from this study shows a high-spin haem feature that was estimated to account for 0.2% of total haem content. Based on 0.2% haem content being several orders of magnitude sub-stoichiometric to the haem content of OmcA, the production of the high-spin haem feature can be attributed to a minimal population of OmcA that denatured during protein purification/handling (not discussed in publication).

A later study also detected a high-spin haem content in the EPR spectrum of OmcA from *S. oneidensis* MR-1 [17]. Based on the relative signal intensities, the high-

spin haem content is higher than in the previous study [14], and may be a stoichiometric amount (i.e. an integer ratio of high-spin haem:OmcA concentrations). It is not uncommon for the haem of a cytochrome to undergo ligand exchange, due to a native reaction mechanism [18], pH-induced change in haem-ligand affinities [19] or sample handling [20]. In the interest of determining the physiological ligation state of OmcA, it is important to ascertain whether or not the variable proportion of high-spin haem content detected is an artefact of sample handling.

This chapter describes the first spectroscopic characterisation of one of the most important cytochromes studied in the DMR process (i.e. OmcA). The purification strategy and spectroscopic characterisation of OmcA_(wt) and two recombinant forms of OmcA are described. OmcA is analysed in this study via UV-Vis and EPR spectroscopy at different pHs to determine any pH-dependence on haem ligation.

2.2 – Results

2.2.1 – The Purification of OmcA_(wt) and two recombinant forms of OmcA

OmcA purified from wild-type *Shewanella oneidensis* MR-1 is named OmcA_(wt) in this study. OmcA_(wt) contains the lipid-anchor motif LXXC at its amino-terminus [4]. As such detergent is required to maintain OmcA_(wt) in solution via the detergent's micellar properties. Concerning purification of OmcA_(wt) from *S. oneidensis* MR-1, buffer containing 5% (v/v) Triton X-100 was used to solubilise *S. oneidensis* cell membranes. Isolated membranes were then subject to two anion exchange chromatography steps, where it was noted that OmcA_(wt) co-eluted with the MtrCAB complex (Fig. A2.2) as observed previously [8, 21]. After anion exchange chromatography, the sample was also put through gel filtration chromatography (See Methods and Materials M.3). A < 10 kDa contaminant protein band is present in the final Coomassie and Silver-stained SDS-PAGE gels. The contaminant has no haem/peroxidase content, and could not be separated from OmcA using pressure filtration with a 30 kDa membrane, nor filtration through a Sephadex PD-10 matrix (Fig. A2.3), showing tight interaction of contaminant with OmcA or similar chromatographic/hydrodynamic radius properties (Fig. 2.1A).

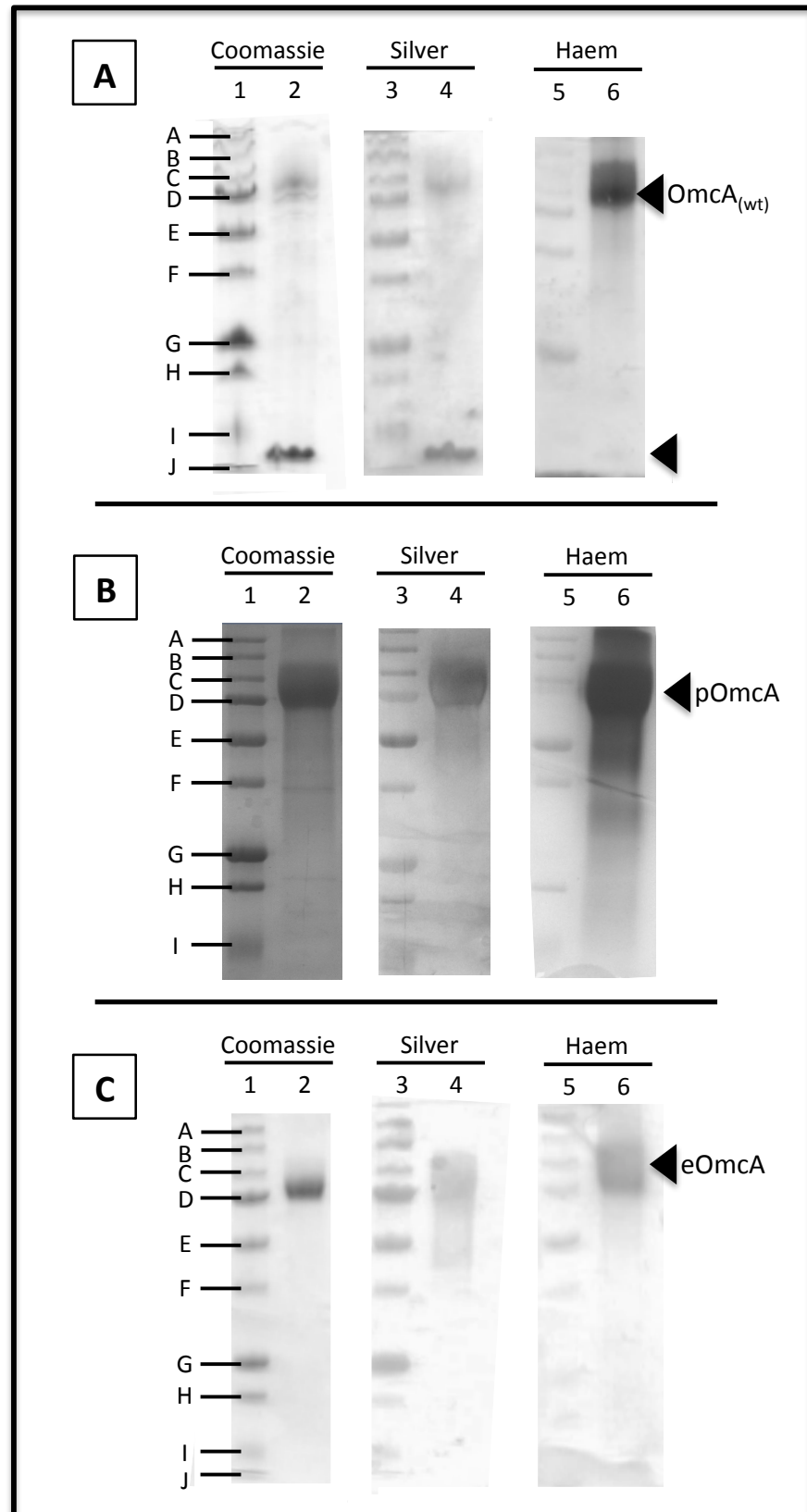


Fig. 2.1 – SDS-PAGE gels of purified OmcA visualised by coomassie, silver and haem staining. Panels A, B and C correspond to OmcA_(wt), pOmcA and eOmcA respectively. Lanes 1, 3 and 5 are molecular weight markers (i.e. A = 250 kDa, B = 150 kDa, C = 100 kDa, D = 75 kDa, E = 50 kDa, F = 37 kDa, G = 25 kDa, H = 15 kDa, I = 10 kDa and J = dye front). Lanes 2, 4 and 6 are the same protein sample of (A) OmcA_(wt), (B) pOmcA and (C) eOmcA that have been coomassie, silver and haem stained.

Table 2.1. – **The Purification of three Forms of OmcA from *S. oneidensis*.** The localisation, yield and haem:polypeptide ratio of OmcA_(wt), pOmcA and eOmcA derived from Fig. 2.2. * = Putative localisation to the periplasm. # = Percentage of cell wet weight.

Protein	Protein localisation	Yield (mg L ⁻¹ cell culture)	A _{410nm} :A _{280nm}
OmcA _(wt)	outer bacterial membrane	54 × 10 ⁻³	3.16
pOmcA	soluble cell lysis extract*	1.1	6.45
eOmcA	media	5.2 0.4%#	6.51

In order to obtain a higher yield of OmcA, of possibly enhanced purity, *Shewanella oneidensis* strain LS 330 was used to express recombinant forms of OmcA. This *Shewanella* strain encodes for a soluble form of OmcA where the amino-terminal polypeptide, which includes the LXXC lipid anchor sequence, is replaced with the amino-terminal amino acid sequence of MtrB as described previously [22-24]. OmcA cloned into this expression system still contains the signal peptide necessary for translocation to the periplasm and targeting to the cytochrome maturation apparatus. Recombinant OmcA that is induced, extracted from the periplasm of lysed cells (see Methods and Materials) and purified is termed “periplasmic soluble OmcA” (i.e. pOmcA, see Fig. 2.1B) in this study. The acyl-terminus hexahistidine metal-affinity tag cloned into the pOmcA protein was utilised in the first purification step, after which pOmcA was purified using anion exchange and gel filtration chromatography (Fig. 2.1B).

As observed for other soluble OMMC constructs [25], the Type II Secretion System of *S. oneidensis* LS 330 also recognises the recombinant form of OmcA and exports it into the extracellular environment of induced cell cultures. Accordingly, this form of OmcA purified from spent, cell-free media is referred to as “extracellular soluble OmcA” (i.e. eOmcA, see Fig. 2.1C). The purification of eOmcA involved three anion exchange steps and a single gel filtration chromatography step (Materials and Methods). Purification of pOmcA and eOmcA increases protein yield, the amount of protein obtained per litre of cell culture, ~20-100 fold respectively (Table 1.1).

2.2.2 – UV-Vis Spectroscopy of purified OmcA_(wt), pOmcA and eOmcA

To compare the different forms of OmcA isolated, UV-Visible electronic absorbance (UV-Vis) and Electron Paramagnetic Resonance (EPR) spectra of OmcA_(wt), pOmcA and eOmcA were measured. Oxidised UV-Vis spectra of all three forms of OmcA consist of a Soret absorption peak at 410 nm, a broad feature at 528 nm with a broad shoulder at 559 nm (Fig. 2.2, black spectra). The relative purity of each OmcA sample can be expressed numerically as the $A_{410\text{ nm}}:A_{280\text{ nm}}$ of the *oxidised* spectra (Table 2.1). This value is a measure of the ratio of haem (i.e. haem soret; $A_{410\text{ nm}}$) and polypeptide content (i.e. tryptophan and tyrosine side chains; $A_{280\text{ nm}}$). The $A_{410\text{ nm}}:A_{280\text{ nm}}$ ratio correlates with the final SDS-PAGE gel of each OmcA form. For example, the impurity present in the OmcA_(wt) sample lowers its the haem:peptide ratio in comparison to pOmcA and eOmcA (Table 2.1).

Upon reduction with sodium dithionite (i.e. $\text{Na}_2\text{S}_2\text{O}_4$) all three OmcA forms share identical spectral features. This entails sharper 551 nm (α -band) and 522 nm (β -band) features, and the Soret (γ) band red-shifts to 420 nm and increases in intensities (see Fig. 2.2, red spectra). The absorption band in the reduced spectra of all OmcA forms seen at 314 nm is produced by the addition of the reducing agent $\text{Na}_2\text{S}_2\text{O}_4$ (see Fig. A2.9). There is no evidence of high-spin haem content in the UV-Vis spectra, usually present as an absorption band in the oxidised spectra in the 600-660 nm range, suggesting all 10 *c*-type haems encoded for are low-spin, hexa-coordinated haems. Although the identity of haem ligands cannot be defined directly by UV-Vis spectra, the absorption bands observed are typical of *bis*-histidine coordinated haem [26].

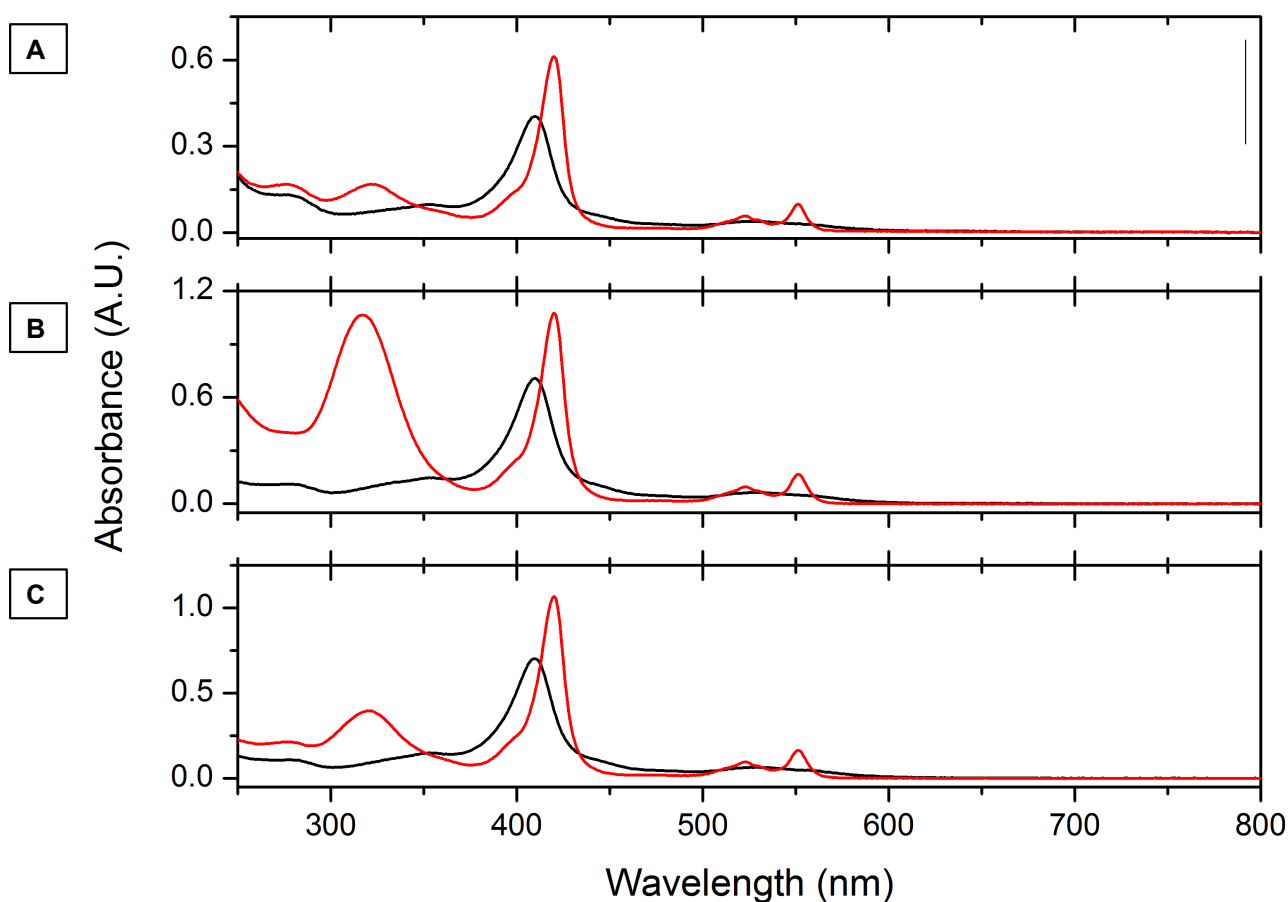


Fig. 2.2 – **UV-Visible redox spectra of purified OmcA.** Oxidised (black) and Na₂S₂O₄-reduced (red) absorption of (A) OmcA_(wt), (B) pOmcA, and (C) eOmcA. Buffer conditions were 20 mM HEPES, pH 7.60, 100 mM NaCl for pOmcA and eOmcA. OmcA_(wt) is in the same buffer conditions with the addition of 0.01 % CHAPS (w/v).

2.2.3 – MCD Spectroscopy of Oxidised pOmcA

The $\epsilon_{410\text{nm}}$ of oxidised eOmcA determined via pyridine-hemochrome assay is $1,644 \pm 3 \text{ mM}^{-1} \text{ cm}^{-1}$ using horse heart cytochrome *c* as a monohaem standard (Fig. 2.3A). This extinction coefficient was used as an estimate for pOmcA in analysis of the MCD data. UV-Vis MCD shows no $\Delta\epsilon$ in the 600-660 nm region, conclusive evidence of no high-spin haem content because the strong magnetic field applied (i.e. 8 T) uncouples any magnetically coupled haem present (Fig. 2.3B). The NIR-MCD spectrum of pOmcA shows the dominant $\Delta\epsilon_{1540\text{nm}} = 8.85 \text{ mM}^{-1} \text{ cm}^{-1} \text{ T}^{-1}$ (Fig. 2.3C). The 1540 nm peak can be attributed to *bis*-nitrogen axial haem co-ordination [27, 28]. The $\Delta\epsilon_{1500\text{nm}}$ of *bis*-histidine coordinated haem is $0.9 \pm 0.1 \text{ mM}^{-1} \text{ cm}^{-1} \text{ T}^{-1}$ per haem [29], and as such the $\Delta\epsilon_{1540\text{nm}}$ band accounts for 10 ± 1 pOmcA haems.

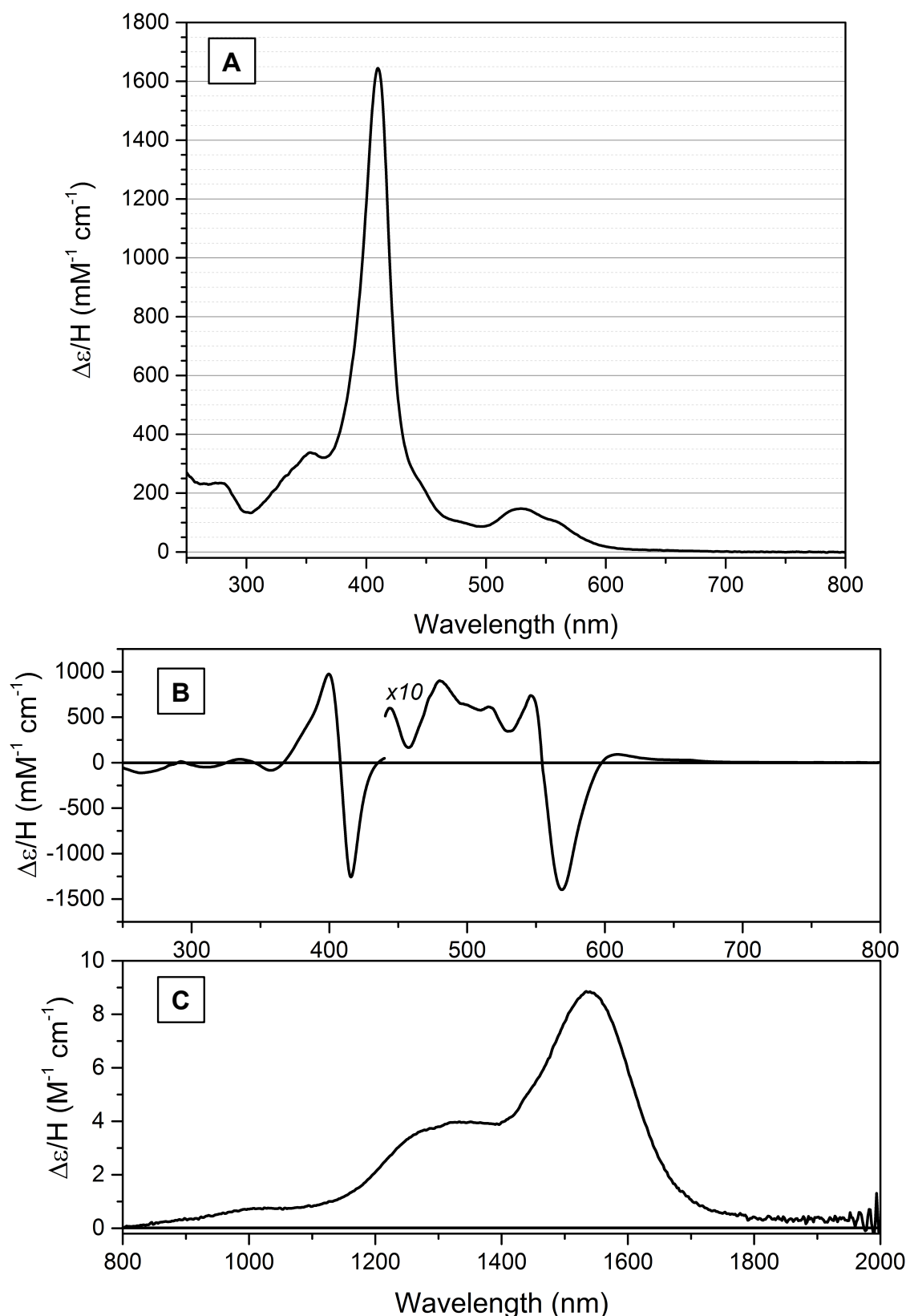


Fig. 2.3 – **The Room Temperature MCD spectrum of oxidised pOmca.** All measurements performed with pOmca in deuterated-buffer at 293 K. (A) A plot of oxidised pOmca extinction coefficient determined by pyridine-hemochrome assay of eOmca. (B) The Circular Dichroism spectrum of oxidised pOmca in the UV-Visible region with *applied* magnetic field ($H = 8$ Tesla). Inset is a 10-fold amplified spectrum obtained by changing the sample path length. (C) Near-Infrared MCD of pOmca ($H = 8$ Tesla). Buffer conditions are 20 mM HEPES, pH 7.60, 0.1 M NaCl.

2.2.4 – EPR Spectroscopy of purified OmcA_(wt), pOmcA and eOmcA

Electron Paramagnetic Resonance (EPR) spectra of all forms of oxidised OmcA were also measured at pH 7.60 for comparison (Fig 2.4). In all spectra similar resonance signals were observed between 150 and 500 mT. In particular, the resonance features of pOmcA and eOmcA are well defined in their respective spectra. However there is a high amount of noise in the OmcA_(wt) spectrum due to relatively weak signals produced by a relatively dilute sample (all spectra are normalised for comparison, Fig 2.4).

Importantly, all signals resolved in the OmcA_(wt) spectrum are observed in the spectra of pOmcA and eOmcA in comparable proportions. There are differences in the two g values between 175 and 225 mT between the three OmcA spectra. The signal between 150 and 175 mT (i.e. $g = 4.3$) has increased in relative signal intensity when comparing the OmcA_(wt) spectrum and the spectra of recombinant OmcA (Fig. 2.4). The $g = 4.3$ signal corresponds with adventitious ferric iron in the EPR resonator cavity or sample that is amplified in Fig. 2.3 by normalisation of the spectrum [26].

Several of the signals observed in OmcA are also present in the EPR spectrum of the oxidised OMMC MtrF from *S. oneidensis* MR-1 [29]. These are the Large g_{\max} (i.e. LGM2 apparent g value, $g_{1app} = 3.18$), LS1 ($g_{1,2,3app} = 2.97, 2.29, 1.54$) and LS2 ($g_{1,2,3app} = 2.87, 2.28, 1.61$) signals are observed in all forms of OmcA. Features unique to the OmcA EPR spectra (i.e. absent in MtrF) are a “Larger” g_{\max} signal (i.e. LGM1 $g_{1app} = 3.58$) and the Low Spin 3 system (i.e. LS3 $g_{1app} \approx 2.66$).

2.2.5 – The Impact of pH on the Spectroscopic Properties of OmcA

UV-Vis measurements of OmcA_(wt) (Fig. 2.5) show that across the pHs measured OmcA_(wt) maintains the same spectral features described earlier (Section 2.2.3). Difference spectra normalised by polypeptide absorbance (i.e. $A_{280\text{ nm}}$; Fig. 2.5 panels C & D) reveal several pH-dependent molar extinction coefficients (i.e. $\Delta\epsilon$). Exchange of OmcA_(wt) from pH 5.60 to 6.60 causes a significant increase in the ϵ_{420} of reduced OmcA_(wt) (Fig. 2.5C). A smaller increase in the ϵ_{420} is apparent in the reduced (pH 6.60 – pH 7.60) difference spectra (see Fig. 2.5D). More apparent in the (pH 6.60 – pH 7.60) difference spectra is that this pH transition (i.e. exchange from pH 6.60 to 7.60) leads to a broad ϵ decrease in the α/β region of both oxidised and reduced spectra.

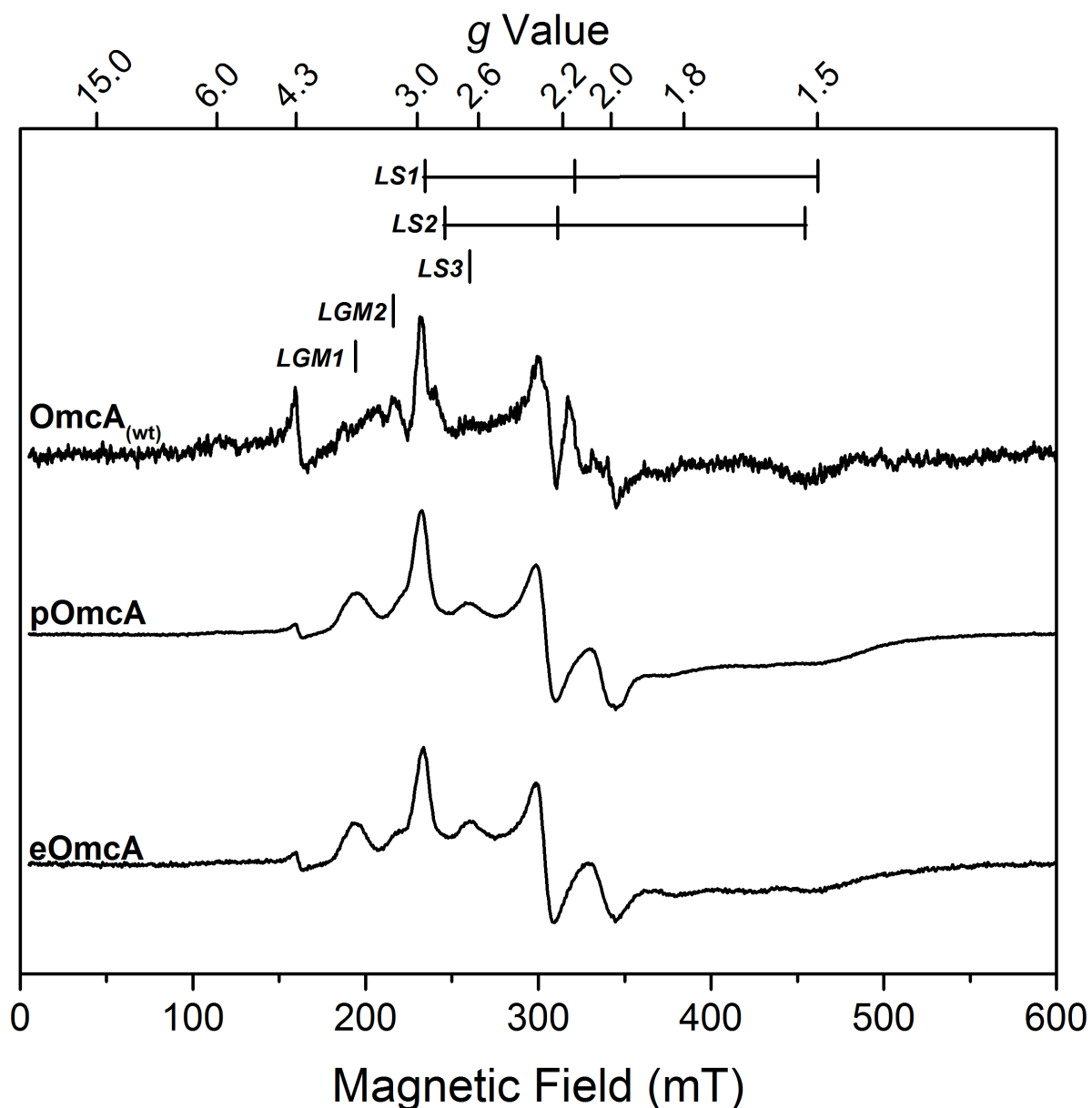


Fig. 2.4 – The EPR spectra of pOmcA and eOmcA in comparison with a $\text{OmcA}_{(\text{wt})}$ preparation. The protein concentrations are 25 μM , 155 μM and 87 μM of the samples $\text{OmcA}_{(\text{wt})}$, pOmcA and eOmcA respectively (in 20 mM HEPES, pH 7.6, 50 mM NaCl, 0.01% CHAPS, 1 % glycerol). The $\text{OmcA}_{(\text{wt})}$ spectrum was amplified 40-fold to make signals comparable. 9.688 GHz, 7 ± 2 K, 2.012×10 mW, Receiver Gain = 6.32×10^4 . The pOmcA and eOmcA spectra were divided by factors of 9 and 4 respectively to make spectra visually comparable.

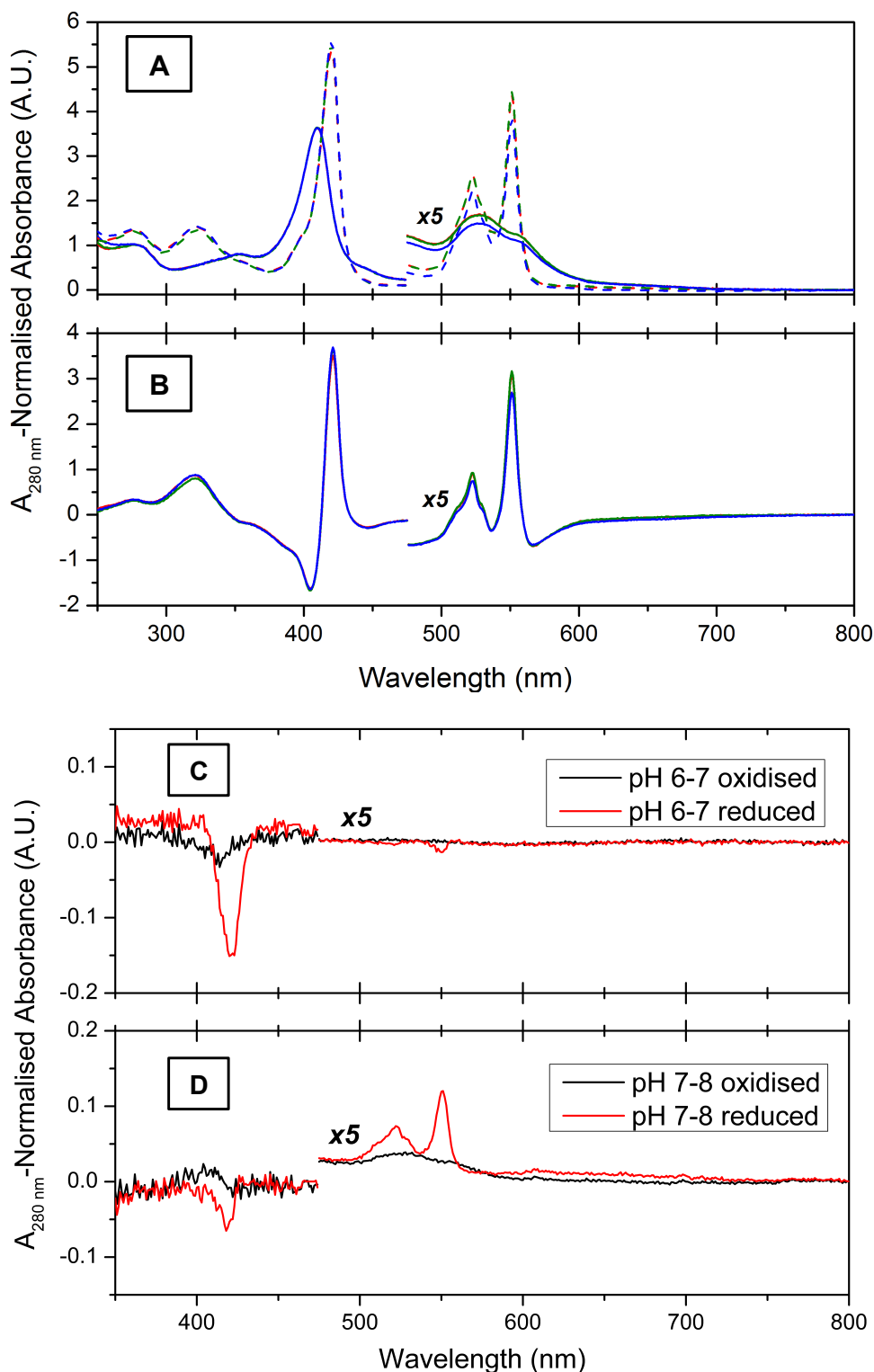


Fig. 2.5 – **The Effect of pH on the Oxidised and the Reduced Spectra of OmcA_(wt)**. (A) Oxidised (solid lines) and Na₂S₂O₄-reduced (dashed lines) spectra were taken of OmcA at pHs 5.60 (red), 6.60 (green) and 7.60 (blue). (B) The reduced minus oxidised spectra (i.e. difference spectra) plot of the absorbance spectra in (A) at each respective pH. pH difference spectra were produced by subtracting spectra of the same redox state in (A) between different pHs; i.e. pH 5.6 – pH 6.6 (C) and pH 6.6 – pH 7.6 (D). Oxidised spectra are black and reduced spectra are red. Spectra were measured of OmcA at these different pHs in both a 2 mm and 1 cm cuvette, the plot multiplied by a factor of 5 (i.e. from 475 – 800 nm). All spectra are normalised to their respective oxidised 280 nm absorbances.

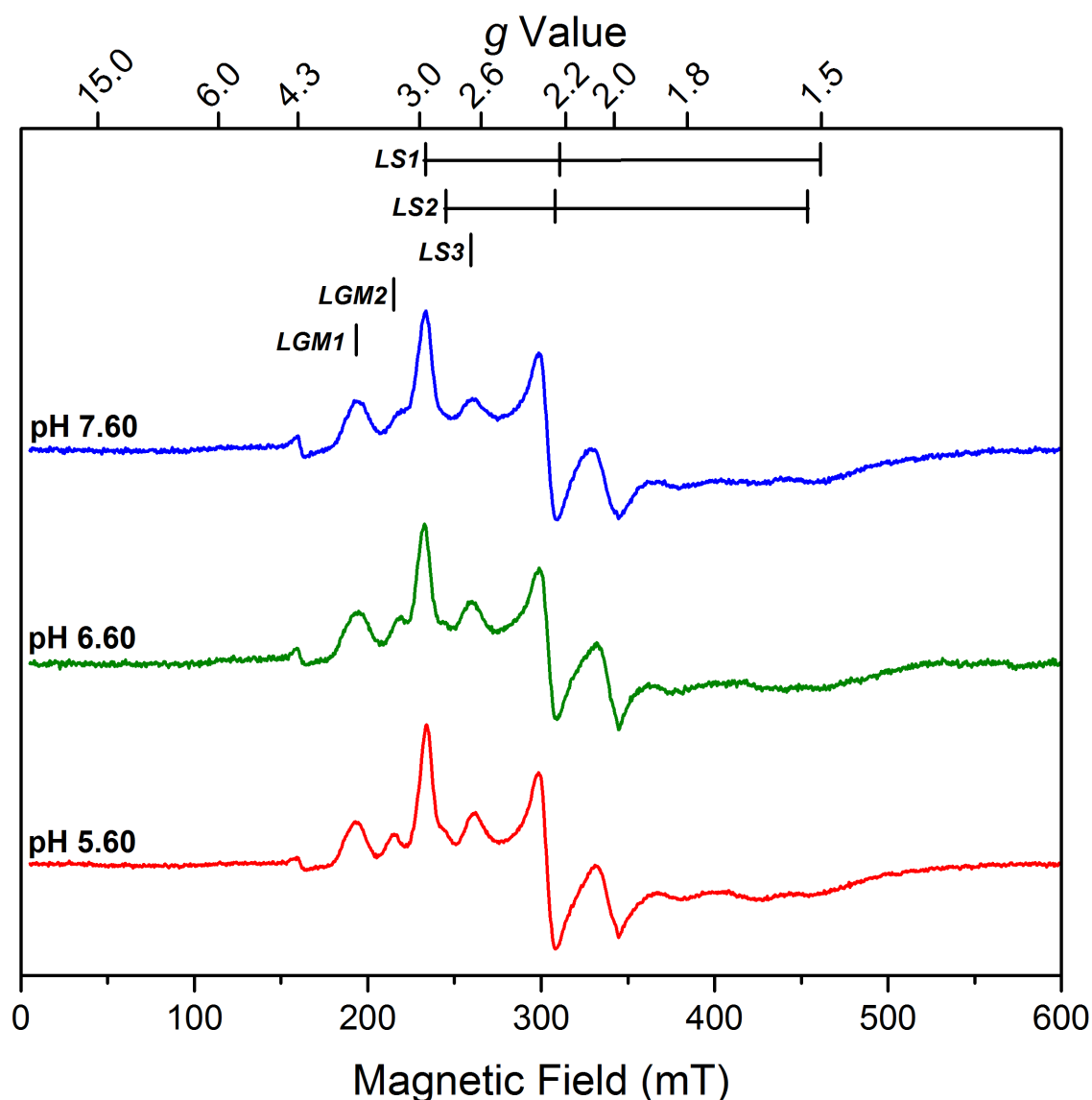


Fig. 2.6 – **The Effect of pH on the Oxidised EPR spectra of eOmCA.** The EPR spectra of eOmCA measured at pH 5.60 (MES buffer, red), 6.60 (PIPES buffer, green) and 7.60 (HEPES buffer, blue). eOmCA concentration is 58 μM . The sample buffer is 20 mM, 50 mM NaCl, 0.01% CHAPS, 1 % glycerol). Due to differences in signal intensities, spectra are normalised to the LS1-peak height.

The EPR spectra of equimolar eOmCA (i.e. 58 μM) samples at pH 5.60, 6.60 and 7.60 reveal negligible qualitative differences. All 5 resonance features observed in OmCA previously are present in eOmCA at all pH values tested (see Fig. 2.6), at intensities of similar relative proportion. However resonance intensity of the entire absorption envelope appears to be largest at pH 5.60, followed by pH 7.60 and then pH 6.60 has the smallest resonance intensity. This is possibly due to sample preparation yielding samples of unequal concentration (as such EPR spectra are

normalised to LS1 g_{1app} peak height in Fig. 2.6). Alternatively, pH could be contributing to partial reduction of eOmCA, although there is no evidence of this in the UV-Vis spectra (Fig. 2.5).

Also apparent is the resolution of LGM2, LS2 and LS3 g_{1app} peaks from the dominant LS1 g_{1app} peak with decrease in pH. The LGM2 g_1 lineshape sharpens from pH 7.60 to pH 6.60, and then decreases by $g_{1app} = 0.06$, whilst further sharpening from pH 6.60 to pH 5.60.

2.3 – Discussion

This chapter describes the successful development of an OmCA purification strategy that produces ≈ 100 fold higher yield than OmCA_(wt), and protein purification to homogeneity (i.e. eOmCA). In this study the recombinant proteins pOmCA and eOmCA are spectroscopically validated as representative of OmCA_(wt). All UV-Vis and EPR absorbance features are recognisably shared by OmCA_(wt), pOmCA and eOmCA, although the dilute OmCA_(wt) sample produces certain signals barely discernible from spectral noise. There is no $g_{\perp} \approx 6$ EPR resonance signal or 600 – 660 nm UV-Vis/MCD spectroscopy absorption band in the corresponding spectra of any forms of OmCA purified in this study. Furthermore, the *bis*-nitrogen coordination of pOmCA's 10 haems indicate that the identical EPR signals observed of OmCA_(wt), pOmCA and eOmCA are produced by the *bis*-nitrogen coordinated haems.

The purification protocol of OmCA_(wt) described (Materials and Methods) results in co-purification of a < 10 kDa contaminant protein. The co-purifying contaminant protein that interacts with OmCA_(wt) may have undetermined redox properties, effectively poisoning the sample in a semi-reduced state. Reduced haem has the spin-state, $S = 1$, which is diamagnetic and thus produces no EPR signal. However there is no evidence of reduced haem in the UV-Vis spectra of OmCA_(wt).

The pH range studied include the physiological conditions of *S. oneidensis* MR-1, i.e. pH 7 – 8 [30]. Exploration of pH-dependant haem ligation changes of OmCA was explored by UV-Vis and EPR spectroscopy. Minor haem-related UV-Vis $\Delta\epsilon$ were observed, all of which are pH-dependent (Figs. 2.5 and 2.6). These UV-Vis $\Delta\epsilon$ are complex to consolidate with the EPR spectra of OmCA. LGM2 lineshape broadening

and g_1 increase of 0.06 from exchange of eOmCA from pH 5.60 – pH 6.60 causes no UV-Vis $\Delta\epsilon$ of (oxidised) OmCA_(wt). Also, LGM2 lineshape broadening from pH 6.60 – pH 7.60 may be responsible for the more significant $\Delta\epsilon$ in the UV-Vis spectra. However, the relevance of this observation is unclear and physiologically vague. Spin quantification of the oxidised eOmCA EPR spectrum would be required to meaningfully interpret difference spectra that could be generated from the data shown in Fig. 2.6. As such this type of analysis will be addressed in Chapter 5.

The lack of high-spin haem features in the EPR, UV-Vis and MCD spectra of OmCA is a strong body of evidence against high-spin/penta-coordinate haem content in OmCA. This is in agreement with the characterisation of OmCA from *S. frigidimarina* NCIMB 400 [14], but contrasts data on OmCA from *S. oneidensis* MR-1 [17] that detects high spin haem in its EPR spectrum. As such, it is worth considering the effect of sample handling/conditions where the high-spin signal was observed. The purification protocol followed in the publication used 2% (v/v) Sarkosyl, a very strong anionic detergent that may have denatured OmCA and cause loss of axial haem ligand(s) [17]. This is corroborated by the low $\epsilon_{410\text{nm}}$ calculated in that study (i.e. 934 mM⁻¹ cm⁻¹ per OmCA molecule [17]) which accounts for ≈ 9 c-type haems ($\epsilon_{410\text{nm}} \approx 110$ mM⁻¹ cm⁻¹ per c-type haem [16]). The pyridine-hemochromogen assay of eOmCA, in agreement with previous studies [14, 15], accounts for approximately 10 haems (10 haems confirmed by $\Delta\epsilon_{1540\text{nm}} = 8.85 \text{ mM}^{-1} \text{ cm}^{-1} \text{ T}^{-1}$ NIR-MCD absorption peak).

References

- 1 Shi, L., Belchik, S. M., Wang, Z., Kennedy, D. W., Dohnalkova, A. C., Marshall, M. J., Zachara, J. M. and Fredrickson, J. K. (2011) Identification and Characterization of UndA(HRCR-6), an Outer Membrane Endoheme c-Type Cytochrome of *Shewanella* sp Strain HRCR-6. *Applied and Environmental Microbiology*. **77**, 5521-5523
- 2 Shi, L., Squier, T. C., Zachara, J. M. and Fredrickson, J. K. (2007) Respiration of metal (hydr)oxides by *Shewanella* and *Geobacter*: a key role for multihaem c-type cytochromes. *Molecular Microbiology*. **65**, 12-20
- 3 Richardson, D. J., Butt, J. N., Fredrickson, J. K., Zachara, J. M., Shi, L., Edwards, M. J., White, G., Baiden, N., Gates, A. J., Marritt, S. J. and Clarke, T. A. (2012) The 'porin-cytochrome' model for microbe-to-mineral electron transfer. *Molecular Microbiology*. **85**, 201-212
- 4 Myers, J. M. and Myers, C. R. (1998) Isolation and sequence of omcA, a gene encoding a decaheme outer membrane cytochrome c of *Shewanella putrefaciens* MR-1, and detection of omcA homologs in other strains of *S. putrefaciens*. *Biochimica Et Biophysica Acta-Biomembranes*. **1373**, 237-251

- 5 Beliaev, A. S. and Saffarini, D. A. (1998) *Shewanella putrefaciens* mtrB encodes an outer membrane protein required for Fe(III) and Mn(IV) reduction. *Journal of Bacteriology*. **180**, 6292-6297
- 6 Heidelberg, J. F., Paulsen, I. T., Nelson, K. E., Gaidos, E. J., Nelson, W. C., Read, T. D., Eisen, J. A., Seshadri, R., Ward, N., Methe, B., Clayton, R. A., Meyer, T., Tsapin, A., Scott, J., Beanan, M., Brinkac, L., Daugherty, S., DeBoy, R. T., Dodson, R. J., Durkin, A. S., Haft, D. H., Kolonay, J. F., Madupu, R., Peterson, J. D., Umayam, L. A., White, O., Wolf, A. M., Vamathevan, J., Weidman, J., Impraim, M., Lee, K., Berry, K., Lee, C., Mueller, J., Khouri, H., Gill, J., Utterback, T. R., McDonald, L. A., Feldblyum, T. V., Smith, H. O., Venter, J. C., Nealson, K. H. and Fraser, C. M. (2002) Genome sequence of the dissimilatory metal ion-reducing bacterium *Shewanella oneidensis*. *Nature Biotechnology*. **20**, 1118-1123
- 7 Fredrickson, J. K., Romine, M. F., Beliaev, A. S., Auchtung, J. M., Driscoll, M. E., Gardner, T. S., Nealson, K. H., Osterman, A. L., Pinchuk, G., Reed, J. L., Rodionov, D. A., Rodrigues, J. L. M., Saffarini, D. A., Serres, M. H., Spormann, A. M., Zhulin, I. B. and Tiedje, J. M. (2008) Towards environmental systems biology of *Shewanella*. *Nature Reviews Microbiology*. **6**, 592-603
- 8 Shi, L., Chen, B. W., Wang, Z. M., Elias, D. A., Mayer, M. U., Gorby, Y. A., Ni, S., Lower, B. H., Kennedy, D. W., Wunschel, D. S., Mottaz, H. M., Marshall, M. J., Hill, E. A., Beliaev, A. S., Zachara, J. M., Fredrickson, J. K. and Squier, T. C. (2006) Isolation of a high-affinity functional protein complex between OmcA and MtrC: Two outer membrane decaheme c-type cytochromes of *Shewanella oneidensis* MR-1. *Journal of Bacteriology*. **188**, 4705-4714
- 9 Donald, J. W., Hicks, M. G., Richardson, D. J. and Palmer, T. (2008) The c-type cytochrome OmcA localizes to the outer membrane upon heterologous expression in *Escherichia coli*. *Journal of Bacteriology*. **190**, 5127-5131
- 10 Myers, J. M. and Myers, C. R. (2001) Role for outer membrane cytochromes OmcA and OmcB of *Shewanella putrefaciens* MR-1 in reduction of manganese dioxide. *Applied and Environmental Microbiology*. **67**, 260-269
- 11 Reardon, C. L., Dohnalkova, A. C., Nachimuthu, P., Kennedy, D. W., Saffarini, D. A., Arey, B. W., Shi, L., Wang, Z., Moore, D., McLean, J. S., Moyles, D., Marshall, M. J., Zachara, J. M., Fredrickson, J. K. and Beliaev, A. S. (2010) Role of outer-membrane cytochromes MtrC and OmcA in the biomineralization of ferrihydrite by *Shewanella oneidensis* MR-1. *Geobiology*. **8**, 56-68
- 12 Beliaev, A. S., Saffarini, D. A., McLaughlin, J. L. and Hunnicutt, D. (2001) MtrC, an outer membrane decaheme c cytochrome required for metal reduction in *Shewanella putrefaciens* MR-1. *Molecular Microbiology*. **39**, 722-730
- 13 Coursolle, D. and Gralnick, J. A. (2010) Modularity of the Mtr respiratory pathway of *Shewanella oneidensis* strain MR-1. *Molecular Microbiology*. **77**, 995-1008
- 14 Field, S. J., Dobbin, P. S., Cheesman, M. R., Watmough, N. J., Thomson, A. J. and Richardson, D. J. (2000) Purification and magneto-optical spectroscopic characterization of cytoplasmic membrane and outer membrane multiheme c-type cytochromes from *Shewanella frigidimarina* NCIMB400. *Journal of Biological Chemistry*. **275**, 8515-8522
- 15 Ross, D. E., Brantley, S. L. and Tien, M. (2009) Kinetic Characterization of OmcA and MtrC, Terminal Reductases Involved in Respiratory Electron Transfer for Dissimilatory Iron Reduction in *Shewanella oneidensis* MR-1. *Applied and Environmental Microbiology*. **75**, 5218-5226
- 16 Margoliash, E. and Frohwirt, N. (1959) Spectrum of horse-heart cytochrome-c. *Biochemical Journal*. **71**, 570-578
- 17 Bodemer, G. J., Antholine, W. A., Basova, L. V., Saffarini, D. and Pacheco, A. A. (2010) The effect of detergents and lipids on the properties of the outer-membrane protein OmcA from *Shewanella oneidensis*. *Journal of Biological Inorganic Chemistry*. **15**, 749-758
- 18 Cheesman, M. R., Ferguson, S. J., Moir, J. W. B., Richardson, D. J., Zumft, W. G. and Thomson, A. J. (1997) Two enzymes with a common function but different heme ligands in the forms as isolated. Optical and magnetic properties of the heme groups in the

- oxidized forms of nitrite reductase, cytochrome cd(1), from *Pseudomonas stutzeri* and *Thiosphaera pantotropha*. *Biochemistry*. **36**, 16267-16276
- 19 Gadsby, P. M. A., Peterson, J., Foote, N., Greenwood, C. and Thomson, A. J. (1987) Identification of the Ligand-Exchange Process in the Alkaline Transition of Horse heart Cytochrome C. *Biochemical Journal*. **246**, 43-54
- 20 Yonetani, T. and Anni, H. (1987) Yeast Cytochrome-C Peroxidase - Coordination and Spin States of Heme Prosthetic Group. *Journal of Biological Chemistry*. **262**, 9547-9554
- 21 Ross, D. E., Ruebush, S. S., Brantley, S. L., Hartshorne, R. S., Clarke, T. A., Richardson, D. J. and Tien, M. (2007) Characterization of protein-protein interactions involved in iron reduction by *Shewanella oneidensis* MR-1. *Applied and Environmental Microbiology*. **73**, 5797-5808
- 22 Eggleston, C. M., Voros, J., Shi, L., Lower, B. H., Droubay, T. C. and Colberg, P. J. S. (2008) Binding and direct electrochemistry of OmcA, an outer-membrane cytochrome from an iron reducing bacterium, with oxide electrodes: A candidate biofuel cell system. *Inorganica Chimica Acta*. **361**, 769-777
- 23 Shi, L., Lin, J. T., Markillie, L. M., Squier, T. C. and Hooker, B. S. (2005) Overexpression of multi-heme C-type cytochromes. *Biotechniques*. **38**, 297-299
- 24 Edwards, M. J., Baiden, N. A., Johs, A., Tomanicek, S. J., Liang, L., Shi, L., Fredrickson, J. K., Zachara, J. M., Gates, A. J., Butt, J. N., Richardson, D. J. and Clarke, T. A. (2014) The X-ray crystal structure of *Shewanella oneidensis* OmcA reveals new insight at the microbe-mineral interface. *Febs Letters*. **588**, 1886-1890
- 25 Edwards, M. J., Hall, A., Shi, L., Fredrickson, J. K., Zachara, J. M., Butt, J. N., Richardson, D. J. and Clarke, T. A. (2012) The Crystal Structure of the Extracellular 11-heme Cytochrome UndA Reveals a Conserved 10-heme Motif and Defined Binding Site for Soluble Iron Chelates. *Structure*. **20**, 1275-1284
- 26 Moore, G. R. and Pettigrew, G. W. (1990) Springer Series in Molecular Biology Cytochromes C: Evolutionary, Structural and Physicochemical Aspects. Moore, G. R. and G. W. Pettigrew. Springer Series in Molecular Biology: Cytochromes C: Evolutionary, Structural and Physicochemical Aspects. Xvi+478p. Springer-Verlag: Berlin, Germany; New York, New York, USA. Illus
- 27 Gadsby, P. M. A. and Thomson, A. J. (1990) Assignment of the Axial Ligands of Ferric Ion in Low-Spin Hemoproteins by Near-Infrared Magnetic Circular-Dichroism and Electron-Paramagnetic Resonance Spectroscopy. *Journal of the American Chemical Society*. **112**, 5003-5011
- 28 Cheesman, M. R., Greenwood, C. and Thomson, A. J. (1991) Magnetic circular-dichroism of hemoproteins. *Advances in Inorganic Chemistry*. **36**, 201-255
- 29 Clarke, T. A., Edwards, M. J., Gates, A. J., Hall, A., White, G. F., Bradley, J., Reardon, C. L., Shi, L., Beliaev, A. S., Marshall, M. J., Wang, Z., Watmough, N. J., Fredrickson, J. K., Zachara, J. M., Butt, J. N. and Richardson, D. J. (2011) Structure of a bacterial cell surface decaheme electron conduit. *Proceedings of the National Academy of Sciences of the United States of America*. **108**, 9384-9389
- 30 Venkateswaran, K., Moser, D. P., Dollhopf, M. E., Lies, D. P., Saffarini, D. A., MacGregor, B. J., Ringelberg, D. B., White, D. C., Nishijima, M., Sano, H., Burghardt, J., Stackebrandt, E. and Nealson, K. H. (1999) Polyphasic taxonomy of the genus *Shewanella* and description of *Shewanella oneidensis* sp. nov. *International Journal of Systematic Bacteriology*. **49**, 705-724

Chapter 3: **Crystallographic Structural Studies of OmcA**

3.1 – Introduction

Protein function is enabled/mediated through its structure, and structural data on the OMMCs is recently becoming available. The crystal structures of the OMMCs MtrF [1] and UndA [2] show conservation of haem packing arrangements and domain folds despite sharing < 24% primary structure identity (Fig. 3.1). Both OMMCs have their polypeptide arranged into 4 domains with the split β -barrel of domains I and III, and two pentahaem domains II and IV (whereas UndA's domain IV is a hexahaem module). However these OMMCs have the least experimental data published of the four major OMMC clades (i.e. MtrF, UndA, OmcA and MtrC [3]).

Analytical Ultracentrifugation and PFV data indicated that MtrC is a component of the MtrCAB complex, and its haem reduction potentials are modulated upon complexation [4, 5]. However, there is limited structural data on how MtrC interfaces the MtrAB module. MtrB has been implicated in the localisation of OmcA (and MtrC) to the outer-membrane [6]. An OmcA:MtrC complex has been isolated with reported higher Fe^{3+} -NTA reduction activity per mg protein than either OmcA or MtrC [7]. The dissociation constant of OmcA:MtrC (and thus the complex) was shown to be salt-sensitive, with k_D doubling from 0 – 150 mM KCl (i.e. 0.5 – 1.0 μM). Utilising cross-linking molecules that identify interactions $\leq 11 \text{ \AA}$, OmcA and MtrC were shown to co-localise within electron tunnelling distance, and as such OmcA is modelled to receive electrons from the periplasm via MtrCAB [8]. In a similar manner, evidence of the OmcA:MtrC interaction still provides limited structural data on the OMMC:OMMC interface [4, 7, 8].

As suggested earlier, OmcA is one of the more heavily studied OMMCs. There is significant data available on OmcA's mineral-binding capacity [9-11]. OmcA localisation to the extracellular surface of the outer membrane [12-14] has been resolved to co-localisation between tight and loosely-associated exopolymeric substance at the outer-membrane [15]. Biophysical data previously published indicates contrasting spin-states of OmcA's haem content [16, 17], which has been addressed in Section 2.2. Gene knockout studies indicate OmcA accounts for $\approx 50\%$ Mn(IV) oxide reduction [18] and $\approx 20\text{-}50\%$ ferric oxide mineral reduction activity of *S. oneidensis* MR-1 [19-21]. Neutron reflectometry data of oxidised and reduced OmcA

in solution provide mechanistic insights into the DMR process [22]. However the atomic resolution given by a crystal structure may facilitate better understanding of the chemistry behind the reaction mechanisms being studied.

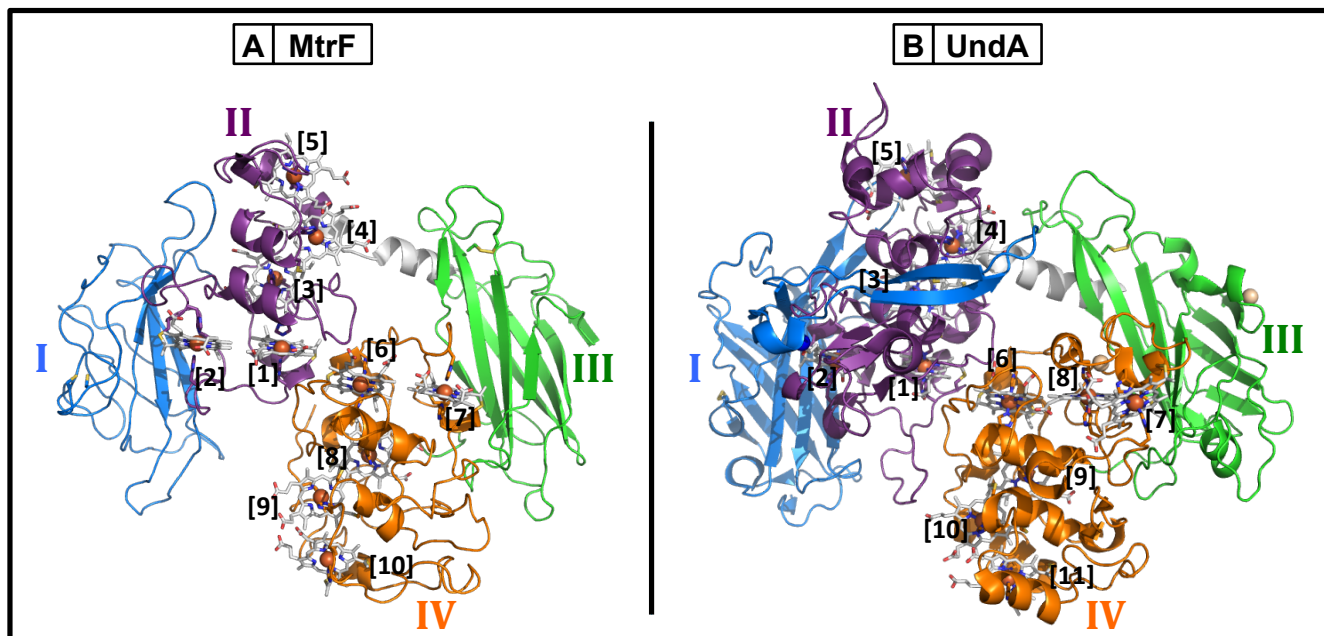


Figure 3.1. – **Previously published OMMC crystal structures.** Domain folds (domain I = blue, II = purple, III = green, IV = orange, linker polypeptide = grey), domain organisation and haem arrangement are maintained between the structures of (A) MtrF and (B) UndA. Blue spheres = calcium atoms/ions, orange spheres = iron atoms/ions, grey spheres = magnesium atoms/ions.

3.2 – Results & Discussion

The amino acid sequence of OmcA (Fig. 3.2) shares features described above for MtrF and UndA (Fig. 3.1, [2, 23]), with two pentahaem binding modules and ample histidine residues that can serve as distal haem ligands. The alignment presented in Fig. 3.2 is annotated with the details of the crystal structure discussed later.

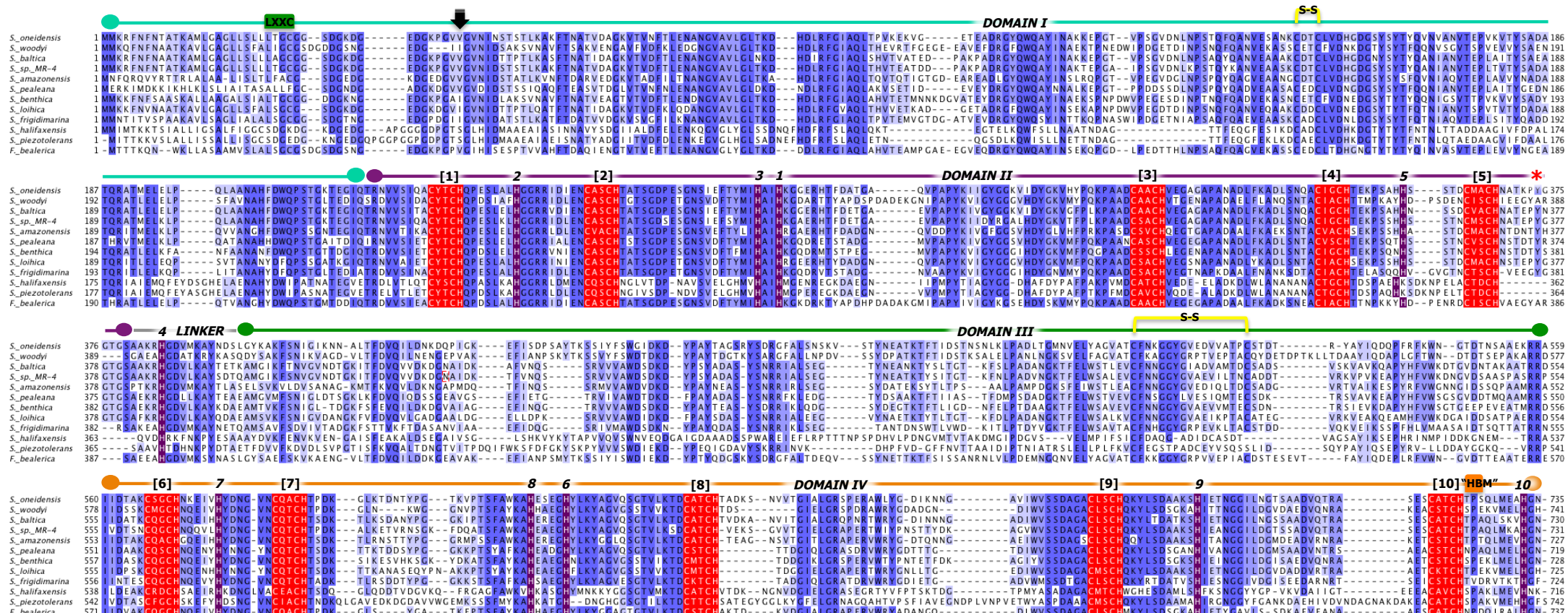


Figure 3.2. – Primary Structure Conservation in OmcA across selected bacterial strains. The primary structure of OmcA from 11 *Shewanella* strains (*Shewanella oneidensis* MR-1, *S. woodyi* ATCC 51908, *S. baltica* OS185, *Shewanella* sp. MR-4, *S. amazonensis* SB2B, *S. pealeana* ATCC 700345, *S. benthica* KT99, *S. loihica* PV-4, *S. frigidimarina* NCIMB 400, *S. halifaxensis* HAW-EB4 and *S. piezotolerans* WP3) and *Ferrimonas balearica* DSM 9799 were aligned using the CLUSTALW service and output made using Jalview. CXXC motifs are in red and numbered in square brackets; green LXXC box = lipid binding motif; yellow S-S bridge = disulphide bridge; * = conserved Y³⁷⁴; orange “HBM” box = conserved histidine-binding motif; distal histidines are in purple and numbered with italics; amino acid conservation are in shades of blue where >80% is the darkest shade. Black arrow denotes first ordered-diffracting residue (i.e. Val⁴³).

3.2.1 – X-Ray Crystal Structure of eOmcA

Based on the purity and yield of protein obtained, eOmcA (which has been spectroscopically validated as significantly representative of OmcA_(wt); Chapter 2) was used in the X-ray crystallography experiments. A stock solution of 10 mg mL⁻¹ eOmcA in 20 mM HEPES, pH 7.60, 0.1 M NaCl was added to a range of trial crystallisation buffer conditions at 16°C and 4°C. Ultimately, 0.5 µL:0.5 µL incubation of stock eOmcA in 0.1 M Bis-TRIS Propane, pH 8.50, 0.1 M MgCl₂ and 20 % (w/v) PEG 20K at 16°C yielded amorphous-shaped crystals, from which native and single-wavelength anomalous diffraction (i.e. SAD) data was collected to 2.7 Å and 3.5 Å resolution respectively. The phase problem was solved processing the SAD dataset, and the crystal structure of eOmcA was solved with 2.7 Å resolution (Fig. 3.3). Crystallography was done in collaboration with Dr Marcus J. Edwards [24].

The crystal structure reveals eOmcA forms crystals with a *P2*₁ space group and unit lattice dimensions of *a* = 92.64, *b* = 245.38, *c* = 135.63 Å and corresponding angles α = 90.00, β = 97.89, γ = 90.00° (full statistics listed in Table 3.1). There are 4 copies of OmcA per asymmetric unit, where several combinations of quaternary structure can be inferred [24]. The soluble form of OmcA crystallised (i.e. eOmcA) has its amino-terminal residues, including the lipid anchor peptide LXXC, substituted with the amino-terminal two amino acids of MtrB [10]. An unknown number of residues of eOmcA's N-terminus are putatively cleaved by signal peptidase and Type II Secretion systems. The electron density data shows ordered diffraction from the 43rd residue onwards (Fig. 3.2).

The crystal structure of OmcA shows that its polypeptide backbone is arranged into the same four domains as observed for UndA and MtrF. Domain I is a split β -barrel region containing a CXXC disulphide bond (Figs. 3.3B & 3.4A) and a loop region that extends across a section of domain II's surface. Domain III is another split β -barrel that also contains a disulphide bond (i.e. CX₁₆C; Figs. 3.3C & 3.4B). Domain II is the amino-terminal pentahaem module, which contains 5 CXXCH *c*-type haem binding motifs, 4 of the 5 distal histidine haem ligands and the 5 thioether-bound *c*-type haems (Fig. 3.3A). A linker α -helix that bridges domains II and III contains haem 4's distal histidine ligand (Fig. 3.3D). Domain II also contains a conserved Y³⁷⁴ residue of interest in solution-state studies discussed later. The distal haem ligand to haem 4 is provided by the linker helix between domains II and III (Fig. 3.3D). Domain IV is the

carboxyl-terminal pentahaem module (Fig. 3.3A). As in domain II there are 5 CXXCH motifs and 5 thioether-bound c-type haems, but all 5 distal histidines for domains IV's haems are in domain IV. The surplus histidine residues in OmcA provide *bis*-histidine ligation of all 10 of OmcA's haems in the crystal structure, and various spectroscopic data confirm this haem ligation is maintained in solution (i.e. via UV-Visible, NIR-MCD and EPR data presented in Chapter 2).

Table 3.1 – **The Statistical details of the eOmcA crystal structure.** Brackets denote highest resolution shell.

	SAD	Native
<u>Data collection</u>	<u>Space group</u>	<u>P2₁</u>
	<u>Cell dimensions</u>	
	- a, b, c (Å)	92.70, 245.64, 135.51
	- α, β, γ (°)	92.64, 245.38, 135.63
	Resolution (Å)	90.00, 97.79, 90.00
	R _{sym} or R _{merge} (%)	91.8 – 3.5 (3.6 – 3.5)
	I/σ(I)	58.1 – 2.7 (2.8 – 2.7)
	Completeness (%)	13.1 (30.3)
	Redundancy	20.5 (9.9)
		99.9 (99.9)
		14.1 (13.1)
		3.0 (2.9)
<u>Refinement</u>		
	Resolution (Å)	2.70
	No. of Reflections	161,229
	R _{work} /R _{free}	0.19/0.23
	<u>No. of atoms</u>	
	- Protein	20,903
	- Ligand/ion	1,728
	- Water	1,748
	<u>Average B-factors</u>	
	- Protein	38.4
	- Ligand/ion	33.1
	- Water	35.0
	<u>R.m.s. deviations</u>	
	- Bond lengths (Å)	0.013
	- Bond angles (°)	0.889

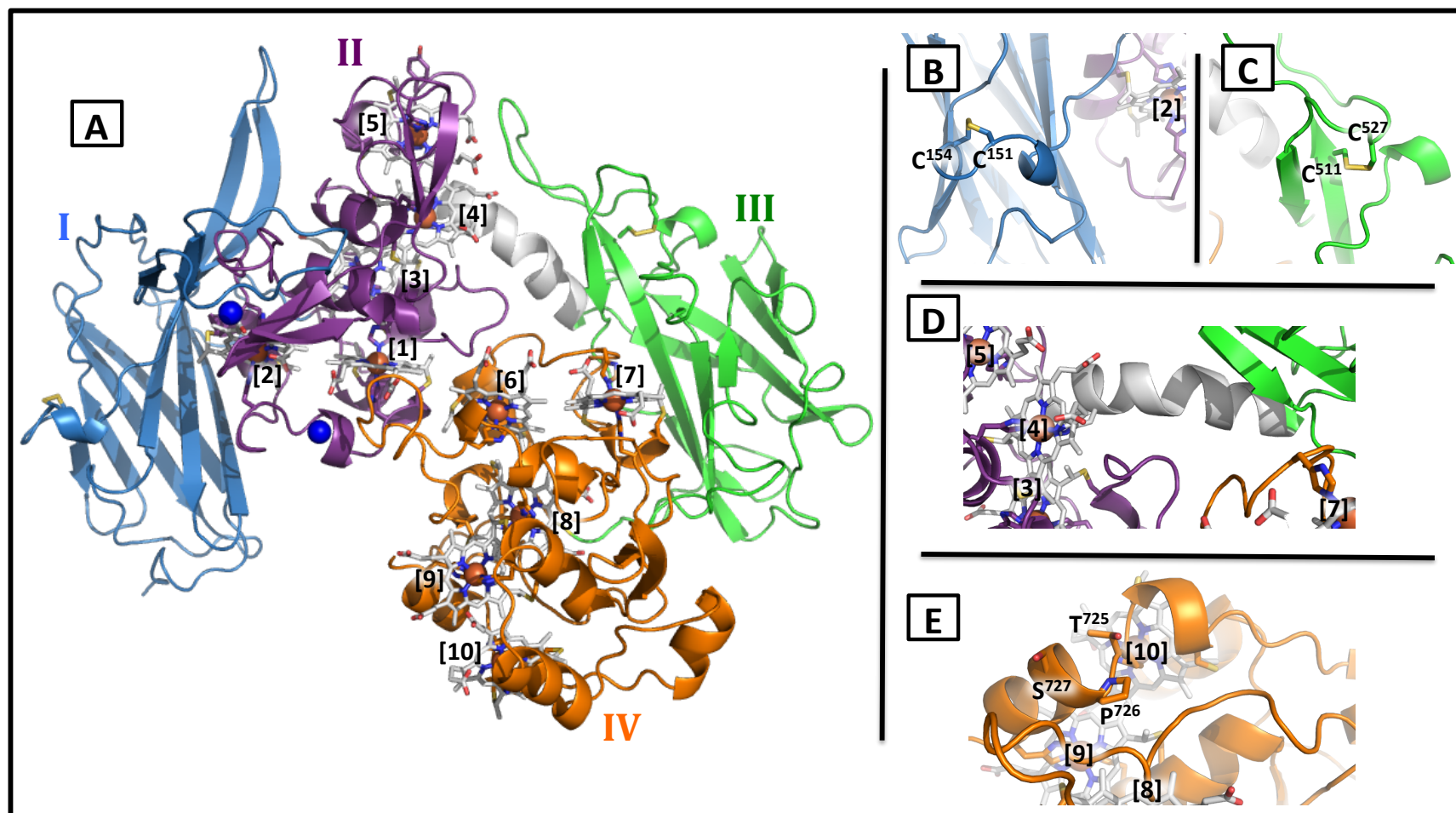


Figure 3.3 – **The Crystal Structure of eOmcA.** Chain A of the 2.70 Å resolution crystal structure of eOmcA shows that (A) OmcA has four domains as in MtrF and UndA (i.e. domain I = blue, II = purple, III = green, IV = orange, linker polypeptide = grey). There is a disulphide bridge present in (B) domain I and (C) domain III. Domains II and III are bridged by a linker α -helix (D) which contains haem 4's distal histidine ligand. (E) The proposed hematite-binding motif adjacent to haem 10. Solvent content = 72%. PDB code 4LMH [24].

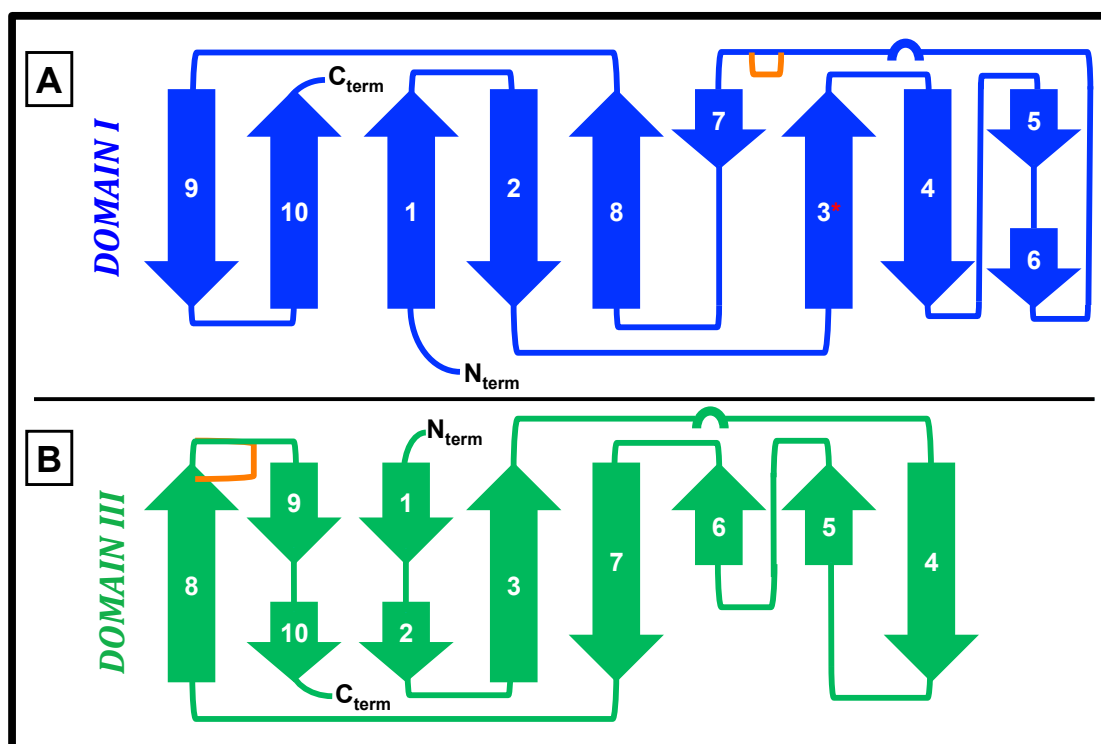


Figure 3.4 – **Cartoon representation of OmcA's split β -barrel domains.** The β -sheets of Domains I (A) and III (B) are represented here with arrows and are numbered in the amino-acyl direction. Disulphide bridges are shown as orange lines and short helices as a semi-circle. The extended β -sheet is marked with a red asterisk. The amino and acyl termini are labelled N_{term} and C_{term} respectively.

The relative orientation of domains II and IV arrange the haems of OmcA in the same staggered cross as observed for MtrF and UndA. This arrangement positions each of OmcA's haems within 7 Å of its closest haem neighbour; sufficiently close to facilitate electron tunnelling. There is an octahaem wire that spans the entire protein (i.e. 65 Å; Fig. 3.5A), and the two additional haems are at opposite sides of the central octahaem, forming a transecting tetrahaem connecting the split β -barrels of domains I and III (i.e. haems 2, 1, 6 and 7; Fig. 3.5B). The “accessory” haems (i.e. haems 2 and 7) are within electron tunnelling distance of flavin/chelated mineral species that could putatively localise to specific regions of domains I and III respectively.

On the carboxyl side of haem 10's distal histidine ligand is a 3 amino acid peptide, $T^{725}P^{726}S^{727}$, that has been inferred to enable OmcA to hydrogen bond to oxide-presenting regions of hematite (i.e. $\alpha\text{-Fe}_2\text{O}_3$) surfaces [25]. Of importance is that this “hematite binding-motif” is surface-exposed (Fig. 3.3E), and hydrogen bonding to this proposed motif would position hematite/mineral within electron tunnelling distance of haem 10 (i.e. 13 – 14 Å via T^{725}). However hydrogen-bonding to the non-conserved S^{727} would place mineral just beyond electron tunnelling distance (i.e. ≈ 17

Å) of haem 10. The capacity of OmcA to hydrogen bond with hematite as part of its mineral reduction mechanism is explored in Chapter 6.

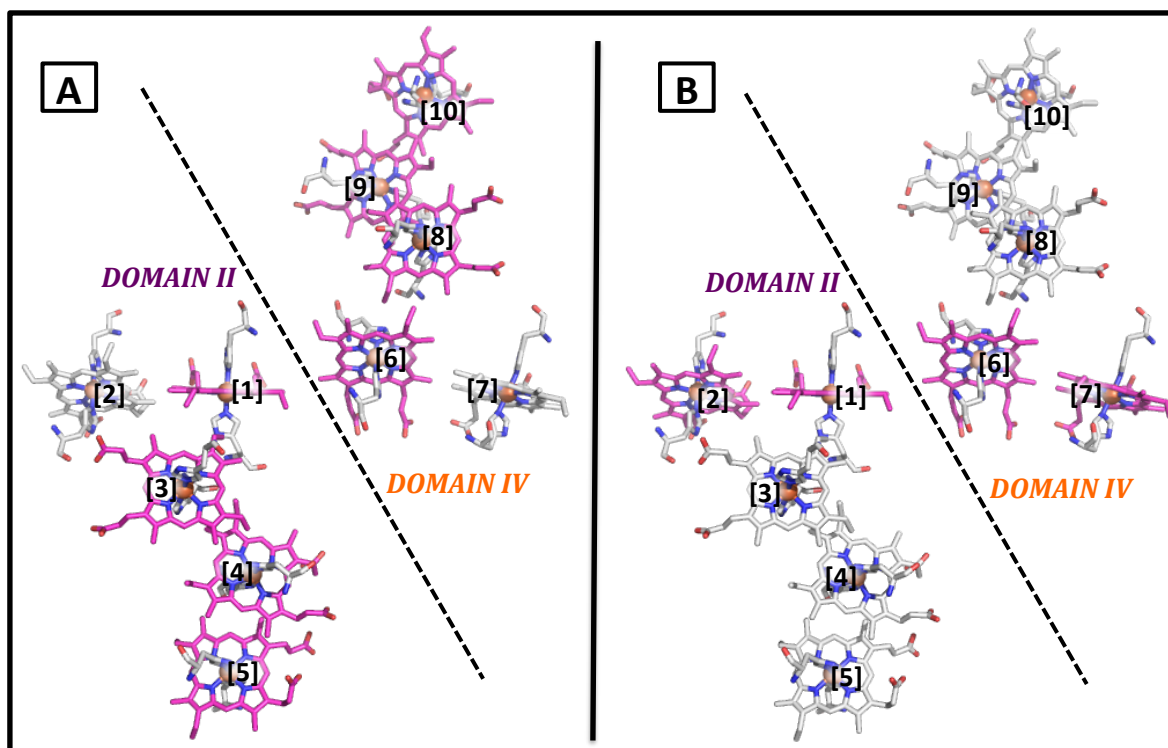


Figure 3.5 – **The arrangements of haems in eOmcA.** The (A) central octahaem (i.e. haems 5, 4, 3, 1, 6, 8, 9 and 10) and (B) transecting tetrahaem (i.e. haems 2, 1, 6 and 7) arrangements of haems in eOmcA are highlighted in pink.

The asymmetric unit of the OmcA crystals has four copies of OmcA, and their arrangement/relative orientation suggests two dimers present per asymmetric unit (Fig. 3.6). The favoured of the two possible dimer-sets is chains A:B and chains C:D. The putative OmcA dimer has non-crystallographic C_2 symmetry, with a screw rotation axis lying along the putative domain II_{Chain A}:II_{Chain B} and domain III_{Chain A}:III_{Chain B} dimer interface (Fig. 3.6). This dimer-set maintains a 9 Å distance between each monomer's haem 5 co-factor. However the low interfacial surface area between eOmcA monomers (i.e. average dimer interface area = 481 Å²) is indicative that such interactions could be a by-product of eOmcA molecules packing into the asymmetric unit, as opposed to maintenance of a physiological interaction.

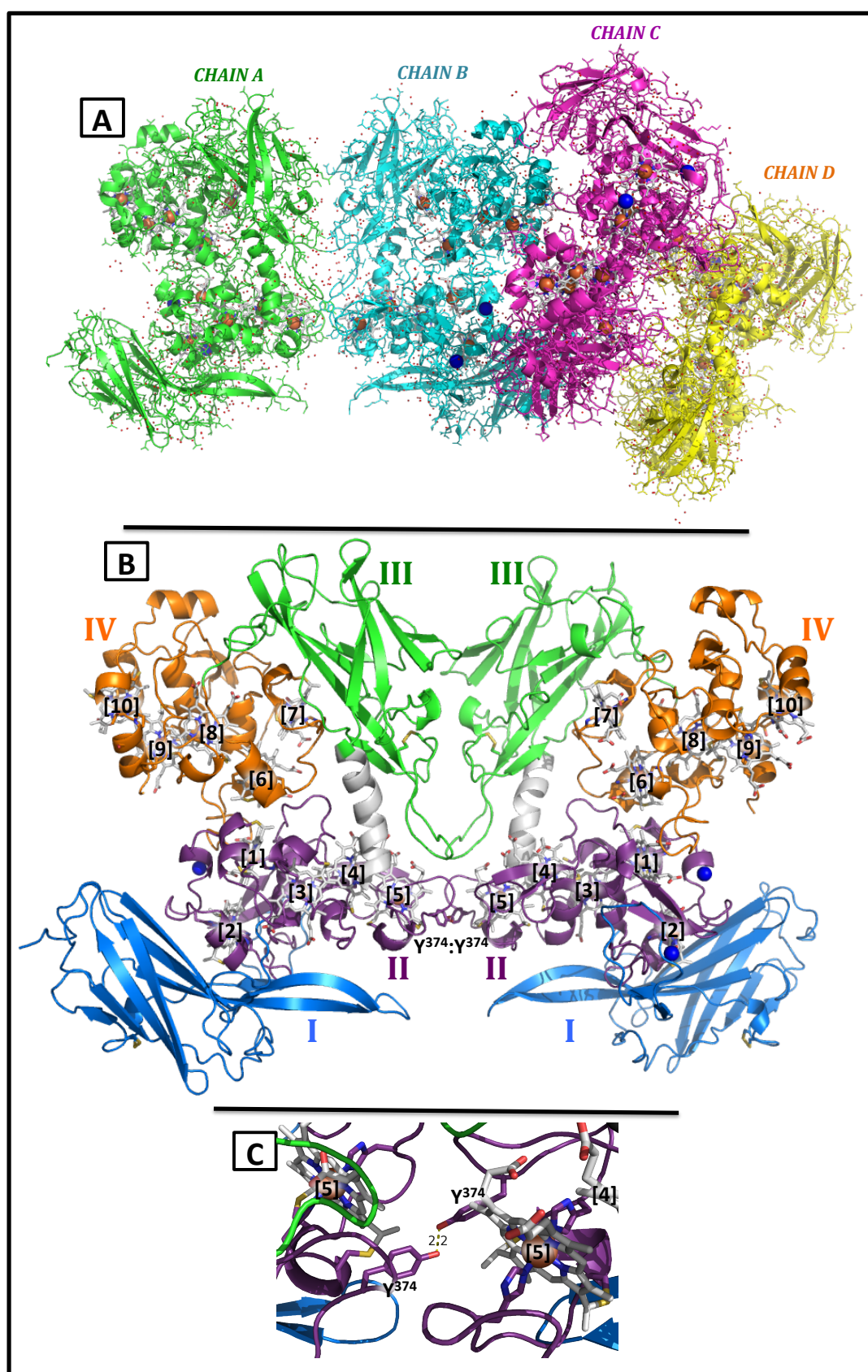


Figure 3.6 – **The Asymmetric Unit of eOmca Crystals.** (A) There are 4 copies of the eOmca molecule per asymmetric unit denoted chains A, B, C and D. (B) Favoured eOmca dimer with 9 Å distance between the two haem 5 groups. Dimer interface area median = 481 Å². (C) Unique putative tyrosine³⁷⁴:tyrosinate³⁷⁴ hydrogen-bond modelled to stabilise the dimer interface (bond length = 2.2 Å).

A unique part of the proposed dimer interface is the proximity of the Y³⁷⁴ residues of each eOmcA molecule. The hydroxyl groups of the Y³⁷⁴ residues face each other 2.2 Å apart, which would qualify as a short hydrogen bond. The hydroxyl residues do not align exactly, which is unfavourable for hydrogen bonding. Furthermore, for the residues to undergo hydrogen bonding with each other it is implicit that one of the two be deprotonated to a tyrosinate to be a hydrogen bond acceptor. At the resolution of the structure the protonation state of either Tyr³⁷⁴ residue cannot be determined.

3.2.2 – The Effect of Y³⁷⁴F Mutation on the Putative Dimer-Interface

Disruption of the putative dimer interface was attempted using site-directed mutagenesis of Tyr³⁷⁴, the residue within 2.2 Å from its homodimeric equivalent residue (Fig. 3.6C). The phase problem was solved using molecular replacement with the eOmcA coordinates (PDB code 4LMH, [24]). Removal of the Tyr³⁷⁴ hydroxyl group by generation of eY³⁷⁴F did not inhibit the formation of the previously observed “homodimeric” interface (Fig. 3.7). The proposed dimer interface is maintained in the eY³⁷⁴F crystal structure despite crystal formation in a different space group (i.e. *P*2₁2₁2, Fig. 3.7). The different space group of the mutant crystal may be the result of the 1.50 difference in pH between eOmcA and eY³⁷⁴F crystallisation conditions.

3.3 – Conclusions

OmcA shares significantly similar domain organisation and haem arrangement to MtrF [1] and UndA [2]. This includes the two pentahaem modules (domain II and IV) that form a staggered haem cross and the split β-barrels domains I and III. The 65 Å central octahaem chain resolved in the crystal structure of eOmcA is befitting of a cytochrome tasked with accepting electrons from MtrC [4, 7, 8] to extracellular electron acceptors [4, 9, 21, 26]. Split β-barrel conformation is common amongst flavin binding domains [27], and flavins putatively bound at domains I or III may come within critical electron tunnelling distance (i.e. 14 Å [28]) of haems 2 or 7 respectively. Semi-flavoquinone has been implied as a co-factor for the OMMCs MtrC and OmcA [29], and domains I and III serve as ideal candidates for such an interaction. This would also provide functional relevance to the arrangement of haems 2 and 7 at alternate sides of the central octahaem chain; i.e. to transfer electrons to

flavin/semiflavoquinone localised to domains I and III respectively. However, there is no experimental data here on the putative OmcA:flavin interaction.

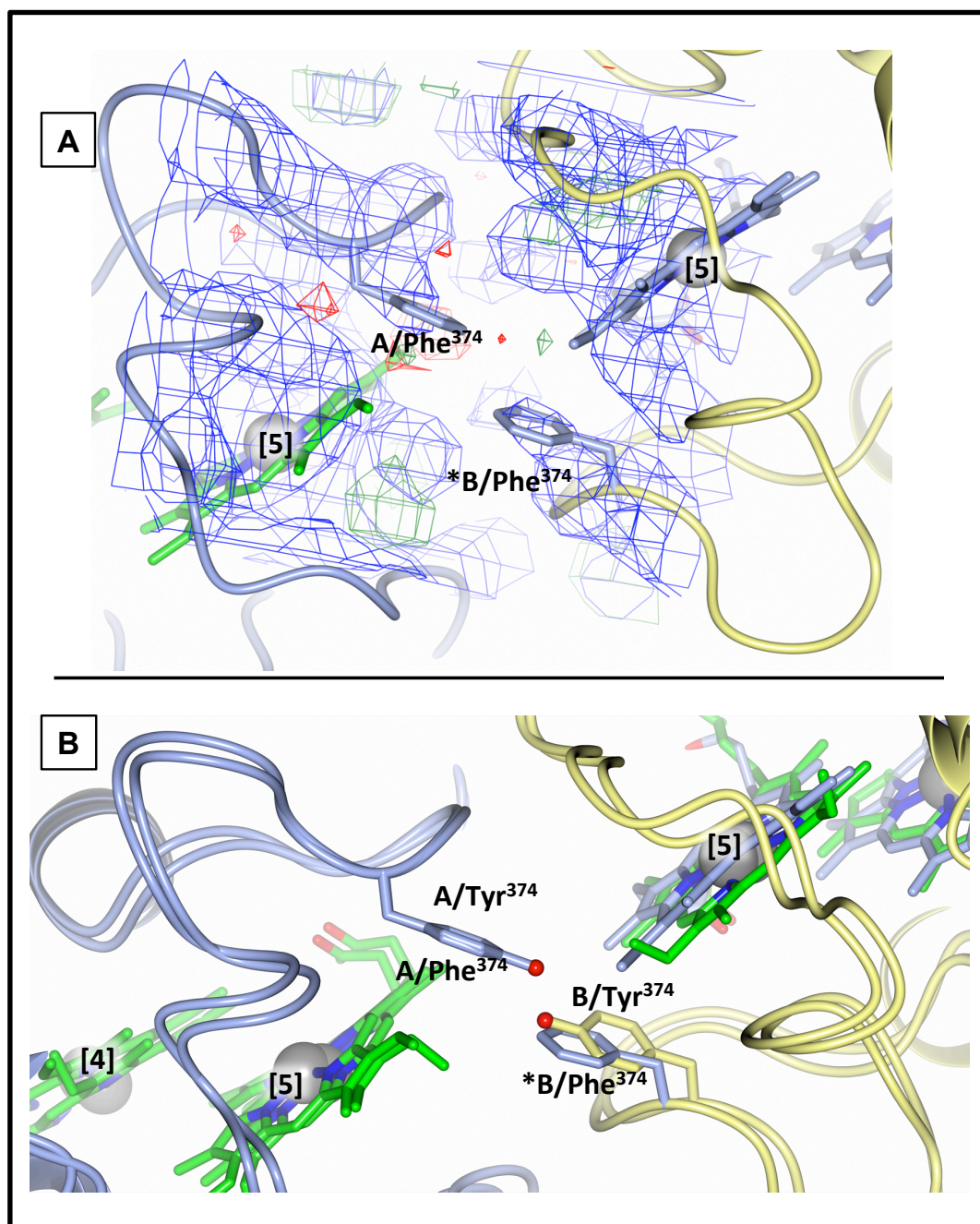


Fig. 3.7 – X-Ray Crystallography of eOmcA eY³⁷⁴F. (A) The proposed dimer interface in the eY³⁷⁴F crystal structure. The experimentally determined $2F_o - F_c$ electron density map (contoured to 1.2σ ; blue), as well as the positive (green) and negative (red) $F_o - F_c$ electron density maps (contoured to 3.0σ) are shown as wire meshes. Chains A (blue) and B (yellow) maintain the molecular interface observed in the eOmcA crystal structure. (B) The super-position of eY³⁷⁴F and eOmcA respective 374th residues in Chain A. Both Phe³⁷⁴ side chains pictured maintain similar proximity and orientation to the Tyr³⁷⁴ side chains of eOmcA's putative dimer pair. Only side-chains of interest are shown (i.e. 374th residue). The eY³⁷⁴F crystal structure was solved to 3.57 Å resolution. * = Molecule from an adjacent asymmetric unit.

Table 3.2 – **The statistical details of the eY³⁷⁴F crystal structure.** Brackets denote highest resolution (i.e. outer) shell.

	Native	
<u>Data collection</u>	Space group	<i>P</i> 2 ₁ 2 ₁ 2
	Cell dimensions	
	- a, b, c (Å)	151.6, 246.4, 84.22
	- α, β, γ (°)	90.00, 90.00, 90.00
	Resolution (Å)	84.2 – 3.7 (16.0 – 3.6)
	<i>R</i> _{sym} or <i>R</i> _{merge} (%)	1.6 (48.8)
	<i>I</i> /σ(<i>I</i>)	42.0 (2.4)
	Completeness (%)	98.0 (100.0)
	Redundancy	5.2 (6.3)
<u>Refinement</u>	Resolution (Å)	3.57
	No. of Reflections	225,979
	<i>R</i> _{work} / <i>R</i> _{free}	0.20/0.26
	No. of atoms	
	- Protein	10,442
	- Ligand/ion	860
	- Water	86
	Average <i>B</i> -factors	
	- Protein	113.72
	- Ligand/ion	96.17
	- Water	129.49
	R.m.s. deviations	
	- Bond lengths (Å)	0.011
	- Bond angles (°)	2.635

In the context of determining OmcA's haem ligation [16, 17], the *bis*-histidine ligation of all 10 haems in eOmcA's crystal structure is supported by the EPR data of OmcA_(wt), pOmcA and eOmcA (see Section 2.2). The *bis*-histidine ligation of OmcA's haem content is further corroborated by the MCD spectra of pOmcA that accounts for 10 ± 1 *bis*-histidine ligated haems (see Section 2.2.4).

The intermolecular contacts between the multiple copies of eOmcA per asymmetric unit suggest that the biological unit of eOmcA crystallised is a homodimer with C2 symmetry. The p*K*_a for deprotonation of tyrosine's hydroxyl is ≈ 10, so at pH 8.50 any putative tyrosinate³⁷⁴ generated would have to be maintained by autocatalytic means. In this instance the surrounding polypeptide deprotonates the Tyr³⁷⁴ hydroxyl, putatively a component part of the dimerization process. To further investigate whether eOmcA is a dimer under physiological conditions, mutation of the

interfacial residue showed that the proposed dimer interface is maintained. This indicates that the putative (wild-type) Y³⁷⁴:Y³⁷⁴ hydrogen-bond is either non-existent, or not fundamental to the dimer interface (i.e. the molecular interface is maintained by other intermolecular interactions).

Considering the physiological localisation of OmcA to the LPS/EPS environment of *Shewanella spp* outer membranes, two of its haems are available for electron exchange (i.e. haems 5 and 10). This was also observed for MtrF [1] and UndA [2]. Amongst OMMCs that putatively bind mineral during DMR [9, 11], it is feasible that structural conservation is observed at the mineral interaction/electron egress site. In the same manner, structural divergence may be expected at the electron ingress site, where MtrF is modelled as an interacting component of the MtrDEF complex, and OmcA and UndA are modelled to accept electrons from the MtrCAB (and possibly MtrDEF) complex(es). There is minimal evidence of such a bias using sequence alignment analysis, but amongst the OMMC crystal structures haem 5 is the most variant in terms of localisation. The propionates of UndA's haem 5 have been rotated $\approx 180^\circ$ in comparison to haem 5 of MtrF [2]. The crystal structure shows that the haem 5 propionates of OmcA have a comparable orientation to haem 5 of MtrF [24], however haem 5 is central to the favoured OmcA dimer model intermolecular interface (Fig. 3.6). As such the previously observed difference in haem 5 orientation between MtrF and UndA supports the model that haem 5 is a common electron ingress site amongst the OMMCs, and serves as the ingress site(s) to an OmcA₂ molecule. Studies indicating that OmcA exists in an oligomeric state attributed the oligomer enhanced electron transfer rates to chelated ferric iron [7], which would be facilitated by haem 5 providing sites of electron exchange between OmcA homodimer components.

However, the structural study of OmcA presented so far reports crystallographic intermolecular interactions, none of which have been confirmed to give OmcA quaternary structure in solution. As such, the apparent molecular weight (MW_{app}) of eOmcA in solution was analysed, and is reported in the following chapter.

References.

- 1 Clarke, T. A., Edwards, M. J., Gates, A. J., Hall, A., White, G. F., Bradley, J., Reardon, C. L., Shi, L., Beliaev, A. S., Marshall, M. J., Wang, Z., Watmough, N. J., Fredrickson, J. K., Zachara, J. M., Butt, J. N. and Richardson, D. J. (2011) Structure of a bacterial cell surface decaheme electron conduit. *Proceedings of the National Academy of Sciences of the United States of America*. **108**, 9384-9389
- 2 Edwards, M. J., Hall, A., Shi, L., Fredrickson, J. K., Zachara, J. M., Butt, J. N., Richardson, D. J. and Clarke, T. A. (2012) The Crystal Structure of the Extracellular 11-heme Cytochrome UndA Reveals a Conserved 10-heme Motif and Defined Binding Site for Soluble Iron Chelates. *Structure*. **20**, 1275-1284
- 3 Edwards, M. J., Fredrickson, J. K., Zachara, J. M., Richardson, D. J. and Clarke, T. A. (2012) Analysis of structural MtrC models based on homology with the crystal structure of MtrF. *Biochemical Society Transactions*. **40**, 1181-1185
- 4 Ross, D. E., Ruebush, S. S., Brantley, S. L., Hartshorne, R. S., Clarke, T. A., Richardson, D. J. and Tien, M. (2007) Characterization of protein-protein interactions involved in iron reduction by *Shewanella oneidensis* MR-1. *Applied and Environmental Microbiology*. **73**, 5797-5808
- 5 Hartshorne, R. S., Reardon, C. L., Ross, D., Nuester, J., Clarke, T. A., Gates, A. J., Mills, P. C., Fredrickson, J. K., Zachara, J. M., Shi, L., Beliaev, A. S., Marshall, M. J., Tien, M., Brantley, S., Butt, J. N. and Richardson, D. J. (2009) Characterization of an electron conduit between bacteria and the extracellular environment. *Proceedings of the National Academy of Sciences of the United States of America*. **106**, 22169-22174
- 6 Myers, C. R. and Myers, J. M. (2002) MtrB is required for proper incorporation of the cytochromes OmcA and OmcB into the outer membrane of *Shewanella putrefaciens* MR-1. *Applied and Environmental Microbiology*. **68**, 5585-5594
- 7 Shi, L., Chen, B. W., Wang, Z. M., Elias, D. A., Mayer, M. U., Gorby, Y. A., Ni, S., Lower, B. H., Kennedy, D. W., Wunschel, D. S., Mottaz, H. M., Marshall, M. J., Hill, E. A., Beliaev, A. S., Zachara, J. M., Fredrickson, J. K. and Squier, T. C. (2006) Isolation of a high-affinity functional protein complex between OmcA and MtrC: Two outer membrane decaheme c-type cytochromes of *Shewanella oneidensis* MR-1. *Journal of Bacteriology*. **188**, 4705-4714
- 8 Zhang, H., Tang, X., Munske, G. R., Zakharova, N., Yang, L., Zheng, C., Wolff, M. A., Tolic, N., Anderson, G. A., Shi, L., Marshall, M. J., Fredrickson, J. K. and Bruce, J. E. (2008) In vivo identification of the outer membrane protein omcA-mtrC interaction network in *Shewanella oneidensis* MR-1 cells using novel hydrophobic chemical cross-linkers. *Journal of Proteome Research*. **7**, 1712-1720
- 9 Xiong, Y. J., Shi, L., Chen, B. W., Mayer, M. U., Lower, B. H., Londer, Y., Bose, S., Hochella, M. F., Fredrickson, J. K. and Squier, T. C. (2006) High-affinity binding and direct electron transfer to solid metals by the *Shewanella oneidensis* MR-1 outer membrane c-type cytochrome OmcA. *Journal of the American Chemical Society*. **128**, 13978-13979
- 10 Eggleston, C. M., Voros, J., Shi, L., Lower, B. H., Droubay, T. C. and Colberg, P. J. S. (2008) Binding and direct electrochemistry of OmcA, an outer-membrane cytochrome from an iron reducing bacterium, with oxide electrodes: A candidate biofuel cell system. *Inorganica Chimica Acta*. **361**, 769-777
- 11 Lower, B. H., Shi, L., Yongsunthon, R., Droubay, T. C., McCready, D. E. and Lower, S. K. (2007) Specific bonds between an iron oxide surface and outer

membrane cytochromes MtrC and OmcA from *Shewanella oneidensis* MR-1. *Journal of Bacteriology*. **189**, 4944-4952

12 Shi, L., Deng, S., Marshall, M. J., Wang, Z. M., Kennedy, D. W., Dohnalkova, A. C., Mottaz, H. M., Hill, E. A., Gorby, Y. A., Beliaev, A. S., Richardson, D. J., Zachara, J. M. and Fredrickson, J. K. (2008) Direct involvement of type II secretion system in extracellular translocation of *Shewanella oneidensis* outer membrane cytochromes MtrC and OmcA. *Journal of Bacteriology*. **190**, 5512-5516

13 Myers, C. R. and Myers, J. M. (2003) Cell surface exposure of the outer membrane cytochromes of *Shewanella oneidensis* MR-1. *Letters in Applied Microbiology*. **37**, 254-258

14 Donald, J. W., Hicks, M. G., Richardson, D. J. and Palmer, T. (2008) The c-type cytochrome OmcA localizes to the outer membrane upon heterologous expression in *Escherichia coli*. *Journal of Bacteriology*. **190**, 5127-5131

15 Cao, B., Shi, L. A., Brown, R. N., Xiong, Y. J., Fredrickson, J. K., Romine, M. F., Marshall, M. J., Lipton, M. S. and Beyenal, H. (2011) Extracellular polymeric substances from *Shewanella* sp HRCR-1 biofilms: characterization by infrared spectroscopy and proteomics. *Environmental Microbiology*. **13**, 1018-1031

16 Field, S. J., Dobbin, P. S., Cheesman, M. R., Watmough, N. J., Thomson, A. J. and Richardson, D. J. (2000) Purification and magneto-optical spectroscopic characterization of cytoplasmic membrane and outer membrane multiheme c-type cytochromes from *Shewanella frigidimarina* NCIMB400. *Journal of Biological Chemistry*. **275**, 8515-8522

17 Bodemer, G. J., Antholine, W. A., Basova, L. V., Saffarini, D. and Pacheco, A. A. (2010) The effect of detergents and lipids on the properties of the outer-membrane protein OmcA from *Shewanella oneidensis*. *Journal of Biological Inorganic Chemistry*. **15**, 749-758

18 Myers, J. M. and Myers, C. R. (2001) Role for outer membrane cytochromes OmcA and OmcB of *Shewanella putrefaciens* MR-1 in reduction of manganese dioxide. *Applied and Environmental Microbiology*. **67**, 260-269

19 Coursolle, D. and Gralnick, J. A. (2010) Modularity of the Mtr respiratory pathway of *Shewanella oneidensis* strain MR-1. *Molecular Microbiology*. **77**, 995-1008

20 Meitl, L. A., Eggleston, C. M., Colberg, P. J. S., Khare, N., Reardon, C. L. and Shi, L. (2009) Electrochemical interaction of *Shewanella oneidensis* MR-1 and its outer membrane cytochromes OmcA and MtrC with hematite electrodes. *Geochimica Et Cosmochimica Acta*. **73**, 5292-5307

21 Reardon, C. L., Dohnalkova, A. C., Nachimuthu, P., Kennedy, D. W., Saffarini, D. A., Arey, B. W., Shi, L., Wang, Z., Moore, D., McLean, J. S., Moyles, D., Marshall, M. J., Zachara, J. M., Fredrickson, J. K. and Beliaev, A. S. (2010) Role of outer-membrane cytochromes MtrC and OmcA in the biomineralization of ferrihydrite by *Shewanella oneidensis* MR-1. *Geobiology*. **8**, 56-68

22 Johs, A., Shi, L., Droubay, T., Ankner, J. F. and Liang, L. (2010) Characterization of the Decaheme c-Type Cytochrome OmcA in Solution and on Hematite Surfaces by Small Angle X-Ray Scattering and Neutron Reflectometry. *Biophysical Journal*. **98**, 3035-3043

23 Myers, J. M. and Myers, C. R. (1998) Isolation and sequence of omcA, a gene encoding a decaheme outer membrane cytochrome c of *Shewanella putrefaciens* MR-1, and detection of omcA homologs in other strains of *S. putrefaciens*. *Biochimica Et Biophysica Acta-Biomembranes*. **1373**, 237-251

24 Edwards, M. J., Baiden, N. A., Johs, A., Tomanicek, S. J., Liang, L., Shi, L., Fredrickson, J. K., Zachara, J. M., Gates, A. J., Butt, J. N., Richardson, D. J. and Clarke,

- T. A. (2014) The X-ray crystal structure of *Shewanella oneidensis* OmcA reveals new insight at the microbe-mineral interface. *Febs Letters*. **588**, 1886-1890
- 25 Lower, B. H., Lins, R. D., Oestreich, Z., Straatsma, T. P., Hochella, M. F., Shi, L. A. and Lower, S. K. (2008) In vitro evolution of a peptide with a hematite binding motif that may constitute a natural metal-oxide binding archetype. *Environmental Science & Technology*. **42**, 3821-3827
- 26 Baron, D., LaBelle, E., Coursolle, D., Gralnick, J. A. and Bond, D. R. (2009) Electrochemical Measurement of Electron Transfer Kinetics by *Shewanella oneidensis* MR-1. *Journal of Biological Chemistry*. **284**, 28865-28873
- 27 Hubbard, T. J. P., Ailey, B., Brenner, S. E., Murzin, A. G. and Chothia, C. (1999) SCOP: a structural classification of proteins database. *Nucleic Acids Research*. **27**, 254-256
- 28 Page, C. C., Moser, C. C., Chen, X. X. and Dutton, P. L. (1999) Natural engineering principles of electron tunnelling in biological oxidation-reduction. *Nature*. **402**, 47-52
- 29 Okamoto, A., Hashimoto, K., Nealson, K. H. and Nakamura, R. (2013) Rate enhancement of bacterial extracellular electron transport involves bound flavin semiquinones. *Proceedings of the National Academy of Sciences of the United States of America*. **110**, 7856-7861

Chapter 4: Solution-state Structural Studies of OmcA

4.1 – Introduction

Verification of OmcA's possible oligomeric state observed in the crystal structure (Fig. 4.1, Section 3.2) was explored and detailed in this chapter. Determination of the apparent molecular weight (i.e. MW_{app}) of eOmcA in solution using a suite of techniques will inform if eOmcA undergoes oligomerisation in solution. As concluded earlier (Section 3.3), the surface areas of the putative dimer interfaces are unfavourable for all oligomer combinations observed (i.e. interfacial area $< 700 \text{ \AA}^2$ [1]). However if the biological unit is an oligomer present in the crystal structure, previous study suggests quaternary structure with enhanced electron transfer activity [2], which favours the two eOmcA dimers of chain A:B + chain C:D per asymmetric unit (i.e. $2eOmcA_2$; Fig. 4.1; [3]). The MW_{app} of eOmcA and $eY^{374}F$ were determined in this study in an attempt to correlate crystal structure observations to the biological unit of OmcA. Based on the lack of evidence in the literature that MtrC undergoes oligomerisation (in the absence of OmcA), the MW_{app} of eMtrC is assessed as a negative control.

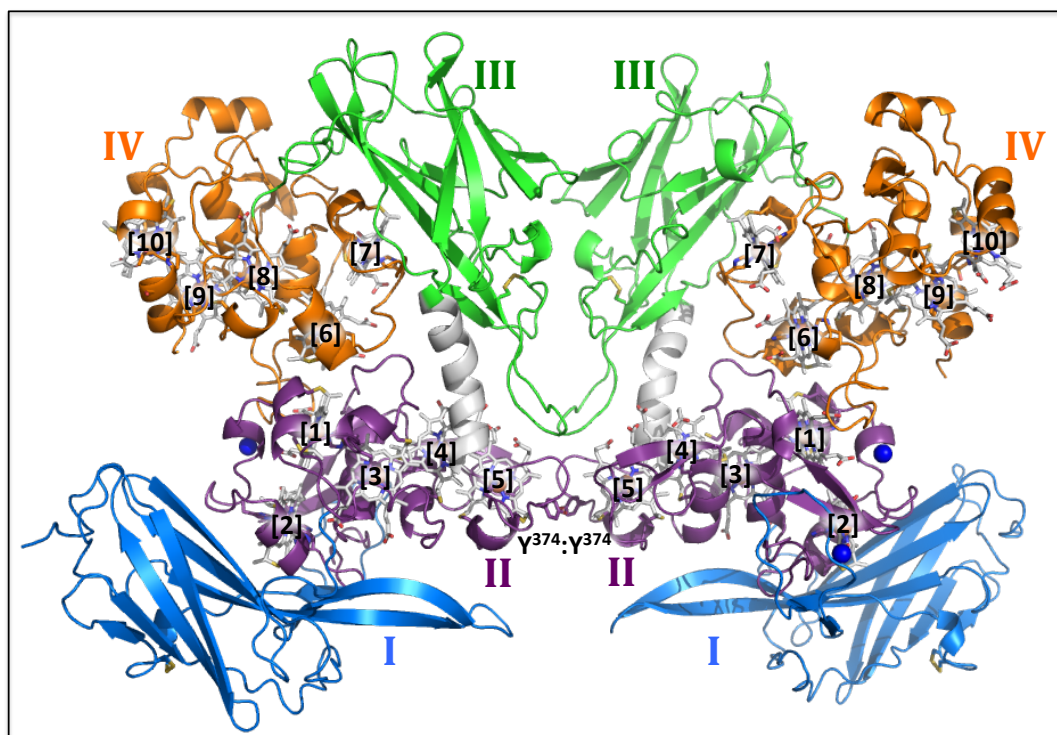


Figure 4.1 – **The Favoured eOmcA “dimer”**. The indication of an OmcA oligomer with enhanced electron transfer activity [2] indicates the intermolecular interaction with 9 \AA distance between adjacent eOmcA molecule haems is the favoured dimer model. Dimer interface area median = 481 \AA^2 .

4.2 – Results

4.2.1 – Analytical Gel Filtration Chromatography (AGFC)

The only published work on OMMC oligomers provides evidence for a salt-sensitive OmcA₂MtrC complex [2]. Salt-sensitivity of putative eOmcA₂ was thus assessed initially with analytical gel filtration. A Superdex S-200 HR 10/30 column was calibrated with proteins of known molecular weight as standards. All AGFC experiments reported in this Chapter were performed with the same calibrated Superdex S-200 HR 10/30 column. The molecular weight standards were run in both 20 mM HEPES, pH 7.60, 0.1 M NaCl and 50 mM BICINE, pH 8.50 (no salt). The extrapolated K_{av} values were plotted to generate semi-logarithmic calibration curves under both salt regimes (Fig. 4.2; fits labelled with equations). The semi-log fits show the fit gradients are near-equal (i.e. $-0.104 - (-0.091) = 0.013$). There is a larger difference between K_{av} axis-intercepts (i.e. $1.596 - 1.463 = 0.133$), all of which accounts for a maximum absolute deviation of 34 kDa for a 200 kDa molecule (i.e. $\pm 15\%$).

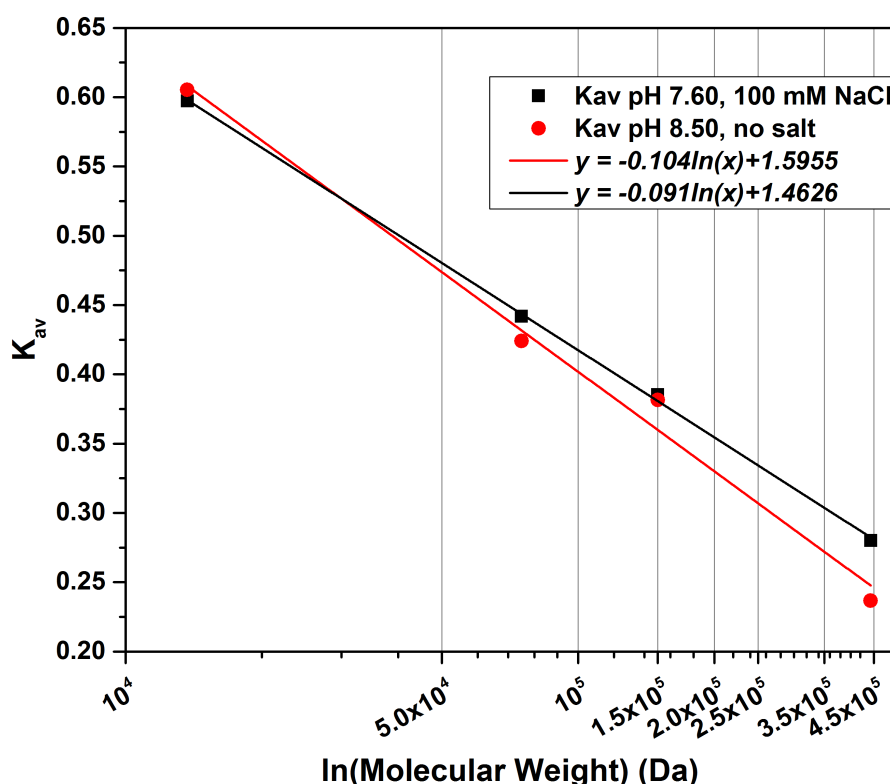


Fig. 4.2 –**Semi-logarithmic calibration curves of the Superdex S-200 column.** Molecular weight standards used are Ribonuclease A (12.7 kDa), Conalbumin (75 kDa), Alcohol dehydrogenase (150 kDa) and Apoferritin (443 kDa) at approximately 1 mg mL⁻¹. The column was calibrated at 0.10 mL min⁻¹ with independent runs of 250 μ L of each molecular weight standard in both 20 mM HEPES, pH 7.60, 0.1 M NaCl and 50 mM BICINE, pH 8.50 (no salt).

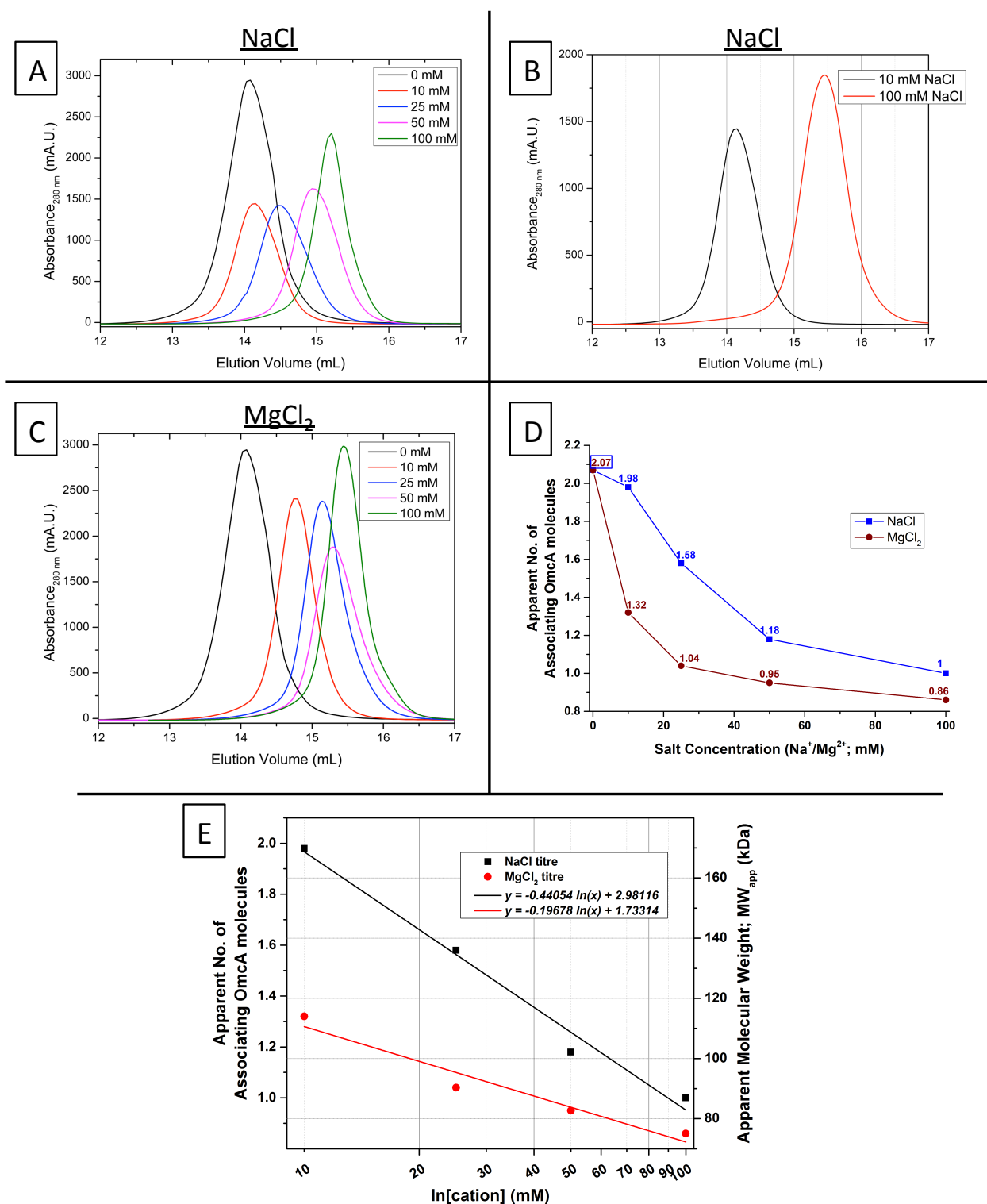


Fig. 4.3 – Chromatograms of eOmCA under different Salt Regimes in Analytical Gel Filtration. Each chromatogram plotted shows the $A_{280\text{nm}}$ monitored during the elution of 0.15 mM eOmCA from a Superdex S-200 gel filtration column. Each experiment was run with 250 μL of protein at 0.1 mL min^{-1} in 50 mM BICINE, pH 8.50 and varying concentrations of either (A) NaCl or (C) MgCl_2 . (B) Equimolar eOmCA (0.13 mM) at the salt extremes analysed to confirm K_{av} changes were not affect by sample dilution/loss. (D) Linear and (E) semi-log_e plot of observed eOmCA stoichiometry relative to salt concentration (as a function of MW_{app}). The semi-log_e fits have Pearson's R correlation co-efficients of 0.992 and 0.973 for NaCl and MgCl_2 titres respectively.

Near-equimolar eOmCA (≈ 0.13 mM) was then run on the calibrated Superdex S-200 under a range of NaCl and then MgCl_2 concentrations (i.e. 0, 10, 25, 50 and 100 mM of each). The concentration of salt was shown to affect the elution volume (V_e) of eOmCA (Fig. 4.3A-C). When elution volume of eOmCA from the calibrated column is extrapolated to apparent molecular weight (MW_{app}), eOmCA appears to elute as a dimer at 0 – 10 mM NaCl (i.e. $\text{MW}_{\text{app}} = 170$ kDa), and a monomer at 100 mM NaCl (Fig. 4.3D and 4.3E). The MW_{app} of eOmCA was also monomeric at $\text{MgCl}_2 > 25$ mM ($\text{MW}_{\text{app}} = 75 - 85$ kDa; Fig. 4.3D and 4.3E). MgCl_2 appears to be twice more effective than NaCl at putatively breaking eOmCA dimerization (i.e. $\frac{\text{MW}_{\text{app}}}{\ln [\text{NaCl}]} : \frac{\text{MW}_{\text{app}}}{\ln [\text{MgCl}_2]} = \frac{-0.44}{-0.20} = 2.20$; Fig. 4.3E).

There is a precedent for performing gel filtration chromatography experiments with $[\text{NaCl}] \approx 100$ mM to neutralise weak electrostatic/hydrophobic interactions between the analyte and the gel filtration matrix [4, 5]. To blanket spurious hydrophobic interactions, control experiments of equimolar eOmCA were performed with the non-ionic detergent octyl-glucopyranoside (OGP). In the presence of 2.25 mM OGP OmCA had a MW_{app} of 152 and 96 kDa with eOmCA in 10 and 100 mM NaCl respectively (Fig. 4.4). However the MW_{app} reported are extrapolated from detergent-free calibration of the Superdex S-200 column, and as such the inferred MW_{app} may not be representative. Nevertheless the difference in MW_{app} of eOmCA between 10 mM and 100 mM NaCl in the presence of OGP (i.e. ≈ 60 kDa) is a 58% increase in MW_{app} ; this change is significant and most likely an actual observation, as opposed to experimental variance.

To further characterise the inferred MW_{app} changes observed on the analytical gel filtration column, a titre of eOmCA load concentration was performed at a consistent “dimeric” salt concentration of 10 mM NaCl (Fig. 4.5). eOmCA concentration was titrated from 103 μM to 0.5 μM to determine if the K_{av} is concentration-dependent. K_{av} does not decrease with decreasing [eOmCA]. eOmCA eluted predominantly at 14.2 mL, excluding [eOmCA] = 103 μM , where elution volume was 14.6 mL. Analytical gel filtration of eOmCA was performed with a buffer containing 10 mM (reduced) DTT. Whilst the MW_{app} was still in accordance with an eOmCA dimer, UV-visible absorbance of the sample revealed partial haem reduction $A_{551 \text{ nm}}$ (Fig. 4.6A). Irreversible production of a peak at $A_{652 \text{ nm}}$ was also observed (i.e.

signal persisted post-dialysis; Fig. 4.6B). Both of these spectroscopic observations were reproduced on an independent batch of eOmCA that was not subject to AGFC (see A4.1).

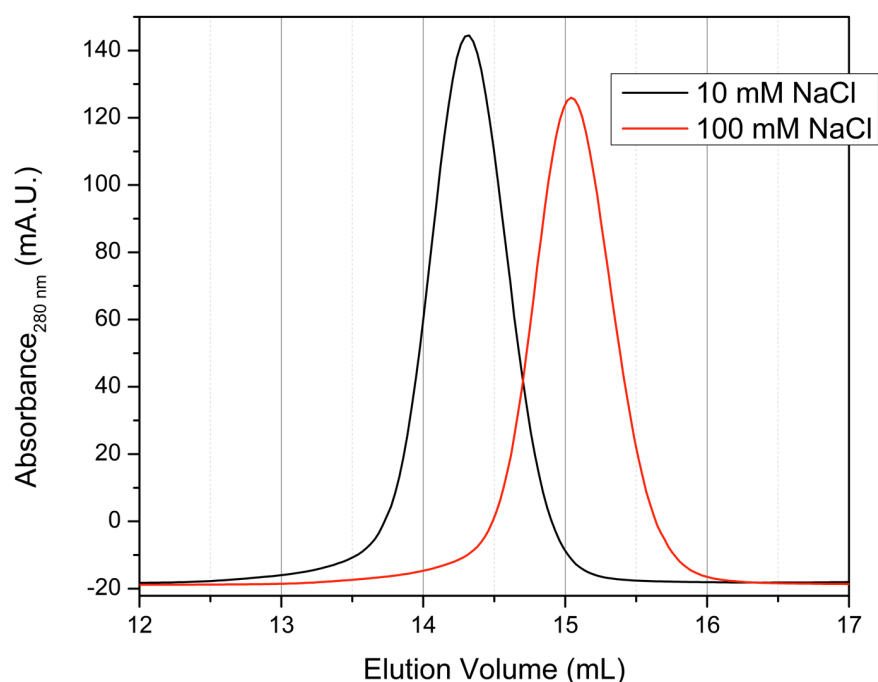


Fig. 4.4 – **Chromatograms of eOmCA elution from OGP-equilibrated Superdex S-200 column.** Equimolar OmCA in pH 8.50, 10 and 100 mM NaCl with 2.25 mM OGP to block non-specific protein:column interactions.

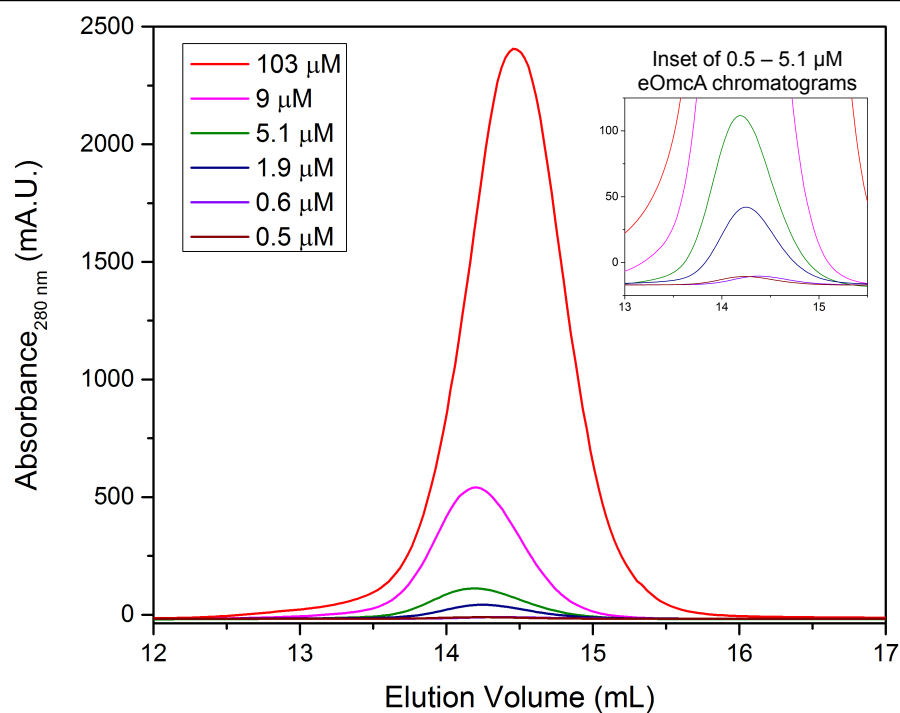


Fig. 4.5 – **Chromatograms of an eOmCA concentration-titration.** eOmCA samples (250 μ L) were run in 50 mM BICINE, pH 8.50, 10 mM NaCl at 0.10 mL min^{-1} . All chromatograms plotted here are produced by the dilution of the same protein sample. Inset emphasises elutions of 5.1 – 0.5 μ M eOmCA.

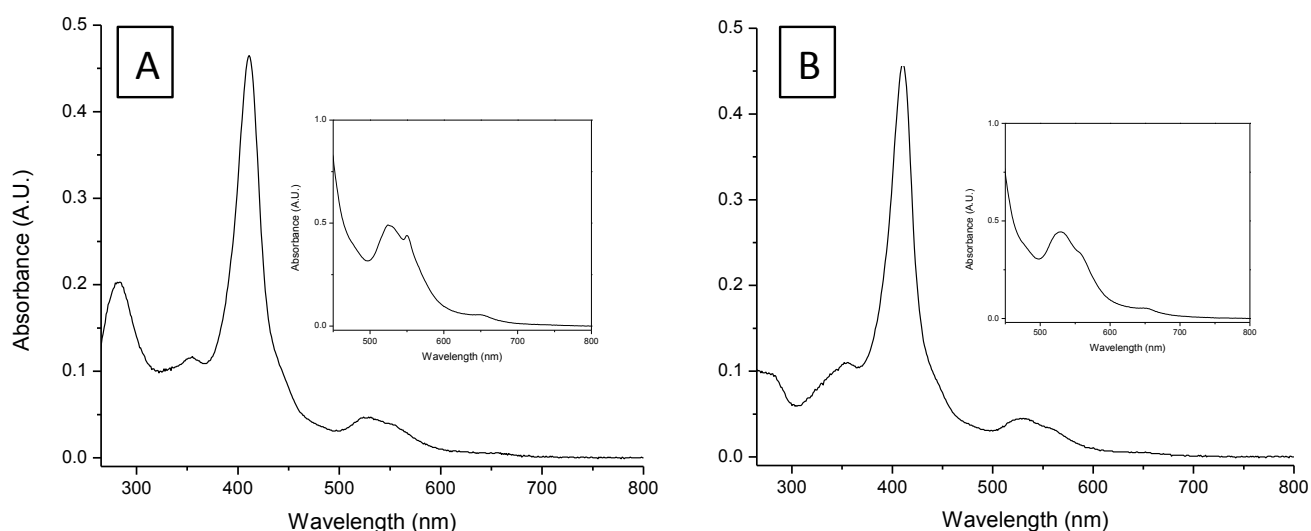


Fig. 4.6 - The effect of DTT reduction on eOmCA. The UV-vis spectra of eOmCA eluted from Superdex S-200 column in 50 mM BICINE, pH 8.50, 10 mM DTT (A) before and (B) after dialysis into 50 mM BICINE, pH 8.50, 0.1 M MgCl₂. Inset spectra cuvette path length is 1 cm and main plots produced from 1 mm path length cuvettes.

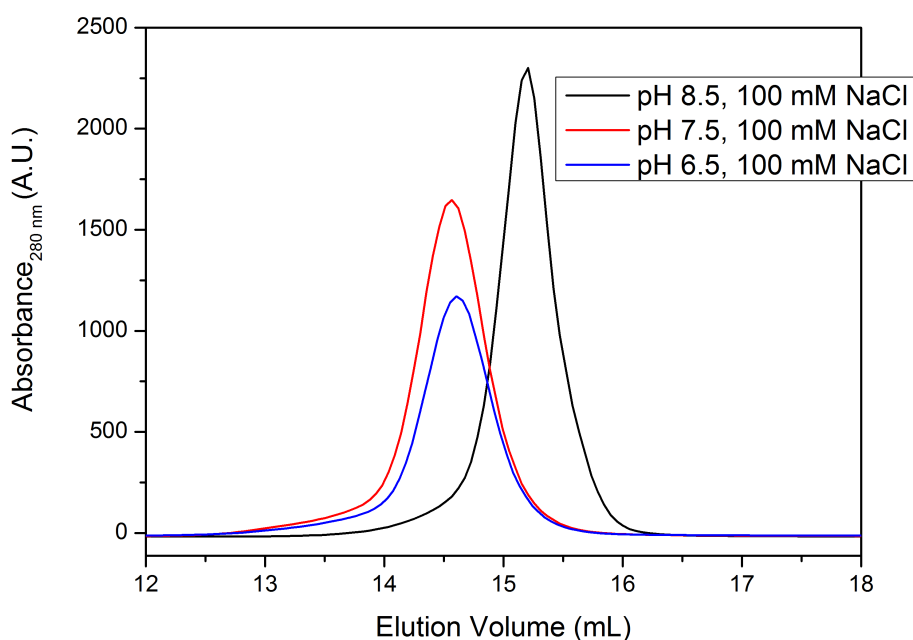


Fig. 4.7 - Chromatograms of an eOmCA pH titration in Analytical Gel Filtration. Near-equimolar eOmCA was run using the same parameters as mentioned previously (on the calibrated Superdex S-200 column) in the presence of 100 mM NaCl and in 20 mM buffers at pH values 6.5 (MES), 7.5 (HEPES) and 8.5 (Bis-TRIS Propane).

Further analytical gel filtration studies involved running eOmCA in pH 8.50, 7.50 and 6.50 buffers with 0.1 M NaCl (Fig. 4.7). The MW_{app} determined at these pHs correlate to a monomer at pH 8.50, and 1.44 molecules associating (i.e. $MW_{app} = 127$ kDa) at both pH 7.50 and 6.50.

4.2.2 – AGFC Column Performance

Column performance was analysed indirectly via analysis of the eOmCA elution peaks. Peak asymmetry (A_s) is uncommon in eOmCA chromatograms (Fig. 4.3) and is compiled in Table 3.1. Peak width at half peak height (W_h) was also used to assess column efficacy. To determine if the resolving efficacy of the column (h) is constant with change in NaCl or $MgCl_2$ concentration, h of eOmCA is solved for at each salt concentration as shown here:

$$h = \frac{L}{5.54 d_p} \left(\frac{W_h}{V_e} \right)^2 = k \left(\frac{W_h}{V_e} \right)^2 \dots (\text{Eqn. 4.1})$$

(h = reduced plate height, L = bed height, d_p = matrix particle diameter, $k = \frac{L}{5.54 d_p}$, W_h = peak width at half peak height, V_e = elution volume)

At 100 mM NaCl (chromatogram in Fig.3.8B):

$$h = k \times \left(\frac{0.73}{15.46} \right)^2 = k \times 2.23 \times 10^{-3}$$

As such peak asymmetry (A_s), half peak height width (W_h), and the variable term that determines the resolution capacity of the column (i.e. $\left(\frac{W_h}{V_e} \right)^2$) during NaCl and $MgCl_2$ titration are compared in Table 3.1.

It is apparent that the variable column efficiency term (i.e. $h \propto \left(\frac{W_h}{V_e} \right)^2$) is constant throughout the majority of NaCl titre chromatograms. This observation, with the assumption of constant matrix particle diameter (d_p) and bed height (L) (i.e. k being constant), means that h is constant at 0 – 100 mM NaCl (Table 4.1). This trend appears to correlate with peak asymmetry (A_s); an A_s value of 1.00 is produced by a symmetric peak. The average A_s of the eOmCA chromatograms is much more variable in the $MgCl_2$ titre than the NaCl titre. W_h is lowered in the presence of $MgCl_2$, and in the asymmetric 100 mM NaCl chromatogram.

Table 4.1 – **Elution peak analysis of eOmca AGFC-salt titre.** The NaCl titre values tabulated are the more consistent of the two titration datasets. In conjunction with monovalent salt usually used in AGFC, average NaCl titre values are used as a benchmark. σ = Standard deviation. # = NaCl titre values inconsistent with average NaCl titre values. * = MgCl_2 titre values consistent with average NaCl titre values.

[NaCl] (mM)	0	10	25	50	100	100 (repeat)	Average ($\pm\sigma$)
A_s	1.04	1.10	1.23 [#]	1.18	1.02	1.06	1.12 \pm 0.08
W_h	0.72	0.67	0.74	0.70	0.48 [#]	0.73	0.71 \pm 0.03
$(W_h \div V_e)^2$ ($\times 10^{-3}$)	2.62	2.25	2.61	2.19	1.00 [#]	2.23	2.38 \pm 0.22
[MgCl ₂] (mM)	0	10	25	50	100		
A_s	1.01*	1.03*	-1.86	1.44	1.37		
W_h	0.71*	0.58	0.61	0.54	0.54		
$(W_h \div V_e)^2$ ($\times 10^{-3}$)	2.55*	1.54	1.62	1.25	1.22		

4.2.3 – Blue Native PAGE

Polyacrylamide gel Electrophoresis was performed with eOmca in the absence of SDS in order to maintain the protein's native fold and preserve putative dimerization interactions (Fig. 4.8). A distinct band of $MW_{app} \approx 160$ kDa is the dominant species observed. There are also discrete bands apparent with $MW_{app} \approx 300$ and 480 kDa, approximately equivalent to homotetramer and homohexameric eOmca complexes. Protein detected with $MW_{app} \geq 720$ kDa is not a distinct band in the lanes and is possibly precipitant. Blue Native PAGE in high [NaCl] buffer has not been performed.

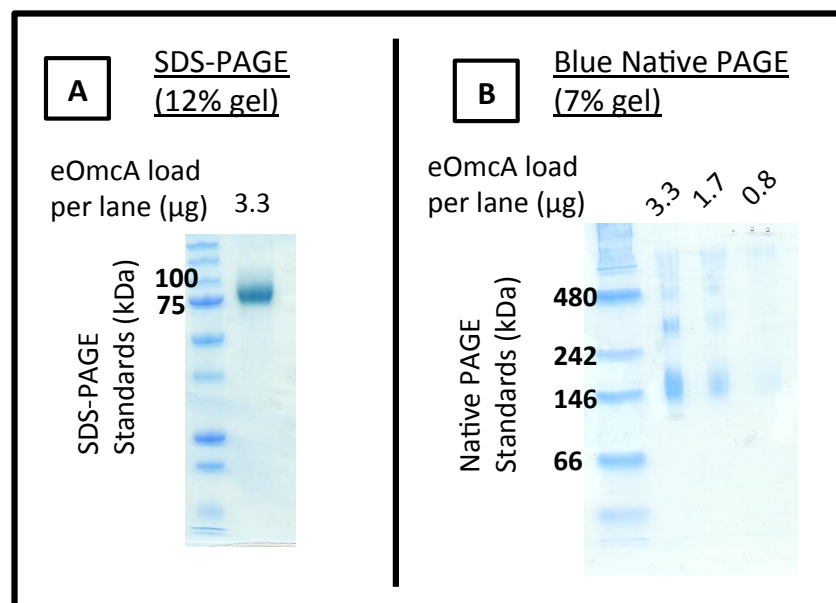


Fig. 4.8 – **Blue Native PAGE of eOmca in low (10 mM) NaCl concentration buffer.** In comparison to eOmca in an SDS-PAGE gel (A), Blue Native PAGE of eOmca (B; in 50 mM BICINE, pH 8.50, 10 mM NaCl) shows a dominant band equivalent to dimeric eOmca and other higher molecular weight species are resolved. For Blue Native PAGE, samples were mixed with Instant Blue Coomassie Stain in a 1 part Coomassie, 3 parts sample ratio. Electrophoresis was performed without SDS in the sample buffer, gel or running buffer. Native PAGE protein standard marker used was Novex NativeMark Unstained Protein Standard.

4.2.4 – Analytical Ultracentrifugation (AUC)

Sedimentation Equilibrium (SE) experiments were performed of pOmca and eOmca. At all concentrations and rotor speeds, a molecular weight of 85 ± 1 kDa was determined for eOmca (Fig. 4.9, Table 4.2). A higher molecular weight was extrapolated from modelling a single globular molecule from the sedimentation absorption profile of pOmca. However, the presence of contaminant in the sample (see Section 2.2) means there is a possibility of pOmca:contaminant interaction contributing to the extrapolated hydrodynamic radius/ MW_{app} .

Table 4.2 – **Sedimentation Equilibrium data of Omca.** The globally fitted data of Omca was based on a least-squares model of a monomeric, non-interacting molecule in solution. All samples were run in 20mM HEPES, pH 7.6, 0.01% CHAPS, 50 mM NaCl, 1% glycerol (see Materials and Methods). * = Run at 7000 and 10000 rpm. ‡ = Run at 8100, 12900 and 16200 rpm.

Sample	Estimated Molecular Weight (Da)	Protein Concentration (μM)	Wavelength monitored (nm)	MW_{app} (Da)
pOmca*	86,059	3.05	450	100,000
		0.87	410	
eOmca‡	86,059	4.36	440	84 – 86,000
		8.71	440	

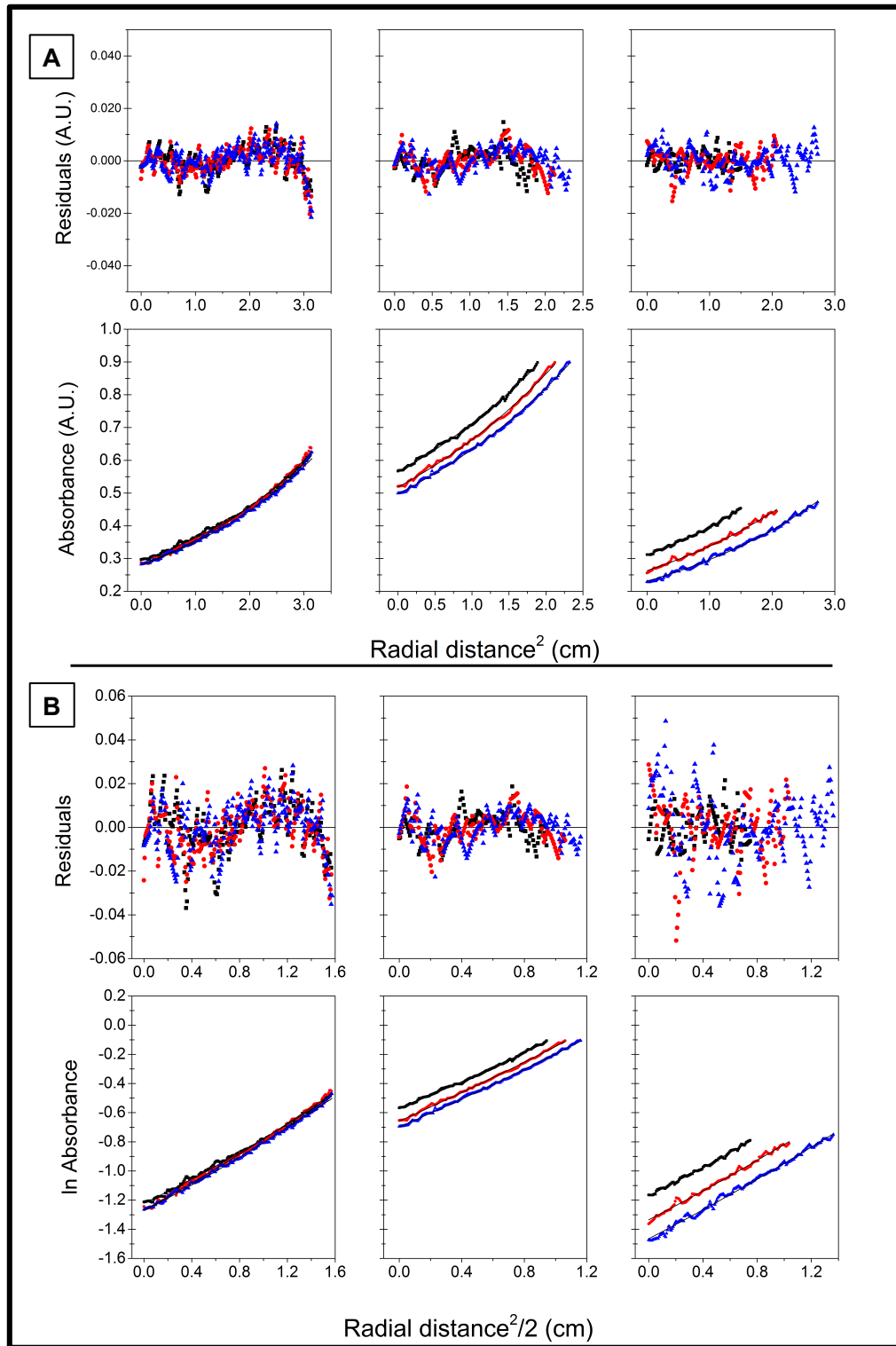


Fig. 4.9 – **Analytical Ultracentrifugation sedimentation profiles of eOmCA.** A Sedimentation Equilibrium experiment of eOmCA was run at three protein concentrations: 0.7 μM (black squares), 3.6 μM (red circles) and 7.0 μM (blue triangles). The globally fitted model from which MW_{app} is derived is plotted for each sample (black line). The experiment was run at three angular velocities: 8100 rpm (left panels), 12900 rpm (middle panels) and 16200 rpm (right panels). For each angular velocity, the residual between each data point the model is in the upper panel. (A) The sedimentation absorbance profiles measured as a function of radial distance² from a reference point (i.e. x). (B) Data presented in (A) manipulated such that global fit gradient = $\frac{M\omega^2}{RT}$. MW_{app} (i.e. M) is thus obtained from this plot's gradient.

4.2.5 – Small Angle X-Ray Scattering (SAXS)

Collaborators in Oakridge National Laboratory collected SAXS data of purified eOmca supplied during the course of this study (Fig. 4.10). Data was collected under a range of [eOmca] (i.e. 2.3 – 18.4 mg mL⁻¹) in low (10 mM) and high (150 mM) NaCl buffers. eOmca was shown to be a monomer in solution under all conditions tested, with a maximum dimension (D_{\max}) of 96 Å and a radius of gyration (R_G) of 30.6 Å ± 0.2, in agreement with previous measurements [6] and the crystal structure presented here (D_{\max} = 97 Å, R_G = 30.2 Å).

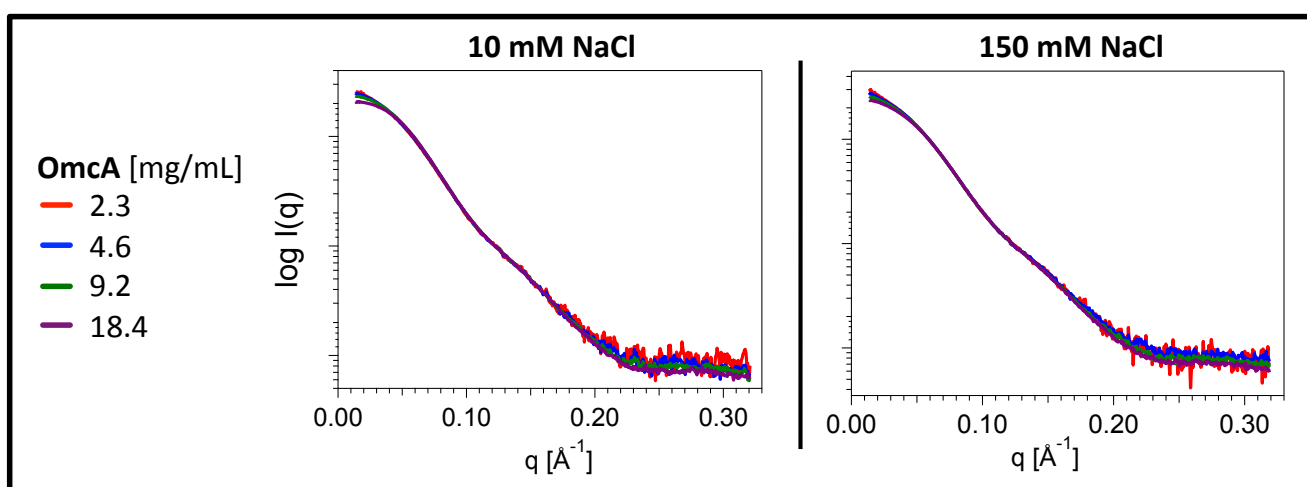


Fig. 4.10 – **SAXS profiles of eOmca**. The SAXS profiles of eOmca at different concentrations in low (10 mM; left panel) and high (150 mM; right panel) NaCl buffers. Buffers contain 50 mM BICINE, pH 8.50, and variable [NaCl].

4.2.6 – Probing the Oligomeric State of eOmca mutant Y³⁷⁴F

AGFC of eOmca mutant Y³⁷⁴F (i.e. eY³⁷⁴F) in 10 mM NaCl buffer shows the protein elutes with a K_{av} corresponding to a MW_{app} intermediate between monomeric and dimeric Omca (Fig 4.11A). Whereas MgCl₂ changed the K_{av} of eOmca twice as effectively as NaCl, the K_{av} of eY³⁷⁴F was barely changed by MgCl₂ (full NaCl titre not measured; Fig. 4.11B).

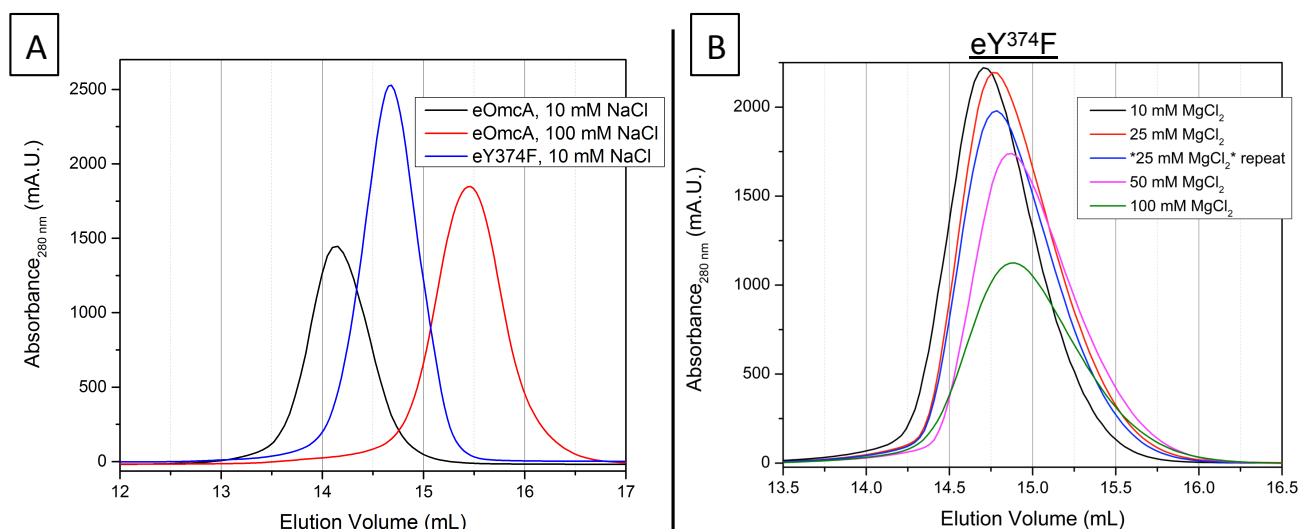


Fig. 4.11 – Analytical Gel Filtration chromatograms of eY³⁷⁴F. (A) Near-equimolar eOmcA elution in 10 mM NaCl (black) and 100 mM NaCl (red) are compared with elution of eY³⁷⁴F in 10 mM NaCl buffer (blue). Each chromatogram is the elution of ≈ 0.1 mM protein concentration from a Superdex S-200 gel filtration column by pure protein absorption at 280 nm. Each experiment was run with 250 μ L of protein at 0.1 mL min⁻¹ in 50 mM BICINE, pH 8.50 and varying [NaCl]. (B) Chromatograms of an eY³⁷⁴F [MgCl₂] titre in Analytical Gel Filtration. eY³⁷⁴F was run using the same parameters as mentioned previously in the presence of 10-100 mM MgCl₂.

4.2.7 – Solution studies of the Oligomeric state of MtrC

Based on the lack of any MtrC oligomerisation evidence in the literature (in the absence of eOmcA), the effect of salt concentration on the K_{av} of the OMMC eMtrC was used as a negative control. Under the salt extremes that produce dimeric and monomeric K_{av} of eOmcA during AGFC (i.e. 10 mM and 100 mM NaCl respectively), eMtrC had MW_{app} values of 128 kDa and 115 kDa respectively, a difference of 13 kDa. An MtrC molecule has a molecular weight of 75 kDa [7-9], as such the cause for the consistent discrepancy between MW_{app} and molecular weight is unclear (Fig. 4.12). Furthermore, SAXS measurements of eMtrC by Oakridge National Laboratory collaborators showed evidence of a higher molecular weight fraction as a function of protein concentration (Fig.4.13). Although higher molecular weight fractionation occurred independent of buffer ionic strength, low [NaCl] produced more distinct fractionation profiles than high [NaCl] buffer, suggesting NaCl inhibited fractionation.

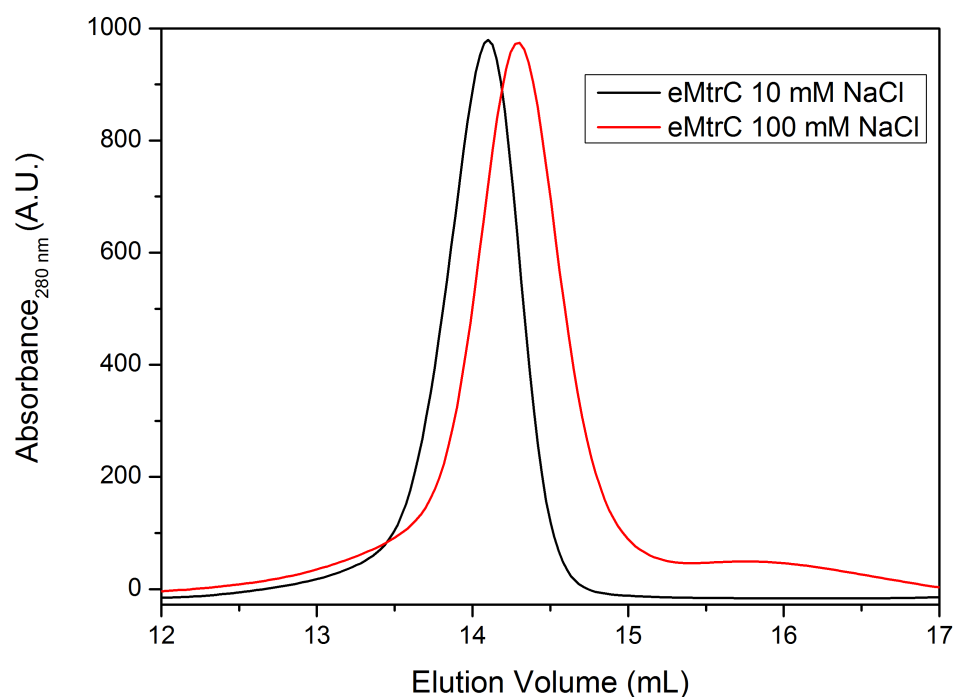


Fig. 4.12 - **Chromatograms of eMtrC under extreme Salt Regimes in Analytical Gel Filtration.** Each chromatogram plotted here was determined by monitoring the elution of 0.1 mM eMtrC from a Superdex S-200 gel filtration column by pure protein absorption at 280 nm. Each experiment was run with 250 μ L of protein at 0.1 mL min⁻¹ in 50 mM BICINE, pH 8.50 and varying concentrations of NaCl.

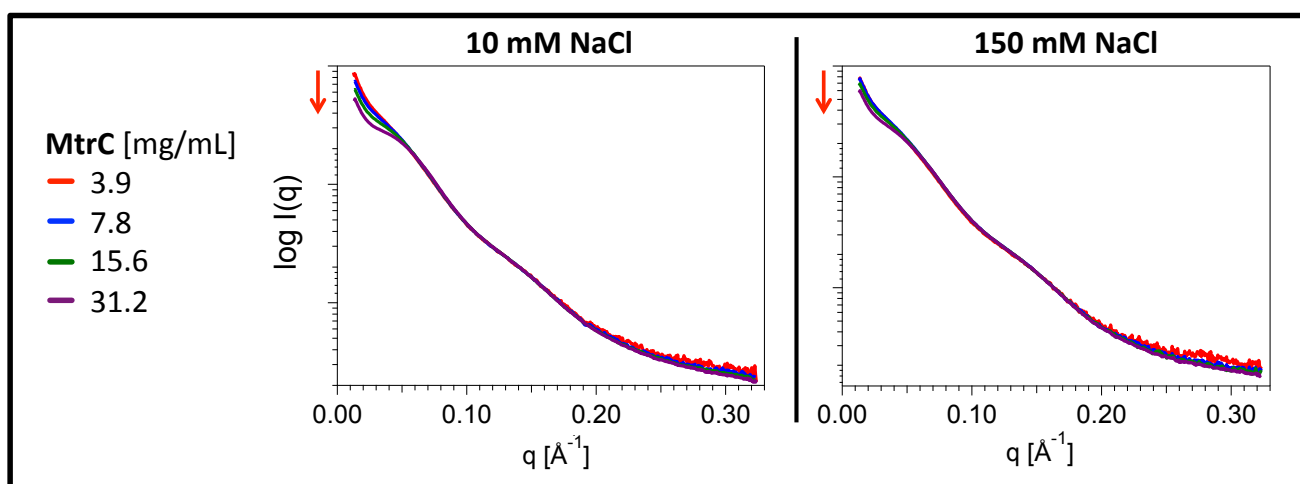


Fig. 4.13 - **SAXS of eMtrC.** The SAXS profiles of eMtrC at low (10 mM; left panel) and high (150 mM; right panel) NaCl concentrations. Buffers contain 50 mM BICINE, pH 8.50, with listed [NaCl]. Red arrow indicates increasing high molecular weight fraction of sample with increasing protein concentration.

4.3 – Discussion

The previous chapter details crystallographic data indicating that the biological unit of eOmCA is a homodimer with C_2 symmetry (Section 3.2). To elucidate whether the quaternary structure apparent in eOmCA crystals is maintained in solution, the apparent molecular weight (MW_{app}) of eOmCA was analysed via analytical gel filtration chromatography (AGFC), blue native PAGE, analytical ultracentrifugation (AUC) and small angle X-ray scattering (SAXS). A cue from the inhibitory effect of ionic strength on the K_D of an isolated OMMC hetero-oligomer complex (putatively OmCA₂MtrC [2]) was followed to perform NaCl and MgCl₂ titrations using AGFC. Changes in K_{av} (implying ΔMW_{app}) were observed with change in both NaCl and MgCl₂ concentrations. eOmCA titrated between a MW_{app} equivalent to a dimer at 10 mM NaCl (i.e. 170 kDa) and a monomer at 100 mM NaCl (i.e. 86 kDa).

In previous data, binding of OmCA to an Al₂O₃ optical waveguide was shown to be salt-sensitive across the range tested (i.e. 4 – 10 mM KCl) [10], which may correlate with the AGFC observations here. The AGFC data of eOmCA can be interpreted such that eOmCA's putative homodimer is sensitive to $[NaCl] > 10$ mM and $[MgCl_2] > 0$ mM. It is not initially clear that the greater ΔK_{av} in the MgCl₂ titre is caused by the divalency of Mg²⁺ compared to monovalent Na⁺, or the presence of twice the $[Cl^-]$ in the MgCl₂-buffers compared to the NaCl-buffers. The possibility of disulphide regulated/covalent homodimerisation by OmCA is ruled out by the presence of 10 mM DTT not shifting the K_{av} of OmCA in the “dimeric”, no salt buffer. Semi-reduced eOmCA eluted from the DTT-equilibrated Superdex S-200 column with an Fe-ligand charge transfer band at 652 nm (Fig. 4.6), a phenomena reproduced with a DTT titration of eOmCA (see A4.1).

Furthermore, previous atomic force microscopy force retraction curves showed OmCA's attraction for hematite AFM probes is twice the magnitude measured for MtrC, however MtrC binds to hematite AFM probes with twice the frequency of OmCA [11]. Both observations correlate well with the OmCA dimer narrative: a putative OmCA₂ molecule would possess twice the number of mineral/hematite affinity sites of MtrC. Concerning binding frequency; monomeric MtrC is approximately half the molecular weight of OmCA₂. According to the Svedberg equation, MtrC should thus have a translational diffusion coefficient (D) twice the magnitude of an OmCA₂ molecule:

$$\frac{M_b}{RT} = \frac{s}{D}$$

$$\Rightarrow D \propto \frac{1}{M_b} \text{Eqn. 4.2}$$

(s = sedimentation coefficient, M_b = buoyant mass, R = gas constant, T = absolute temperature)

This would account for MtrC's capacity to bind to hematite with twice the frequency of OmcA₂.

AGFC and SAXS of eMtrC was performed as a negative control because (in the absence of OmcA [2]) there is no evidence of MtrC existing as an oligomer in the literature. SAXS data contrasted this: eMtrC has a distinct high-molecular weight fractionation SAXS profile that is salt-sensitive, whereas there is no distinct sign of a high-molecular weight population in eOmcA at either [NaCl] (Fig. 4.10). Also, eMtrC has an MW_{app} intermediate to an MtrC monomer:dimer in low and high [NaCl] according to AGFC (i.e. $\Delta MW_{app} = 13$ kDa). The K_{av} of eOmcA shifted with a change in pH, which may explain the inaccurate MW_{app} extrapolated for eMtrC. Alternatively, eOmcA's putative dimeric state is less sensitive to ionic strength below pH 8.50. OmcA binding to Al₂O₃ and α -Fe₂O₃ (i.e. hematite) waveguides has been shown to also be pH sensitive, and that maximal OmcA binding to both waveguides occurs near OmcA's calculated isoelectric point (pI \approx 7) [10].

To ensure column efficiency was not altered by performing AGFC in [NaCl] < 100 mM, or in MgCl₂ buffers, the eOmcA chromatograms were analysed for peak asymmetry (A_s , Eqn. M.5) and column resolution efficacy (i.e. reduced plate height, h) via the term $(\frac{W_h}{V_e})^2$ (Eqn. 4.1). Whereas this is typically performed with molecular standards known to be chemically inert to the column matrix, the data already exists to qualitatively assess column efficiency with eOmcA. The data indicates that whereas a NaCl-titre has no effect on column efficiency, MgCl₂ increases the asymmetry of eOmcA elution peaks and produces atypical $(\frac{W_h}{V_e})^2$ values. The free oxide groups present in dextran polymers that constitute the Superdex column matrix can chelate metal cations [12-14], including Mg²⁺ and ferric iron [15]. This may affect matrix pore sizes, modulating the column's retention capacity. However, as discussed earlier it is ideal to assess column efficacy with molecules experimentally shown to not interact

with the column matrix, and the effects observed may be due to the promotion/inhibition of non-specific protein:matrix interaction(s). As such, it is unclear whether MgCl_2 affected putative eOmCA homodimerisation or the Superdex matrix's resolution capacity. Furthermore, it is unclear whether or not the ΔK_{av} of the [NaCl] titre is based purely on changing column resolution capacity via promotion/inhibition of non-specific protein:matrix interaction(s).

To explore the possibility of low/high salt concentrations promoting protein:column matrix interactions (and ultimately MW_{app}), the column was equilibrated with the non-ionic detergent OGP to saturate/blanket any non-specific interaction. Whereas K_{av} of eOmCA in 10 mM and 100 mM NaCl shifted in the presence of OGP, the extent of ΔK_{av} is no longer proportional to a dimer and monomer respectively. It is possible that the change in MW_{app} at 10 mM and 100 mM NaCl is because the column was calibrated without OGP. Since ΔMW_{app} with $\Delta[\text{salt}]$ was maintained in the presence of OGP (i.e. $\Delta MW_{app} \approx 60 \text{ kDa}$), it is likely that there is no non-specific/hydrophobic column interaction contributing to ΔK_{av} .

All chromatograms in the salt titrations of eOmCA display single elution peaks. The single peak phenomenon persists when K_{av} is proportional to an MW_{app} intermediate to an eOmCA monomer or dimer (i.e. at $10 \text{ mM} < [\text{NaCl}] < 100 \text{ mM}$ and $0 < [\text{MgCl}_2] < 50 \text{ mM}$ respectively). This is a different observation from what would be expected for a protein in equilibrium between monomeric and dimeric states, whereby a change in the amount of protein eluting at either dimeric or monomeric elution volumes would produce two elution peaks. However, if the OmCA homodimerisation kinetic rate is very fast, it may be possible that intermediate phases of the monomer:dimer equilibrium are resolved as single elution peaks of eOmCA in chromatograms.

eY³⁷⁴F maintains the single peak phenomenon in the "dimeric" 10 mM NaCl buffer, which corroborates the working model of mutagenic dimer-interface disruption. A MgCl_2 titre of eY³⁷⁴F was performed with the intention of inhibiting homodimerisation, and the K_{av} of eY³⁷⁴F was much less sensitive to increasing $[\text{MgCl}_2]$ than eOmCA. Whereas it is apparent that eY³⁷⁴F MW_{app} is less sensitive to MgCl_2 , the knowledge that MgCl_2 is likely to affect column resolution efficacy further complicates interpreting these results. Furthermore, persistence of the proposed dimer interface in the eY³⁷⁴F crystal structure indicates that other interactions may facilitate the

intermolecular interface observed in the eOmCA crystal structure. As such the eOmCA “dimer” may be an artefact of molecules packing into the asymmetric unit during crystal formation, and the Y³⁷⁴F mutation maintains enough intermolecular contacts to maintain general wild-type (i.e. eOmCA) crystal packing arrangement.

Titration of the concentration of eOmCA loaded onto the Superdex S-200 column had no effect on K_{av} and thus MW_{app} . Either eOmCA concentrations tested in this experiment were not lower than the homodimeric dissociation constant (i.e. $<0.5 \mu M$ [2]), or more simply the ΔK_{av} of eOmCA is not being affected by a change in molecular weight.

Blue native PAGE of eOmCA corroborated the AGFC and crystal structure eOmCA dimer data. However, as with AGFC, molecular weight standards used to calibrate the polyacrylamide gel or gel filtration column are globular molecules, whereas the OMMC structures obtained so far show they possess ellipsoid morphology. As such the accuracy of the MW_{app} determined in the AGFC dataset is dependent on the molecular standards having a similar molecular shape to the analyte. Furthermore, in SDS-PAGE, OmCA (molecular weight = 86 kDa) migrates to a $MW_{app} \approx 75$ kDa (Section 2.2.1), putatively because 20 haem propionate groups covalently bound to the denatured polypeptide per OmCA molecule change OmCA’s mass:charge ratio. Natively folded eOmCA may blanket/neutralise many haem propionate groups during blue native PAGE. The added issue of different molecular shapes between analyte and molecular weight markers make it unclear if the MW_{app} observed during AGFC and blue native PAGE is representative of eOmCA. A necessary experiment would be native PAGE of eOmCA in “monomeric” and “dimeric” buffers to observe a [salt]-dependent shift in eOmCA band on a native PAGE gel. However the inability to reproduce eOmCA oligomers using techniques that don’t require molecular weight standards (i.e. SAXS, AUC) does not support the OmCA dimer model.

The major issue with the eOmCA dimer model (besides the intermediate elution peaks and stability of the apparent Y³⁷⁴F crystallographic interaction) is the mixed implications from other solution-state techniques. AUC of pOmCA produce MW_{app} equivalent to OmCA oligomers, however the SDS-PAGE gels of the samples show contaminants that could interfere with OmCA’s sedimentation. A possible cause for the discrepancy in MW_{app} derived from different techniques could be that the exopolysaccharide (EPS) environment OmCA is putatively embedded in at the

extracellular surface of the outer bacterial membrane (i.e. EPS depth $\geq 0.5 \mu\text{m}$ [16]) is mimicked by the dextran polymer of the AGFC column matrix [17]. Ion-exchange “chromatographic” properties have been attributed to the biofilm content of a river [18] based on the resolution of K^+ and Br^- elution profiles. Furthermore, resolution of these ions is directly proportional to length of passage through the river. Particulate minerals goethite and kaolinite have been shown to compete with Cu^{2+} ions for sorption sites in *Pseudomonas putida* and *Bacillus thuringiensis* biofilms [19]. As such, it may be possible that flavin secretion also functions to release/“elute” reduced mineral from metal sorption sites of the EPS via chelation [20], freeing the EPS to adsorb oxidized mineral for DMR. In this instance, putative disruption of OmcA_2 at high $[\text{NaCl}]$ or intermediate $[\text{MgCl}_2]$ may be representative of dimer disruption by $\text{Fe}^{2+}/\text{Mn}^{2+}$ and other mineral turnover products.

Of the four solution-structure techniques used to determine the MW_{app} of eOmcA, two techniques identify putative eOmcA oligomers, and two indicate eOmcA is a monomer under the experimental conditions tested. The limited dimer interfacial surface area in the eOmcA crystal structure correlates with inconsistent solution-structure data, in the context of a salt-sensitive OmcA dimerization-working model. As such monomeric OmcA is the most likely biological unit that exists at the outer membrane of *S. oneidensis* MR-1. In this model, the oligomeric MW_{app} determined for eOmcA via AGFC is an artefact of the experiment. The AGFC column would thus interact with monomeric eOmcA in a manner inhibited by an increase in NaCl or MgCl_2 concentration. This is indicative of a repulsive electrostatic interaction, where eOmcA monomers are titrated into the AGFC column void volume with decrease in salt concentration. Exposed polar groups of the AGFC column and eOmcA charged surface residues would be neutralised in the presence of salt. As such, the conclusion from this study is that OmcA exists exclusively as a monomer in solution. However, as discussed, the crystal structure of eOmcA may hold cues to OmcA quaternary structure interactions observed in other studies [2], and AGFC data presented here may indicate that these interactions are promoted in the presence of polysaccharide such as EPS or AGFC column matrix.

References.

- 1 Rupp, B. (2010) Biomolecular Crystallography: Principles, Practice, and Application to Structural Biology. Garland Science
- 2 Shi, L., Chen, B. W., Wang, Z. M., Elias, D. A., Mayer, M. U., Gorby, Y. A., Ni, S., Lower, B. H., Kennedy, D. W., Wunschel, D. S., Mottaz, H. M., Marshall, M. J., Hill, E. A., Beliaev, A. S., Zachara, J. M., Fredrickson, J. K. and Squier, T. C. (2006) Isolation of a high-affinity functional protein complex between OmcA and MtrC: Two outer membrane decaheme c-type cytochromes of *Shewanella oneidensis* MR-1. *Journal of Bacteriology*. **188**, 4705-4714
- 3 Edwards, M. J., Baiden, N. A., Johs, A., Tomanicek, S. J., Liang, L., Shi, L., Fredrickson, J. K., Zachara, J. M., Gates, A. J., Butt, J. N., Richardson, D. J. and Clarke, T. A. (2014) The X-ray crystal structure of *Shewanella oneidensis* OmcA reveals new insight at the microbe-mineral interface. *Febs Letters*. **588**, 1886-1890
- 4 Ricker, R. D. and Sandoval, L. A. (1996) Fast, reproducible size-exclusion chromatography of biological macromolecules. *Journal of Chromatography A*. **743**, 43-50
- 5 Hong, P., Koza, S. and Bouvier, E. S. P. (2012) A review Size-Exclusion Chromatography for the analysis of protein biotherapeutics and their aggregates. *Journal of Liquid Chromatography & Related Technologies*. **35**, 2923-2950
- 6 Johs, A., Shi, L., Droubay, T., Ankner, J. F. and Liang, L. (2010) Characterization of the Decaheme c-Type Cytochrome OmcA in Solution and on Hematite Surfaces by Small Angle X-Ray Scattering and Neutron Reflectometry. *Biophysical Journal*. **98**, 3035-3043
- 7 Myers, C. R. and Myers, J. M. (2002) MtrB is required for proper incorporation of the cytochromes OmcA and OmcB into the outer membrane of *Shewanella putrefaciens* MR-1. *Applied and Environmental Microbiology*. **68**, 5585-5594
- 8 Hartshorne, R. S., Jepson, B. N., Clarke, T. A., Field, S. J., Fredrickson, J., Zachara, J., Shi, L., Butt, J. N. and Richardson, D. J. (2007) Characterization of *Shewanella oneidensis* MtrC: a cell-surface decaheme cytochrome involved in respiratory electron transport to extracellular electron acceptors. *Journal of Biological Inorganic Chemistry*. **12**, 1083-1094
- 9 Hartshorne, R. S., Reardon, C. L., Ross, D., Nuester, J., Clarke, T. A., Gates, A. J., Mills, P. C., Fredrickson, J. K., Zachara, J. M., Shi, L., Beliaev, A. S., Marshall, M. J., Tien, M., Brantley, S., Butt, J. N. and Richardson, D. J. (2009) Characterization of an electron conduit between bacteria and the extracellular environment. *Proceedings of the National Academy of Sciences of the United States of America*. **106**, 22169-22174
- 10 Eggleston, C. M., Voros, J., Shi, L., Lower, B. H., Droubay, T. C. and Colberg, P. J. S. (2008) Binding and direct electrochemistry of OmcA, an outer-membrane cytochrome from an iron reducing bacterium, with oxide electrodes: A candidate biofuel cell system. *Inorganica Chimica Acta*. **361**, 769-777
- 11 Lower, B. H., Shi, L., Yongsunthorn, R., Droubay, T. C., McCready, D. E. and Lower, S. K. (2007) Specific bonds between an iron oxide surface and outer membrane cytochromes MtrC and OmcA from *Shewanella oneidensis* MR-1. *Journal of Bacteriology*. **189**, 4944-4952
- 12 Wuenschell, G. E., Naranjo, E. and Arnold, F. H. (1990) Aqueous 2-phase metal affinity extraction of heme-proteins. *Bioprocess Engineering*. **5**, 199-202

- 13 Raize, O., Argaman, Y. and Yannai, S. (2004) Mechanisms of biosorption of different heavy metals by brown marine macroalgae. *Biotechnology and Bioengineering*. **87**, 451-458
- 14 Cakic, M., Mitic, Z., Nikolic, G. S., Ilic, L. and Nikolic, G. M. (2008) The investigations of bioactive copper(II) complexes with reduced low-molar dextran. *Spectroscopy-an International Journal*. **22**, 177-185
- 15 McCarthy, J. T., Regnier, C. E., Loebertmann, C. L. and Bergstralh, E. J. (2000) Adverse events in chronic hemodialysis patients receiving intravenous iron dextran - A comparison of two products. *American Journal of Nephrology*. **20**, 455-462
- 16 Stukalov, O., Korenevsky, A., Beveridge, T. J. and Dutcher, J. R. (2008) Use of atomic force microscopy and transmission electron microscopy for correlative studies of bacterial capsules. *Applied and Environmental Microbiology*. **74**, 5457-5465
- 17 Vu, B., Chen, M., Crawford, R. J. and Ivanova, E. P. (2009) Bacterial Extracellular Polysaccharides Involved in Biofilm Formation. *Molecules*. **14**, 2535-2554
- 18 Freeman, C., Chapman, P. J., Gilman, K., Lock, M. A., Reynolds, B. and Wheeler, H. S. (1995) Ion-exchange mechanisms and the entrapment of nutrients by river biofilms. *Hydrobiologia*. **297**, 61-65
- 19 Fang, L., Cai, P., Li, P., Wu, H., Liang, W., Rong, X., Chen, W. and Huang, Q. (2010) Microcalorimetric and potentiometric titration studies on the adsorption of copper by *P. putida* and *B. thuringiensis* and their composites with minerals. *Journal of Hazardous Materials*. **181**, 1031-1038
- 20 Albert, A. (1953) Quantitative studies of the avidity of naturally occurring substances for trace metals .3. Pteridines, riboflavin and purines. *Biochemical Journal*. **54**, 646-654

Chapter 5: Spectropotentiometric Studies of OmcA using EPR

5.1 – Introduction

5.1.1 – Paramagnetic Resolution of c-type Haems to Characterise OMMCs

Chapter 2 detailed how the oxidation state of OmcA's haems affect its UV-Vis spectrum. Previously this behaviour has been used to monitor a potentiometric titration of OmcA from *S. frigidimarina* NCIMB400 [1]. However it is evident that all haems contribute to the single absorbance feature monitored (i.e. $A_{552\text{ nm}}$), a consequence of the absorbance being produced by charge-transfer events arising from a $\pi \rightarrow \pi^*$ transition at each of the 10 c-type haems [2]. As such the structural insights gained from the X-ray crystal structure of OmcA (from *S. oneidensis* MR-1; Chapter 3) do not enhance interpretation of previous UV-Vis potentiometric data, because the haems are spectroscopically indistinguishable using this method.

Electron Paramagnetic Resonance (EPR) spectroscopy provides much greater spectral resolution of the OmcA haems; at least 5 different resonance features are resolved in the (as prepared) oxidised spectra of OmcA (Fig. 2.4). The spectral resolution of identical c-type haem cofactors in OmcA is based on EPR measuring the resonance of a given haem's unpaired electron(s). The spin state of the haem iron ion is dependent on the strength of the ligand field in comparison to the energy required for the iron's valence electrons to populate all 5 haem d orbitals. A weak crystal field typical of penta-coordinate haem leaves all 5 d orbitals with the same energy, (i.e. the d orbitals are degenerate). In this instance the electrons populate all of the degenerate orbitals according to Hund's rule. As such in a weak crystal field, ferric haem iron has a spin state, $S = \frac{5}{2}$, referred to as high-spin (Fig. 5.1). The spin state of ferrous high-spin haem is $S = 2$, and because it is diamagnetic the haem displays no paramagnetic resonance. The strong ligating field enforced by *bis*-histidine ligation splits the degenerate d orbitals into the t_{2g} and e_g orbital populations, resulting in a low-spin state (i.e. $S = \frac{1}{2}$; Fig. 5.1). The diamagnetic spin state of ferrous low-spin haem, $S = 0$, means reduced haem (high-spin or low-spin) displays no paramagnetic resonance. The unpaired electron resonance measured by EPR is sensitive to a haem's molecular environment. As such resonance from multiple haems populate different EPR signals based on their unique molecular environment.

	Weak Ligand Field		Strong Ligand Field	
	High-spin: $S = \frac{5}{2}$		Low-spin: $S = \frac{1}{2}$	
Spin state:				
Haem Iron (III) valence orbital energy:				
Ligand Field effect:	Strong Axial Distortion		Axial Distortion	Rhombic Distortion
Example Haem Ligation:				
Conceptual Resonance Shape:	$g_x = g_y < g_z$ 		$g_x = g_y > g_z$ 	$g_x \neq g_y \neq g_z$

Fig. 5.1 – **The Effect of Ligation on Ferric Haem Spin State.** In the context of haem ligation in OmcA, penta-coordinate and *bis*-histidine haem ligation is depicted below with corresponding valence orbital relative energy. Note, all 5 d orbitals in the weak ligand field are degenerate. Dashed lines indicate splitting of orbital degeneracy as a function of ligand field strength. The magnitude of haem resonance in Cartesian coordinate components g_x , g_y and g_z is depicted in “Conceptual Resonance Shape”. In “Example Haem Ligation” pentagons depict imidazole haem ligands. Table adapted from [2] and [3].

Haem resonance is differentiated by g value, a microwave frequency-independent constant value that indicates resonance feature position. Specific experiments are required to determine the sample's Cartesian components of a given resonance feature, which is further complicated considering the multiple orientations of resonating haems within the decahaem OmcA in solution. As such the microwave absorbance detected is the average resonance of randomly oriented sample molecules. A derivative of the sample's microwave absorbance is measured, facilitating identification of resonance features. Low-spin ferric haem typically has rhombic distortion to its ligand field. This increases orbital degeneracy (Fig. 5.1), which produces a “rhombic trio” derivative spectrum, with positive, bi-signate and negative peaks (Fig. 5.2).

Haem-ligating amino acid side chains/solvent/substrate have been well documented to dictate the g value of a haem's EPR signal [2, 4, 5]. The 10 haems of OmcA have been experimentally determined as *bis*-histidine ligated via NIR-MCD (Section 2.2) and X-ray crystallography (Section 3.2). In the context of *bis*-histidine ligated haem, histidine charge and *bis*-imidazole plane dihedral angle (i.e. φ) affect haem resonance, and consequently g value (Fig. 5.3). Haem ligated with near-parallel *bis*-imidazole planes (e.g. Fig. 5.3C) produces resonance where $3.0 \geq g_1 > 2.9$ (Fig. 5.3D) [6]. According to previous OMMC-EPR nomenclature on MtrF, this signal has been referred to as Low-Spin 1 (i.e. LS1) [7]. Haems ligated by near-perpendicular imidazole groups (e.g. Fig. 5.2B) produce EPR signal with enhanced “rhombic” nature (i.e. larger $g_{1-3} = g_1 - g_3$ value), with $3.7 \geq g_1 \geq 3.1$ (Fig. 5.3D) [6]. Paramagnetic resonance in the range of $3.7 \geq g_1 \geq 3.1$ has been referred to as Large g_{\max} (i.e. LGM) [7]. Deprotonation of a haem-ligating histidine N_δ produces a diagnostic signal, previously referred to as Low-Spin 2 (i.e. LS2) [7]. The relatively “axial” LS2 signal, where $2.9 > g_1 > 2.8$ (Fig. 5.3D), has a $g_{1-3}(\text{LS2}) < g_{1-3}(\text{LS1})$ [8]. In the EPR spectra of OmcA (Section 2.2) there are two populations of LGM signals (i.e. LGM1 and LGM2), and a highly axial LS3 resonance feature. The g values of a low-spin c-type (ferric) haem are distributed such that $\sum_{i=1}^3 g_i^2 = 16.0$ [2, 3], and so decrease in g_1 causes concomitant increase in g_2 and/or g_3 value, affecting g_{1-3} values.

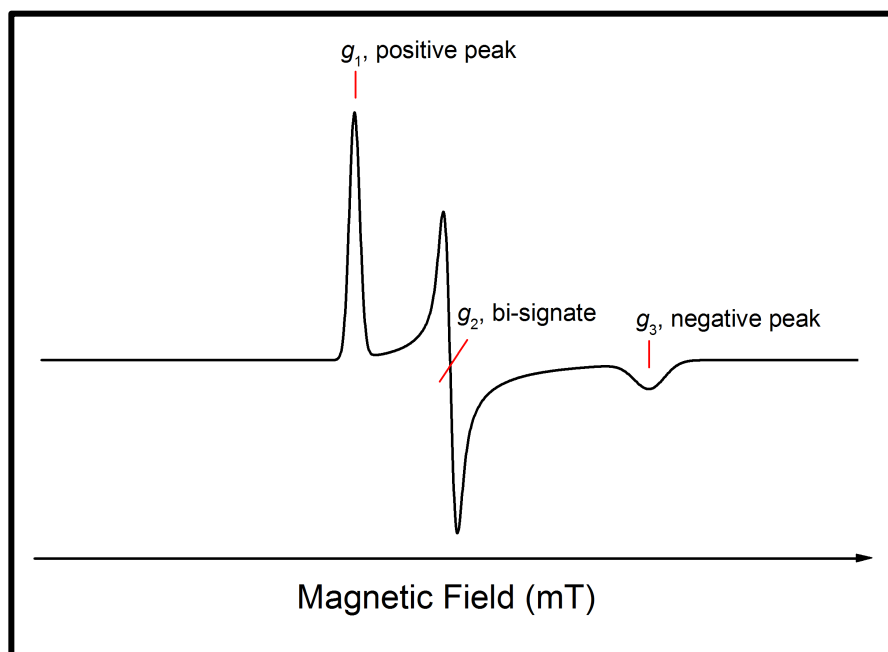


Fig. 5.2 – **The Nature of Low-Spin, Rhombic Haem Paramagnetic Resonance.** The lineshape of a “rhombic trio”, the 1st derivative of microwave absorbance resonance features that is typical of a low-spin ferric haem. The g value breadth is variable.

The major benefit of using EPR to study OMMCs is the spectroscopic resolution of multiple haems within a cytochrome based on differential molecular environments of the c -type haems. As such, the haem content of OMMCs can be spectroscopically resolved according to oxidation state and molecular environment in a potentiometric titre. This can provide a basis of assigning redox active windows to haem populations with particular structural components.

The EPR data presented in Section 2.2 indicates that OmcA (all forms isolated) produces several paramagnetic resonance features, which is expected for a decahaem cytochrome, and has been reported for OmcA previously [1, 9]. Furthermore, there is no spectroscopic or crystallographic evidence for high-spin (i.e. penta-coordinate) haem in any isolated form of OmcA, nor any detectable $g_{\perp} \approx 6.0$ EPR signal in eOmcA at the pH range tested (Section 2.2), in contrast with a previous publication [9]. Experimental data presented in this chapter is a potentiometric titration of eOmcA, including spectral simulation and spin quantitation.

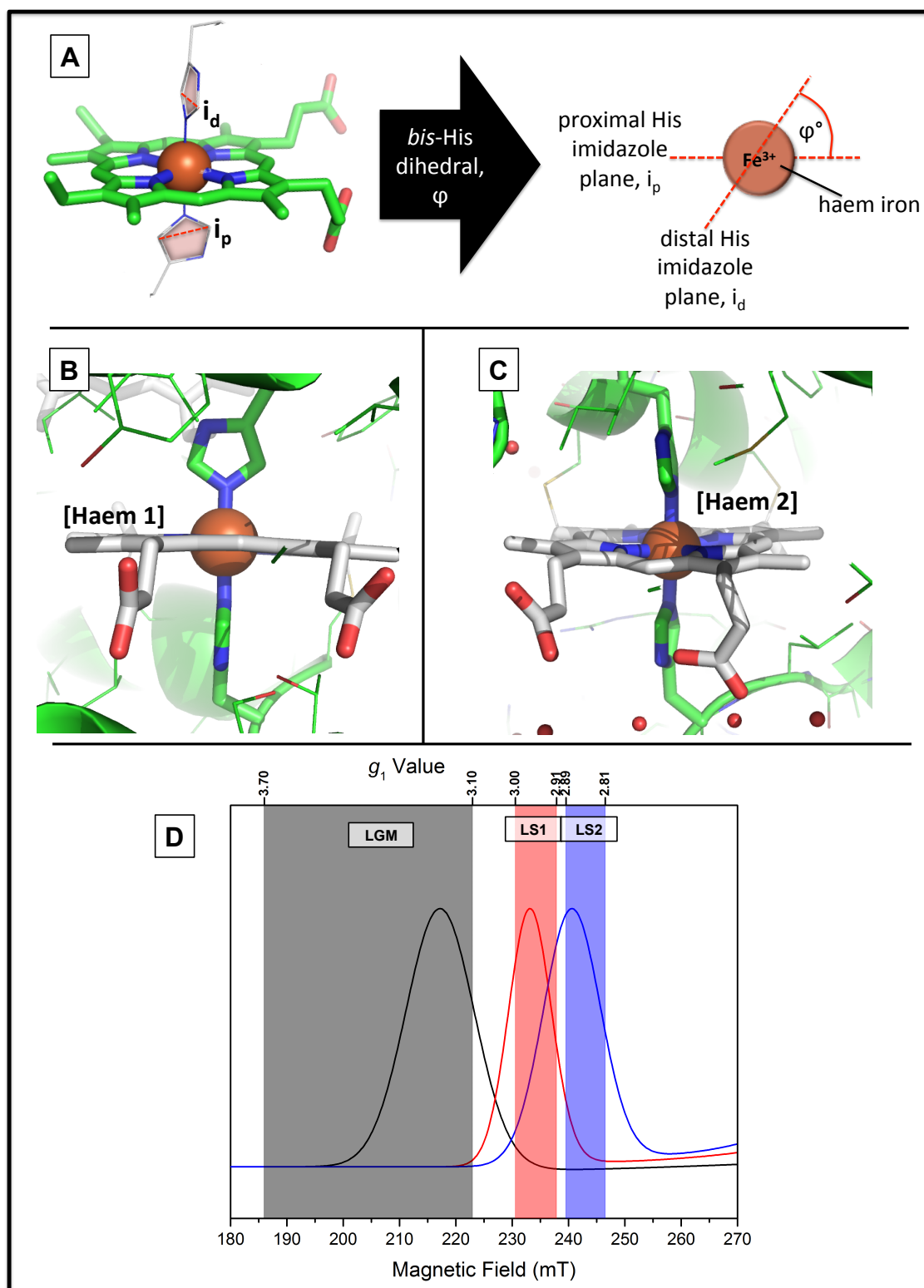


Fig. 5.3 – **Determination of the *bis*-histidine dihedral (φ) angle and examples in eOmca.** (A) The angle between a haem's proximal and distal histidine imidazole planes (i.e. i_p and i_d respectively). (B) Haem 1 of eOmca has an average $\varphi = 68^\circ$. (C) Haem 2 of eOmca has an average $\varphi = 12^\circ$. (D) Comparison of common *bis*-histidine *c*-type haem ligations on the nature of EPR signals. Perpendicular histidine imidazole planes produce a Large g_{\max} (LGM) signal and parallel histidine imidazole planes produce the relatively axial signal (labelled Low Spin 1: LS1). Imidazolate ligated-haem produces a signal of greater axial resonance (LS2). Signal nomenclature from the EPR spectrum of MtrF [7].

5.2 – Results

5.2.1 – An Overview of the *EPR-monitored Potentiometric Titration of eOmcA*

Potentiometric titration of 145 μM eOmcA was performed using chemical titrants (see Section M.4) in an anaerobic glovebox. Equimolar samples of eOmcA, poised at the listed reduction potentials (Fig. 5.4), were frozen in $\text{N}_2(l)$ before EPR measurements were recorded. Equilibration of protein with target sample potential was achieved using redox mediators (listed in Section M.4).

The potentiometric redox titre samples of eOmcA were measured under identical spectrometer and sample conditions (Section M.4). The EPR spectra of eOmcA across the potentials measured (i.e. +0.20 V to -0.42 V vs S.H.E.) show that there is no evidence of detectable $g_{\perp} \approx 6.0$ at any sample redox potential measured (Fig. 5.4). All resonance features observed during the titre appear to be similar to those observed in the EPR spectra reported of air-oxidised samples reported in Section 2.2. It is concluded that there is no high-spin haem content, only low-spin ferric haem produced resonance features during redox transformation of eOmcA.

Preliminary analysis of signal intensity via assessment of g_1 peak height shows that the haems producing the different signals monitored have different redox behaviour (Fig. 5.5). The LS3 signal (i.e. $g_{1\text{app}} \approx 2.60$) is detectable until sample potential < -0.10 V vs S.H.E., whereas LGM1 resonance (i.e. $g_{1\text{app}} = 3.58$) loses detectable intensity below -0.30 V vs S.H.E. (Fig. 5.5). The inflexion in the LGM1 signal intensity apparent at -0.10 V vs S.H.E. indicates multi-component resonance produced by multiple haems in eOmcA. Furthermore, resolution of the sample potential-dependence of various signal intensities supports the model that different haem populations produce these signals. However, further data interpretation requires simulation of the individual EPR signals.

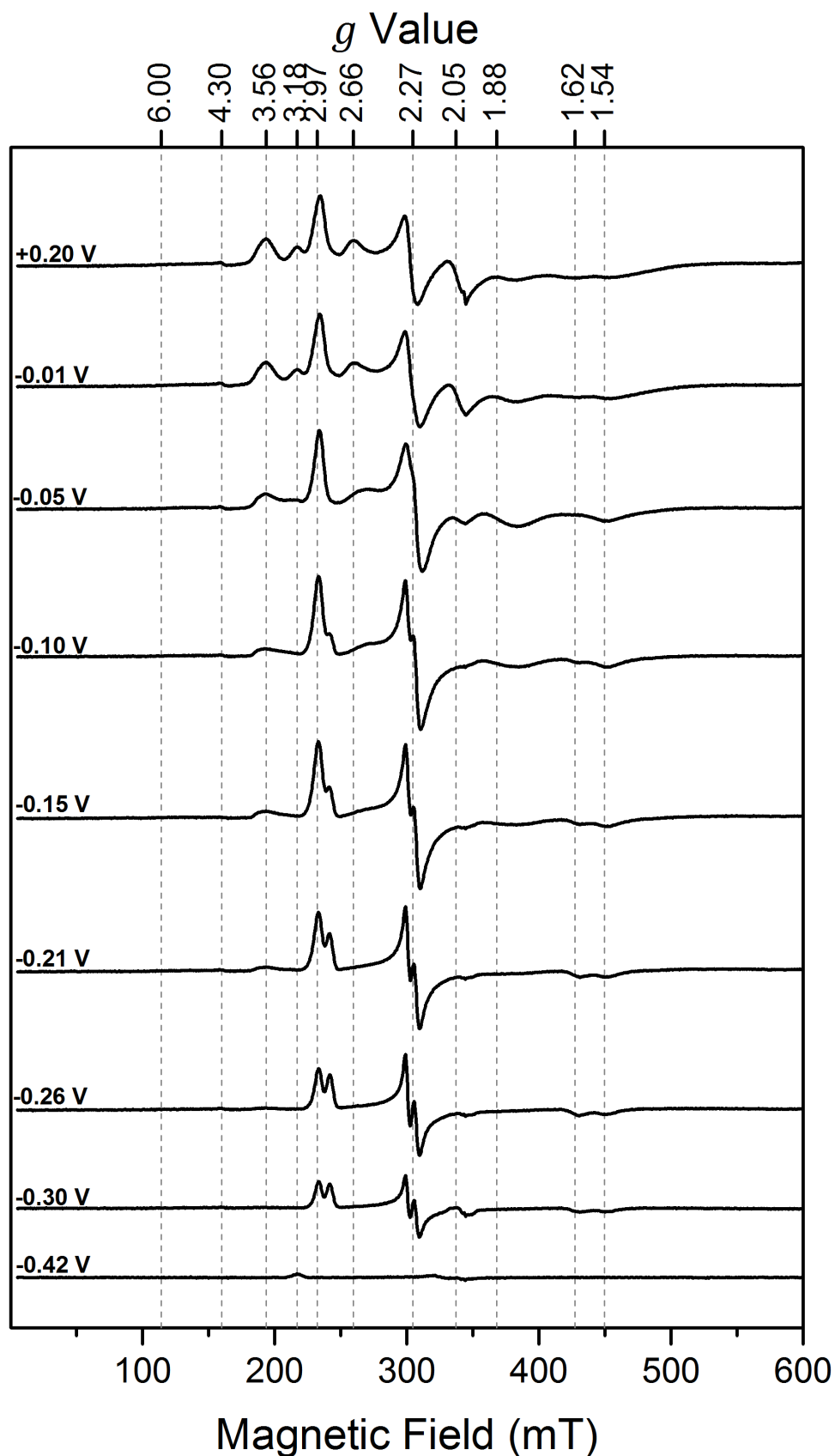


Fig. 5.4 – **EPR-monitored potentiometric titration of eOmcA.** eOmcA (145 μM) was poised at the potentials listed and EPR spectra measured. EPR spectra were measured at 9.688 GHz, 7 ± 2 K, 2.012 mW. eOmcA was in 20 mM HEPES, pH 7.60, 50 mM NaCl, 0.01% CHAPS, 1% glycerol.

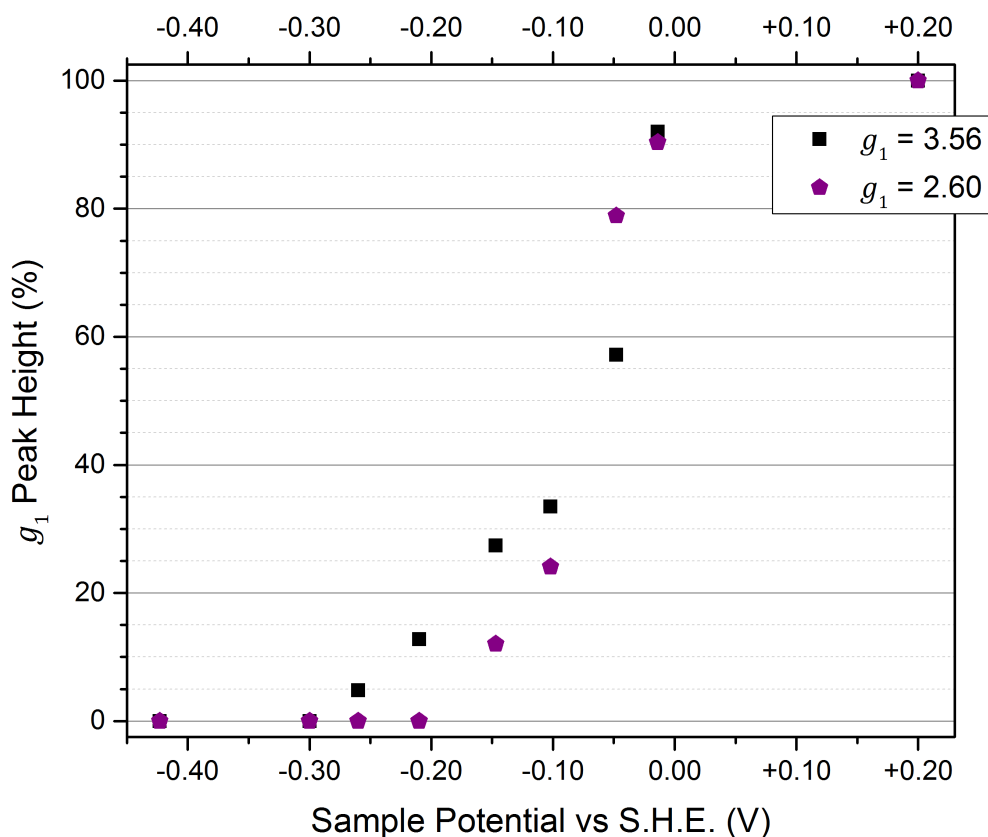


Fig. 5.5 – **The Dependence of eOmCA EPR Signal Intensity on Sample Potential.** EPR signals assessed are LGM1 (i.e. $g_{1app} = 3.56$) and LS3 (i.e. $g_{1app} = 2.60$). Signal intensity is determined by g_1 peak height.

5.2.2 – Simulation of eOmCA's EPR Signals

The potentiometric redox titres of eOmCA measured under identical conditions (Fig. 5.4) were simulated using WinEPR (ver. 1.25, Bruker Analytische Messtechnik GmbH). Determining the g values of each haem signal's rhombic trio was the first step to simulating each spectrum. The lineshape of each g value was modelled by assessing the Field Strength width of each g value (in Gauss). Each resonance feature is simulated separately. The individual contributions are summed and simulation quality is then assessed by analysis of the residual spectrum and simulation parameters are adjusted in an iterative manner until there is negligible residual resonance signal. As introduced, the guiding principle of $\sum_{i=1}^3 g_i^2 = 16.0$ for low-spin haem informs the determination of g values amongst compound linesapes.

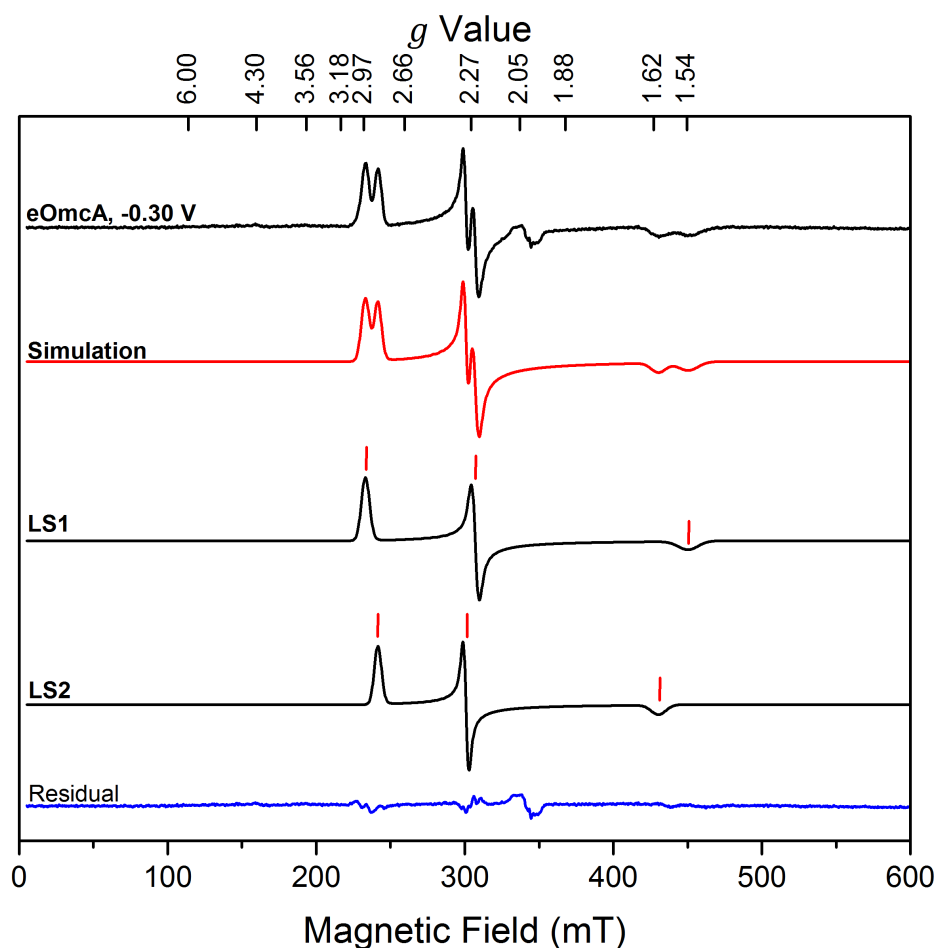


Fig. 5.6 – **The Simulation of eOmcA's -0.30 V vs S.H.E. EPR spectrum.** Simulation (red) of the measured spectrum (black) is a summation of the resonance feature simulations listed below (black). The g values of each signal are marked (in order of g_1, g_2, g_3 with increasing Magnetic Field) with red markers on each signal simulation and compiled in Table 5.1. Residual spectrum (blue) = measured spectrum – spectrum simulation.

Table 5.1 – **The g values of eOmcA poised at -0.30 V vs S.H.E..** The g value lineshape is modelled by Field Strength width of g value (in Gauss), listed below respective g value.

EPR Signal	Signal g values			$\sum_{i=1}^3 g_i^2$
	g_1	g_2	g_3	
LS1	2.970	2.285	1.544	16.34
<i>lineshape (Gauss)</i>	54.0	43.0	135.0	
LS2	2.874	2.280	1.608	16.04
<i>lineshape (Gauss)</i>	48.0	32.0	100.0	

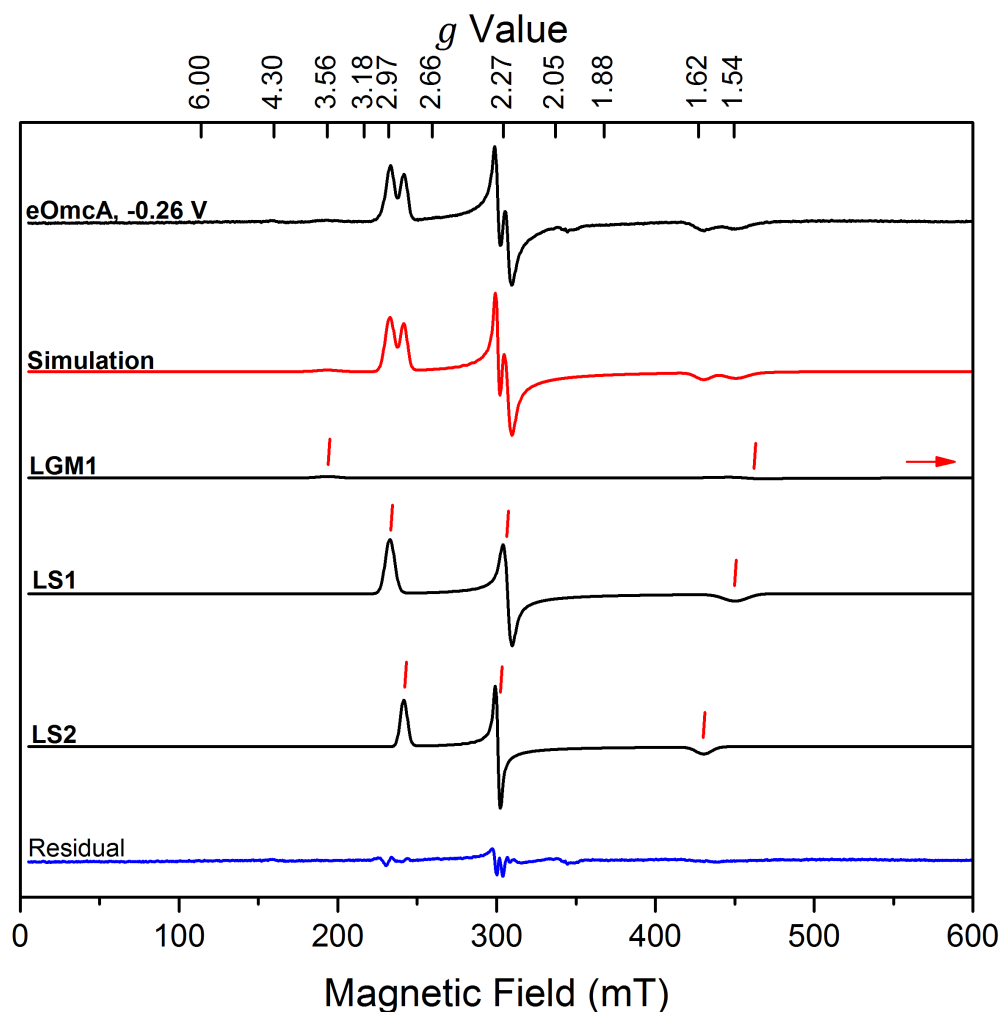


Fig. 5.7 – **The Simulation of eOmcA's -0.26 V vs S.H.E. EPR spectrum.** Simulation (red) of the measured spectrum (black) is a summation of the resonance feature simulations listed below (plotted individually, lower, black). The g values of each signal are marked (in order of g_1, g_2, g_3) with red markers on each signal simulation and compiled in Table 5.2. The estimated g value beyond the magnetic field measured is indicated with a red arrow.

Table 5.2 – **The g values of eOmcA poised at -0.26 V vs S.H.E..**

EPR Signal	Signal g values			$\sum_{i=1}^3 g_i^2$
	g_1	g_2	g_3	
LGM1	3.576	1.515	1.020	16.12
<i>lineshape (Gauss)</i>	130.0	180.0	200.0	
LS1	2.975	2.256	1.537	16.30
<i>lineshape (Gauss)</i>	58.0	45.0	150.0	
LS2	2.867	2.302	1.608	16.11
<i>lineshape (Gauss)</i>	44.0	25.0	100.0	

The approach to simulating the measured EPR spectra of the eOmcA titration was to simulate the simplest EPR spectrum first (i.e. eOmcA at -0.30 V vs S.H.E.; Fig. 5.6). The rhombic trios identified at this sample potential were $g_{1,2,3} = 2.97, 2.29, 1.54$ (i.e. LS1) and $g_{1,2,3} = 2.87, 2.28, 1.61$ (i.e. LS2, see Table 5.1). Small changes in g value and rhombic trio linewidth were consistently employed to account for all spectral features. These signal parameters informed simulation of the -0.26 V EPR spectrum (Fig. 5.7, core simulation parameters in Table 5.2). In addition to LS1 and LS2 signals, an LGM1 contribution is also required to fully account for all spectral features at -0.26 V (Fig. 5.7; Table 5.2). In accordance with the $\sum_{i=1}^3 g_i^2 = 16.0$ rule for low-spin c -type haem, the g_3 peak of the LGM1 signal was estimated to be outside the magnetic field that was measured.

The signal parameters from the -0.26 V spectrum informed the simulation of the -0.21 V spectrum (not shown). Amplification of the simulated signals of the -0.26 V LGM1, LS1 and LS2 resonances was sufficient to reproduce the spectrum measured. The spectrum at -0.15 V, contained the additional LGM2 and LS3 resonance signals (Fig. 5.8; Table 5.3), and these signals informed the simulation of the remaining spectra, including +0.20 V (Fig. 5.9; Table 5.4). As such, all resonance features observed in the EPR spectra in the potentiometric titration of eOmcA have been simulated.

Simulation of each spectrum required minor lineshape and g value modification to the rhombic trio parameters of each resonance signal. The LS2 signal shows significant lineshape change during the potentiometric titration (Fig. 5.10). The LS2 lineshape changes the most from -0.01 V to +0.20 V with broadening of the g_2 and g_3 features, but negligible changes in g values. There is also a trend of small LS2 lineshape broadening of $g_{1,2,3}$ with increase in sample potential. It is apparent that the LS3 $\sum_{i=1}^3 g_i^2$ is consistently less than 16.0 (Tables 5.3 and 5.4). The LS3 signal undergoes significantly more lineshape and g value changes, including the presence of two LS3 species at -0.05 V (i.e. LS3-1 and LS3-2, Fig. 5.10B). The LS3-2 signal at -0.05 V has near-identical g values to the LS3 signal observed at -0.15 V, but with a broadened g_2 lineshape. The LS3-2 resonance is absent from potentials above -0.05 V, and the LS3-1 resonance g values and lineshape first observed at -0.05 V are maintained up until complete eOmcA oxidation at +0.20 V.

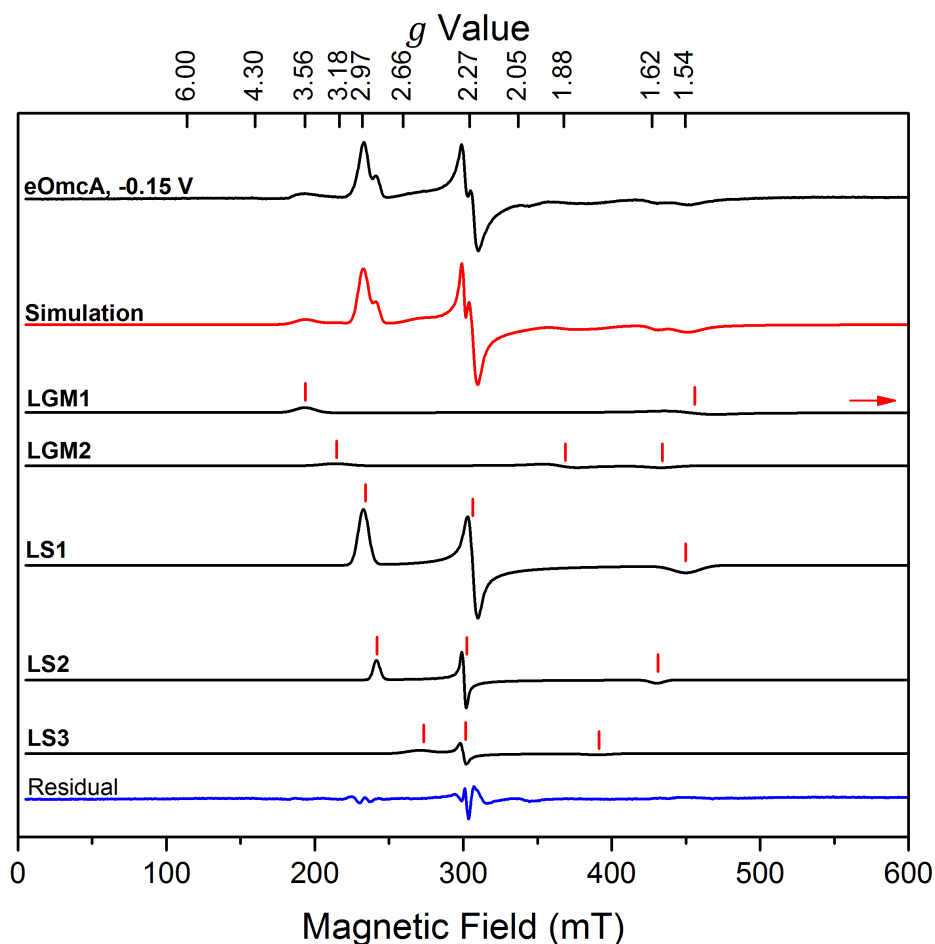


Fig. 5.8 – **The Simulation of eOmCA's -0.15 V vs S.H.E. EPR spectrum.** Simulation (red) of the measured spectrum (black) is a summation of the resonance feature simulations listed below (plotted individually, lower, black). The g values of each signal are marked (in order of g_1, g_2, g_3) with red markers on each signal simulation and compiled in Table 5.3. The estimated g value beyond the magnetic field measured is indicated with a red arrow.

Table 5.3 – **The g values of eOmCA poised at -0.15 V vs S.H.E..**

EPR Signal	Signal g values			$\sum_{i=1}^3 g_i^2$
	g_1	g_2	g_3	
LGM1	3.576	1.53	1.020	16.17
<i>lineshape (Gauss)</i>	130.0	270.0	400.0	
LGM2	3.235	1.895	1.595	16.60
<i>lineshape (Gauss)</i>	120.0	180.0	180.0	
LS1	2.976	2.26	1.537	16.33
<i>lineshape (Gauss)</i>	69.0	54.0	180.0	
LS2	2.867	2.304	1.608	16.11
<i>lineshape (Gauss)</i>	44.0	23.0	90.0	
LS3	2.57	2.31	1.77	15.07
<i>lineshape (Gauss)</i>	160.0	30.0	150.0	

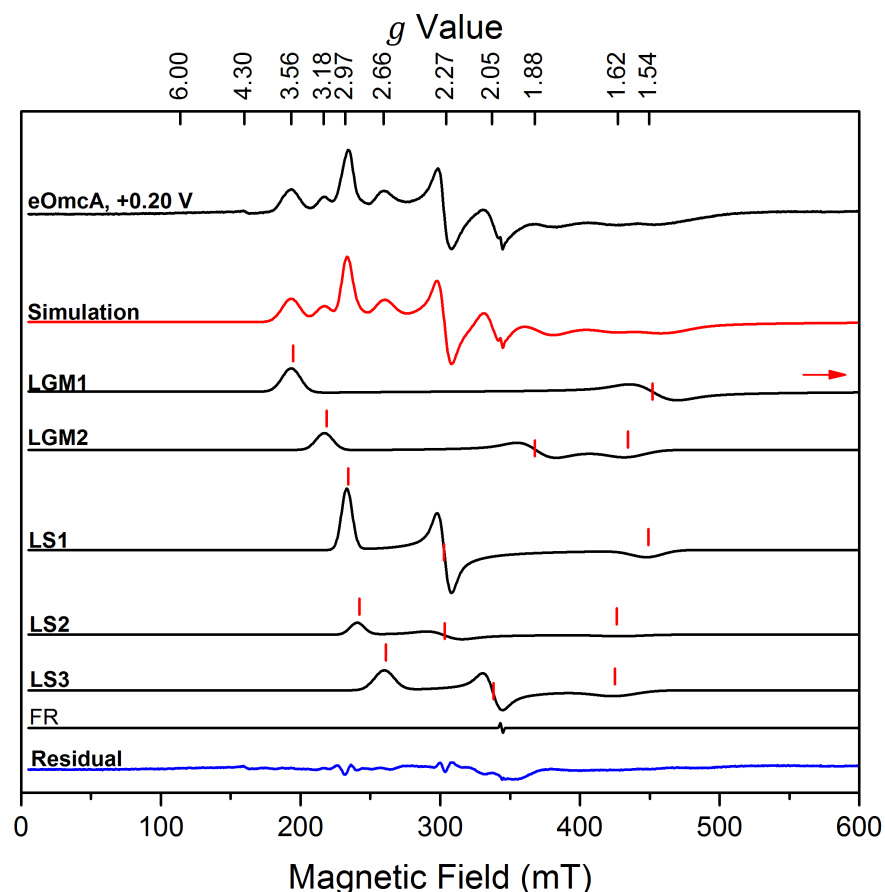


Fig. 5.9 – **The Simulation of eOmcA's Oxidised EPR spectrum.** Simulation (red) of the measured spectrum (black) is a summation of the resonance feature simulations listed below (plotted individually, lower, black). The g values of each signal are marked (in order of g_1 , g_2 , g_3) with red markers on each signal simulation and compiled in Table 5.4. The estimated g value beyond the magnetic field measured is indicated with a red arrow. FR is the simulation of free radical signal observed; $g = 2.00$.

Table 5.4 – **The g values of eOmcA poised at +0.20 V vs S.H.E..**

EPR Signal	Signal g values			$\sum_{i=1}^3 g_i^2$
	g_1	g_2	g_3	
LGM1	3.576	1.530	1.020	16.17
<i>lineshape (Gauss)</i>	130.0	270.0	400.0	
LGM2	3.182	1.875	1.595	16.22
<i>lineshape (Gauss)</i>	120.0	220.0	264.0	
LS1	2.970	2.285	1.544	16.43
<i>lineshape (Gauss)</i>	75.0	80.0	220.0	
LS2	2.874	2.280	1.608	16.04
<i>lineshape (Gauss)</i>	100.0	200.0	300.0	
LS3	2.658	2.045	1.620	13.87
<i>lineshape (Gauss)</i>	140.0	110.0	300.0	

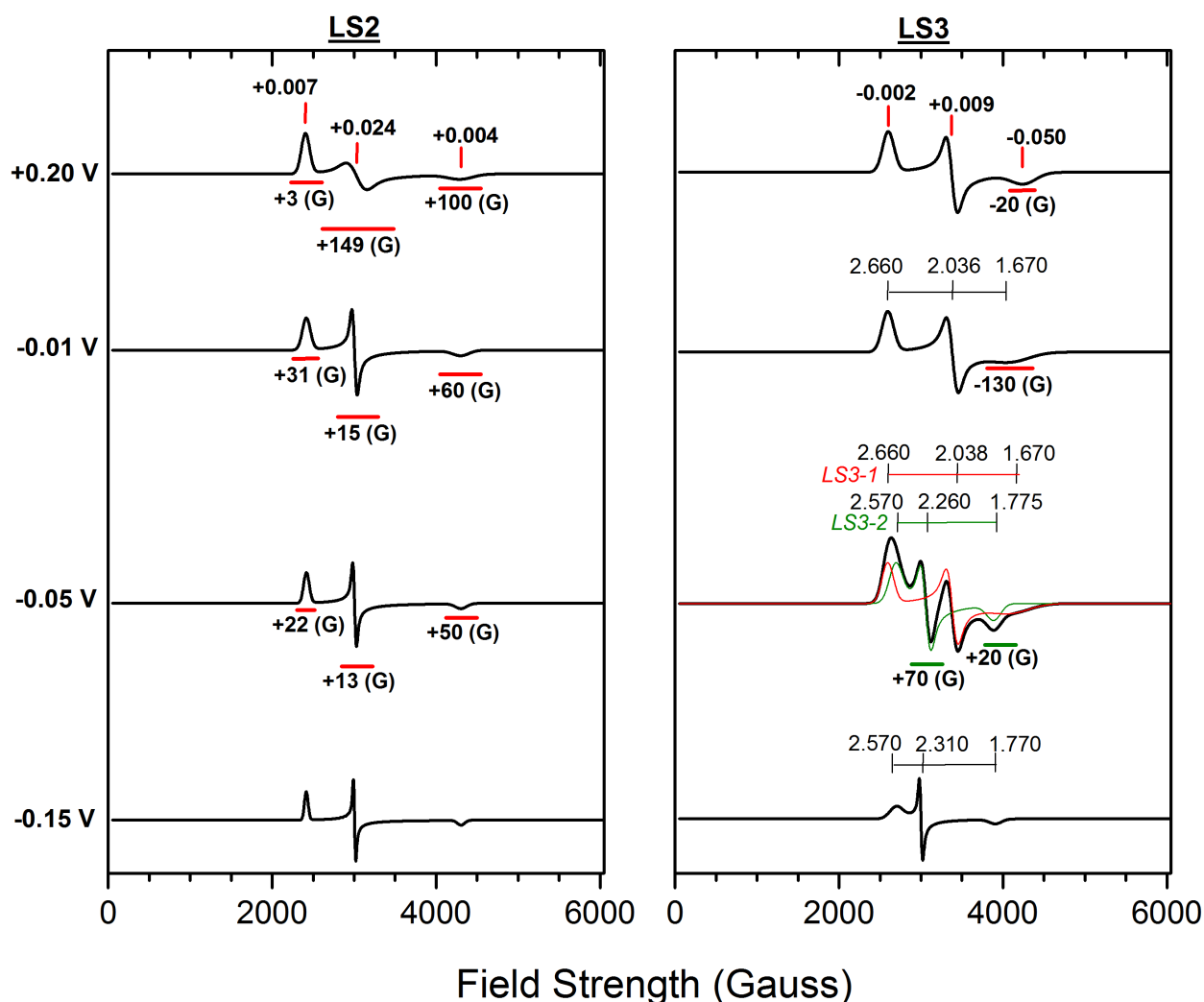


Fig. 5.10 – **The variable lineshapes in eOmCA’s EPR Potentiometric Titration.** The variable lineshapes and Δg of (A) LS2 and (B) LS3 EPR signals at the sample potentials listed. All signals are normalized for comparison. The lineshapes of LS2 below the potentials plotted here maintain near-identical g values and lineshape. EPR signal amplitudes have been normalized for comparison. LS3-1 (red plot) and LS3-2 (green plot) signals are two independent resonance features at -0.05 V that have been modelled as intermediate resonance lineshapes, as the LS3 lineshapes transitions from its form at -0.15 V to +0.20 V.

5.2.3 – Spin Quantitation of eOmca's EPR Redox Titre

Each (low-spin) oxidised c-type haem has 1 unpaired 3d electron, giving it $S = \frac{1}{2}$ (i.e. has a single spin). Spin quantitation of individual resonance features indicates the number of haems producing each resonance feature. As such there are 10 spins expected from spin quantitation of all resonance features per oxidised eOmca molecule. The EPR spectrum of a 1 mM CuSO₄, 10 mM EDTA solution was measured as a spin quantitation external standard (see Section M.4). Pyridine-hemochrome assay of eOmca reveals that its 410 nm molar extinction coefficient, $\epsilon_{410 \text{ nm}} = 1.644 \times 10^3 \text{ mM}^{-1} \text{ cm}^{-1} \pm 30$ (Figure 2.3A). From this the number of paramagnetic spins per eOmca molecule for each signal was quantified (Fig. 5.11A). Cu²⁺-spin standard quantitation shows the fully oxidised spectrum (i.e. at +0.20 V vs S.H.E.) has 10.23 spins per eOmca molecule.

A plot of total spins per eOmca molecule against sample potential suggests that the mid-point potentials of eOmca's haems can be divided into high potential and low potential groups (i.e. 5 haems titrate from -0.05 V to -0.15 V, and the remaining 5 haems titrate from -0.15 V to -0.42 V; Fig. 5.11A). A plot of individual resonance feature spins per eOmca molecule against sample potential shows that LGM2, LS3 and the majority of LGM1 signal contributes to the low potential group of haems whilst LS1, LS2 and a proportion of LGM1 signal contributes to the high potential group of haems. It is apparent that all haems are reduced at -0.42 V, and there is negligible haem oxidation between 0.00 V and +0.20 V (i.e. increase in spins per molecule) indicating eOmca is fully oxidised at +0.20 V.

A plot of individual resonance feature spins per eOmca molecule against sample potential provides the basis to fit the Nernst equation. From the Nernst fit, reduction potentials of paramagnetically resolved haem populations can be derived. As such spin quantitation should provide near-integer values for each signal according to the number of contributing species, which is not the case for eOmca (Fig. 5.11B). As such, assignment of EPR signals to structurally resolved haem populations requires interpretation of results and is addressed in the Discussion Section. Nernst simulation of the EPR-monitored potentiometric titration is therefore addressed in the Discussion (Section 5.3).

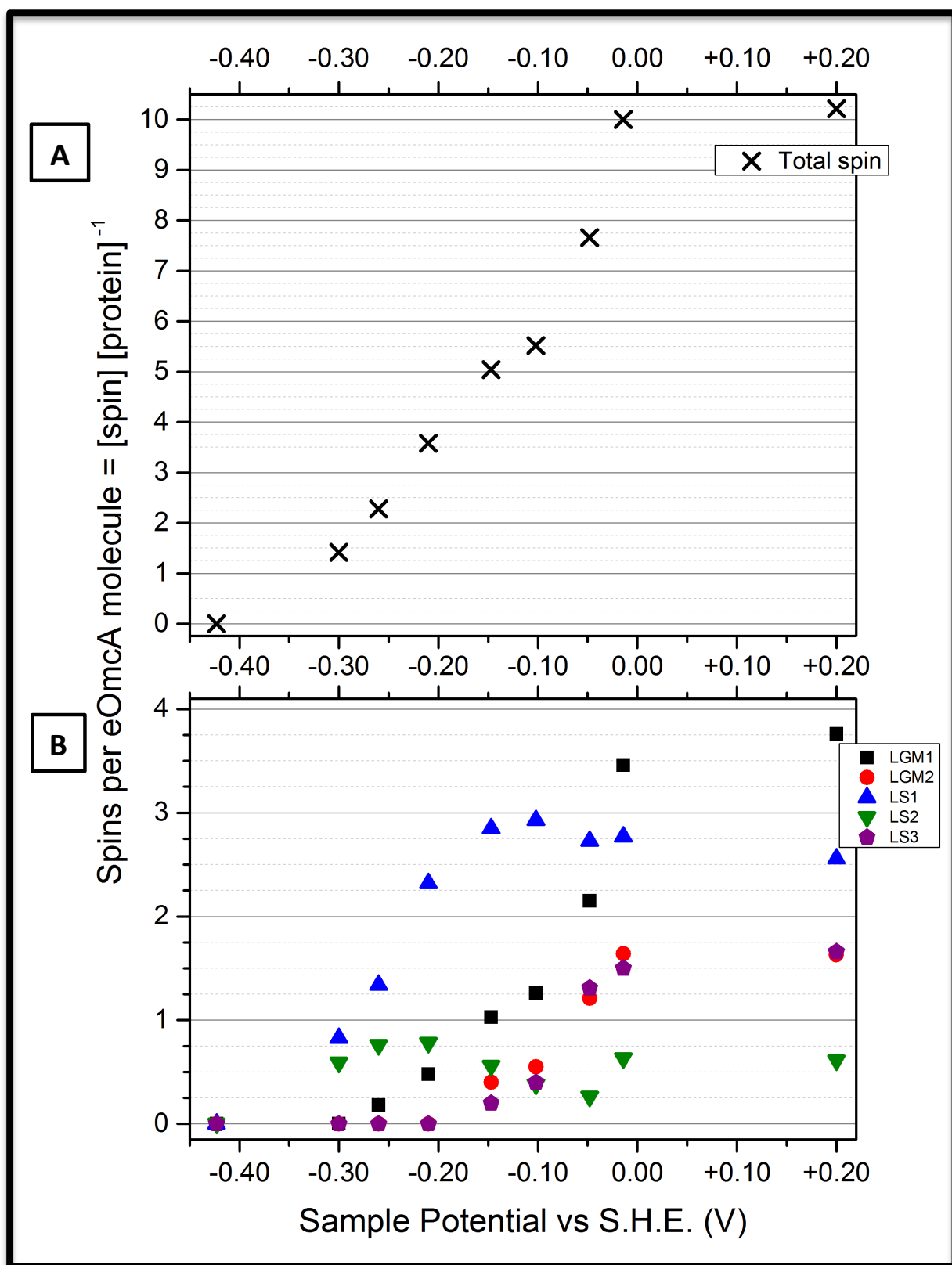


Fig. 5.11 – **Spin Quantitation of eOmca's EPR Resonance Features across Potentiometric Titration.** (A) The total spins per eOmca molecule at each sample potential. The EPR signals of eOmca quantitate to 10.23 spins per eOmca molecule at +0.20 V, and 0.00 spins at -0.42 V. (B) The number of spins quantified per eOmca for each resonance feature, at each sample potential. The LS3 contributions at -0.05 V (i.e. LS3-1 and LS3-2) are combined. Spin quantitation is informed by protein concentration provides oxidised haem per eOmca molecule.

5.3 – Discussion

5.3.1 – Correlating Spin Quantitation with eOmcA Haem Ligation

Correlation between spin quantitation of eOmcA's EPR spectrum and the eOmcA crystal structure is required to attribute resonance signals to specific haem populations. As introduced, *bis*-imidazole dihedral angle, φ , affects haem EPR signal produced [6]. The dihedral angles observed in eOmcA are compiled in Table 5.5. A study correlating g_1 value and φ indicates that LS1 resonance (i.e. $2.9 < g_1 \leq 3.0$) is produced by $\varphi < 30^\circ$, and LGM resonance (i.e. $g_1 > 3.1$) is produced by $\varphi > 45-60^\circ$ [10]. More specifically, LGM resonance can be arbitrarily resolved such that LGM1 signal (i.e. $3.1 < g_1 < 3.3$) originates from $\varphi > 60^\circ$, and LGM2 signal (i.e. $g_1 < 3.3$) originates from $30^\circ < \varphi < 60^\circ$. Assessing eOmcA by this criteria, predicted EPR signal according to φ is in Table 5.5.

The only haem-ligating histidine residue candidate for a de-protonated N_δ atom in the eOmcA structure (which would produce LS2 resonance) is His³⁵⁹ of haem 5. The Ser³⁵⁶ hydroxyl group is 2.5 Å away from the N_δ atom in question. Although the hydroxyl group cannot solely de-protonate the N_δ atom, the proximity of Ser³⁵⁶ to the N_δ atom could putatively stabilise N_δ atom deprotonation by providing steric hinderance. In order for hydrogen bonding to occur between the two residues the His³⁵⁹ N_δ atom needs to be deprotonated to be the hydrogen bond acceptor to Ser³⁵⁶'s hydroxyl group. Furthermore, the His³⁵⁹ N_δ atom must be deprotonated to be within 2.5 Å of Ser³⁵⁶'s hydroxyl group to avoid hydroxyl:hydrogen steric repulsion. The Ser³⁵⁶ hydroxyl group also hydrogen bonds with a H₂O molecule, part of an extensive hydrogen-bonding H₂O network that extends to both proprionate groups of haem 5 and one haem 4 proprionate. The haem proprionates may drive His³⁵⁹ N_δ atom deprotonation that is mediated by the associated network of water molecules (Fig. 5.12). The unfavourable nature for this de-protonation event may explain the sub-stoichiometric quantity of LS2 resonance in oxidised eOmcA and throughout the potentiometric titre. It is also possible that the experimental pH of 7.60 is near the pK_a of the His³⁵⁹ deprotonation event (i.e. within eOmcA).

Table 5.5 – **The Haem-ligating *bis*-histidine Dihedral Angles in the crystal structure of eOmcA.** There are 4 molecules of eOmcA in the asymmetric unit of the crystals from which the structure was solved (i.e. chains A, B, C and D). The *bis*-histidine dihedrals of equivalent haems from each molecule copy were averaged in order to assign EPR signals to specific haems. Haems with resonance features originating from unique structural properties (present in all 4 molecules of eOmcA in the asymmetric unit) are listed under “Putative Unique Ligation”. The origin of the LS3 signal is explored later. Please note that the angles measured are subject to the error of the resolution of the structure (i.e. 2.8 Å). σ = standard deviation.

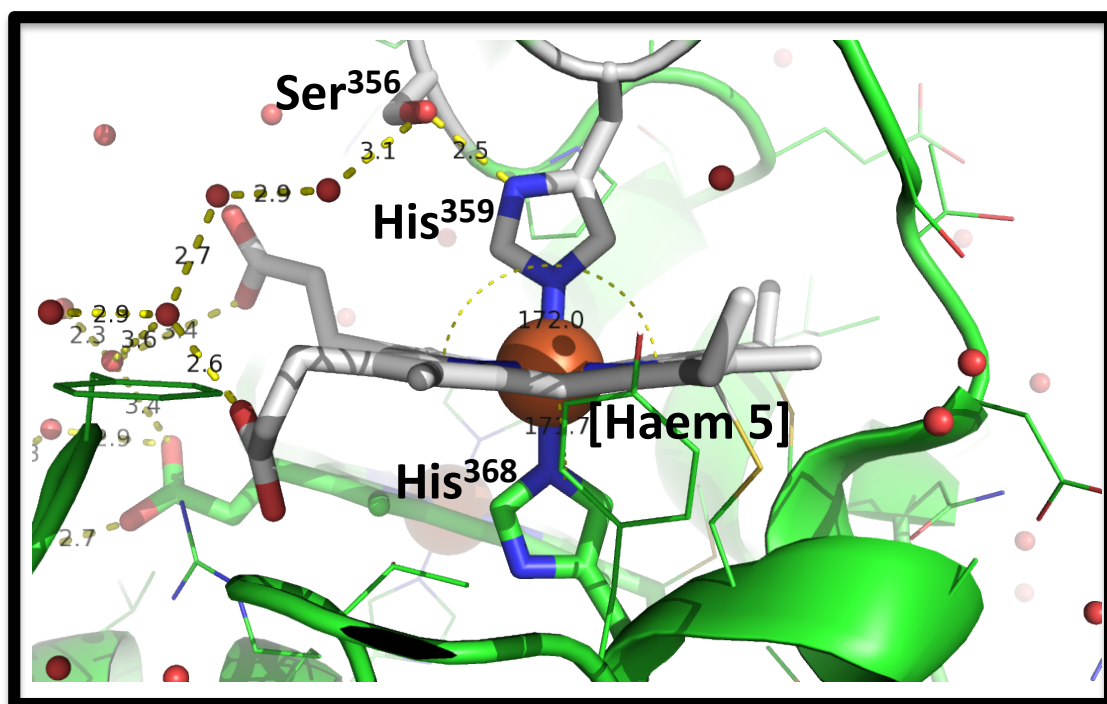
Haem No.	Chain <i>bis</i> -His dihedral, φ (°)				Average <i>bis</i> -His dihedral (°)	σ	Assigned EPR Signal	Putative Unique Ligation
	A	B	C	D				
1	76	49	79	67	68	14	LGM1	-
2	1	30	5	12	12	13	LS1	-
3	75	63	72	76	72	6	LGM1	-
4	7	12	18	16	13	5	LS1	-
5	24	7	30	24	21	10	LS2	Ser ³⁵⁶ :His ³⁵⁹ (2.5 Å)
6	76	74	81	84	79	5	LGM1	-
7	61	41	64	37	51	14	LGM2	-
8	48	38	43	44	43	4	LGM2	-
9	42	48	40	57	47	8	LGM2	-
10	47	74	85	80	72	17	LGM1	-

There is significant agreement between the spin quantitation of the +0.20 V vs S.H.E. spectrum and interpretation of the *bis*-imidazole dihedral angles presented in Table 5.5. It is worth considering that spin quantitation only provides net resonance feature changes. A further complication is that the crystal structure of eOmcA is not of potentiometrically poised protein, but air-oxidised eOmcA.

As discussed, pH has been shown to affect haem molecular environment and cause changes in haem resonance signal. This complicates confidence in attributing air-oxidised molecular environments to haems at pH 8.50 to eOmcA at pH 7.60 that has been equilibrated to +0.20 V vs S.H.E. by potentiometric poisoning. However, as shown by the pH transition of eOmcA from pH 7.60 to 6.60, eOmcA’s haem molecular environment does not always change significantly.

Also, the likelihood of resonance signal quantitation of +0.20 V-poised eOmcA corresponding well to eOmcA’s crystal structure with haem molecular environment changes is low. OmcA is expected to exist in circum-neutral environments (i.e. closest to pH 6.60 [11]); the inferred conformational changes may still be a physiologically

relevant adaptation of the OMMC to temporal pH variance. Also, there is negligible net change in haem molecular environment between air-oxidised eOmca from pH 7.60 to pH 6.60.



5.3.2 – Exploring the Origin of Low Spin 3 Resonance

Consolidating the unique LS3 signal ($g_1 = 2.66$) with the *bis*-histidine haem ligation that is seen in OmcA is complex. Similar g_1 values annotated in the cytochrome literature are produced by anionic or conjugated species ligation of ferric *b* or *c*-type haems (see Table 5.6), aside from the sole example of putative *bis*-histidine coordination in leghaemoglobin ($g_1 = 2.69$ [13]). The publication states “approximately half” of the sample’s haem population exists in the low-spin state (i.e. $g_{1,2,3} = 2.59, 2.24, 1.72$). The crystal structure published of oxidised lupin leghaemoglobin does not display the *bis*-histidine haem ligation population present in the EPR sample measured [14]. NIR-MCD and crystallographic data identify the *bis*-histidine ligation of all eOmcA’s haem content.

The $\sum_{i=1}^3 g_i^2$ (LS3) < 16.0 (i.e. ≈ 14.0), and it is possible that the LS3 signal is produced by the coupled spins of two or more adjacent haems. Although 1.66 LS3 spins have been quantified, the LS3 signal maintains an atypical $\sum_{i=1}^3 g_i^2$ value. Part of signal quantitation involves normalising the signal double-integral to the distribution of g values amongst the magnetic field measured (i.e. g_{av} , see Section M.4), meaning the $\sum_{i=1}^3 g_i^2$ value is incorporated into the normalised double-integral calculation such that:

$$\iint (EPR\ signal)_{Norm} \propto \frac{3}{2 \times \sqrt{\frac{\sum_{i=1}^3 g_i^2}{3}}} \dots \text{Eqn 5.1}$$

(Where $\iint (EPR\ signal)_{Norm}$ = Normalised EPR signal double integral)

As such, a smaller $\sum_{i=1}^3 g_i^2$ value would produce a greater $\iint (EPR\ signal)_{Norm}$ and subsequently a larger LS3 spin quantitation. Whereas the mathematical consideration in Eqn. 5.1 is intended to normalise various resonance features, there may be additional normalisation requirements for the highly axial LS3 resonance because of the signal’s atypical $\sum_{i=1}^3 g_i^2$ value.

Also, inspection of the LS2 and LS3 resonance intensities show reduction of the LS3 resonance population occurs concomitantly with the increase of LS2 spin intensity (Fig. 5.11B). This fits the experimental model where reduction of a higher potential haem component of a coupled haem population (i.e. producing LS3 resonance) decreases spin coupling. In this model the lower potential haem component of the

spin-coupled population is un-coupled and produces a different resonance signal (i.e. LS2 resonance).

Whereas there is no LS3 resonance in the EPR spectrum of MtrF, spin-coupling is attributed to quantitation of ≈ 8 spins per oxidised protein, suggesting loss of detected resonance to spin-coupling in the decahaem [7]. Experimental verification that LS3 resonance is a spin-coupled signal requires multi-frequency EPR, which was beyond the scope and timescale of this study. Whereas coupled LS3 resonance has an impact on signal integration, and subsequent spin quantitation, the effect is apparently minor for eOmcA (i.e. decrease in spins quantified) and does not detract from conclusions made in this study.

Significant lineshape change in the LS3 signal throughout the potentiometric titration may be due to conformational changes modulating haem environment(s) as a function of sample potential (Fig. 5.10). A large variety of conformers amongst the LS3 haem population would likely produce many intermediates and broader composite resonance feature than those observed. However the resolution of specific LS3 signal g values and lineshape species throughout the titre is thus more likely brought about by defined (and thus spectroscopically resolved) conformational changes during oxidation/reduction of eOmcA. This working model is supported by the subtle lineshape changes in the LS2 signal above sample potential > -0.15 V vs S.H.E., suggesting changes in the haem environments of LS2 and LS3 haem population environments as a function of sample potential.

The working model of the LS3 signal being a coupled resonance feature implies that reduction of eOmcA to -0.15 V vs S.H.E. produces the two LS3 resonances observed as a result of resonance un-coupling. It is possible that the variable LS3 signal g values and lineshape may also be attributed to variability in spin-coupled inter-haem distance as a function of potential-dependent conformational changes. Previously published evidence for conformational changes in OmcA was provided by a ≈ 7 Å difference in the maximal dimension of oxidised and reduced OmcA SAXS envelopes [15].

Table. 5.6 – **Compilation of Low-Spin *b* and *c* type Haem Ligand Sets that produce LS3 Paramagnetic Resonance.** The haem ligands compiled are those with $2.70 \geq g_1 \geq 2.50$. The cytochromes presented here contain predominantly *b* haems. However *b* and *c*-type haems are identical molecules, the covalent bond of *c*-type haems to the polypeptide is not known to produce differential paramagnetic features. * = phenol ring modelled to bind haem parallel to porphyrin ring, ^ = modified *b* haem that is covalently bound to polypeptide [16], # = haem not *bis*-histidine ligated in structure, but His⁶³ is adjacent to distal haem pocket and putatively available to ligate the haem.

<i>g</i> ₁ Value	Haem Ligation	Corroborating Data	Haem Type	Cytochrome	Reference
2.50	cysteinate:histidine	Crystal Structure	<i>b</i>	cytochrome P450	[17]
2.52	histidine:tyrosinate	Resonance Raman	<i>b</i>	hemoglobin	[18]
2.54	histidine:hydroxide	-	<i>b</i>	leghemoglobin	[13]
2.56	histidine:thiolate adduct	NIR-MCD	<i>b</i>	myoglobin	[5]
2.59	histidine:sulphide	-	<i>b</i>	myoglobin	[19]
2.65	histidine:phenol adduct	NIR-MCD	<i>b</i>	leghemoglobin	[5]
2.66, 2.67	histidine: phenol adduct*	Resonance Raman	<i>b</i>	myeloperoxidase	[20]
2.67	histidine:selenocyanate	-	<i>b</i>	myoglobin	[19]
2.68	histidine:azide adduct	-	<i>b</i> [^]	myeloperoxidase	[21]
2.69	<i>bis</i> -histidine	Crystal Structure [14] [#]	<i>b</i>	leghemoglobin	[13]
2.70	histidine:hydroxide	-	<i>c</i>	cytochrome <i>c</i> peroxidase	[22]

5.3.3 – Fitting the Nernst Equation to eOmCA's Spin Quantitated Potentiometric Titre

The haems of eOmCA titrate from +0.08 V to -0.42 V vs S.H.E. and have mid-point potentials (i.e. $E_{m,7.6}$) that could be divided into five high potential haems (i.e. $E_{m,H} = -0.05 \text{ V} > E_{m,7.6} > -0.15 \text{ V}$) and five low potential haems (i.e. $E_{m,L} = -0.15 \text{ V} > E_{m,7.6} > -0.42 \text{ V}$) (Fig. 5.13). The Nernst fits show there are three high-potential LGM1 haems that titrate from +0.08 V to -0.12 V (Fig. 5.13), all with simulated $E_{m,7.6} = -0.05 \text{ V}$ (Table 5.7). The two LGM2 haems titrate from +0.07 V to -0.23 V with simulated $E_{m,7.6} = -0.06 \text{ V}$ and -0.12 V. Although three haems were identified with a φ modelled to produce LGM2 resonance (i.e. $30^\circ < \varphi < 60^\circ$, Table 5.6), spin quantitation consistently identifies ≈ 2 LGM2 spins per eOmCA molecule (Fig. 5.13). As such the dihedral angle: paramagnetic resonance model presented may need adjusting. Alternatively, a haem of the modelled LGM2 population (i.e. haems 7, 8 and 9) is a candidate to couple to the LS2 resonance haem population to generate LS3 resonance. The coupled LS3 resonance titrates from -0.15 V to +0.07 V, (i.e. $E_{m,7.6} = -0.08 \text{ V}$). As such the $E_{m,H}$ haem population consists of 6 haems.

In contrast the 4th LGM1 haem titrates from -0.12 V to -0.31 V (i.e. $E_{m,7.6} = -0.22 \text{ V}$). The two LS1 haems titrate from -0.09 V to -0.42 V, with derived $E_{m,7.6} = -0.24 \text{ V}$ and $E_{m,7.6} = -0.30 \text{ V}$. Spin intensity of the LS2 is lost in spin-coupling to produce the LS3 resonance, and so the absolute sample potential-dependency of the LS2 population's oxidation state is unknown. However with the data available, the LS2 haem population has an $E_{m,7.6} = -0.36 \text{ V}$, in agreement with the distinct remnant of LS2 resonance that remains between -0.15 to -0.30 V. As such 4 haems constitute the $E_{m,L}$ haem population.

Table 5.7 – eOmCA's Derived Mid-point Potentials of its EPR-monitored Redox Titre. EPR signals were fitted to an $n = 1$ oxidative Nernst derivative. The mid-point potentials ($E_{m,7.6}$) extrapolated were obtained by modelling the number of haem contributions per resonance population according to eOmCA's structure. * = 1 haem assigned to resonance population despite sub-stoichiometric spins quantitated.

EPR Signal	Spins Quantified	No. of Haems Assigned	$E_{m,7.6}$ vs S.H.E. (V)			
			1	2	3	4
LGM1	3.76	4	-0.05	-0.05	-0.05	-0.22
LGM2	1.63	2	-0.06	-0.12		
LS1	2.56	2	-0.24	-0.30		
LS2	0.61	1*	-0.36			
LS3	1.66	1	-0.08			

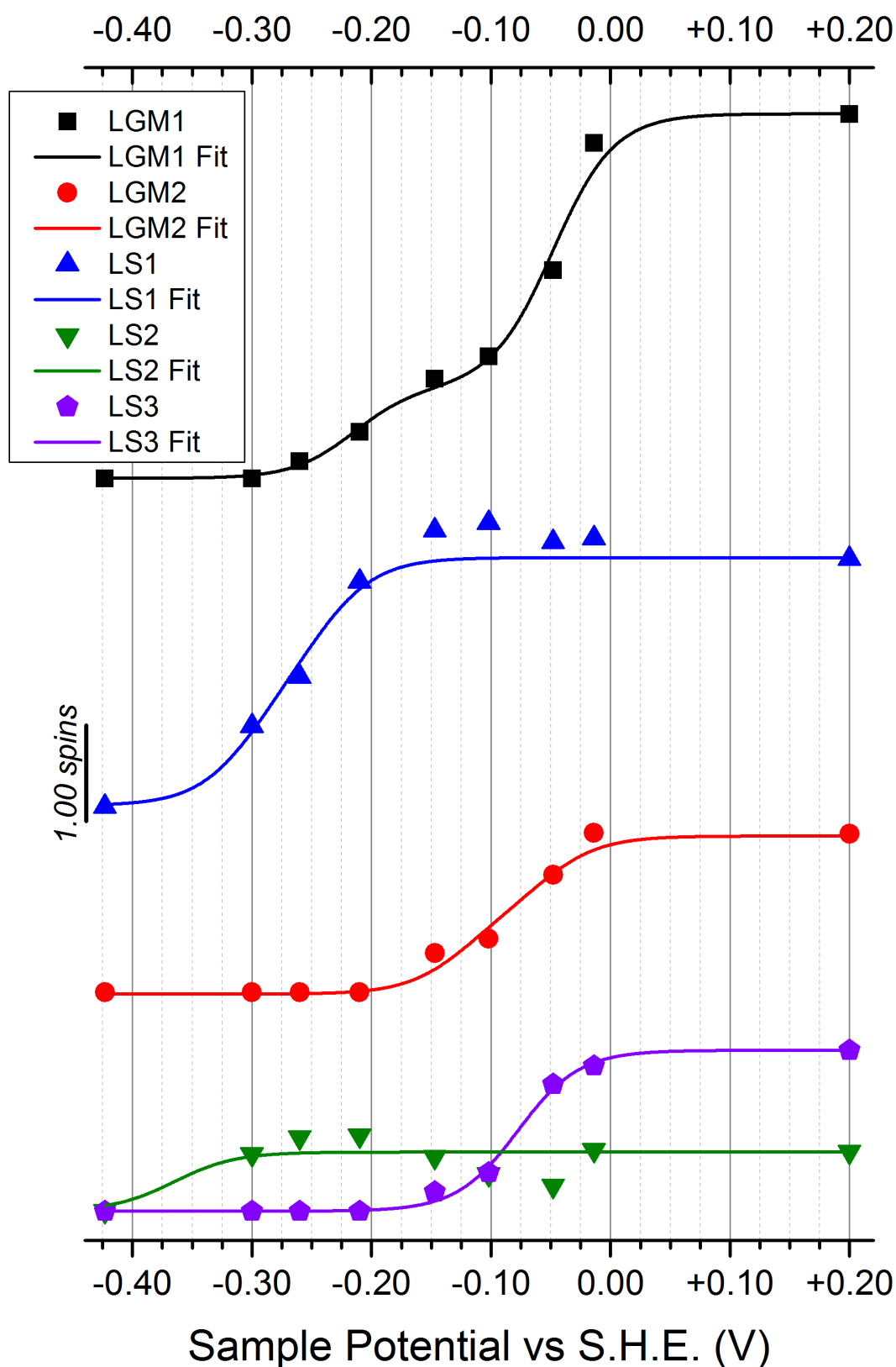


Fig. 5.13 – **The Nernst Fit to Spin Quantitation of eOmca's EPR Resonance Features.** Nernst simulation (lines) of resonance signal spins per eOmca molecule (symbols). Spins per eOmca molecule (symbols) was fitted to an $n = 1$ derivative of the Nernst equation (see Section M.4). The number of haems assigned as described in Table 5.7 has informed the Nernst fit. There fit to LS2 signal intensity may be affected by its atypical sample potential-dependency.

Comparison of the potentiometric properties of eOmca identified in this chapter with those of the other major OMMC clades is performed in Chapter 6, where the potentiometric titration of eUndA is reported.

5.3.4 – Quantitative Analysis of eOmca at different pHs

Spin quantitation of the EPR spectrum of eOmca poised at +0.20 V vs S.H.E. is compared to spin quantitation of air-oxidised eOmca at pH 7.60, 6.60 and 5.60 (presented in Section 2.2). Between poised (i.e. +0.20 V vs S.H.E.) and air-oxidised eOmca at pH 7.60, the LGM1 Δ spins value of -1.96 shows loss of 2 LGM1 haems that transition resonance features. This is corroborated by +1.62 spins quantified in the LS1 and LS3 populations between the two samples (Fig. 5.14). However, as discussed earlier, interpretation of LS3 signal spin quantitation is complicated by its spin-coupled nature and $\sum_{i=1}^3 g_i^2$ value. Transition of eOmca from pH 7.60 to 6.60 produces negligible net change in eOmca resonance population. Transition of eOmca from pH 6.60 to pH 5.60 produces Δ spins = -1.44 in LS1 resonance, accounted for predominantly in LS3 resonance (i.e. Δ spins = +1.08).

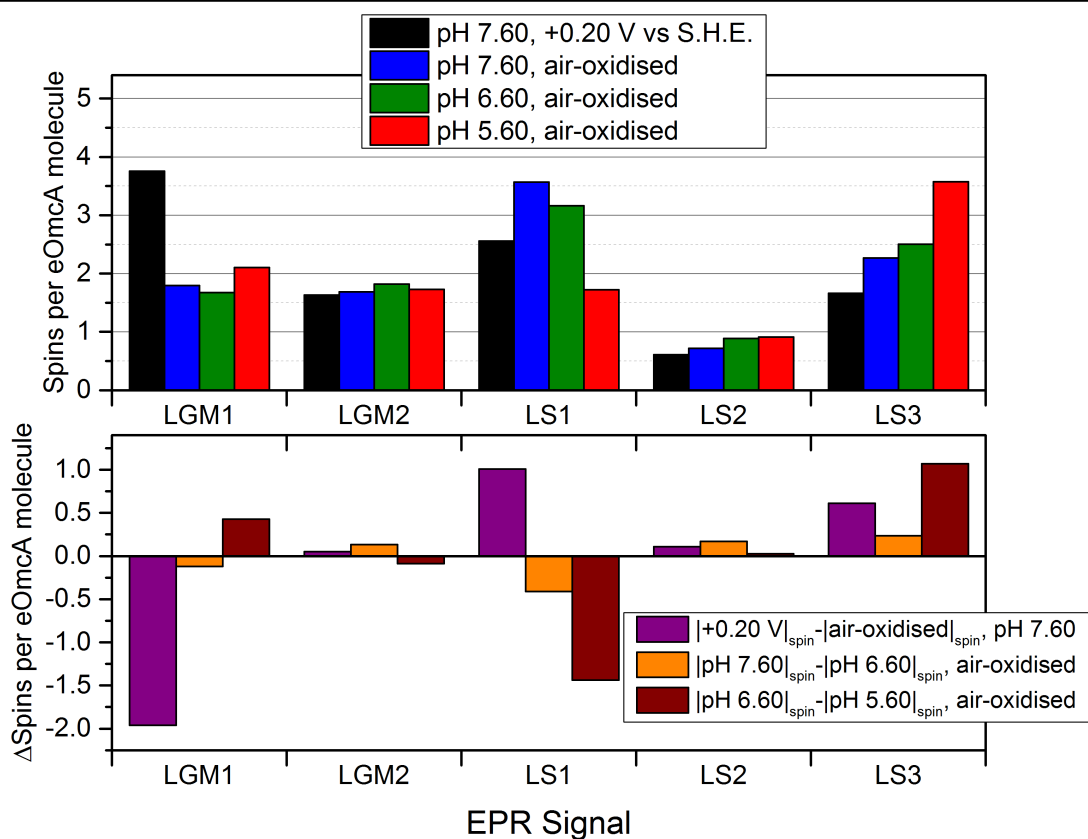


Fig. 5.14 - **Paramagnetic Resonance Population changes in eOmca as a function of pH.** (Upper panel) The spins per eOmca molecule of each resonance feature, equivalent to haems per molecule, are plotted as a function of pH. (Lower panel) Change in spins (Δ Spins) per eOmca molecule of resonance populations between conditions specified inset.

Where net changes in resonance populations are observed, the LS3 population consistently changes. Changes in pH value most likely produce conformational change(s) by changing amino acid protonation states. Conformational changes in the structurally similar OMMC MtrF have been modelled *in silico* to be a dynamic function of structural flexibility [12]. Furthermore OmcA has been shown to undergo conformational changes as a function of oxidation state [15]. As such it is likely that conformational changes vary inter-haem distances, producing concomitant change in spin-coupling and thus LS3 spin quantitation.

The pH-sensitivity of eOmcA's paramagnetic resonance features share similarities to the pH-sensitivity of haem absorption features reported of OmcA_(wt) in Chapter 2 (i.e. oxidised and reduced α and β region $\Delta\epsilon$). The largest $\Delta\epsilon$ observed were between pH 6.60 and pH 7.60. Whilst this doesn't correlate directly with EPR spectra quantitation presented here, it may explain the difference between poised (i.e. +0.20 V) and air-oxidised eOmcA spectral quantitation. As such, small differences in pH value and oxidation state (see Section 5.3.2) may significantly alter the molecular environment of eOmcA haem(s).

In conclusion, the EPR spectrum of eOmcA corroborates the haem ligation and *bis*-histidine dihedral angles observed in the eOmcA crystal structure. Furthermore, the reduction potentials of haem populations paramagnetically resolved in eOmcA are appropriate for a cytochrome responsible to reduce mineral TEA.

References

- 1 Field, S. J., Dobbin, P. S., Cheesman, M. R., Watmough, N. J., Thomson, A. J. and Richardson, D. J. (2000) Purification and magneto-optical spectroscopic characterization of cytoplasmic membrane and outer membrane multiheme c-type cytochromes from *Shewanella frigidimarina* NCIMB400. *Journal of Biological Chemistry*. **275**, 8515-8522
- 2 Moore, G. R. and Pettigrew, G. W. (1990) Springer Series in Molecular Biology Cytochromes C: Evolutionary, Structural and Physicochemical Aspects. Moore, G. R. and G. W. Pettigrew. Springer Series in Molecular Biology: Cytochromes C: Evolutionary, Structural and Physicochemical Aspects. Xvi+478p. Springer-Verlag: Berlin, Germany; New York, New York, USA. Illus
- 3 Palmer, G. (1985) The electron paramagnetic resonance of metalloproteins. *Biochemical Society Transactions*. **13**, 548-560

- 4 Gadsby, P. M. A., Peterson, J., Foote, N., Greenwood, C. and Thomson, A. J. (1987) Identification of the Lignad-Exchange Process in the Alkaline Transition of Horse heart Cytochrome C. *Biochemical Journal*. **246**, 43-54
- 5 Gadsby, P. M. A. and Thomson, A. J. (1990) Assignment of the Axial Lignads of Ferric Ion in Low-Spin Hemoproteins by Near-Infrared Magnetic Circular-Dichroism and Electron-Paramagnetic Resonance Spectroscopy. *Journal of the American Chemical Society*. **112**, 5003-5011
- 6 Walker, F. A., Huynh, B. H., Scheidt, W. R. and Osvath, S. R. (1986) Models of the Cytochromes-b - Effect of Axial Ligand Plane Orientation on the EPR and Mössbauer-Spectra of Low-Spin Ferrihemes. *Journal of the American Chemical Society*. **108**, 5288-5297
- 7 Clarke, T. A., Edwards, M. J., Gates, A. J., Hall, A., White, G. F., Bradley, J., Reardon, C. L., Shi, L., Beliaev, A. S., Marshall, M. J., Wang, Z., Watmough, N. J., Fredrickson, J. K., Zachara, J. M., Butt, J. N. and Richardson, D. J. (2011) Structure of a bacterial cell surface decaheme electron conduit. *Proceedings of the National Academy of Sciences of the United States of America*. **108**, 9384-9389
- 8 Gadsby, P. M. A. and Thomson, A. J. (1982) Identification of the Imidazolate Anion as a Ligand in Metmyoglobin by Near-Infrared Magnetic Circular-Dichroism Spectroscopy. *Febs Letters*. **150**, 59-63
- 9 Bodemer, G. J., Antholine, W. A., Basova, L. V., Saffarini, D. and Pacheco, A. A. (2010) The effect of detergents and lipids on the properties of the outer-membrane protein OmcA from *Shewanella oneidensis*. *Journal of Biological Inorganic Chemistry*. **15**, 749-758
- 10 Yatsunyk, L. A., Dawson, A., Carducci, M. D., Nichol, G. S. and Walker, F. A. (2006) Models of the cytochromes: Crystal structures and EPR spectral characterization of low-spin bis-imidazole complexes of (OETPP)Fe-III having intermediate ligand plane dihedral angles. *Inorganic Chemistry*. **45**, 5417-5428
- 11 Venkateswaran, K., Moser, D. P., Dollhopf, M. E., Lies, D. P., Saffarini, D. A., MacGregor, B. J., Ringelberg, D. B., White, D. C., Nishijima, M., Sano, H., Burghardt, J., Stackebrandt, E. and Nealson, K. H. (1999) Polyphasic taxonomy of the genus *Shewanella* and description of *Shewanella oneidensis* sp. nov. *International Journal of Systematic Bacteriology*. **49**, 705-724
- 12 Smith, D. M. A. and Rosso, K. M. (2014) Possible Dynamically Gated Conductance along Heme Wires in Bacterial Multiheme Cytochromes. *Journal of Physical Chemistry B*. **118**, 8505-8512
- 13 Appleby, C. A., Blumberg, W. E., Peisach, J., Wittenberg, B. A. and Wittenberg, J. B. (1976) Leghemoglobin .3. Electron-Paramagnetic Resonance and Optical Spectral Study of Free Protein and its complexes with Nicotinate and Acetate. *Journal of Biological Chemistry*. **251**, 6090-6096
- 14 Harutyunyan, E. H., Safonova, T. N., Kuranova, I. P., Popov, A. N., Teplyakov, A. V., Obmolova, G. V., Rusakov, A. A., Vainshtein, B. K., Dodson, G. G., Wilson, J. C. and Perutz, M. F. (1995) The Structure of deoxy-Leghemoglobin and oxy-Leghemoglobin from Lupin. *Journal of Molecular Biology*. **251**, 104-115
- 15 Johs, A., Shi, L., Droubay, T., Ankner, J. F. and Liang, L. (2010) Characterization of the Decaheme c-Type Cytochrome OmcA in Solution and on Hematite Surfaces by Small Angle X-Ray Scattering and Neutron Reflectometry. *Biophysical Journal*. **98**, 3035-3043
- 16 Fiedler, T. J., Davey, C. A. and Fenna, R. E. (2000) X-ray crystal structure and characterization of halide-binding sites of human myeloperoxidase at 1.8 angstrom resolution. *Journal of Biological Chemistry*. **275**, 11964-11971

- 17 Girvan, H. M., Seward, H. E., Toogood, H. S., Cheesman, M. R., Leys, D. and Munro, A. W. (2007) Structural and spectroscopic characterization of P450BM3 mutants with unprecedented P450 heme iron ligand sets - New heme ligation states influence conformational equilibria in P450BM3. *Journal of Biological Chemistry*. **282**, 564-572
- 18 Das, T. K., Couture, M., Lee, H. C., Peisach, J., Rousseau, D. L., Wittenberg, B. A., Wittenberg, J. B. and Guertin, M. (1999) Identification of the ligands to the ferric heme of *Chlamydomonas* chloroplast hemoglobin: Evidence for ligation of tyrosine-63 (B10) to the heme. *Biochemistry*. **38**, 15360-15368
- 19 Sono, M. and Dawson, J. H. (1982) Formation of Low-Spin Complexes of Ferric Cytochrome P-450-CAM with Anionic Ligands - Spin State and Ligand Affinity comparison to Myoglobin. *Journal of Biological Chemistry*. **257**, 5496-5502
- 20 Hori, H., Fenna, R. E., Kimura, S. and Ikeda-saito, M. (1994) Aromatic Substrate Molecules Bind at the Distal Heme Pocket of Myeloperoxidase. *Journal of Biological Chemistry*. **269**, 8388-8392
- 21 Wever, R. and Bakkenist, A. R. J. (1980) Interaction of Myeloperoxidase with Ligands as studied by EPR. *Biochimica Et Biophysica Acta*. **612**, 178-184
- 22 Yonetani, T. and Anni, H. (1987) Yeast Cytochrome-C Peroxidase - Coordination and Spin States of Heme Prosthetic Group. *Journal of Biological Chemistry*. **262**, 9547-9554

Chapter 6: **Potentiometric Studies of UndA, a homologue of OmcA in several** ***Shewanella spp***

6.1 – Introduction

The genome of *Shewanella oneidensis* MR-1 and other *Shewanella spp* encodes for the OMMCs MtrF, MtrC and OmcA (i.e. the *mtr* gene cluster Fig. 1.4) [1, 2]. The undecahem cytochrome *undA* is encoded for in *Shewanella spp* that omit *omcA* in their *mtr* gene cluster [2], as such UndA is postulated as a functional analogue of OmcA [3]. Chapter 5 presents an EPR study of eOmcA's redox properties. This complements the redox properties presented for the OMMCs MtrC [4] and MtrF [5], indicating electroactive coverage amongst the OMMCs studied so far. All three OMMCs display redox activity across potential windows that span +0.08 V to to -0.47 V vs S.H.E.. EPR allows a degree of correlation between protein structure and resonance populations in each case. The availability of the UndA structure means measurement of its EPR-monitored potentiometric titration can also be correlated to its structure for comparison with the other OMMCs, including its functional analogue OmcA. This may help identify functional differences/similarities amongst the OMMCs.

There is high structural conservation of haem arrangement observed between OMMCs (see Section 3.2, [6]). The additional, "11th" haem of UndA is inserted between haems 6 and 7 of MtrF/OmcA haem arrangements, with minimal disruption to the surrounding polypeptide [7]. The haem is referred to as haem 7 in the publication of the structure, whereas in the context of comparing haem arrangement conservation amongst the OMMCs, the additional haem is referred to as haem 7' in this chapter. Fig. 6.1 is a comparison of *bis*-histidine dihedral angles (i.e. φ) amongst OMMC crystal structures currently available. Of the ten haems comparable amongst the OMMCs, six haems have $\Delta\varphi \leq 30^\circ$, namely haems 1, 2, 3, 8, 9 and 10 (discounting UndA's haem 7' that has no haems in comparable position in the other OMMCs). Furthermore, haems 8 – 10 have $\Delta\varphi \leq 15^\circ$ between UndA, OmcA and MtrF. As such, the EPR-monitored potentiometric titration of UndA is reported here for comparison with its functional analogue UndA, and to contextualise φ conservation between haems 8 – 10.

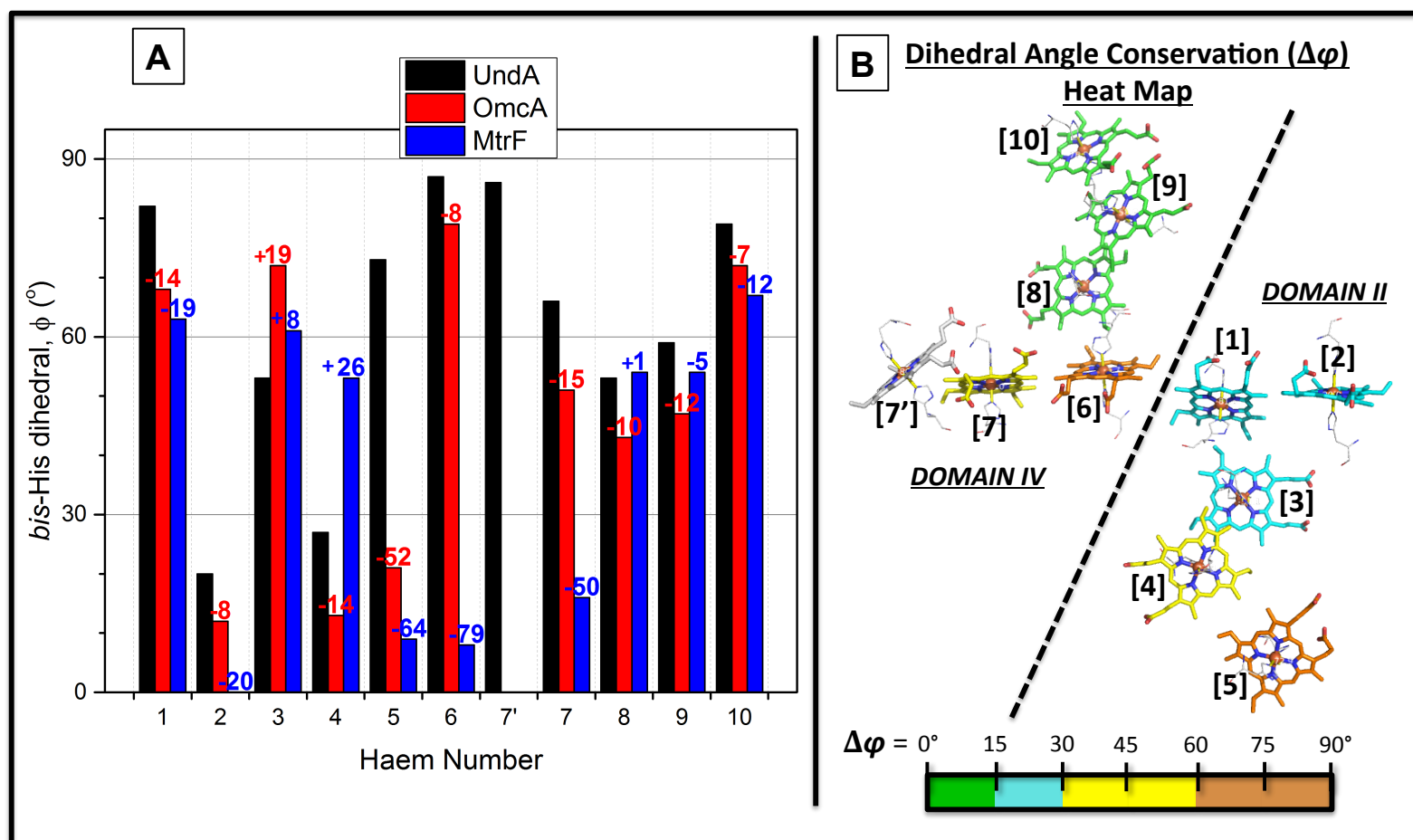


Fig. 6.1 – **OMMC *bis*-histidine dihedral angle conservation.** (A) The *bis*-histidine dihedral angles of haems of UndA, OmcA and MtrF. Difference in dihedral angle between UndA and other OMMCs are labeled above each haem's dihedral plot. (B) The *bis*-histidine dihedral angle conservation heat map. Haems are colour-coded with the largest dihedral angle difference ($\Delta\phi$) between each OMMC haem, and mapped onto UndA's haems.

6.2 – Results

6.2.1 – EPR-Monitored Redox Titre of eUndA

A solution of 86 μM eUndA, kindly provided by Dr Marcus J. Edwards (UEA), was poised at sample potentials ranging from +0.18 V to -0.47 V vs S.H.E., where the protein is fully oxidised and fully reduced at these respective potentials (Fig. 6.2). Equimolar samples of eUndA, poised at the listed reduction potentials (Fig. 6.2), were frozen in $\text{N}_2(\text{l})$ before EPR measurements were recorded, as was done for eOmcA (Section 5.2). As in OmcA, there is no $g_{\perp} \approx 6.0$ at any sample potential measured. All resonance features are indicative of low-spin, ferric, $S = \frac{1}{2}$ haem that is reduced to ferrous, $S = 0$ haem with decrease in sample potential. The fully oxidised eUndA EPR spectrum (i.e. +0.18 V vs S.H.E.) displays four of the five types of resonance populations observed in OmcA, namely LGM1, LGM2, LS1 and LS2 (identified by g_1 values, Fig. 6.2).

6.2.2 – Simulation of eUndA's EPR Signals

The procedure used to simulate the complex spectrum of eUndA was as described for eOmcA, Chapter 5. The simplest spectrum, containing a sole resonance population (i.e. -0.34 V vs S.H.E., Fig. 6.3) was simulated first. The signal simulation was then used to inform simulation of the more positive spectra until all resonance features of the fully oxidised spectrum could be accounted for.

There is a sole resonance feature present at -0.34 V vs S.H.E. is LGM2 (LGM2 $g_{1,2,3} = 3.19, 2.13$ and 1.32 ; Fig. 6.3). At -0.28 V vs S.H.E., LGM1 and LS1 resonance signals are present alongside LGM2 resonance (Fig. 6.4), and the LS2 signal is detected at sample potential ≥ -0.09 V vs S.H.E. (Fig. 6.5). Multiple forms of EPR signals, such as LS3-1 and LS3-2 simulations for the LS3 signal of eOmcA at -0.05 V vs S.H.E., were not required to simulate eUndA. The signal simulations of the -0.09 V vs S.H.E. spectrum were used to model the 0.00 V and +0.18 V vs S.H.E. spectra, as no additional resonance features or lineshape and g value adjustments were required (Fig. 6.6).

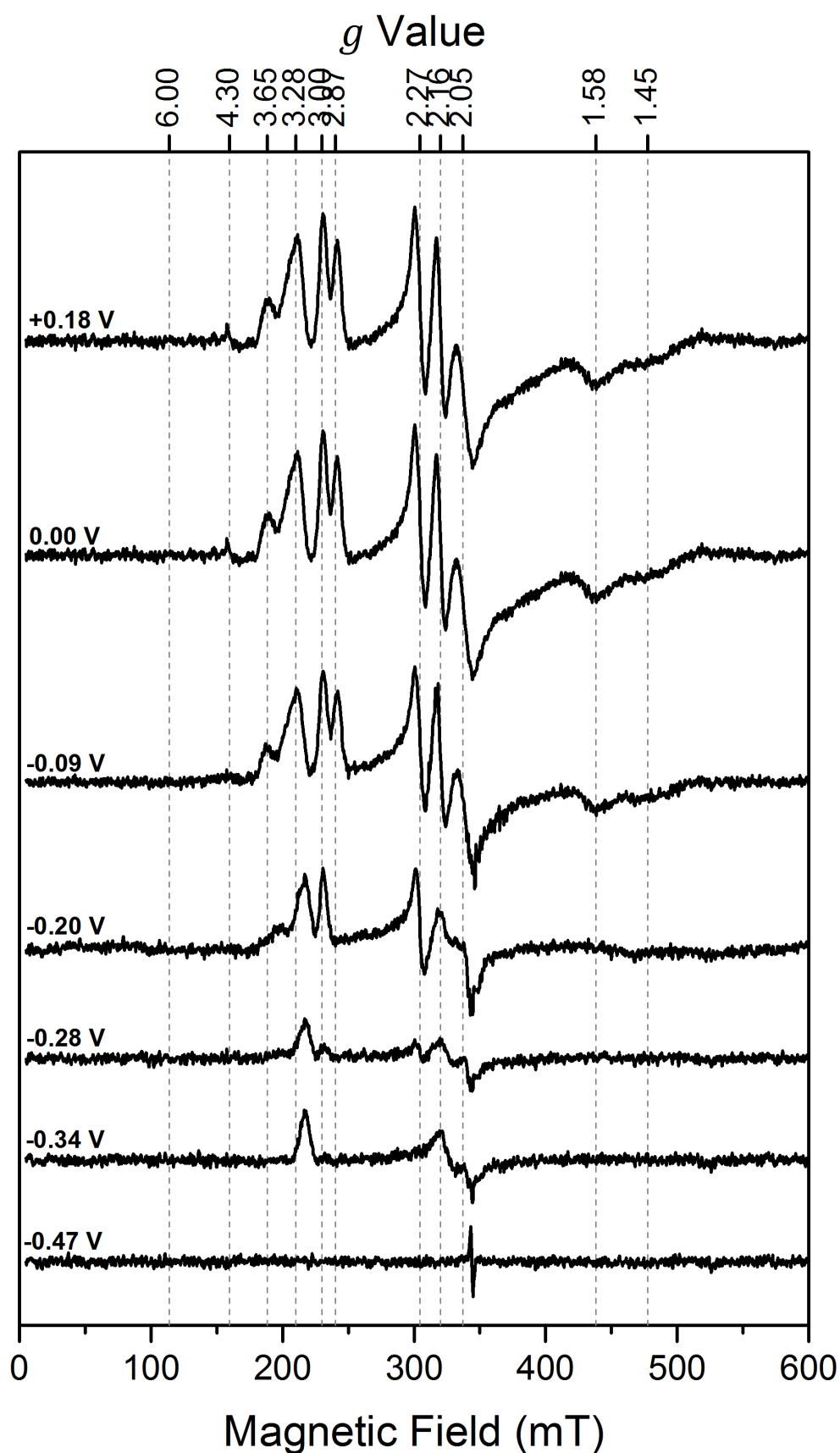


Fig. 6.2 – **EPR-monitored potentiometric titration of eUndA.** EPR spectra of eUndA (86 μ M) poised at the sample potentials listed. EPR spectra were measured at 9.688 GHz, 7 ± 2 K, 2.012 mW. eUndA was in 20 mM HEPES, pH 7.60, 50 mM NaCl, 0.01% CHAPS, 1% glycerol. * = radical contribution from redox mediators.

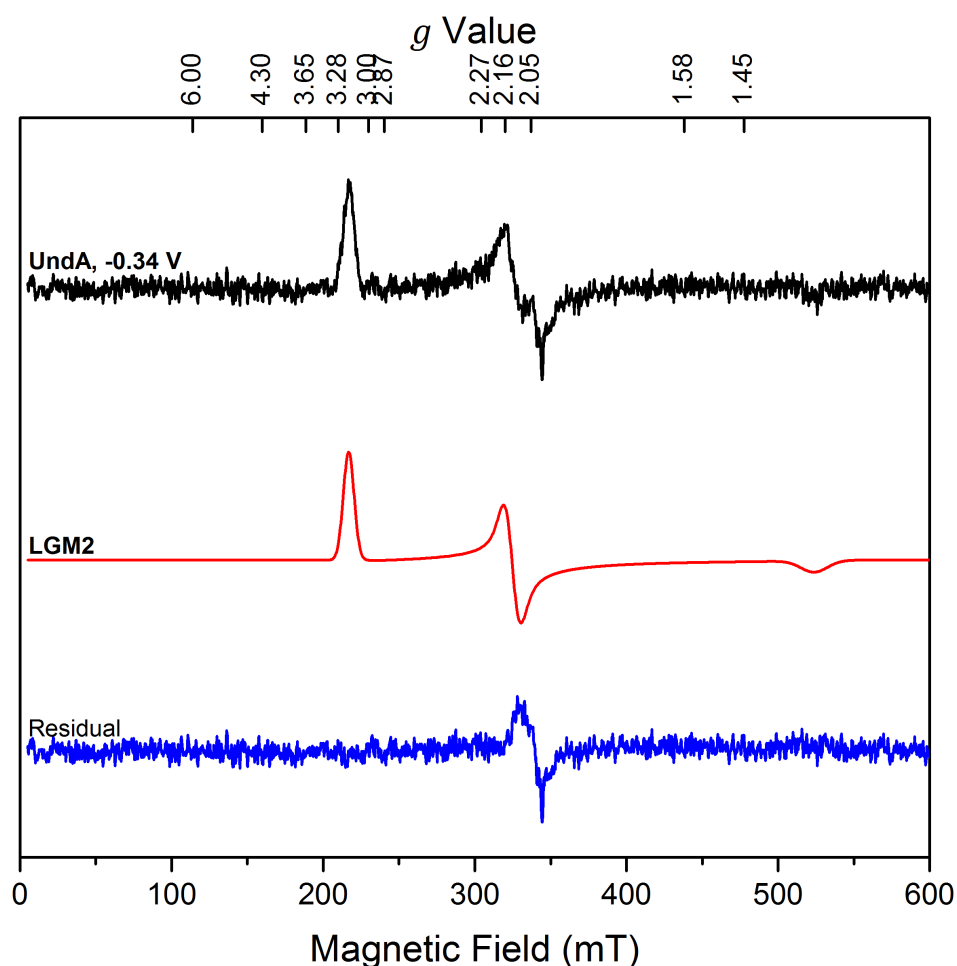


Fig. 6.3 – **Simulation of eUndA's -0.34 V vs S.H.E. EPR spectrum.** Simulation (red) of the measured spectrum (top, black) is composed solely of the LGM2 resonance signal. The g values of the signal is marked (in order of g_1, g_2, g_3) as red lines on each signal simulation and compiled in Table 6.1. Residual spectrum (blue) = measured spectrum – spectrum simulation.

Table 6.1 – **The g values of eUndA poised at -0.34 V vs S.H.E..** The g value lineshape is modelled by Field Strength width of g value (in Gauss; 1,000 Gauss = 0.1 mT), listed below respective g value.

EPR Signal	Signal g values			$\sum_{i=1}^3 g_i^2$
	g_1	g_2	g_3	
LGM2	3.190	2.130	1.320	16.46
<i>lineshape</i> (Gauss)	70.0	90.0	180.0	

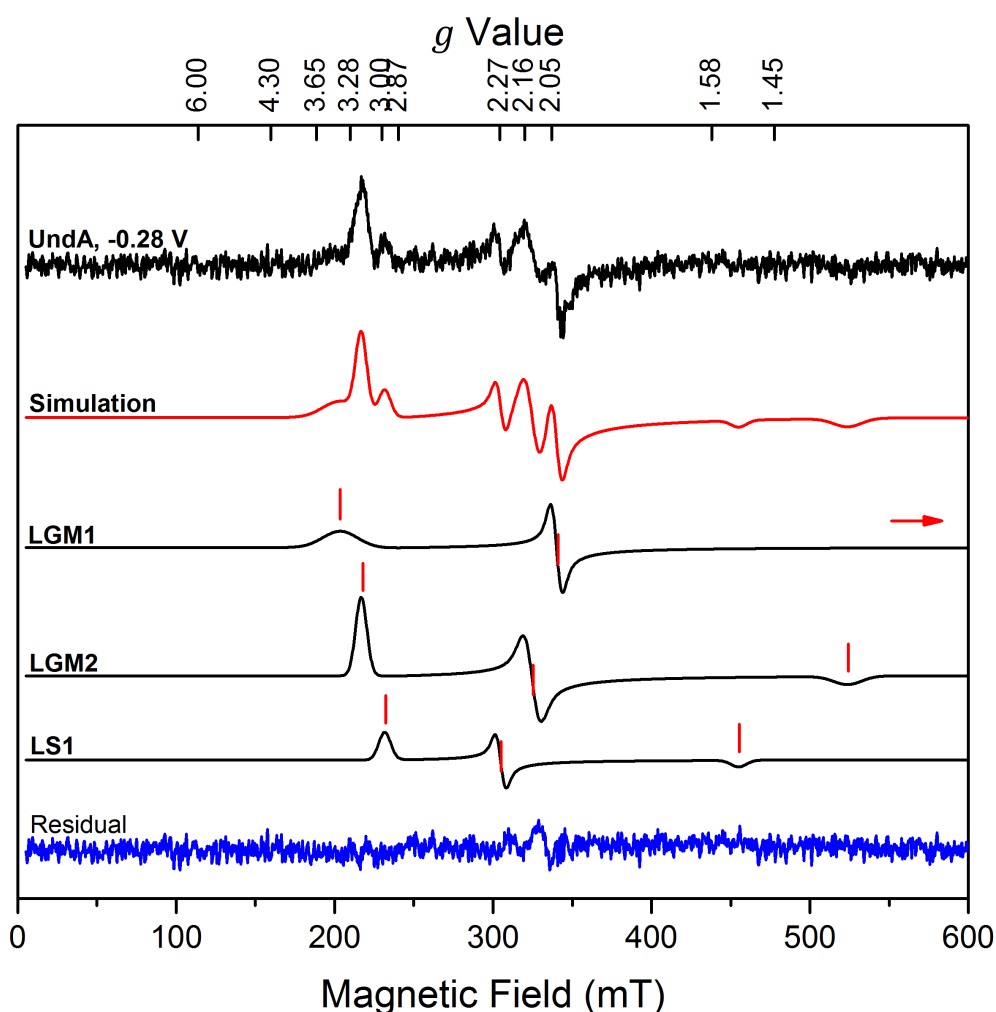


Fig. 6.4 – **Simulation of eUndA's -0.28 V vs S.H.E. EPR spectrum.** Simulation (red) of the measured spectrum (top, black) is a summation of the resonance feature simulations listed below. The LGM1, LGM2 and LS1 components of the spectrum are plotted individually (lower, black). The g values of each signal are marked (in order of g_1, g_2, g_3) as red lines on each signal simulation and compiled in Table 6.2.

Table 6.2 – **The g values of eUndA poised at -0.28 V vs S.H.E..** The g value lineshape is modelled by Field Strength width of g value (in Gauss), listed below respective g value.

EPR Signal	Signal g values			$\sum_{i=1}^3 g_i^2$
	g_1	g_2	g_3	
LGM1	3.400	2.035	1.020	16.74
<i>lineshape (Gauss)</i>	220.0	60.0	180.0	
LGM2	3.190	2.130	1.320	16.46
<i>lineshape (Gauss)</i>	70.0	90.0	180.0	
LS1	2.988	2.270	1.520	16.13
<i>lineshape (Gauss)</i>	75.0	55.0	100.0	

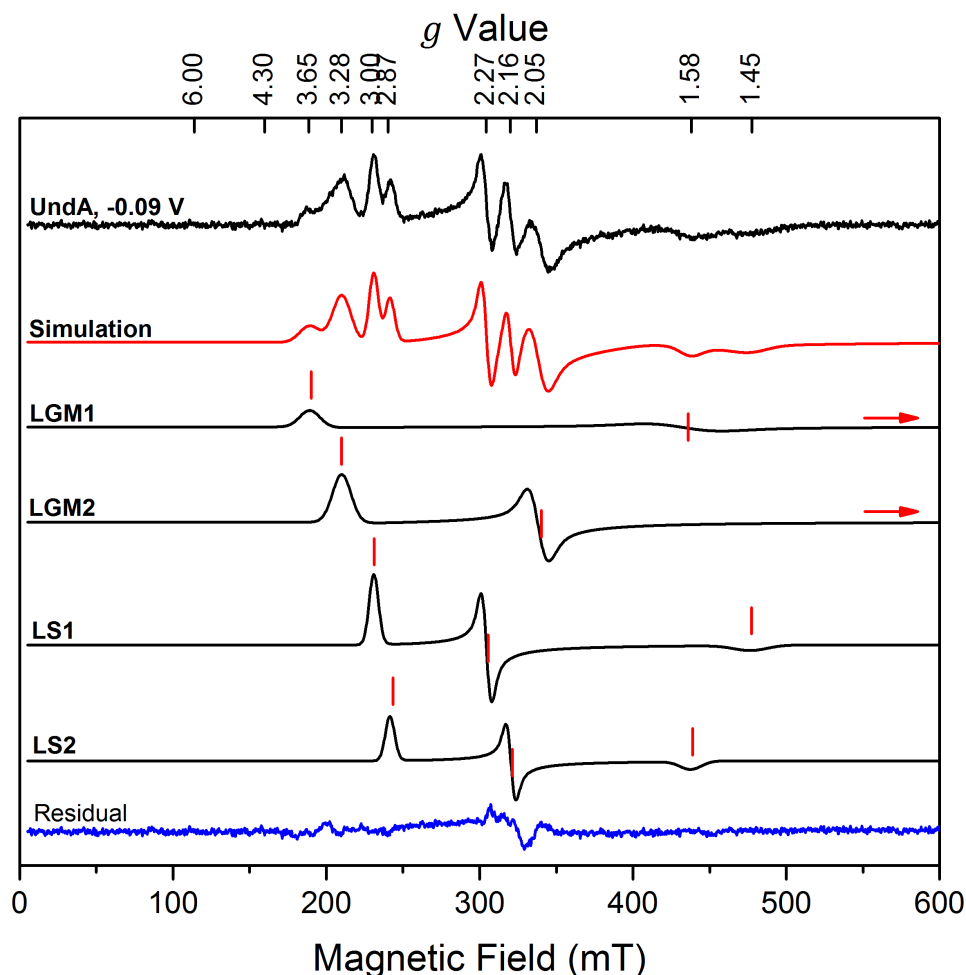


Fig. 6.5 – **Simulation of eUndA's -0.09 V vs S.H.E. EPR spectrum.** Simulation (red) of the measured spectrum (top, black) is a summation of the resonance feature simulations listed below. The LGM1, LGM2, LS1 and LS2 components of the spectrum are plotted individually (lower, black). The g values of each signal are marked (in order of g_1, g_2, g_3) as red lines on each signal simulation and compiled in Table 6.3.

Table 6.3 – **The g values of eUndA poised at -0.09 V vs S.H.E..** The g value lineshape is modelled by Field Strength width of g value (in Gauss), listed below respective g value.

EPR Signal	Signal g values			$\sum_{i=1}^3 g_i^2$
	g_1	g_2	g_3	
LGM1	3.650	1.600	1.020	16.92
<i>lineshape (Gauss)</i>	130.0	400.0	180.0	
LGM2	3.280	2.048	1.020	15.99
<i>lineshape (Gauss)</i>	150.0	120.0	180.0	
LS1	2.995	2.272	1.450	16.23
<i>lineshape (Gauss)</i>	60.0	55.0	220.0	
LS2	2.865	2.159	1.580	15.37
<i>lineshape (Gauss)</i>	60.0	52.0	140.0	

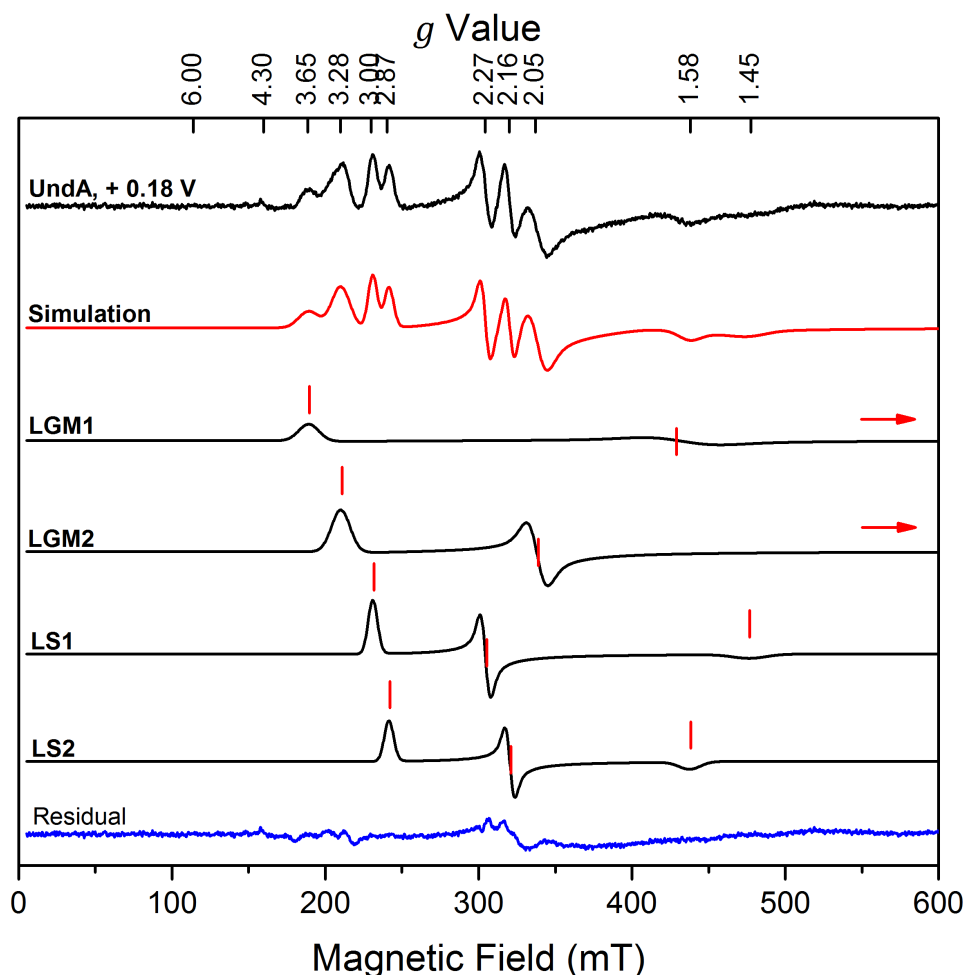


Fig. 6.6 – **Simulation of eUndA's +0.18 V vs S.H.E. EPR spectrum.** Simulation (red) of the measured spectrum (top, black) is a summation of the resonance feature simulations listed below. The LGM1, LGM2, LS1 and LS2 components of the spectrum are plotted individually (lower, black). The g values of each signal are marked (in order of g_1, g_2, g_3) as red lines on each signal simulation and compiled in Table 6.4.

Table 6.4 – **The g values of eUndA poised at +0.18 V vs S.H.E..** The g value lineshape is modelled by Field Strength width of g value (in Gauss), listed below respective g value.

EPR Signal	Signal g values			$\sum_{i=1}^3 g_i^2$
	g_1	g_2	g_3	
LGM1	3.650	1.600	1.020	16.92
<i>lineshape (Gauss)</i>	130.0	400.0	180.0	
LGM2	3.280	2.048	1.020	15.99
<i>lineshape (Gauss)</i>	150.0	120.0	180.0	
LS1	2.995	2.272	1.450	16.23
<i>lineshape (Gauss)</i>	60.0	55.0	220.0	
LS2	2.865	2.159	1.580	15.37
<i>lineshape (Gauss)</i>	60.0	52.0	140.0	

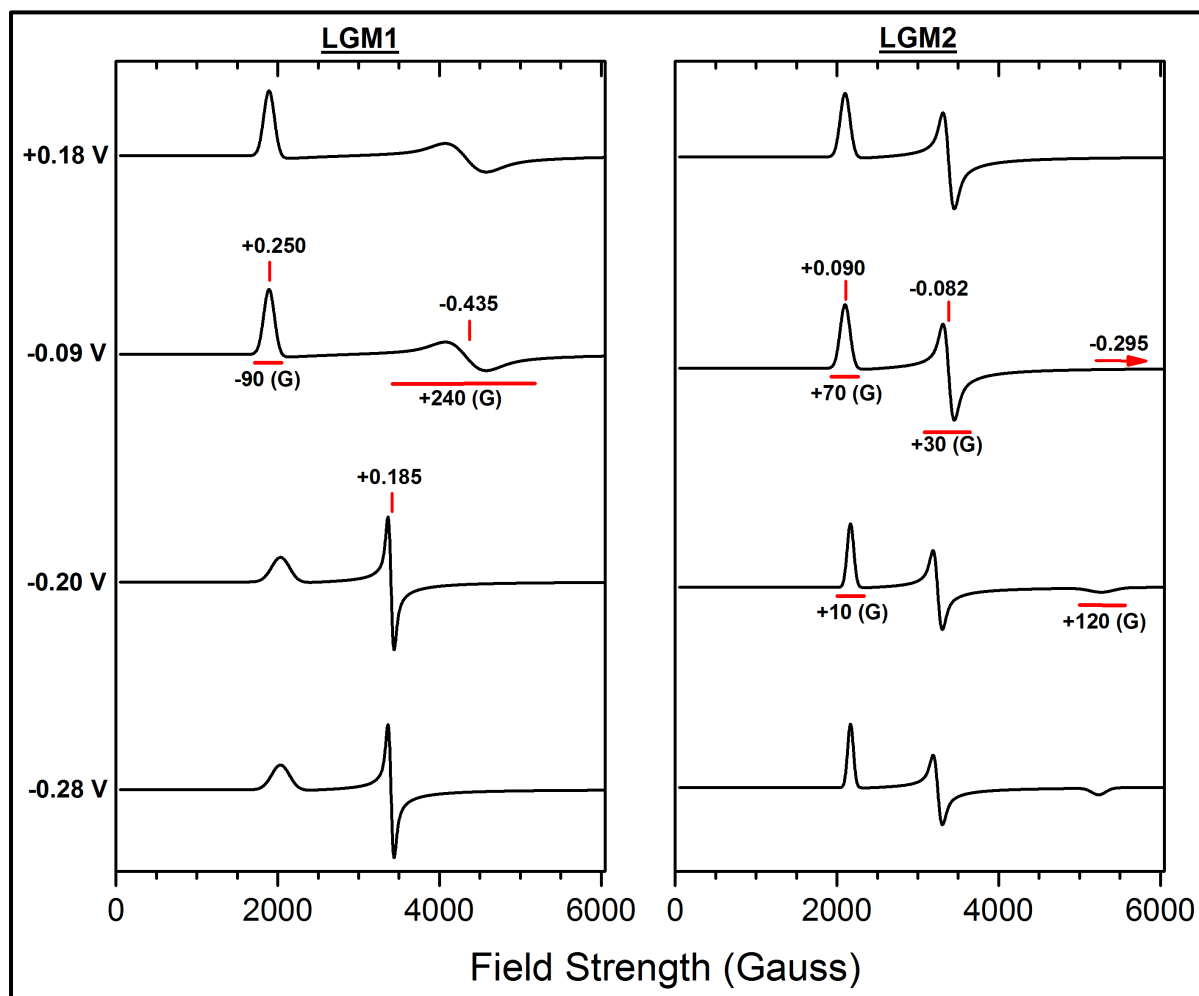


Fig. 6.7 – **The variable lineshapes in eUndA’s EPR Potentiometric Titration.** The variable lineshapes and Δg of LGM1 (left panel) and LGM2 (right panel) EPR signals at the sample potentials listed (vs S.H.E). At a given sample potential the difference between -0.09 V and -0.20 V lineshape and Δg changes are labelled on the -0.09 V spectra. The change in LS1 g_3 value (+0.050) and g_3 lineshape (+120.0 Gauss) between -0.34 V and -0.28 V vs S.H.E. is not plotted.

The guiding principle of $\sum_{i=1}^3 g_i^2 = 16.0$ for low-spin haem, is consistently disobeyed by the LGM1 ($\sum_{i=1}^3 g_i^2 > 16.7$) and LS2 ($\sum_{i=1}^3 g_i^2 < 15.4$) resonance features of eUndA. From -0.34 V to -0.28 V, the LGM2 $\sum_{i=1}^3 g_i^2 \approx 16.4$, but at sample potential ≥ -0.09 V, $\sum_{i=1}^3 g_i^2 \approx 16.0$. As indicated by changes in $\sum_{i=1}^3 g_i^2$, there are g value and lineshape changes that occur to the LGM1 and LGM2 resonance features (Fig. 6.7). There is also a small change in LS1 g_3 value and lineshape between -0.34 V and -0.28 V vs S.H.E..

6.2.3 – Spin Quantitation of eUndA’s EPR Redox Titre

Integration of eUndA’s resonance features was calibrated using the integration of 1 mM CuSO_4 solution standard (as described in Section 5.2). In conjunction with experimentally determined $\epsilon_{410\text{nm}}$ of eUndA = $1.599 \times 10^3 \text{ mM}^{-1} \text{ cm}^{-1}$ (Fig. A2.11), spin

integration was converted to spins per eUndA molecule. The fully oxidised spectrum (i.e. at +0.18 V vs S.H.E.) accounted for 10.96 spins per eUndA molecule. When analysing total spins per eUndA molecule (Fig. 6.9), eUndA's haems titrate with a high potential population of five haems ($E_{m,H}$ titrates from -0.09 V to -0.20 V) and a low potential population of six haems ($E_{m,L}$ titrates from -0.20 V to -0.47 V).

Spin quantitation of individual resonance features indicates the number of haems producing each resonance feature. At +0.18 V vs S.H.E., there are 3.59 LGM1 spins, 2.67 LGM2 spins, 1.82 LS1 spins and 2.87 LS2 spins per eUndA molecule. Each (low-spin) oxidised *c*-type haem has 1 unpaired 3d electron, giving it $S = \frac{1}{2}$ (i.e. has a single spin). On this basis spin quantitation should provide near-integer values for each signal. This is not entirely the case for eUndA. As such, assignment of EPR signals to specific haems and derivation of haem population reduction potentials is addressed in the Discussion.

6.3 – Discussion

6.3.1 – Correlating Spin Quantitation with eUndA Haem Ligation

Assessment of *bis*-histidine dihedral angle (i.e. φ) shows UndA is dominated by $\varphi > 45^\circ$ (Tables 6.5). This is consistent with the spectrum of oxidised eUndA that shows high LGM content (i.e. $g_1 > 3.1$ for ≈ 6 haems) relative to the LS populations (i.e. $2.8 < g_1 \leq 3.0$ for ≈ 5 haems; Tables 6.5). Positioning of a carboxylate group within hydrogen-bonding distance (i.e. ≈ 3.0 Å) of histidine N_δ atoms indicate that there are two putative histidinate-ligated haems present in UndA (i.e. haems 4 and 9; Fig. 6.8, Table 6.5). These histidinate-ligated haems would thus produce LS2 resonance (i.e. $2.8 < g_1 < 2.9$). Spin quantitation permits allocation of LGM1, LGM2 and LS1 resonance to haems such that $\varphi_{LGM1} > \varphi_{LGM2} > \varphi_{LS1}$ (Table 6.5).

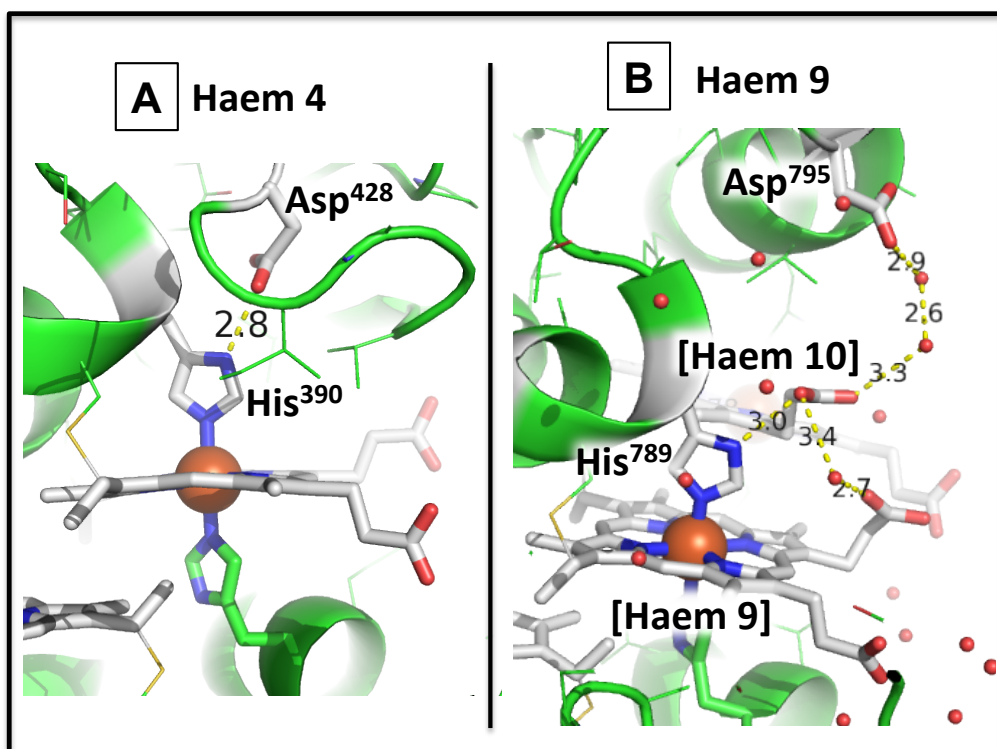


Fig. 6.8 – **The Putative Histidinate haem ligands of haems 4 and 9.** (A) Haem 4 has been assigned LS2 resonance because its proximal ligand His³⁹⁰ undergoes putative deprotonation by Asp⁴²⁸. (B) Haem 9 has been assigned LS2 resonance based on its proximal ligand His⁷⁸⁹ undergoes putative deprotonation by a propionate group of haem 10. This propionate is connected to a propionate group of haem 9 and Asp⁷⁹⁵ via H₂O-networks.

Table 6.5 – **The *bis*-histidine Dihedral angles measured in the crystal structure of UndA.** With only 1 molecule of UndA in the asymmetric unit of the UndA crystal structure (3UCP), *bis*-histidine dihedral averaging is not possible. Haems with putative histidinate ligation environments are detailed in the respective column. Please note that the angles measured are subject to the error of the resolution of the structure (i.e. 1.8 Å).

Haem No.	3UCP Labelling	Average <i>bis</i> -His dihedral (°)	Assigned EPR Signal	Putative Histidinate Ligation (bond length)
1	1	82	LGM1	-
2	2	20	LS1	-
3	3	53	LS1	-
4	4	27	LS2	His ³⁹⁰ :Asp ⁴²⁸ (2.8 Å)
5	5	73	LGM2	-
6	6	87	LGM1	-
7'	7	86	LGM1	-
7	8	66	LGM2	-
8	9	53	LGM2	-
9	10	59	LS2	His ⁷⁸⁹ :Haem 10-Haem 9-Asp ⁷⁹⁵ (3.0 Å)
10	11	79	LGM1	-

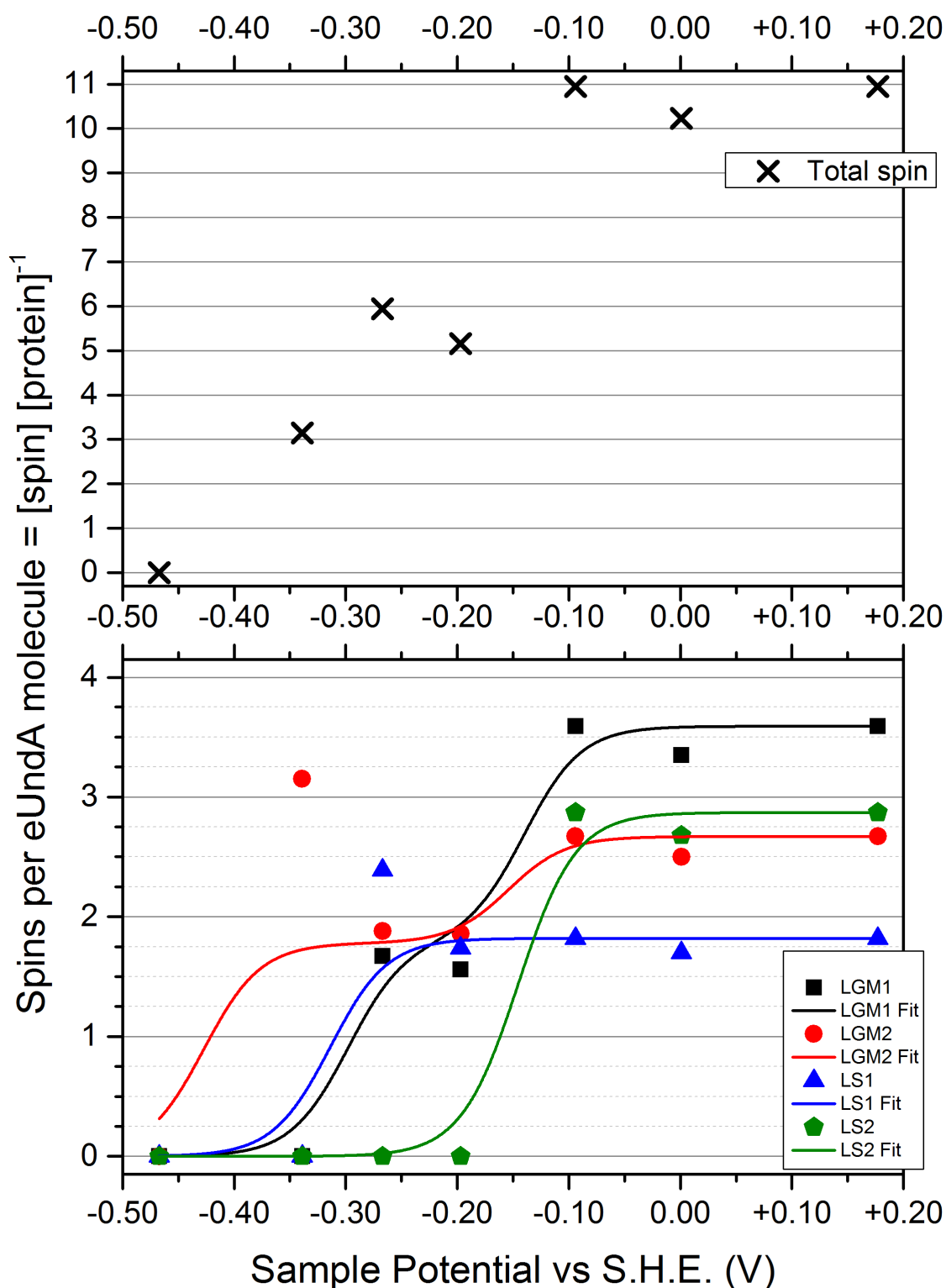


Fig. 6.9 – Spin Quantitation of eUndA’s EPR Resonance Features and Nernst Fit of Spin Quantitation. (Upper panel) The EPR signals of eUndA quantitate to 10.96 spins per eUndA molecule at +0.18 V, and 0.00 spins at -0.47 V. The LGM1 and LGM2 signals of eUndA have sample potential-dependent intensities that decrease consistently with decreasing sample potential. However the LS1 and LS2 signal intensities do not consistently decrease with decrease in sample potential. (Lower panel) Spins per eUndA molecule (symbols) was fitted to an $n = 1$ derivative of the Nernst equation (see Section M.4). The number of haems assigned to each resonance population informed the Nernst fit, as described in Table 6.6.

Although the potentiometric titration of eUndA is a low-resolution dataset, several mid-point potentials of haem populations were still spectroscopically-resolved. Nernst simulation of the EPR signal intensities (i.e. spins per molecule) indicate that the $E_{m,H}$ haem population have a derived $E_{m,7.6}$ range = $-0.14 \text{ V} \geq E_{m,7.6} \geq -0.15 \text{ V}$. Also, the $E_{m,L}$ population has an $E_{m,7.6}$ range = $-0.30 \text{ V} \geq E_{m,7.6} \geq -0.43 \text{ V}$ (Table 6.6). The non-integer values of spins per oxidised eUndA molecule indicate mixed populations of haem environments. In this model a monohaem population produces more than one resonance feature, as in eOmcA (Section 5.3). This complicates correlating quantitated spins directly to the structural properties of dihedral angle and histidinate haem ligation compiled in Table 6.6.

The $\sum_{i=1}^3 g_i^2$ for LGM1 and LS2 signals of oxidised eUndA deviate notably from 16.0 (Table 6.4). The $\sum_{i=1}^3 g_i^2$ of each resonance feature informs the normalised resonance double-integral, as discussed in Section 5.3. As with the LS3 signal of eOmcA, the $\sum_{i=1}^3 g_i^2 < 16.0$ of eUndA's LS2 signal is modelled to result in over-quantitation of the LS2 haem population (i.e. 2.82 spins per oxidised eUndA is assigned to two haems). In the same manner, the $\sum_{i=1}^3 g_i^2 > 16.0$ of eUndA's LGM1 signal results in under-quantitation (i.e. four haems assigned to the 3.59 spins quantitated).

Table 6.6 – The Derived Mid-point Potentials of eUndA via an EPR-monitored Redox Titre. EPR signals were fitted to an $n = 1$ oxidative Nernstian derivative. Mid-point potentials ($E_{m,7.6}$) resolved were obtained by simulating the number of haem contributions expected according to the crystal structure (see Table 6.5). Haems are not listed in order of derived $E_{m,7.6}$.

EPR Signal	Spins Quantified	No. of Haems Assigned	$E_{m,7.6}$ vs S.H.E. (V)				Haem Candidates
			1	2	3	4	
LGM1	3.59	4	-0.14	-0.14	-0.30	-0.30	1, 6, 7', 10
LGM2	2.67	3	-0.15	-0.43	-0.43		5, 7, 8
LS1	1.82	2	-0.31	-0.31			2, 3
LS2	2.87	2	-0.15	-0.15			4, 9

6.3.2 – Comparison of OMMC Spectropotentiometric Properties

Previous studies show that the EPR spectra of MtrC and MtrF possess similar sets of resonance features to the other OMMCs (i.e. LGM, LS1 and LS2 signals), expected for c-type haems [5, 8]. The comparison of the potentiometric properties of spectroscopically resolved haem populations between eUndA, eOmcA and MtrF is shown in Fig. 6.12 (spectral simulation and spin quantitation of the MtrC EPR spectra was not performed due to time constraints). Chapter 3 details the high tertiary structure conservation between the OMMCs. Fig. 6.1 also shows conservation of *bis*-histidine dihedral angle between the OMMCs MtrF, OmcA and UndA. Comparison shows there are 6 out of the 10 haems that have $\Delta\varphi \leq 30^\circ$ (Fig. 6.1). In particular, the high conservation of the *bis*-histidine dihedrals of haems 8 – 10 (i.e. $\Delta\varphi \leq 15^\circ$, OmcA haem equivalents) indicates conservation of domain IV's haem environments.

Considering the higher resolution of the UndA crystal structure, and that haems 8 and 9 of MtrF with a dihedral angle of 54° have also been assigned LGM and LS1 resonance respectively indicate that 53° is the transition angle. This is in agreement with a review correlating *bis*-histidine dihedral with g_1 value that indicates the LGM:LS1 transition dihedral angle = $40^\circ < \varphi < 65^\circ$ [9]. However the LGM2 haem population of eOmcA (i.e. haems 7 and 9) has an average dihedral angle of $49^\circ \pm 10$. The transition dihedral angle that differentiates LGM resonance from LS1 resonance, when comparing EPR spin quantitation and crystal structures of OMMCs, is tentatively assigned as 53° . For comparison, φ of the OMMCs has been compiled in Table 6.7 to compare φ identified via EPR and crystallography.

Table. 6.7 – **Comparison of OMMC *bis*-histidine Dihedral resolved via EPR and Crystallography.** Note that 8 out of 10 haems were accounted for in the oxidised MtrF spectrum [5]. * = Whereas $\varphi \geq 53^\circ$ corresponds to LGM resonance, LS2 and LS3 resonance do not correspond to φ . As such, LS2 (and LS3) resonance populations are accounted for in brackets. # = The presence of one LGM resonance population in MtrF's EPR spectrum provides no spectroscopic resolution of *bis*-histidine dihedral, φ .

OMMC	$\varphi \geq 60^\circ$		$60^\circ \geq \varphi \geq 30^\circ$		$30^\circ \geq \varphi$	
	Structure	EPR	Structure	EPR	Structure	EPR*
eUndA	6	4	3	3	2	2 (+2)
eOmcA	4	4	3	2	3	2 (+2)
MtrF	3	2	3	0 [#]	4	5 (+1)

With experimental resolution of the critical LGM:LS1 transition φ (i.e. 53°), full interpretation of the eOmcA potentiometric titre presented in Section 5.2 is possible. Haem 8, with average $\varphi = 43^\circ \pm 4$, is most likely to produce LS1 resonance. As such, haem 4's proximity to haem 5 make the haem 4:5 dihaem a candidate spin-couple, coupling out eOmcA's LS2 resonance to produce the LS3 signal observed. The renewed conclusions to the eOmcA potentiometric titre discussed are presented in Table 6.8.

Table 6.8 – eOmcA's Revised Mid-point Potential Assignments from its EPR-monitored Redox Titre. EPR signals were fitted to an $n = 1$ oxidative Nernst derivative. The mid-point potentials ($E_{m,7.6}$) extrapolated were obtained by modelling the number of haem contributions per resonance population according to eOmcA's structure. Haems are not listed in order of derived $E_{m,7.6}$. * = 1 haem assigned to resonance population despite sub-stoichiometric spins quantitated. † = Assigned due to tentative 53° LGM:LS1 transition φ . # = Assigned coupled signal to neighbouring haem 5.

EPR Signal	Spins Quantified	No. of Haems Assigned	$E_{m,7.6}$ vs S.H.E. (V)				Haem Candidates
			1	2	3	4	
LGM1	3.76	4	-0.05	-0.05	-0.05	-0.22	1, 3, 6, 10
LGM2	1.63	2	-0.06	-0.12			7, 9
LS1	2.56	2	-0.24	-0.30			2, 8 [†]
LS2	0.61	1*	-0.36				5
LS3	1.66	1	-0.08				5:4 [#]

The oxidised MtrF molecule provides near-integer spin-quantitation of its resonance populations [5], which is different in comparison with spin-quantitation of fully oxidised eOmcA and eUndA EPR spectra. As in eOmcA, it is likely that one or more haem populations of eUndA produce multiple resonance features. This complicates assignment of resonance signals to eUndA haems according to *bis*-histidine dihedral angle, φ , as in Section 5.3. However φ is used to assign the EPR signals observed to specific haem populations in eUndA (according to Table 6.5).

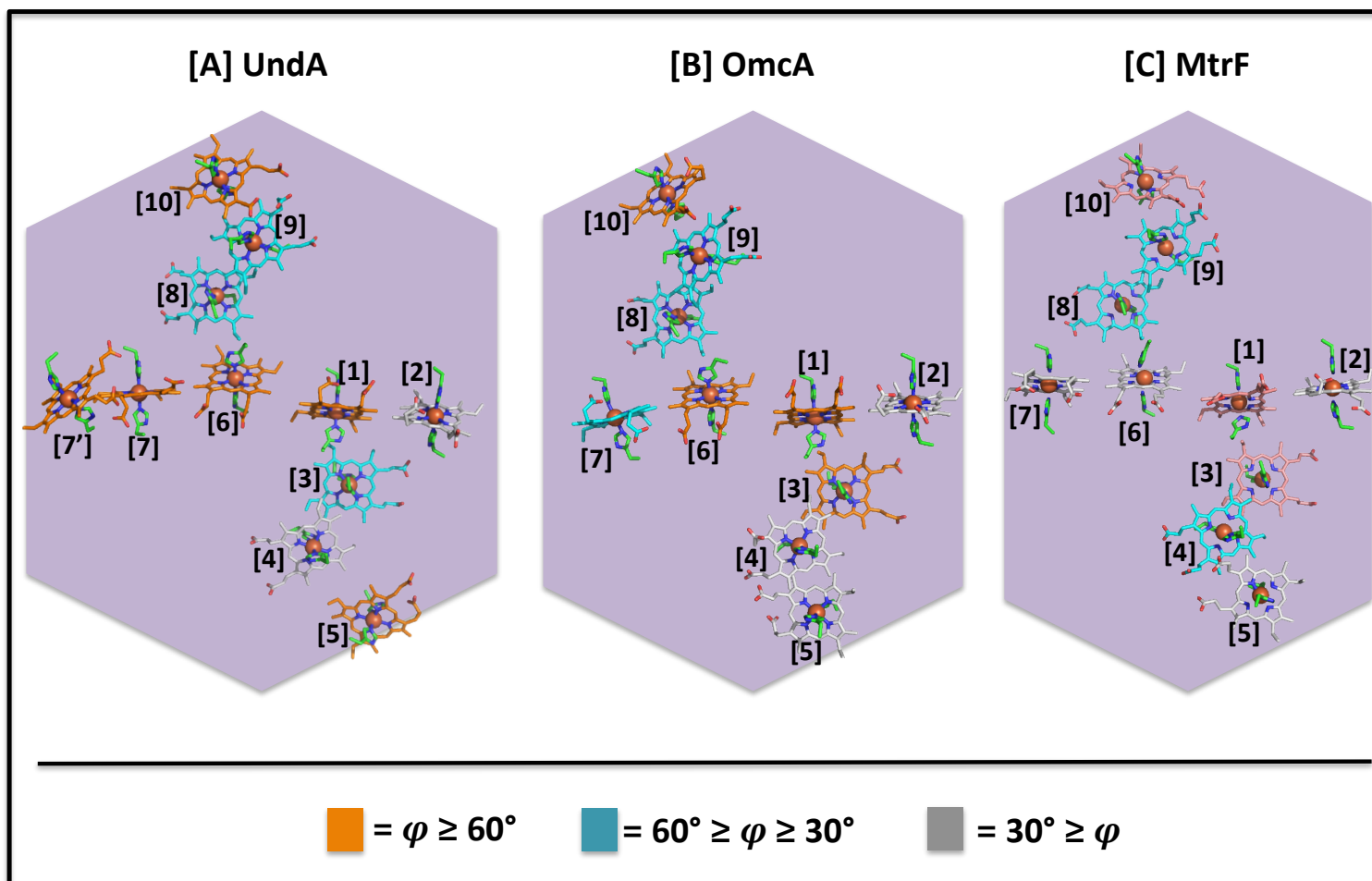


Fig. 6.10 – Comparison of haem dihedral angle arrangement amongst UndA, OmcA and MtrF. The *bis*-histidine dihedrals of OMMC haems are shown as colour-coded haems, and presented as described in Table 6.7: $\varphi \geq 60^\circ$, $60^\circ \geq \varphi \geq 30^\circ$ and $30^\circ \geq \varphi$.

Potentiometric characterisation of OmcA and UndA using EPR shows that the two OMMCs share similar potential windows with MtrC [4] and MtrF [5] (i.e. +0.08 to -0.43 V for OmcA; 0.00 to -0.47 V for UndA). However both the $E_{m,L}$ and $E_{m,H}$ haem populations of UndA have lower $E_{m,7.6}$ ranges than those of OmcA (Fig. 6.11). The $E_{m,L}$ and $E_{m,H}$ haem populations of UndA also have more discrete potential distribution from each other, however this may be a function of the low-resolution dataset.

The LGM and LS populations of eOmcA and MtrF share similar electro-active ranges, but eUndA's LGM haem population has a more negative reduction potential (Fig. 6.12A), as is the case for all eUndA's haems (Fig. 6.12C). All OMMC LS resonance features titrate over a similar potential range (Fig. 6.12B), and the crystallographically resolved dihedrals show highly conserved arrangement of haems where $\Delta\varphi \leq 30^\circ$ (Fig. 6.1). Comparison of the LGM (i.e. LGM1 and LGM2) and LS (i.e. LS1, LS2 and LS3) resonance populations of eOmcA and eUndA indicate that φ does not dictate haem reduction potential. This correlates well with factors such as solvent exposure and surrounding polypeptide environment dielectric properties determining a haem's reduction potential [10].

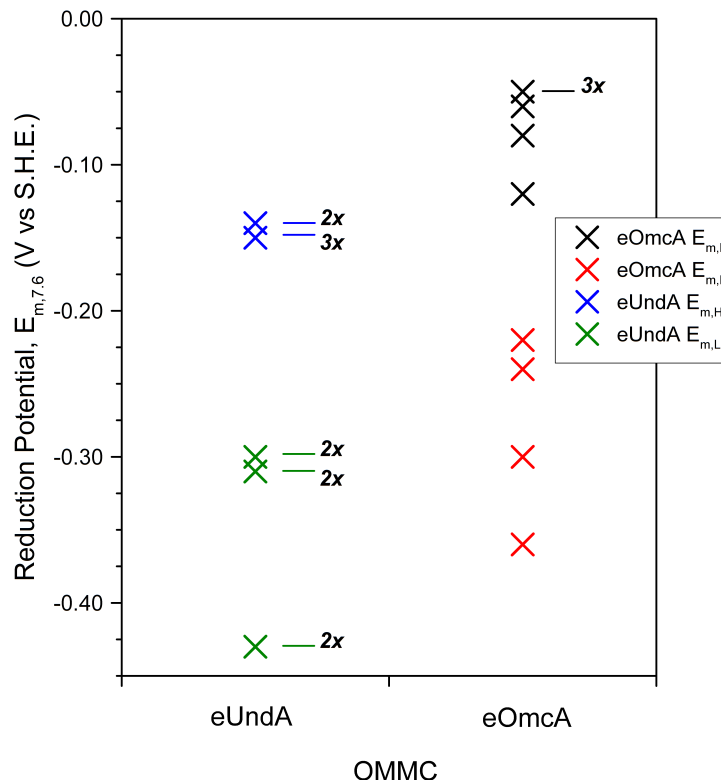


Fig. 6.11 – **Comparison of Reduction Potentials between OmcA and UndA.** Mid-point potentials compiled were determined using EPR at pH 7.60. The number of haems that share a given reduction potential are numbered adjacent to its respective data point.

The significance of φ conservation is unclear. Localisation of φ conservation to domain IV's C-terminal trihaem, as opposed to random distribution of matching φ , indicates functional φ maintenance (i.e. conservation) as opposed to spontaneous correlation. Comparison of OmcA and UndA redox titres shows that conservation of φ does not correlate with $E_{m,7.6}$ (Fig. 6.12). Furthermore, MtrF's haem 10 was resolved as the lowest potential haem [5], whereas the lowest potential haem in OmcA is putatively haem 5 (Table 6.8), implying opposing electron transfer directionality. The spectroscopic resolution of the LS2 haem population's high reduction potential of eUndA (putatively haems 4 and 9) still provides no indication of electron transfer directionality in eUndA. As such the inferred opposite directionality proposed between the MtrF and OmcA may be the basis for differential OMMC function. The *in silico* model of the MtrC crystal structure indicated that haems 8 and 10 may be histidinate ligated [11], and according to the published EPR potentiometric titre monitored this putative LS2 population has at least one low reduction potential component (i.e. haem reduced below -0.45 V vs S.H.E.) [8].

The current potentiometric data supports the working model that MtrC/F interact with their respective porin-cytochrome modules via the electron ingress site haem 10, whereas OmcA's unique localisation between tight and loosely-associating EPS [12] may require haem 5 to be its electron ingress site. As such this may be the functional basis for *Shewanella spp* encoding several structurally similar OMMCs within its *mtr* gene cluster.

The mid-point potential of mineral substrates of *S. oneidensis* MR-1 (i.e. lepidocrocite $E_{m,7} = -0.10$ V, hematite $E_{m,7} = -0.12$ V, goethite $E_{m,7} = -0.16$ V vs S.H.E. [13]) indicate differential roles for OMMCs according to their respective E_m . Whereas it is energetically favourable for all of UndA's haems to reduce the minerals listed (i.e. $E_{m,7.6} \leq -0.14$ V), it is only energetically favourable for electron transfer from OmcA's tetrahaem $E_{m,L}$ population (i.e. $E_{m,7.6} \leq -0.22$ V) to reduce mineral TEA. Mid-point potentials of MtrF derived from PFE indicate that only a putative pentahaem $E_{m,L}$ population (i.e. $E_{m,7.0} \leq -0.15$ V) can reduce mineral TEA [5]. Qualitative assessment of the EPR-monitored potentiometric titration indicates that of the eight haems quantitated per MtrF molecule, three have $E_{m,7.5} \leq -0.15$ V. As such all three major OMMC clades have the capacity to reduce the ferric mineral TEAs, but may not utilise their entire haem content based on their reduction potentials.

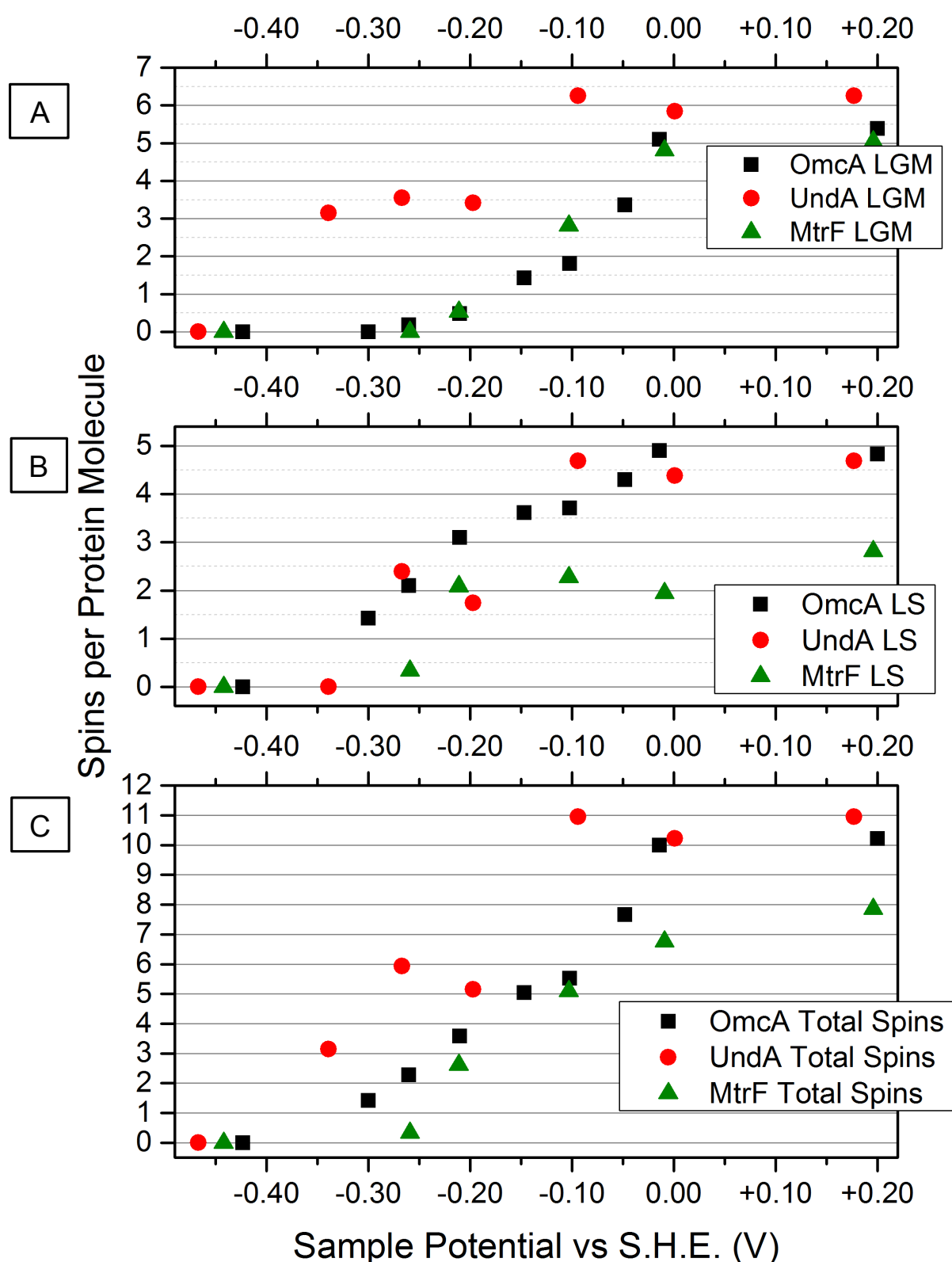


Fig. 6.12 – Comparison of the Potentiometric Properties of UndA, OmcA and MtrF's LGM and LS Haem populations. (A) The potentiometric titration of eUndA, eOmcA and MtrF's LGM resonance population(s). This includes the LGM population of MtrF, and the LGM1 and LGM2 populations of eOmcA and eUndA. (B) The potentiometric titration of eUndA, eOmcA and MtrF's LS resonance populations. This includes the LS1 and LS2 populations of MtrF and eUndA, and the LS1, LS2 and LS3 populations of eOmcA. (C) The potentiometric titration of eUndA, eOmcA and MtrF's sum resonance. All resonance features observed of each protein were added for each protein to generate this plot.

Although energetically unfavourable, multi-cofactor oxidoreductases do not exclusively transfer electrons from a low potential co-factor to a high potential co-factor [14]. EPR provides spectral resolution of the $E_{m,H}$ and $E_{m,L}$ haem populations of eOmcA and eUndA. It is possible that the haem mid-point potentials are distributed such that the ΔE_m between OMMC electron egress site(s) and mineral TEA is favourable. However elaborate *in silico* determination of reduction potentials of MtrF's haems indicate that its haems are not arranged in ascending order of reduction potential within the cytochrome [15]. Although there is high conservation of domain fold between the OMMCs, differences in haem solvent exposure and differential haem environments likely contribute to the differences in potentiometric properties reported here between MtrF, OmcA and UndA. The MtrAB:MtrC interaction that modulates haem reduction potentials also indicates the scope for the E_m of OMMC haems to be modulated by their interaction with protein interaction partners [4]. OmcA and UndA could thus have similar set/distribution of reduction potentials to MtrF and MtrC *in vivo*. MtrC's interaction with OmcA [16-18] may also shift the redox poise of OmcA's haems *in vivo*, and a similar interaction may occur in *Shewanella* spp that encode for UndA.

The MtrCAB complex modulates the reduction potential spanned by MtrA and MtrC components such that electron transfer from MtrCAB to mineral TEA is favourable [4]. As such, recent evidence of semiquinone co-factors for MtrC and OmcA has been indicated to contribute to the mechanism of DMR by enhancing OMMC oxidation kinetics [19].

The full context of OmcA's extracellular localisation is that the 9 nm-long cytochrome is embedded in an exopolysaccharide matrix 0.5 μ m deep [20]. More specifically, OmcA co-localises with the tight and loosely-associating exopolymeric substance (EPS) [12]. How this contributes to the mid-point potentials of OMMC haems and/or affects the DMR mechanism has not been detected/determined. However, correlating physico-chemical observations of purified protein to cellular function is addressed in the next chapter.

References

- 1 Heidelberg, J. F., Paulsen, I. T., Nelson, K. E., Gaidos, E. J., Nelson, W. C., Read, T. D., Eisen, J. A., Seshadri, R., Ward, N., Methe, B., Clayton, R. A., Meyer, T., Tsapin, A., Scott, J., Beanan, M., Brinkac, L., Daugherty, S., DeBoy, R. T., Dodson, R. J., Durkin, A. S., Haft, D. H., Kolonay, J. F., Madupu, R., Peterson, J. D., Umayam, L. A., White, O., Wolf, A. M., Vamathevan, J., Weidman, J., Impraim, M., Lee, K., Berry, K., Lee, C., Mueller, J., Khouri, H., Gill, J., Utterback, T. R., McDonald, L. A., Feldblyum, T. V., Smith, H. O., Venter, J. C., Nealson, K. H. and Fraser, C. M. (2002) Genome sequence of the dissimilatory metal ion-reducing bacterium *Shewanella oneidensis*. *Nature Biotechnology*. **20**, 1118-1123
- 2 Fredrickson, J. K., Romine, M. F., Beliaev, A. S., Auchtung, J. M., Driscoll, M. E., Gardner, T. S., Nealson, K. H., Osterman, A. L., Pinchuk, G., Reed, J. L., Rodionov, D. A., Rodrigues, J. L. M., Saffarini, D. A., Serres, M. H., Spormann, A. M., Zhulin, I. B. and Tiedje, J. M. (2008) Towards environmental systems biology of *Shewanella*. *Nature Reviews Microbiology*. **6**, 592-603
- 3 Shi, L., Belchik, S. M., Wang, Z., Kennedy, D. W., Dohnalkova, A. C., Marshall, M. J., Zachara, J. M. and Fredrickson, J. K. (2011) Identification and Characterization of UndA(HRCR-6), an Outer Membrane Endecaheme c-Type Cytochrome of *Shewanella* sp Strain HRCR-6. *Applied and Environmental Microbiology*. **77**, 5521-5523
- 4 Hartshorne, R. S., Reardon, C. L., Ross, D., Nuester, J., Clarke, T. A., Gates, A. J., Mills, P. C., Fredrickson, J. K., Zachara, J. M., Shi, L., Beliaev, A. S., Marshall, M. J., Tien, M., Brantley, S., Butt, J. N. and Richardson, D. J. (2009) Characterization of an electron conduit between bacteria and the extracellular environment. *Proceedings of the National Academy of Sciences of the United States of America*. **106**, 22169-22174
- 5 Clarke, T. A., Edwards, M. J., Gates, A. J., Hall, A., White, G. F., Bradley, J., Reardon, C. L., Shi, L., Beliaev, A. S., Marshall, M. J., Wang, Z., Watmough, N. J., Fredrickson, J. K., Zachara, J. M., Butt, J. N. and Richardson, D. J. (2011) Structure of a bacterial cell surface decaheme electron conduit. *Proceedings of the National Academy of Sciences of the United States of America*. **108**, 9384-9389
- 6 Edwards, M. J., Baiden, N. A., Johs, A., Tomanicek, S. J., Liang, L., Shi, L., Fredrickson, J. K., Zachara, J. M., Gates, A. J., Butt, J. N., Richardson, D. J. and Clarke, T. A. (2014) The X-ray crystal structure of *Shewanella oneidensis* OmcA reveals new insight at the microbe-mineral interface. *Febs Letters*. **588**, 1886-1890
- 7 Edwards, M. J., Hall, A., Shi, L., Fredrickson, J. K., Zachara, J. M., Butt, J. N., Richardson, D. J. and Clarke, T. A. (2012) The Crystal Structure of the Extracellular 11-heme Cytochrome UndA Reveals a Conserved 10-heme Motif and Defined Binding Site for Soluble Iron Chelates. *Structure*. **20**, 1275-1284
- 8 Hartshorne, R. S., Jepson, B. N., Clarke, T. A., Field, S. J., Fredrickson, J., Zachara, J., Shi, L., Butt, J. N. and Richardson, D. J. (2007) Characterization of *Shewanella oneidensis* MtrC: a cell-surface decaheme cytochrome involved in respiratory electron transport to extracellular electron acceptors. *Journal of Biological Inorganic Chemistry*. **12**, 1083-1094
- 9 Yatsunyk, L. A., Dawson, A., Carducci, M. D., Nichol, G. S. and Walker, F. A. (2006) Models of the cytochromes: Crystal structures and EPR spectral characterization of low-spin bis-imidazole complexes of (OETPP)Fe-III having intermediate ligand plane dihedral angles. *Inorganic Chemistry*. **45**, 5417-5428
- 10 Moore, G. R. and Pettigrew, G. W. (1990) *Springer Series in Molecular Biology Cytochromes C: Evolutionary, Structural and Physicochemical Aspects*.

- Moore, G. R. and G. W. Pettigrew. Springer Series in Molecular Biology: Cytochromes C: Evolutionary, Structural and Physiocochemical Aspects. Xvi+478p. Springer-Verlag: Berlin, Germany; New York, New York, USA. Illus
- 11 Edwards, M. J., Fredrickson, J. K., Zachara, J. M., Richardson, D. J. and Clarke, T. A. (2012) Analysis of structural MtrC models based on homology with the crystal structure of MtrF. *Biochemical Society Transactions*. **40**, 1181-1185
 - 12 Cao, B., Shi, L. A., Brown, R. N., Xiong, Y. J., Fredrickson, J. K., Romine, M. F., Marshall, M. J., Lipton, M. S. and Beyenal, H. (2011) Extracellular polymeric substances from *Shewanella* sp HRCR-1 biofilms: characterization by infrared spectroscopy and proteomics. *Environmental Microbiology*. **13**, 1018-1031
 - 13 White, G. F., Shi, Z., Shi, L., Wang, Z. M., Dohnalkova, A. C., Marshall, M. J., Fredrickson, J. K., Zachara, J. M., Butt, J. N., Richardson, D. J. and Clarke, T. A. (2013) Rapid electron exchange between surface-exposed bacterial cytochromes and Fe(III) minerals. *Proceedings of the National Academy of Sciences of the United States of America*. **110**, 6346-6351
 - 14 Nitschke, W. and Rutherford, A. W. (1989) Tetraheme Cytochrome-C Subunit of *Rhodopseudomonas viridis* characterized by EPR. *Biochemistry*. **28**, 3161-3168
 - 15 Smith, D. M. A. and Rosso, K. M. (2014) Possible Dynamically Gated Conductance along Heme Wires in Bacterial Multiheme Cytochromes. *Journal of Physical Chemistry B*. **118**, 8505-8512
 - 16 Shi, L., Chen, B. W., Wang, Z. M., Elias, D. A., Mayer, M. U., Gorby, Y. A., Ni, S., Lower, B. H., Kennedy, D. W., Wunschel, D. S., Mottaz, H. M., Marshall, M. J., Hill, E. A., Beliaev, A. S., Zachara, J. M., Fredrickson, J. K. and Squier, T. C. (2006) Isolation of a high-affinity functional protein complex between OmcA and MtrC: Two outer membrane decaheme c-type cytochromes of *Shewanella oneidensis* MR-1. *Journal of Bacteriology*. **188**, 4705-4714
 - 17 Zhang, H., Tang, X., Munske, G. R., Zakharova, N., Yang, L., Zheng, C., Wolff, M. A., Tolic, N., Anderson, G. A., Shi, L., Marshall, M. J., Fredrickson, J. K. and Bruce, J. E. (2008) In vivo identification of the outer membrane protein omcA-mtrC interaction network in *Shewanella oneidensis* MR-1 cells using novel hydrophobic chemical cross-linkers. *Journal of Proteome Research*. **7**, 1712-1720
 - 18 Ross, D. E., Ruebush, S. S., Brantley, S. L., Hartshorne, R. S., Clarke, T. A., Richardson, D. J. and Tien, M. (2007) Characterization of protein-protein interactions involved in iron reduction by *Shewanella oneidensis* MR-1. *Applied and Environmental Microbiology*. **73**, 5797-5808
 - 19 Okamoto, A., Hashimoto, K., Nealson, K. H. and Nakamura, R. (2013) Rate enhancement of bacterial extracellular electron transport involves bound flavin semiquinones. *Proceedings of the National Academy of Sciences of the United States of America*. **110**, 7856-7861
 - 20 Stukalov, O., Korenevsky, A., Beveridge, T. J. and Dutcher, J. R. (2008) Use of atomic force microscopy and transmission electron microscopy for correlative studies of bacterial capsules. *Applied and Environmental Microbiology*. **74**, 5457-5465

Chapter 7: **The Functional Consequences of Mutations near Haem 10 of** **OmcA**

7.1 – Introduction

Recent crystal structure data has shown that there is significant tertiary structure conservation amongst OMMCs: their polypeptides are organised into two split β -barrel domains and two pentahaem domains (a hexahaem domain for UndA) [1, 2]. However, beyond identifying split β -barrels and the orientation of haems, the structural data obtained does not differentiate the OMMCs significantly. The split β -barrels identified are possible flavin-interaction domains [3]. However, the question of whether electron transfer to mineral TEA occurs via direct contact or flavin shuttling (see Section 1.3.5) is not clarified by the structural data.

7.1.1 – Current Knowledge of OmcA Function

As predicted by identification of 10 CXXCH motifs [4], OmcA is a decahaem electron transfer protein [5, 6] with an electro-active range (i.e. +0.08 V to -0.42 V vs S.H.E.) that resolves into the low and high potential haem populations (i.e. $E_{m,L}$ and $E_{m,H}$ respectively, Section 5.3). A property of OMMCs that is unique amongst cytochromes is their localisation to the extracellular surface of the outer-bacterial membrane of *S. oneidensis* [7, 8] and *Escherichia coli* cells when heterologously expressed [9]. OmcA co-localises to both the tight and loosely-associating EPS [10], and is shown to be the most sensitive OMMC to whole cell proteinase K digestion [7]. OmcA's extracellular localisation positions it to interact with the MtrCAB complex [11, 12], putatively via MtrC [5]. The putative OmcA_xMtrC_y complex has an enhanced Fe³⁺-NTA reduction rate per mg of protein compared to its components [8]. Gene deletion studies show OmcA accounts for \approx 50% of *S. oneidensis* Mn(IV) oxide reduction activity [13, 14] and \approx 25 – 50% Fe(III) mineral reduction activity [15-17]. However $\Delta mtrC\Delta mtrF$ deletion strains have negligible Fe(III) citrate, Fe₂O₃ and FMN reduction rates [15, 18], implying that the inferred expression of *omcA* as the sole OMMC is not sufficient to maintain wild-type DMR capacity. Within the literature there has been an emphasis on OmcA's capacity to bind hematite, which will be reviewed in the discussion.

7.1.2 – Building on Current Knowledge of OmcA with Mutagenic Studies

With a significant body of knowledge on OmcA's role in DMR, there is no function ascribed to OmcA's polypeptide content aside from the lipid binding motif (i.e. LXXC), haem binding motifs (i.e. CXXCH) and distal haem ligands resolved via X-ray crystallography. Of interest is whether there is optimisation of OmcA's polypeptide for protein interaction partners, extracellular localisation, but especially reduction of insoluble mineral TEA. OMMCs with the capacity to tunnel electrons to TEA within 14 Å of its electron egress site [19] may not require polypeptide that is optimised for substrate interaction.

A "hematite-binding" peptide motif was determined from co-sedimentation of phage capsules expressing a library of peptide sequence and hematite [20]. A derived motif was then truncated according to the OMMC amino acid sequences to the peptide Thr/Ser-Pro-Thr/Ser, and a single "hematite-binding motif" was identified in both OmcA and MtrC. The localisation of the putative hematite-binding motif adjacent to haem 10's CXXCH motif in both OmcA and MtrC indicates a model of electron transfer directionality where haem 10 is the electron egress site. The motif was proposed to facilitate hydrogen bonding to oxide-presenting surfaces of hematite via the motif's hydroxyl groups, however many mineral substrates have oxide-presenting surfaces. Furthermore, there are several solvent-exposed hydroxyl groups that exist in OmcA [2], and putatively MtrC. The peptide motif determined may be considered to be a putative "mineral interaction peptide" (MIP).

As such, the study presented in this Chapter details several site-directed mutations made and their effect on OmcA's structure, potentiometric properties, and mineral reduction capacity via mineral reduction assays developed in collaboration with Dr Liang Shi and Dr Dave Kennedy of the Pacific National Laboratory, USA.

7.2 - Results

7.2.1 – Crystallographic Confirmation of Successful Mutagenesis

The mutants generated for the study, and the rationale for each mutation is described in Table 6.1. Both extracellular and LXXC-containing forms of OmcA were generated for each mutant, named eOmcA and mOmcA respectively. The soluble (i.e. eOmcA) form of the MIP mutants was generated to confirm that the desired site-directed mutation existed in the protein.

The eOmcA MIP mutant T⁷²⁵G (referred to as eT⁷²⁵G) was purified to homogeneity, using anion exchange and gel filtration chromatography, (described in Section M.3.3; Fig. 7.1). Confirmation of the desired mutation was subsequently obtained through successful crystallography experiments resulting in a 2.8 Å resolution structure of eT⁷²⁵G. As expected for point mutation of a surface residue in a >700 amino acid protein, the tertiary structure observed for eOmcA (hereon describing wild-type eOmcA) is maintained in eT⁷²⁵G. This includes maintenance of domain fold into two split β-barrels, two pentahaem binding domains and haem localisation. The orientation of amino acid side chains have varied between eOmcA and eT⁷²⁵G crystal structures, which is most likely due to different crystal condition pH values producing different side chain protonation states (Section M.6).

Concerning the proposed MIP, the Thr⁷²⁵ side chain is successfully mutated to Gly⁷²⁵ (Fig. 7.2). The Gln⁷²⁸ side-chain of eOmcA localises within hydrogen bonding distance of the His⁷²⁴ side chain position. The molecular environment of the proposed MIP indicates a secondary structural effect of the T⁷²⁵G mutation: the wild-type Gln⁷²⁸ hydrogen bond with the proximal His⁷²⁴ ligand of haem 10 is non-existent in the eT⁷²⁵G mutant.

By comparison, the crystal structure of purified eP⁷²⁶G obtained (Fig 7.1B) indicates that there is negligible change in side chain orientation of the MIP residues between eP⁷²⁶G and eOmcA (Fig. 7.2). Also, the Gln⁷²⁸ side chain maintains comparable orientation and distance from the proximal His⁷²⁴ ligand of haem 10 in the 2.1 Å resolution eP⁷²⁶G structure, although the inferred bond angle is unfavourable.

Table 7.1. – **The *S. oneidensis* mutant strains used to study the putative MIP in OmcA.** *S. oneidensis* MR-1 and several $\Delta mtrC\Delta omcA$ strains encoding various *omcA*⁺ mutants were used to determine the functional consequences of the respective mutations to hematite reduction. There were eOmcA-producing strains made of the majority of the mutants listed. * = N.B. *S. oneidensis* MR-1 produces OmcA and MtrC, both containing the putative MIP.

Genome Deletion	<i>in trans omcA</i> ⁺	eOmcA LS #	mOmcA LS #	Rationale
MR-1 (i.e. None)	N/A	N/A	N/A	Physiological hematite reduction capacity.*
$\Delta mtrC\Delta omcA$	None (+empty pBAD202)	785		Removal of OMMCs with putative mineral interaction peptide.
	<i>omcA</i> _(wt) ⁺	330	786	Determine complementation of hematite reduction phenotype.
	T ⁷²⁵ G	838	787	Ser/Thr ⁷²⁵ is the only conserved hydrogen-bonding residue of the MIP in OmcA
	P ⁷²⁶ V	821	788	Sequence alignment of OmcA of <i>Shewanella spp</i> shows Pro ⁷²⁶ is highly conserved and only replaced by Val in <i>S. frigidimarina</i> . The 70% conservation for Pro within the MIP determined was otherwise replaced with Val (5%) and 3 other amino acids (25%) [20].
	P ⁷²⁶ G	819	807	Molecular modelling indicated replacement of Pro with Gly in MIP permitted structural flexibility inhibitory to hydrogen bonding with hematite [20].
	T ⁷²⁵ G:S ⁷²⁷ G	820	823	Total removal of hydrogen bonding capacity of amino acid side chains from MIP
	C ⁷²⁷ ins	839	808	A peptide at the crystallographic OmcA "dimer"-interface observed is T ⁵²⁵ PCS ⁵²⁸ . C727 insertion is an attempt to mimic this peptide and identify an alternate MIP. Maintenance of <i>omcA</i> _(wt) ⁺ hematite reduction would indicate the additional TPCS sequence generated adjacent to haem 10's CXXCH is an alternate MIP.
	Y ³⁷⁴ F	822	844	Determine functional effect of removing hydrogen-bonding capacity of conserved Try ³⁷⁴ at crystallographic interface.
	C ⁵²⁷ V	840	845	Determine functional effect of disrupting the disulfide bridge near the proposed interface.

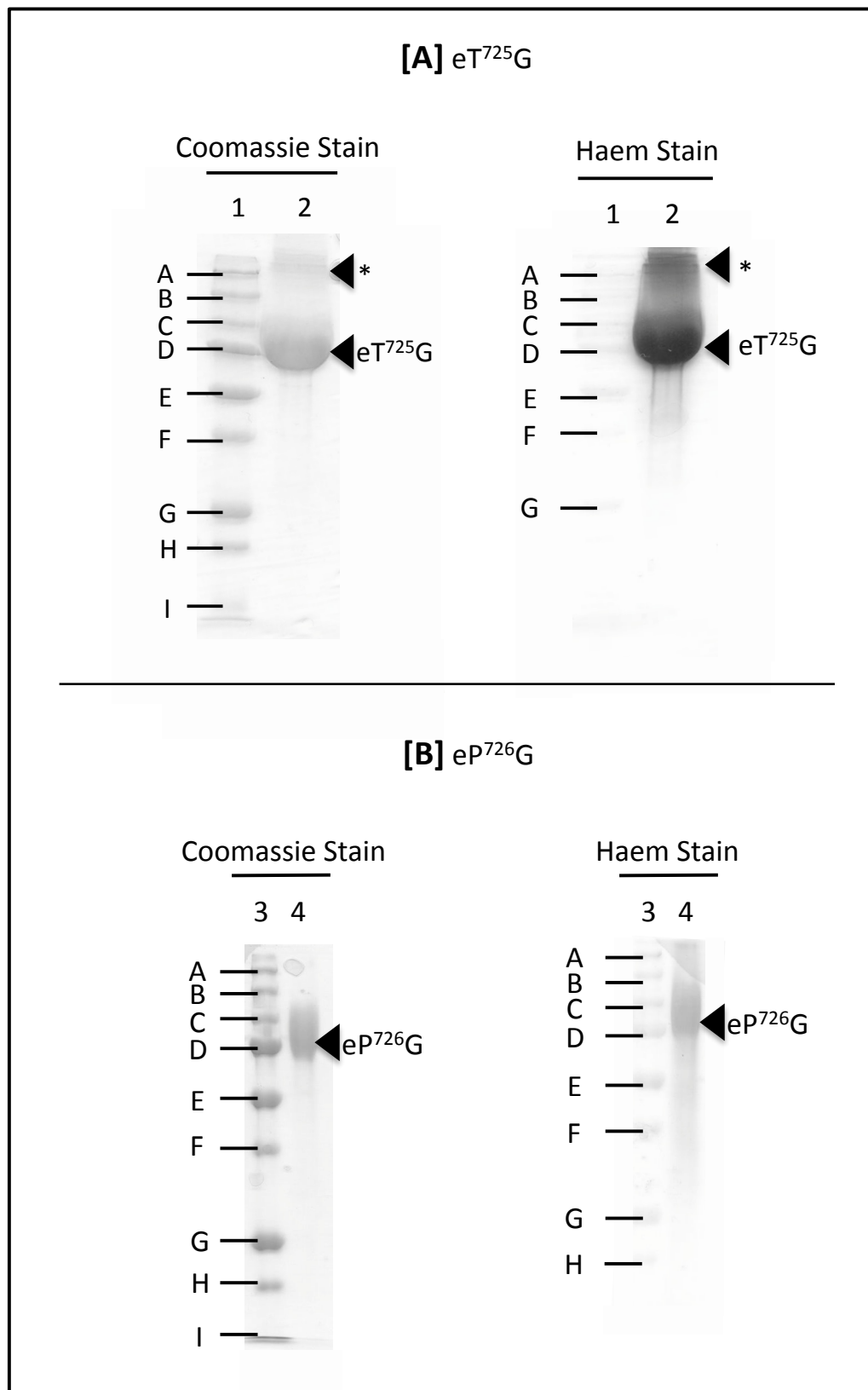


Figure 7.1 – Purification of eT⁷²⁵G and eP⁷²⁶G. Coomassie (left panel) and Haem-stained (right panel) SDS-PAGE gels of the same purified (A) eT⁷²⁵G and (B) eP⁷²⁶G samples respectively. Lanes 1 & 3 contain molecular weight markers, lane 2 & 4 contain pure eT⁷²⁵G and eP⁷²⁶G respectively. Molecular weight markers are: A = 250 kDa, B = 150 kDa, C = 100 kDa, D = 75 kDa, E = 50 kDa, F = 37 kDa, G = 25 kDa, H = 15 kDa and I = 10 kDa. Note that the eT⁷²⁵G migrates to the same MW_{app} of eOmcA. * = Artefact of overloading gel with protein.

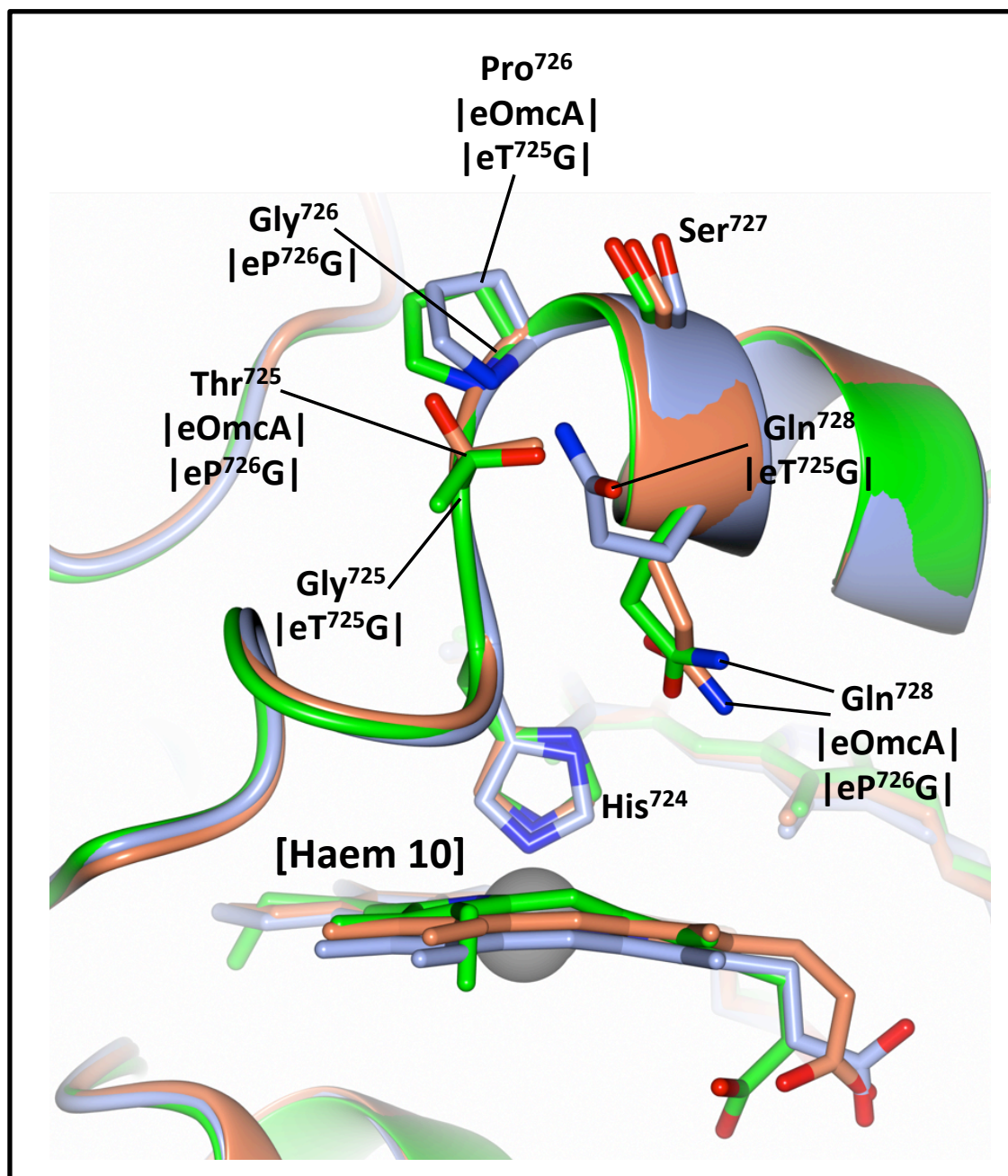


Figure 7.2 – **Comparison of the MIP X-ray Crystal Structures of eOmcA, eT⁷²⁵G and eP⁷²⁶G.** The X-ray crystal structures of eOmcA (green), eT⁷²⁵G (blue) and eP⁷²⁶G (orange) are superimposed. Mutated or unique conformers of side chain residues are labelled independently, whereas side chains of identical amino acid and conformation have been labelled once. $|x|$ = Protein identity. Only amino acid side chains of interest are shown, the distal histidine ligand of haem 10 is omitted (which is present in all MIP mutants crystallised). The crystal structures of eT⁷²⁵G and eP⁷²⁶G were resolved to 2.8 Å and 2.1 Å respectively.

7.2.2 – Potentiometric Properties of $eT^{725}G$

An EPR-monitored potentiometric titration of the $eT^{725}G$ mutant was performed to detect a secondary effect on the reduction potentials of $eT^{725}G$'s haems. As such $eT^{725}G$ was poised at comparable reduction potentials to the eOmCA EPR titre, under identical protein concentration and buffer conditions (i.e. 145 μM $eT^{725}G$ in 20 mM HEPES, pH 7.60, 50 mM NaCl, 1% glycerol, 0.01% CHAPS). The baseline-subtracted spectra measured are presented in (Fig. 7.3). Analysis of the $eT^{725}G$ EPR spectra is performed in this chapter without spectrum simulation and spin quantitation.

The fully oxidised EPR spectrum of $eT^{725}G$ (i.e. +0.24 V vs S.H.E.) maintained the LGM1, LGM2, LS1 and LS3 EPR signals observed in oxidised eOmCA (Section 5.2). The LS2 EPR signal of $eT^{725}G$ is not readily resolved from the LS1 signal until sample potential is reduced to -0.15 V vs S.H.E., very similar to the LS2 signal in the eOmCA potentiometric titre (Section 5.2).

Several qualitative differences are apparent between the eOmCA and $eT^{725}G$ EPR spectropotentiometric titres at comparable sample potentials (Fig 7.4). The presence of a radical signal (i.e. $g_{app} = 2.001$) at sample potentials $\leq +0.04$ V vs S.H.E. is unlikely to be produced by reduced viologen-based mediators ($E_{m,7} = -0.44$ V vs S.H.E.). In the spectrum of $eT^{725}G$ poised at +0.04 V vs S.H.E., a very broad bi-signate feature at $g_{app} = 1.22$ is not observed in eOmCA at any sample potential (Fig. 7.4A). Also, a LGM2 $g_{1,app}$ shift of +0.10 to 3.28 occurs at -0.15 V vs S.H.E., but at all other sample potentials LGM2 $g_{1,app}$ retains its eOmCA value (i.e. $g_{1,app} = 3.18$; Fig. 7.4B).

In the absence of complete simulation of all spectra in the $eT^{725}G$ EPR potentiometric titre, $g_{1,app}$ peak height (directly proportional to signal concentration) is plotted against sample potential to indicate the electroactive ranges of the haem populations resolved. However, $g_{1,app}$ peak height is not normalised as accurately as normalised double integral for signal absorption envelope (Section M.4), so quantitative analysis cannot be performed. Using $g_{1,app}$ peak height, the sample potential at which resonance haem populations are initially reduced are unclear. However all $eT^{725}G$ EPR signals are reduced within 50 mV of their eOmCA counterparts (Fig. 7.5). The LGM1 signal appears to titrate across the sample potential measured, suggesting contributions from multiple haems as in eOmCA. The apparent increase in LGM2 signal at -0.15 V vs S.H.E. corresponds with the sudden change in $g_{1,app}$ (Fig. 7.4B). The apparent increase in LS1 signal between +0.04 V and -0.10 V vs S.H.E.

corresponds with the inability to resolve LS1 and LS2 $g_{1,app}$ peaks without spectral simulation, resulting in compound LS1 + LS2 $g_{1,app}$ peak height measured above -0.15 V vs S.H.E. and an inability to measure LS2 signal $g_{1,app}$ peak height in the same reduction potential range.

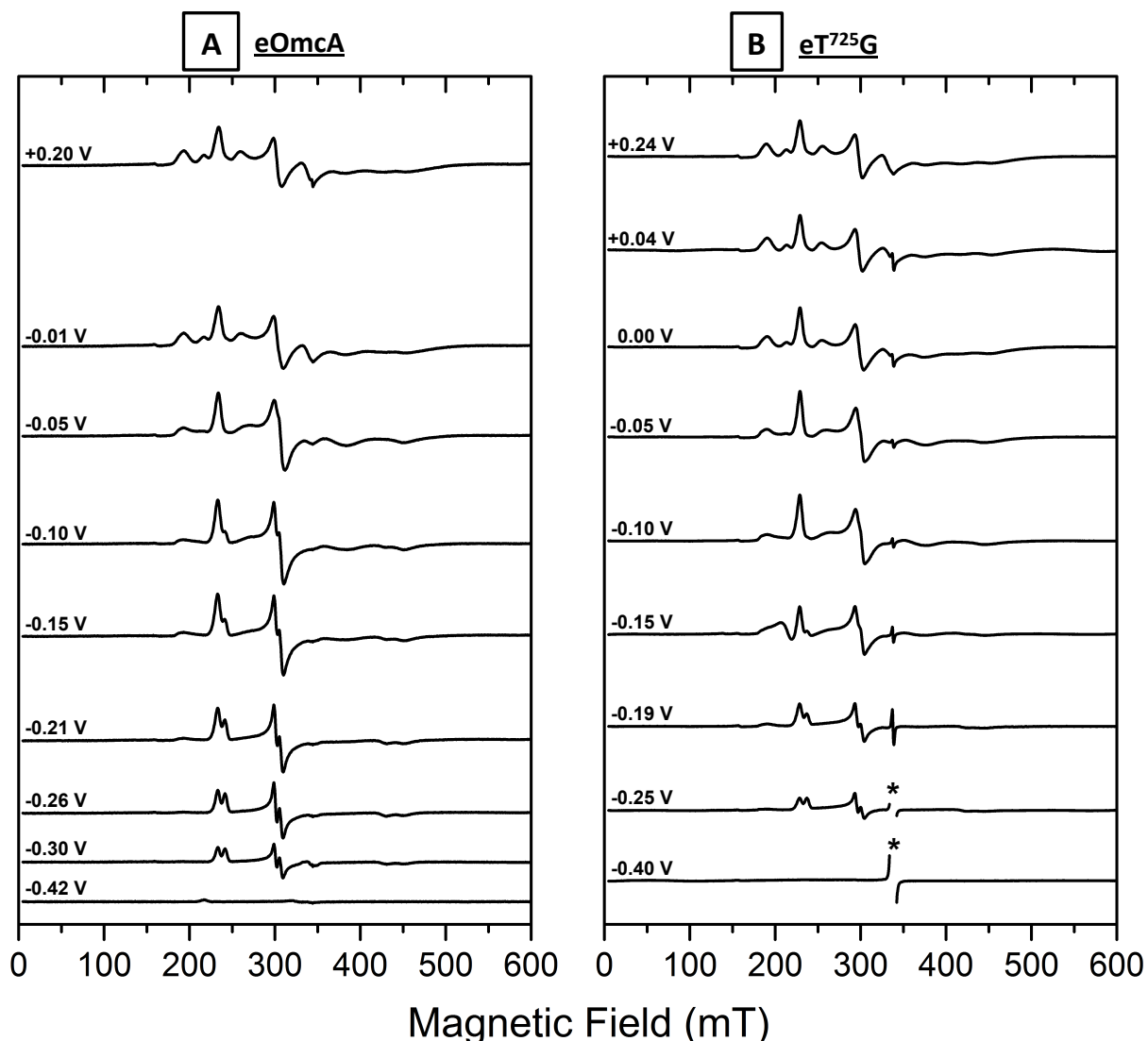


Fig. 7.3 – EPR-monitored potentiometric titration of eT⁷²⁵G. (A) EPR spectra of eOmcA (145 μ M) poised at the sample potentials listed (presented in Section 4.2). EPR spectra were measured at 9.69 GHz, 7 K \pm 2, 2.012 mW. (B) EPR spectra of eT⁷²⁵G (145 μ M) poised at the sample potentials listed. EPR spectra were measured at 9.46 GHz, 10 K \pm 0.1, 2.007 mW and multiplied by a factor of 6 for comparison with eOmcA. Both eOmcA and eT⁷²⁵G were poised in 20 mM HEPES, pH 7.60, 50 mM NaCl, 0.01% CHAPS, 1% glycerol. All sample potentials listed are vs S.H.E. * = Radical contribution removed for comparison.

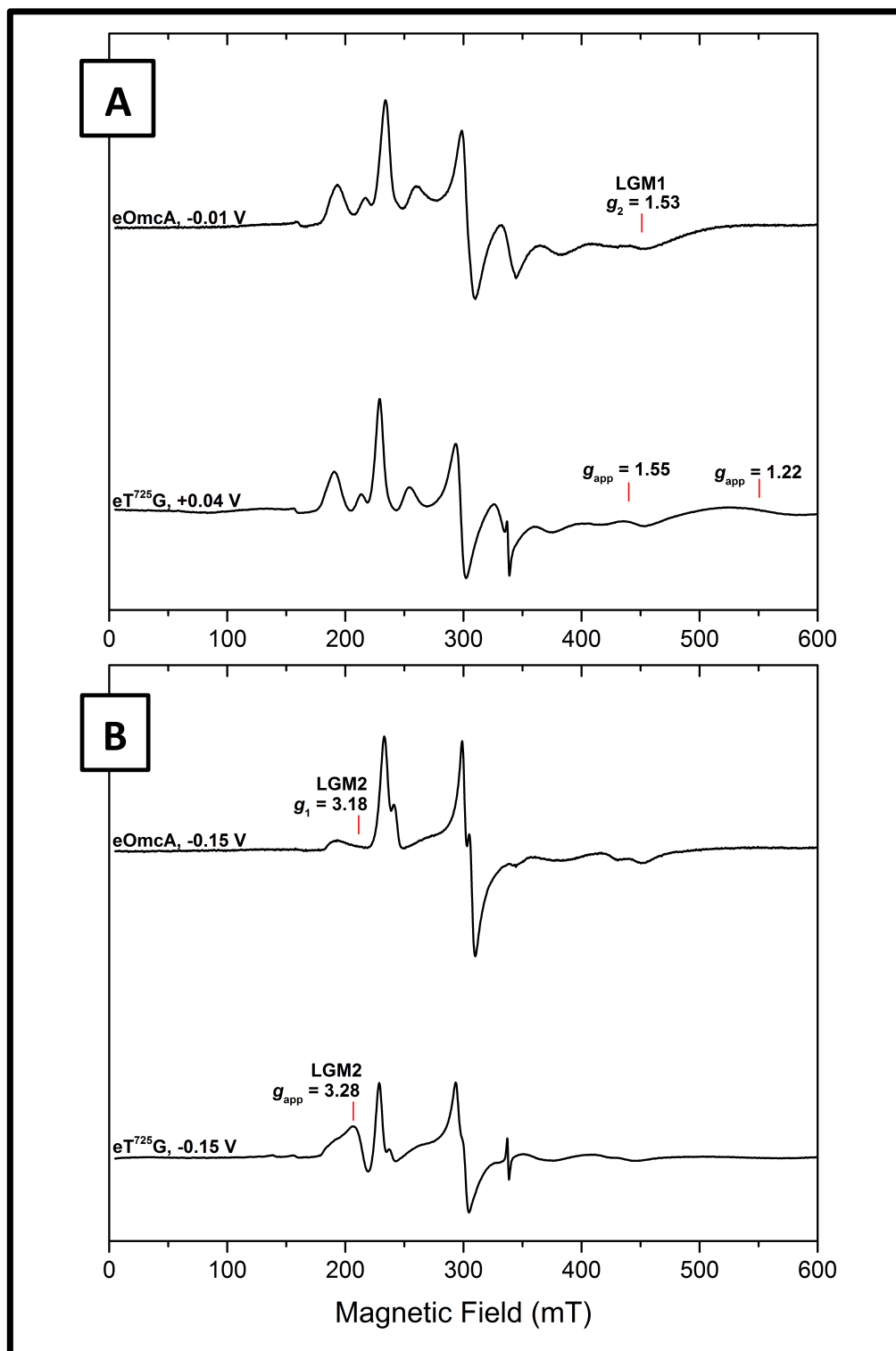


Fig. 7.4 – Comparison of eT⁷²⁵G EPR spectral features with eOmCA and Signal peak height. (A) Comparison of eOmCA at -0.01 V and eT⁷²⁵G at +0.04 V vs S.H.E.. (B) Comparison of eOmCA and eT⁷²⁵G at -0.15 V vs S.H.E.. eT⁷²⁵G spectra multiplied by factor of 6 to account for differences in measurement parameters.

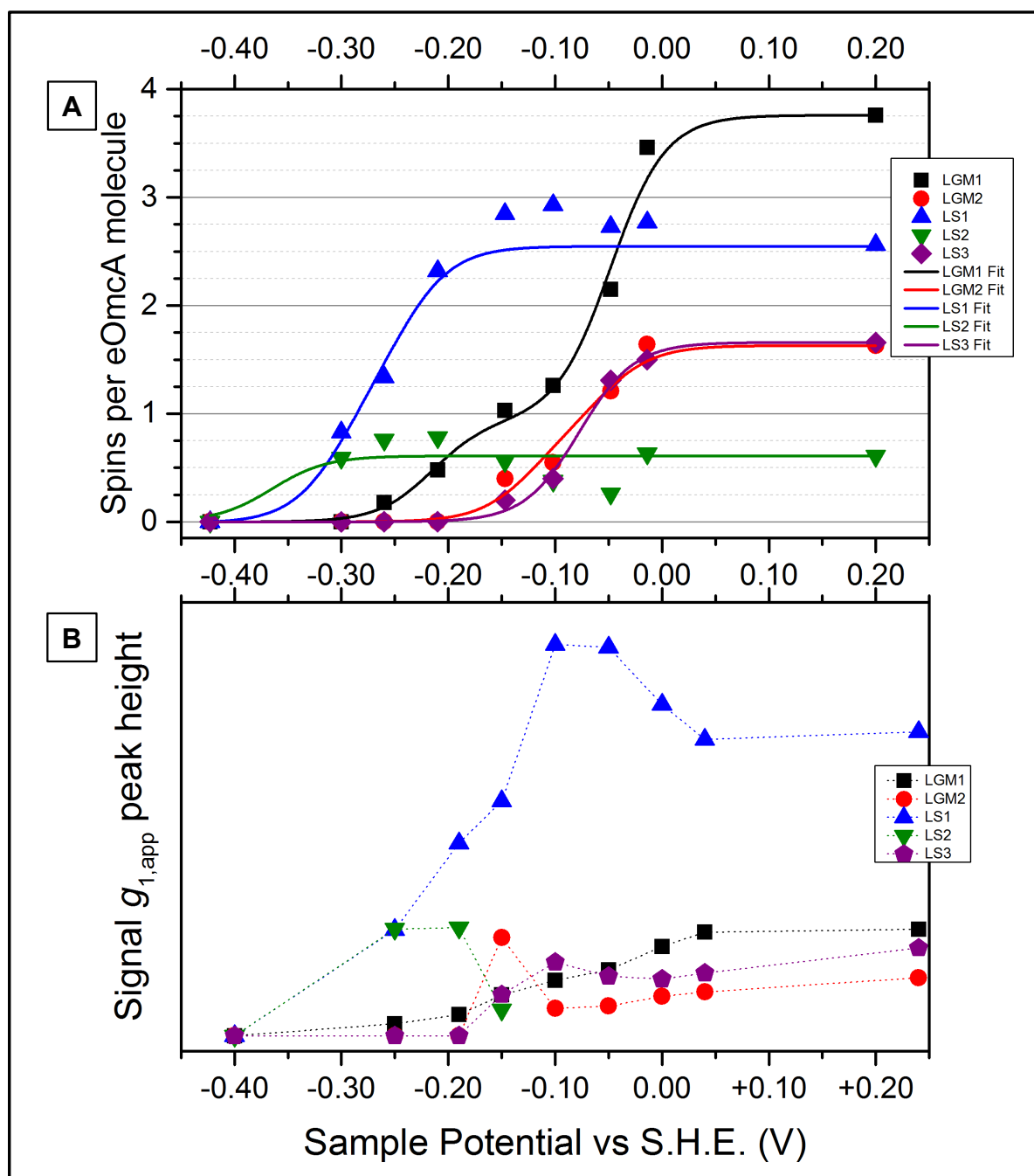


Fig. 7.5 – **Sample potential-dependence of eT⁷²⁵G EPR $g_{1,app}$ peak height in comparison to eOmCA spin quantitation.** (A) The spin quantitation of the eOmCA potentiometric titre as described in Section 5.3. (B) The apparent peak height of each EPR signal's g_1 is plotted according to sample potential.

7.2.3 – Localisation of mOmCA in *S. oneidensis* mutant cells

The OmCA MIP mutants generated encoding the native, amino-terminal LXXC motif (i.e. mOmCA mutants) were designed in order to assess the effect of the mutations on the DMR process in whole cells. However, the localisation of the recombinant mOmCA protein cloned into *S. oneidensis* $\Delta mtrC\Delta omcA$ cells (designated LS strain # 784) was determined.

Localisation of mOmca mutants was determined, based on proteinase K digest assay of whole cells expressing respective recombinant mOmca, to ensure that mOmca was correctly localised to the extracellular surface of the outer bacterial membrane [8] (Fig. 7.6). Expression of mOmca (i.e. wild-type mOmca) and mT⁷²⁵G in *S. oneidensis* LS 786 and 787 cells (respectively) was confirmed by haem-stained SDS-PAGE gels and western blotting (Fig. 7.6). Furthermore, both mOmca and mT⁷²⁵G proteins were confirmed to be accessible to complete digestion by proteinase K incubation with *S. oneidensis* whole cells (Fig. 7.6).

7.2.4 – Whole Cell Mineral Reduction Assay of Omca MIP mutants

The *Shewanella* spp strains *S. oneidensis* MR-1, *S. oneidensis* LS 785 and MIP mOmca mutants listed in Table 7.1 were tested for their capacity to reduce synthesised hematite when supplied with the physiological carbon source lactate. *S. oneidensis* cells were grown in anaerobic M1 minimal media with 20 mM sodium-D,L-lactate as the carbon source and 4.67 mM α -Fe₂O₃ (i.e. hematite) as the terminal electron acceptor. The ferrozine assay is used to detect 1 M HCl extracted Fe²⁺ [23]. Over the 120 hour time-period monitored, the $\Delta mtrC\Delta omca$ *S. oneidensis* strain loses $\approx 90\%$ of the *S. oneidensis* MR-1 hematite reduction capacity (i.e. MR-1 [Fe²⁺] at 48 hours = 0.20 mM; Fig. 7.7A). However, *in trans* mOmca expression (i.e. containing wild-type *omca* MIP; *omca*⁺) produces Fe²⁺ levels comparable to *S. oneidensis* MR-1 (i.e. [Fe²⁺] at 48 hours = 0.21 mM). There is noticeably large error in *omca*⁺ Fe²⁺ concentration measured.

Although the DMR process has been shown to be more complex (Section 1.3.5), the presence of MIP in Omca and MtrC of *S. oneidensis* MR-1 make the *S. oneidensis* $\Delta mtrC\Delta omca$, wild-type mOmca mutant (i.e. LS strain # 786) the positive control for analysis of $\Delta mtrC\Delta omca$ background mOmca MIP mutants. As such the Fe²⁺ concentrations of MIP mOmca mutant strains are assessed as a percentage of wild-type mOmca Fe²⁺ concentration. Of the MIP mOmca mutants, the mT⁷²⁵G (i.e. mOmca T⁷²⁵G mutant) and mT⁷²⁵G:S⁷²⁷G share the same phenotype; consistent $\approx 85\%$ decrease in Fe²⁺ concentration over 120 hours. Mutants expressing Pro⁷²⁶ substitution mutants displayed less than 40% decrease in wild-type mOmca Fe²⁺ production. *Shewanella* cells with the insertional mutation mC⁷²⁷_{ins} displayed a consistent $\approx 60\%$ decrease in Fe²⁺ concentration.

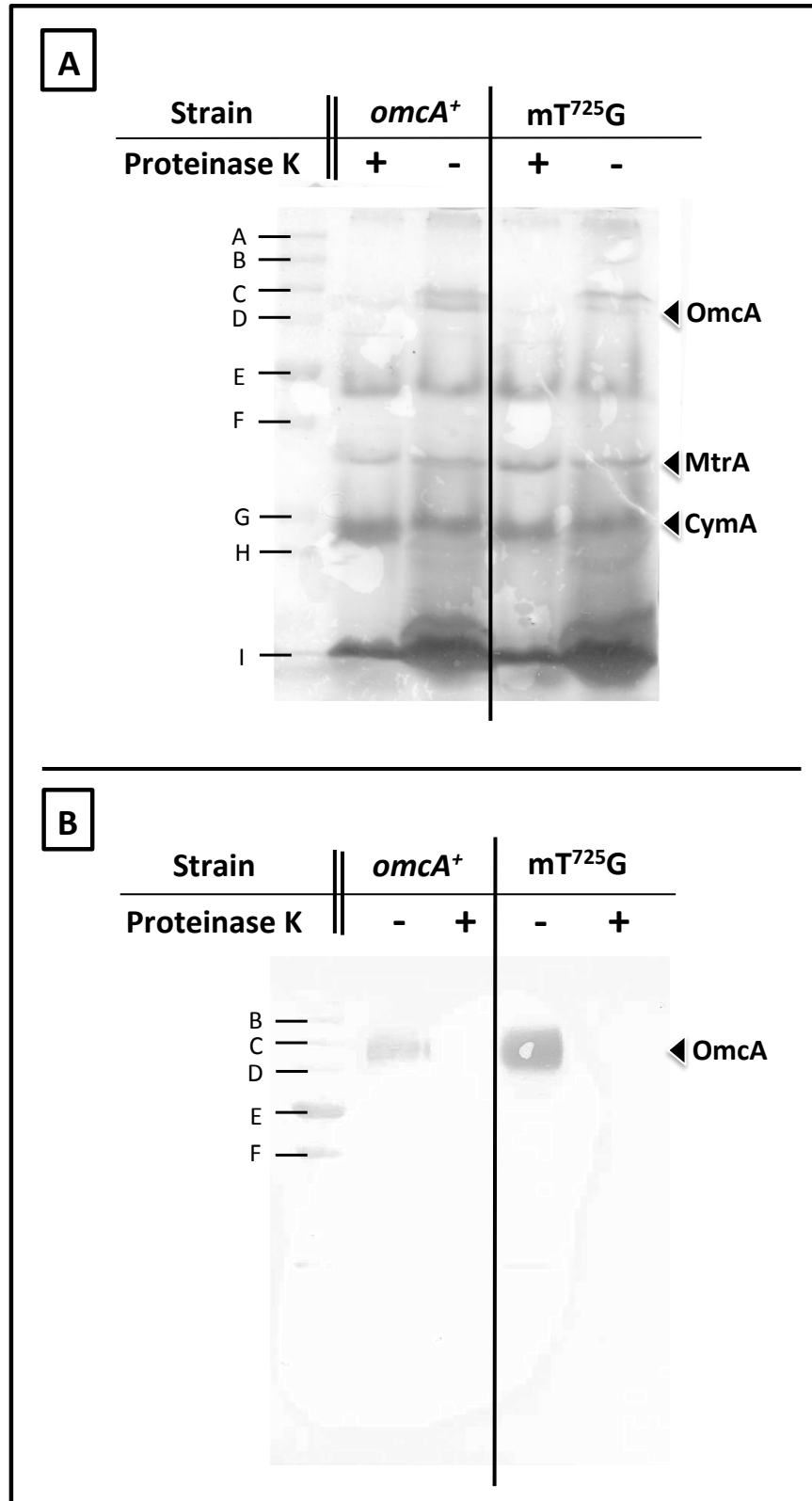


Fig. 7.6 – **Localisation of mOmcA determined by whole cell incubation with Proteinase K.** Identical samples of cells incubated with (+) and without (-) proteinase K were visualised using (A) haem-staining and (B) alkaline phosphatase staining of anti-OmcA IgG. MtrA and CymA visualised in the haem-stained gel were inferred from migration through the SDS-PAGE gel according to the following references [11, 21, 22].

Other mOmca mutants were made (i.e. point mutations outside the MIP) for assessment of their effect on Omca oxidoreductase function. The lipid anchor-containing crystallographic dimer interfacial mutant (i.e. mY³⁷⁴F) has negligible effect on hematite reduction after 24 hours, but decreases hematite reduction by ≈30% from 48 to 120 hours. Also, the removal of domain III's disulphide bond (i.e. mC⁵²⁷V) results in a ≈30-40% decrease in Fe²⁺ production.

7.3 – Discussion

The Thr⁷²⁵ residue has been shown to be of significant structural and functional importance to Omca. The only conserved hydrogen-bonding residue within the MIP is Thr⁷²⁵ (see primary structure alignment, Section 3.2). This is most notably observed by the ≈85% decrease in omca⁺ hematite reduction capacity of both mT⁷²⁵G and mT⁷²⁵G:S⁷²⁷G expressing strains. An mS⁷²⁷G *S. oneidensis* strain has not been tested to resolve the contribution of both hydroxyl-containing MIP residues to the mT⁷²⁵G:S⁷²⁷G phenotype. The P⁷²⁶V substitution maintains wild-type activity as predicted in the publication that predicted the MIP, however the P⁷²⁶G contrasts predictions of that publication because it maintains wild-type hematite reduction activity [20].

The T⁷²⁵G mutation has a secondary effect to the orientation of Gln⁷²⁸ near the haem 10 environment. There are noticeable qualitative consequences to a few spectra of the EPR potentiometric titre of eT⁷²⁵G (i.e. at +0.04 V and -0.15 V vs S.H.E.). The bi-signate feature observed at +0.04 V vs S.H.E. (i.e. $g_{app} = 1.22$), and apparent shift of the LGM2 population from the eOmca LGM2 g_1 of 3.18 to $g_{1,app} = 3.28$ at -0.15 V vs S.H.E. in eT⁷²⁵G did not appear to correlate to changes in resonance population reduction potential(s).

Consolidation of hematite reduction, structural and EPR data is complicated. Considering that haem 10 has been assigned to the LGM1 resonance population, the $g_{app} = 1.22$ feature is best attributed to the middle derivative (i.e. g_2 value) of a variant LGM1 signal ($g_2 = 1.53$ in eOmca, see Section 5.2). There has been no other evidence of variation in the LGM1 signal in eOmca. However it is possible that 1 of the 4 LGM1 haems in eT⁷²⁵G has a unique g_2 value, at least at +0.04 V vs S.H.E.. This would not only corroborate haem 10's EPR signal assignment, but also a putative high $E_{m,7.6}$ (i.e. -0.05 V vs S.H.E.) considering appearance of $g_{app} = 1.22$ by partial reduction of haem 10

producing resolution of its g_2 value. However spectrum simulation and spin quantitation of the potentiometric titre as presented in Chapters 5 and 6 would be required to confirm LGM1 population reduction between +0.24 and +0.04 V vs S.H.E.

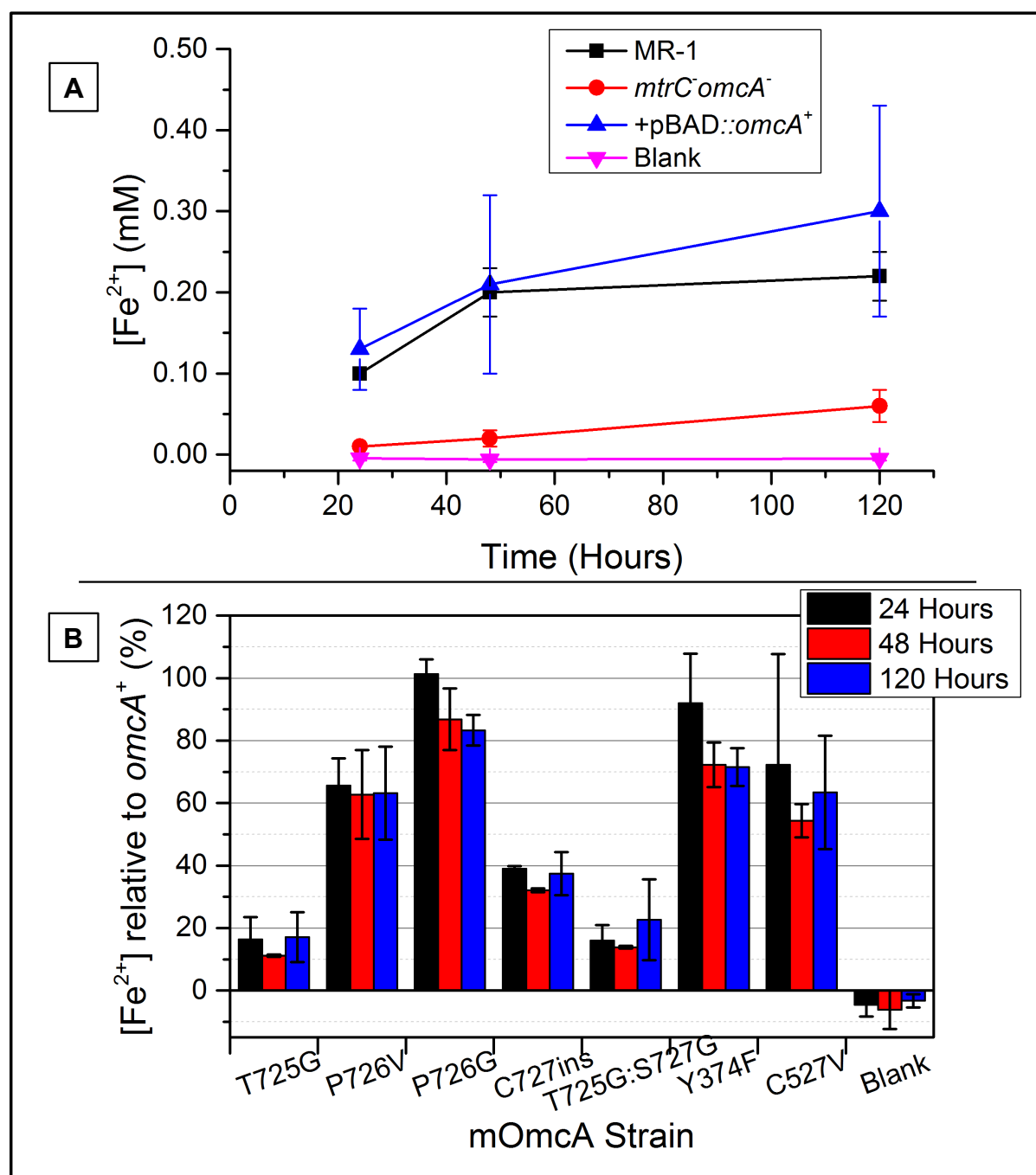


Figure 7.7 – Hematite Reduction Capacity of *S. oneidensis* mOmca mutants. (A) The hematite reduction capacity of *S. oneidensis* MR-1 and complementation of $\Delta mtrC\Delta omcA$ by wild-type mOmca expression *in trans*. Fe²⁺ concentration determined by ferrozine assay. (B) Hematite reduction capacity of *S. oneidensis* mOmca site-directed mutants focused on the MIP and two structural site-directed mutants (i.e. mY³⁷⁴F and mC⁵²⁷V). Fe²⁺ concentration presented as percentage of positive control *omcA*⁺. Cells were grown in M1 minimal media with 20 mM D,L-lactate and 4.67 mM α -Fe₂O₃ (i.e. 9.34 mM Fe³⁺).

The unique LGM2 $g_{1,app}$ of 3.28 at -0.15 V vs S.H.E. that is not observed in eOmCA may also be a consequence of the T⁷²⁵G substitution. In this instance, haem 10 would produce the LGM2 signal and have a relatively low $E_{m,7.6}$.

It is important to note that the reduction potential ranges spanned by the eT⁷²⁵G EPR signals are within 50 mV of their respective eOmCA EPR signals. Supported by the maintenance of the same resonance signals observed in eOmCA, the eT⁷²⁵G EPR spectra confirm crystal structure observations that the point mutation has not significantly affected the protein tertiary structure and haem environments. As such, the ~85% decrease in $omcA^+ Fe^{2+}$ production by the T⁷²⁵G substitution is unlikely to be caused by a change in haem 10's mid-point potential. Therefore haem 10's high $E_{m,7.6}$ LGM1 signal is unlikely to change, and the unique LGM2 feature at -0.15 V vs S.H.E. is unlikely to be produced by haem 10.

The recombinant mOmCA protein expressed has been determined to localise to the extracellular surface of the outer bacterial membrane, and hematite reduction has been substantially decreased by Thr⁷²⁵ substitution. This decrease in hematite turnover occurs despite no apparent change to the reduction potentials of eOmCA's haems caused by T⁷²⁵G substitution and re-orientation of the Gln⁷²⁸ side-chain away from haem 10. This data indicates OmCA's documented capacity to establish a chemical bond with hematite [24-26] may be mediated via the MIP.

OmCA's capacity to interact/bind mineral as part of the mineral reduction mechanism has been heavily studied and may be a component of OmCA's differential function. OmCA's co-sedimentation with, and reduction of hematite has been correlated via UV-vis and intrinsic OmCA peptide fluorescence [24]. Binding of OmCA to an α -Fe₂O₃ (i.e. hematite) waveguide has been shown to be pH-sensitive, and maximal OmCA binding occurs near OmCA's calculated isoelectric point [25] (i.e. estimated pI = 6.2 – 6.4 [4, 11]).

Affinity between OmCA (and MtrC) monolayers and hematite-coated atomic force microscopy (AFM) probes has been detected [26]. As discussed in Chapter 4, OmCA had twice the measured attraction for hematite AFM probes than MtrC, however MtrC binds to hematite AFM probes with twice the frequency of OmCA. Chapter 4 explored the possibility of OmCA existing as a dimer in solution, and although monomeric MtrC molecules with half the number of putative hematite binding motifs and twice the diffusion coefficient correlates with the OmCA dimer

model, this working model is negated by the contrasting data on OmcA stoichiometry. A study indicating conformational changes in OmcA according to OmcA's oxidation state also contains neutron reflectivity data suggesting OmcA adsorbs to hematite via its largest surface [27]. Considering the putative MIP determined [20], the localisation of the MIP to OmcA's external polypeptide surface makes the hematite-binding via the proposed peptide possible (Fig. 7.1). Simulation of OmcA:hematite docking/interaction is possible *in silico* with the crystal structure data, but may require more experimental cues to determine all possible mineral interaction sites in OmcA.

The precedent for OMMCs to bind their substrate is supported by crystal structures of UndA with $(\text{Fe}^{3+})_2\text{-NTA}_2\cdot 2\text{H}_2\text{O}$ and $(\text{Fe}^{3+})_3\text{-citrate}_3\cdot 2\text{H}_2\text{O}$ bound to specific arginine side chains within 9 Å of haem 7 [1]. Whereas the ferric chelate binding site resolved in UndA is different from the proposed HBM in MtrC and OmcA, this still provides evidence that the 70 – 90 kDa of polypeptide in OMMCs may have evolved to bind substrate as well as house, orient and poise haem reduction potentials. Although citrate is a naturally occurring molecule in the environment, ferric citrate chelates are scarce and not as yet known to be part of the DMR process. Nitrilotriacetic acid is not found in the environment, however it can possible that UndA has developed a ferric chelate binding site, most likely part of a chelate reduction mechanism.

Despite the wealth of supporting literature, the only experimentally confirmed evidence for the functional role Thr⁷²⁵ from this study is the position of the Gln⁷²⁸ side-chain and the hematite reduction phenotype observed. Differential co-sedimentation assay of hematite with eOmcA and eT⁷²⁵G would indicate that Thr⁷²⁵ is necessary to establish chemical bonding with hematite as a rate-limiting step for electron transfer from OmcA to hematite. Preliminary experiments performed indicate there is negligible difference in co-sedimentation with hematite and either eOmcA or eT⁷²⁵G.

Several components to the DMR process have been identified beyond direct haem:mineral electron transfer: i.e. flavin mediation [28], semiflavoquinone-cofactor contact [29], the biofilm state [30, 31] and cell motility [32]. However OmcA's co-localisation to the tight and loosely-associating EPS is likely to position OmcA to facilitate hydrogen bond formation with mineral TEA [10].

The different minerals utilised as TEA by *S. oneidensis* have a variety of morphologies and chemical characteristics. Hematite is one of *Shewanella's* most chemically stable respiratory substrates [33]. However *S. oneidensis* cells also respire

on the much less stable ferric mineral ferrihydrite [16]. Such a variety of chemical morphologies and stabilities lend the scope for multiple approaches of electron transfer to these insoluble substrates. The OMMC crystal structures show the possibility of OMMCs to utilise both direct haem and flavin shuttling mechanisms to reduce mineral TEA substrate. It is possible that different OMMCs employ both mechanisms to different degrees according to their polypeptide content, giving reason to multiple OMMCs encoded in the *mtr* gene cluster of *Shewanella spp.*

References

- 1 Edwards, M. J., Hall, A., Shi, L., Fredrickson, J. K., Zachara, J. M., Butt, J. N., Richardson, D. J. and Clarke, T. A. (2012) The Crystal Structure of the Extracellular 11-heme Cytochrome UndA Reveals a Conserved 10-heme Motif and Defined Binding Site for Soluble Iron Chelates. *Structure*. **20**, 1275-1284
- 2 Edwards, M. J., Baiden, N. A., Johs, A., Tomanicek, S. J., Liang, L., Shi, L., Fredrickson, J. K., Zachara, J. M., Gates, A. J., Butt, J. N., Richardson, D. J. and Clarke, T. A. (2014) The X-ray crystal structure of *Shewanella oneidensis* OmcA reveals new insight at the microbe-mineral interface. *Febs Letters*. **588**, 1886-1890
- 3 Clarke, T. A., Edwards, M. J., Gates, A. J., Hall, A., White, G. F., Bradley, J., Reardon, C. L., Shi, L., Beliaev, A. S., Marshall, M. J., Wang, Z., Watmough, N. J., Fredrickson, J. K., Zachara, J. M., Butt, J. N. and Richardson, D. J. (2011) Structure of a bacterial cell surface decaheme electron conduit. *Proceedings of the National Academy of Sciences of the United States of America*. **108**, 9384-9389
- 4 Myers, J. M. and Myers, C. R. (1998) Isolation and sequence of *omcA*, a gene encoding a decaheme outer membrane cytochrome c of *Shewanella putrefaciens* MR-1, and detection of *omcA* homologs in other strains of *S-putrefaciens*. *Biochimica Et Biophysica Acta-Biomembranes*. **1373**, 237-251
- 5 Shi, L., Chen, B. W., Wang, Z. M., Elias, D. A., Mayer, M. U., Gorby, Y. A., Ni, S., Lower, B. H., Kennedy, D. W., Wunschel, D. S., Mottaz, H. M., Marshall, M. J., Hill, E. A., Beliaev, A. S., Zachara, J. M., Fredrickson, J. K. and Squier, T. C. (2006) Isolation of a high-affinity functional protein complex between OmcA and MtrC: Two outer membrane decaheme c-type cytochromes of *Shewanella oneidensis* MR-1. *Journal of Bacteriology*. **188**, 4705-4714
- 6 Ross, D. E., Brantley, S. L. and Tien, M. (2009) Kinetic Characterization of OmcA and MtrC, Terminal Reductases Involved in Respiratory Electron Transfer for Dissimilatory Iron Reduction in *Shewanella oneidensis* MR-1. *Applied and Environmental Microbiology*. **75**, 5218-5226
- 7 Myers, C. R. and Myers, J. M. (2003) Cell surface exposure of the outer membrane cytochromes of *Shewanella oneidensis* MR-1. *Letters in Applied Microbiology*. **37**, 254-258
- 8 Shi, L., Deng, S., Marshall, M. J., Wang, Z. M., Kennedy, D. W., Dohnalkova, A. C., Mottaz, H. M., Hill, E. A., Gorby, Y. A., Beliaev, A. S., Richardson, D. J., Zachara, J. M. and Fredrickson, J. K. (2008) Direct involvement of type II secretion system in extracellular translocation of *Shewanella oneidensis* outer membrane cytochromes MtrC and OmcA. *Journal of Bacteriology*. **190**, 5512-5516

- 9 Donald, J. W., Hicks, M. G., Richardson, D. J. and Palmer, T. (2008) The c-type cytochrome OmcA localizes to the outer membrane upon heterologous expression in *Escherichia coli*. *Journal of Bacteriology*. **190**, 5127-5131
- 10 Cao, B., Shi, L. A., Brown, R. N., Xiong, Y. J., Fredrickson, J. K., Romine, M. F., Marshall, M. J., Lipton, M. S. and Beyenal, H. (2011) Extracellular polymeric substances from *Shewanella* sp HRCR-1 biofilms: characterization by infrared spectroscopy and proteomics. *Environmental Microbiology*. **13**, 1018-1031
- 11 Ross, D. E., Ruebush, S. S., Brantley, S. L., Hartshorne, R. S., Clarke, T. A., Richardson, D. J. and Tien, M. (2007) Characterization of protein-protein interactions involved in iron reduction by *Shewanella oneidensis* MR-1. *Applied and Environmental Microbiology*. **73**, 5797-5808
- 12 Zhang, H., Tang, X., Munske, G. R., Zakharova, N., Yang, L., Zheng, C., Wolff, M. A., Tolic, N., Anderson, G. A., Shi, L., Marshall, M. J., Fredrickson, J. K. and Bruce, J. E. (2008) In vivo identification of the outer membrane protein omcA-mtrC interaction network in *Shewanella oneidensis* MR-1 cells using novel hydrophobic chemical cross-linkers. *Journal of Proteome Research*. **7**, 1712-1720
- 13 Myers, J. M. and Myers, C. R. (2001) Role for outer membrane cytochromes OmcA and OmcB of *Shewanella putrefaciens* MR-1 in reduction of manganese dioxide. *Applied and Environmental Microbiology*. **67**, 260-269
- 14 Bucking, C., Popp, F., Kerzenmacher, S. and Gescher, J. (2010) Involvement and specificity of *Shewanella oneidensis* outer membrane cytochromes in the reduction of soluble and solid-phase terminal electron acceptors. *FEMS Microbiology Letters*. **306**, 144-151
- 15 Coursolle, D. and Gralnick, J. A. (2010) Modularity of the Mtr respiratory pathway of *Shewanella oneidensis* strain MR-1. *Molecular Microbiology*. **77**, 995-1008
- 16 Reardon, C. L., Dohnalkova, A. C., Nachimuthu, P., Kennedy, D. W., Saffarini, D. A., Arey, B. W., Shi, L., Wang, Z., Moore, D., McLean, J. S., Moyles, D., Marshall, M. J., Zachara, J. M., Fredrickson, J. K. and Beliaev, A. S. (2010) Role of outer-membrane cytochromes MtrC and OmcA in the biomineralization of ferrihydrite by *Shewanella oneidensis* MR-1. *Geobiology*. **8**, 56-68
- 17 Meitl, L. A., Eggleston, C. M., Colberg, P. J. S., Khare, N., Reardon, C. L. and Shi, L. (2009) Electrochemical interaction of *Shewanella oneidensis* MR-1 and its outer membrane cytochromes OmcA and MtrC with hematite electrodes. *Geochimica Et Cosmochimica Acta*. **73**, 5292-5307
- 18 Coursolle, D., Baron, D. B., Bond, D. R. and Gralnick, J. A. (2010) The Mtr Respiratory Pathway Is Essential for Reducing Flavins and Electrodes in *Shewanella oneidensis*. *Journal of Bacteriology*. **192**, 467-474
- 19 Page, C. C., Moser, C. C., Chen, X. X. and Dutton, P. L. (1999) Natural engineering principles of electron tunnelling in biological oxidation-reduction. *Nature*. **402**, 47-52
- 20 Lower, B. H., Lins, R. D., Oestreich, Z., Straatsma, T. P., Hochella, M. F., Shi, L. A. and Lower, S. K. (2008) In vitro evolution of a peptide with a hematite binding motif that may constitute a natural metal-oxide binding archetype. *Environmental Science & Technology*. **42**, 3821-3827
- 21 Myers, C. R. and Myers, J. M. (1992) Location of cytochromes to the outer-membrane of anaerobically grown *Shewanella putrefaciens* MR-1. *Journal of Bacteriology*. **174**, 3429-3438
- 22 Myers, C. R. and Myers, J. M. (1997) Cloning and sequence of *cymA* a gene encoding a tetraheme cytochrome c required for reduction of iron(III), fumarate,

- and nitrate by *Shewanella putrefaciens* MR-1. *Journal of Bacteriology*. **179**, 1143-1152
- 23 Stookey, L. L. (1970) Ferrozine - A new spectrophotometric reagent for iron. *Analytical Chemistry*. **42**, 779-&
- 24 Xiong, Y. J., Shi, L., Chen, B. W., Mayer, M. U., Lower, B. H., Londer, Y., Bose, S., Hochella, M. F., Fredrickson, J. K. and Squier, T. C. (2006) High-affinity binding and direct electron transfer to solid metals by the *Shewanella oneidensis* MR-1 outer membrane c-type cytochrome OmcA. *Journal of the American Chemical Society*. **128**, 13978-13979
- 25 Eggleston, C. M., Voros, J., Shi, L., Lower, B. H., Droubay, T. C. and Colberg, P. J. S. (2008) Binding and direct electrochemistry of OmcA, an outer-membrane cytochrome from an iron reducing bacterium, with oxide electrodes: A candidate biofuel cell system. *Inorganica Chimica Acta*. **361**, 769-777
- 26 Lower, B. H., Shi, L., Yongsunthon, R., Droubay, T. C., McCready, D. E. and Lower, S. K. (2007) Specific bonds between an iron oxide surface and outer membrane cytochromes MtrC and OmcA from *Shewanella oneidensis* MR-1. *Journal of Bacteriology*. **189**, 4944-4952
- 27 Johs, A., Shi, L., Droubay, T., Ankner, J. F. and Liang, L. (2010) Characterization of the Decaheme c-Type Cytochrome OmcA in Solution and on Hematite Surfaces by Small Angle X-Ray Scattering and Neutron Reflectometry. *Biophysical Journal*. **98**, 3035-3043
- 28 Lies, D. P., Hernandez, M. E., Kappler, A., Mielke, R. E., Gralnick, J. A. and Newman, D. K. (2005) *Shewanella oneidensis* MR-1 uses overlapping pathways for iron reduction at a distance and by direct contact under conditions relevant for biofilms. *Applied and Environmental Microbiology*. **71**, 4414-4426
- 29 Okamoto, A., Hashimoto, K., Nealson, K. H. and Nakamura, R. (2013) Rate enhancement of bacterial extracellular electron transport involves bound flavin semiquinones. *Proceedings of the National Academy of Sciences of the United States of America*. **110**, 7856-7861
- 30 Teal, T. K., Lies, D. P., Wold, B. J. and Newman, D. K. (2006) Spatiometabolic stratification of *Shewanella oneidensis* biofilms. *Applied and Environmental Microbiology*. **72**, 7324-7330
- 31 McLean, J. S., Pinchuk, G. E., Geydebrekht, O. V., Bilskis, C. L., Zakrajsek, B. A., Hill, E. A., Saffarini, D. A., Romine, M. F., Gorby, Y. A., Fredrickson, J. K. and Beliaev, A. S. (2008) Oxygen-dependent autoaggregation in *Shewanella oneidensis* MR-1. *Environmental Microbiology*. **10**, 1861-1876
- 32 Harris, H. W., El-Naggar, M. Y. and Nealson, K. H. (2012) *Shewanella oneidensis* MR-1 chemotaxis proteins and electron-transport chain components essential for congregation near insoluble electron acceptors. *Biochemical Society Transactions*. **40**, 1167-U1129
- 33 Larsen, O. and Postma, D. (2001) Kinetics of reductive bulk dissolution of lepidocrocite, ferrihydrite, and goethite. *Geochimica Et Cosmochimica Acta*. **65**, 1367-1379

Chapter 8:

Discussion & Future Perspectives on the Role of OmcA in DMR

8.1 – Introduction

There is extensive data on the localisation of the OMMC OmcA to the extracellular surface of the outer bacterial membrane (Section 7.2, [1, 2]). At the outer bacterial membrane, the various structural and redox properties identified in the previous chapters are the basis of OmcA's capacity to mediate the DMR process in *Shewanella spp.* As discussed in Chapter 7, obtaining the crystal structure of a protein typically provides cues as to how its function is executed. The OMMC crystal structures provided information on the domain structure, haem orientations and cues on electron ingress/egress sites previously unknown [3-5], but do not provide explicit clarification of electron transfer directionality. Paramagnetically resolved spectropotentiometric properties of OMMC haem populations provide cues to the electron transfer directionality, but there are also many other questions pertaining to OmcA function and the DMR process in *Shewanella spp.*

8.2 – Electron Ingress/Egress Sites and OmcA Orientation at the Outer Membrane

During DMR electrons reach the outer bacterial membrane at MtrA of the MtrCAB heterotrimer. The orientation of OMMCs at the extracellular surface of the outer bacterial membrane will correspond to the electron ingress and egress sites of each respective OMMC. The OMMC MtrC will need to localise at least one haem within electron tunneling distance of MtrA's electron egress site, which is facilitated by the putative β -barrel MtrB [6].

OmcA has a slightly different orientation at the outer membrane of *S. oneidensis* MR-1 in comparison to MtrC. Haem 10 is resolved as the lowest potential haem in MtrF via an EPR spectropotentiometric titration. The same technique identifies haem 5 as the lowest potential haem in OmcA (Sections 5.2 and 5.3). Differing electron transfer directionality may be the basis of how the OMMCs of *Shewanella spp.* contribute to DMR. MtrF is a component of the MtrDEF complex postulated to interact with the MtrDE porin-cytochrome module as MtrC does with MtrAB [3, 6]. This interaction is postulated to occur via the experimentally resolved lowest potential haem, haem 10 [3]. Currently the only data on the orientation of MtrC's interface with MtrAB is inferred from the *in silico* model of the MtrC that

indicates haems 8 and 10 may be histidinate ligated [7]. Combined with at least one low reduction potential component of their putative EPR signal during a potentiometric titre (i.e. LS2 population fully reduced below -0.45 V vs S.H.E. [8]), it is possible MtrC receives electrons from MtrA via haem 10.

8.2.1 – Details of the OmcA:MtrC Interaction

OmcA's association to the outer bacterial membrane is mediated by its lipid anchor and interaction with MtrC [9-12]. Without *omcA* being encoded in an operon with a dedicated porin-cytochrome module like *mtrC* or *mtrF*, OmcA's lipid anchor and interaction with MtrC are modelled to contribute to OmcA's co-localisation to the tight and loosely-associating exopolymeric substance [13], most likely at the interface of both EPS fractions. As a functional analogue of OmcA, UndA could also be envisaged to substitute for OmcA in the EPS of *Shewanella spp* that do not encode for *omcA*. Cross-linker molecules with 6.4 Å and 11.4 Å linker arms indicate specific OmcA polypeptides that putatively contribute to its interaction with MtrC [11]. Mapping these polypeptides onto the structure of OmcA shows that domains I and III are strongly implicated in the OmcA:MtrC interaction (Fig. 7.1). The two linker molecules used provide over-lapping results: the 11.4 Å linker molecule implicates three polypeptides (one in domain I and two in domain III) whereas six polypeptides are implicated with the 6.4 Å linker molecule (in domains II, III and IV).

Interaction sites in both domains II and IV of OmcA detected with the 6.4 Å linker molecule did not corroborate specific electron transfer directionality along the central octahaem of OmcA. It is not entirely clear how the shorter linker molecule has cross-linked more polypeptides in OmcA. Perhaps structural flexibility, facilitated by OMMC domain movements [14], were anchored with the 6.4 Å linker molecule. Considering this working model, OmcA appears to use domains I and III to interact with MtrC, and all OmcA's surfaces may transiently interact with MtrC (Fig. 8.1). However this contrasts a model of OmcA orienting a specific electron ingress site for reduction by MtrC, and may indicate an error in the putative interactions detected. In the *in silico* structural model of MtrC generated [7], it is apparent that MtrC contains the split β -barrels present in all other major OMMC clades. Domains III and IV of MtrC were implicated in the OmcA:MtrC interaction via the 6.4 Å and 11.4 Å linker arms. However the experimentally determined MtrC coordinates are necessary to build an interaction model.

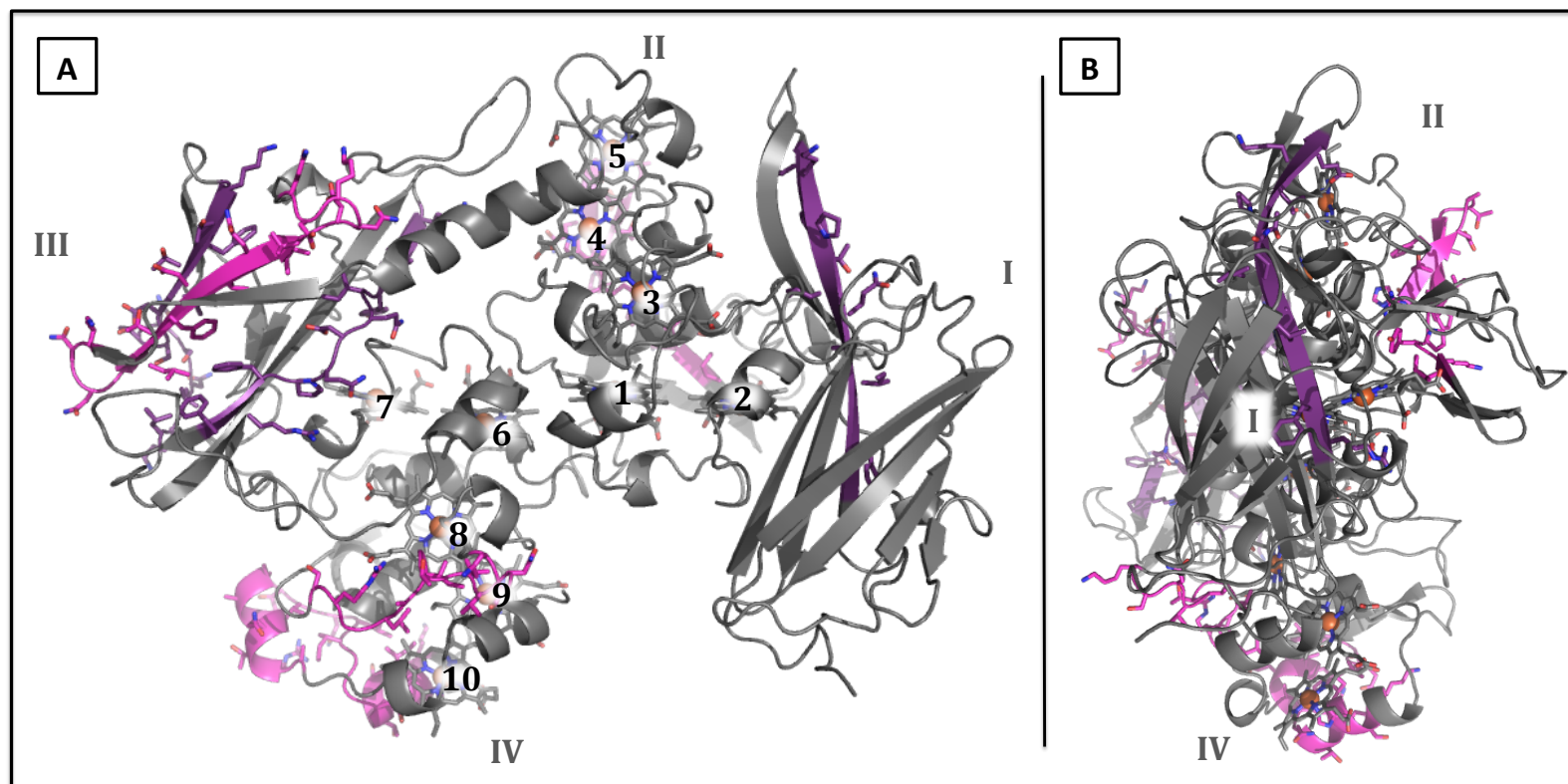


Table 8.1 – **The putative MtrC interaction sites in OmcA.** According to cross-linking experiments, polypeptides of OmcA implicated in interaction with MtrC have been highlighted [11]. Polypeptides implicated by the 6.4 Å cross-linker are pink and polypeptides implicated by both the 6.4 Å and 11.4 Å cross-linkers are purple.

Data that indicates OmcA interacts with hematite via a mineral interaction peptide (MIP) suggests electron transfer directionality [15]. The MIP is adjacent to haem 10's CXXCH motif, and would putatively localise hematite within 14 Å of haem 10. This indicates haem 10 as the putative electron egress site of OmcA. Mutagenic work focusing on the MIP indicated that removal of the hydroxyl containing residues decreased hematite reduction by ~80% (Section 7.2). However since little is known about the orientation of OmcA or any OMMC at the extracellular surface of the outer bacterial membrane, the hydroxylated residues of the MIP could be participating in a number of molecular interactions. This includes interaction with electron source MtrC, interaction with the outer membrane, or other proteins that contribute to OmcA's localisation. As discussed in Section 7.3, co-sedimentation of hematite and OmcA MIP mutants would address the existence of chemical bonding via the MIP.

8.3 – The OmcA “Interactome” of the Outer Bacterial Membrane

As mentioned earlier, OmcA's co-localisation between the tight and loosely associating EPS is modelled to be mediated by its lipid anchor and interaction with MtrC [9, 12, 13]. OmcA may thus be suspended further from the extracellular surface of the outer bacterial membrane via its interaction with MtrC. Several outer membrane proteins have also been implicated to interact with OmcA at the extracellular surface of *S. oneidensis* MR-1 [11], several of which were isolated from the EPS of *Shewanella* sp. strain HRCR-6 [13]. Since *Shewanella* simultaneously expresses structurally similar OMMCs (i.e. MtrC and OmcA [16-18]), these cytochromes may have differential roles dictated by their localisation.

Beyond protein:protein interactions, it is unknown whether the lipopolysaccharide (LPS) and exopolysaccharide (EPS) extracellular content may also provide useful or inhibitory interactions to OMMC:mineral electron transfer. The association of multihaem cytochromes with biofilm matrix components has been shown *Shewanella* sp. HRCR-1 [13]. OmcA (maximum dimension ~10 nm) would be embedded within an EPS matrix ~0.5 µm deep [19] where OmcA is modelled to reduce mineral TEA. As such, direct haem contact or direct semiquinone contact mechanisms of mineral TEA reduction may be disrupted by the presence of the LPS/EPS OMMC environment. In the same manner it is conceivable that electron shuttling or conductive pili are utilised by *Shewanella* spp biofilms to overcome the

unknown OMMC:mineral distance. Any additional interactions that contribute to OmcA's unique EPS localisation and capacity to reduce mineral TEA from within the EPS could be explored by probing extracted EPS (using the protocol established by [13]) with tagged OmcA as an *in situ* pull-down assay.

8.4 – The Role of the Biofilm State in DMR

The EPS of several bacterial species has been shown to regulate access of various molecules into the biofilm matrix. *Pseudomonas putida* and *Bacillus thuringiensis* biofilms have been shown to adsorb Cu^{2+} [20], and the minerals goethite and kaolinite compete with Cu^{2+} for metal sorption sites on the surface of these bacteria. A river biofilm has been attributed ion-exchange “chromatographic” properties due to resolution of K^+ and Br^- elution [21]. Ionic resolution was determined to be directly proportionally to the length of passage through the river. The capacity of flavins to chelate metal ions [22] may be employed by *Shewanella spp* biofilms to “elute” reduced mineral from metal sorption sites of the EPS. In this model, flavin secretion frees the metal adsorption sites of the EPS from reduced mineral, to adsorb oxidized mineral TEA for DMR. In this instance, disruption of the putative OmcA₂ molecule at high [NaCl] or intermediate [MgCl₂] (see Section 4.2) may be representative of DMR inhibition by mineral turnover products (i.e. $\text{Fe}^{2+}/\text{Mn}^{2+}$) resulting in dimer disruption. However contrasting oligomeric data of OmcA negates the OmcA dimer model (see Chapter 4).

Both the aforementioned cellular components (i.e. LPS and especially EPS) have been implicated in the alternate growth state of bacteria as surface-associated microbial cell colonies called biofilms [23]. The capacity for a bacterial colony to express genes in a spatially differentiated manner, whilst adherent to a physical substrate differentiates “planktonic” and biofilm cultures [24]. *Shewanella spp* can adopt the biofilm state [25, 26]. The relevance of the biofilm state to bacteria that perform DMR is not entirely clear, as most bacteria are modelled to exist as biofilms without requiring the physical substrate as its respiratory substrate [24, 27].

A comparison of planktonic and biofilm protein expression of *S. oneidensis* MR-1 cells detects up-regulation of cellular agglutination protein AggA. The type IV pili and haem degradation/iron acquisition enzymes are down-regulated [28], putatively to

protect the cytochromes utilised during in anaerobic respiration processes such as DMR in *Shewanella spp* [16].

8.4.1 – Conductive Pili in Biofilms

The initial stages of *S. oneidensis* biofilm formation have been characterised [26]. Mannose-sensitive hemagglutinin type IV pilus biosynthesis and pilus retraction deletion mutants displayed significant impairment in their ability to adhere to surfaces. Mutations hindering motility affected the ability of the biofilm colonies to form (wild-type) pronounced three-dimensional structures. The up-regulation of type IV pili and auto-aggregation protein AggA have also been detected in biofilms [28]. This may address the role of pili in *Shewanella* biofilms: instead of a conduit for electron conduction, pili contribute to cell motility within *Shewanella* biofilm colonies on the “physico-respiratory” biofilm substrate [29]. However studies measuring the conductive nature of isolated *Shewanella* pili have applied physiological potential differences across isolated pili and identified pili conduction [30].

8.4.2 – Quorum Sensing and Multiple Roles for Flavin in *Shewanella* Biofilms

Quorum sensing and spatiotemporal cellular differentiation are defining characteristics specific to biofilms [31, 32]. In quorum sensing (QS), auto-inductive signalling molecules are released into the extracellular environment, and cell density dictates signal concentration that is transduced and to trigger biofilm formation when signal concentration reaches a certain threshold [33]. Several *Shewanella spp* (including *S. oneidensis* MR-1) have been shown to be susceptible to species non-specific QS “AI-2” molecules [34]. Several QS-regulated proteins are up-regulated in *Shewanella spp* biofilms [28]. AI-2 receptors have been shown to recognise a broader variety of molecules than other quorum sensing receptors [35], including riboflavin [36]. This correlates with up-regulation of the flavin synthesis pathway component RibB in biofilms of *S. oneidensis* MR-1 [28]. Considering the wealth of data listed in Section 1.3.5 on the roles flavins have been assigned in DMR, it may be convoluted to study if secreted flavins also participate in quorum sensing.

Several QS antagonists have been discovered and developed [37], and these can be used in combination with a series of flavin synthesis/secretion knockout strains and flavin supplementation to investigate expression of QS-regulated genes. Flavins have been recently shown to enhance simulated OMMC-to-mineral electron transfer kinetics when in an OMMC-bound, semiflavoquinone state (i.e. direct

semiflavoquinone contact, Section 1.3.5) [38]. Considering the detection of secreted FMN and riboflavin by *Shewanella spp* biofilms [39-41], it is possible flavins released beyond a *Shewanella* cell's EPS function as QS signal molecules.

8.4.3 – Spatiotemporal cellular differentiation and the porin-cytochrome module in *Shewanella* biofilms

Cellular differentiation involves heterogeneity in protein expression profiles according to cellular location within biofilm colonies and biofilm maturity. In *S. oneidensis* biofilms, cellular differentiation manifests as up-regulation of β -barrel protein component of the hetero-trimeric outer membrane mineral reduction complex (i.e. MtrB) [25]. The only experimental data on the involvement of MtrDEF in DMR is in *S. oneidensis* biofilms grown under 50 % dissolved oxygen tension in a continuous culture chemostat [42]. Neither biofilm was grown anaerobically or in the presence of alternate respiratory substrates [25, 42]. The up-regulation of *mtrB* was observed at the centre of mature biofilm colonies of *S. oneidensis* MR-1 [25], whereas MtrDEF expression was not correlated to cellular location [42].

As discussed in Chapter 7, OmcA has been investigated for its capacity to facilitate adsorption to and reduction of the ferric mineral hematite (i.e. α -Fe₂O₃). Several studies indicate purified OmcA has affinity for hematite [15, 43, 44], and hematite adsorption of purified OmcA has also been correlated to its capacity to reduce hematite [45]. Previous whole cell experiments on the effect of *omcA* knockout mutant strains have produced mixed hematite-reduction phenotypes. Phenotypes of *omcA* and *mtrC* knockout mutants indicated that both OMMCs contributed to reduction of a hematite electrode by *S. oneidensis* cells [46]. Linking cell adsorption to hematite reduction, measurements of soluble Fe production and hematite slide surface coverage indicated decreased hematite reduction but wild-type hematite surface coverage by *omcA* knockout *S. oneidensis* biofilms [47]. These results suggest *S. oneidensis* biofilm adsorption to hematite is not mediated solely via OmcA, as type IV pilus and AggA up-regulation indicate. Also it can be inferred that cytochromes do not facilitate adsorption of biofilm cells to the physical substrate. However, OmcA is one of the OMMCs required for utilisation of the physico-respiratory mineral substrate hematite, and may function in a similar manner during DMR with other ferric and manganese mineral TEAs.

In conclusion, OmcA's physicochemical properties corroborate the mineral reduction properties experimentally identified in both the results presented in this thesis and within the literature. Further insight into the interaction partners of OmcA, how it functions within the EPS and the role of biofilm formation on its respiratory substrate is required to fully understand the chemical processes required for DMR.

References.

- 1 Donald, J. W., Hicks, M. G., Richardson, D. J. and Palmer, T. (2008) The c-type cytochrome OmcA localizes to the outer membrane upon heterologous expression in *Escherichia coli*. *Journal of Bacteriology*. **190**, 5127-5131
- 2 Shi, L., Deng, S., Marshall, M. J., Wang, Z. M., Kennedy, D. W., Dohnalkova, A. C., Mottaz, H. M., Hill, E. A., Gorby, Y. A., Beliaev, A. S., Richardson, D. J., Zachara, J. M. and Fredrickson, J. K. (2008) Direct involvement of type II secretion system in extracellular translocation of *Shewanella oneidensis* outer membrane cytochromes MtrC and OmcA. *Journal of Bacteriology*. **190**, 5512-5516
- 3 Clarke, T. A., Edwards, M. J., Gates, A. J., Hall, A., White, G. F., Bradley, J., Reardon, C. L., Shi, L., Beliaev, A. S., Marshall, M. J., Wang, Z., Watmough, N. J., Fredrickson, J. K., Zachara, J. M., Butt, J. N. and Richardson, D. J. (2011) Structure of a bacterial cell surface decaheme electron conduit. *Proceedings of the National Academy of Sciences of the United States of America*. **108**, 9384-9389
- 4 Edwards, M. J., Hall, A., Shi, L., Fredrickson, J. K., Zachara, J. M., Butt, J. N., Richardson, D. J. and Clarke, T. A. (2012) The Crystal Structure of the Extracellular 11-heme Cytochrome UndA Reveals a Conserved 10-heme Motif and Defined Binding Site for Soluble Iron Chelates. *Structure*. **20**, 1275-1284
- 5 Edwards, M. J., Baiden, N. A., Johs, A., Tomanicek, S. J., Liang, L., Shi, L., Fredrickson, J. K., Zachara, J. M., Gates, A. J., Butt, J. N., Richardson, D. J. and Clarke, T. A. (2014) The X-ray crystal structure of *Shewanella oneidensis* OmcA reveals new insight at the microbe-mineral interface. *Febs Letters*. **588**, 1886-1890
- 6 Hartshorne, R. S., Reardon, C. L., Ross, D., Nuester, J., Clarke, T. A., Gates, A. J., Mills, P. C., Fredrickson, J. K., Zachara, J. M., Shi, L., Beliaev, A. S., Marshall, M. J., Tien, M., Brantley, S., Butt, J. N. and Richardson, D. J. (2009) Characterization of an electron conduit between bacteria and the extracellular environment. *Proceedings of the National Academy of Sciences of the United States of America*. **106**, 22169-22174
- 7 Edwards, M. J., Fredrickson, J. K., Zachara, J. M., Richardson, D. J. and Clarke, T. A. (2012) Analysis of structural MtrC models based on homology with the crystal structure of MtrF. *Biochemical Society Transactions*. **40**, 1181-1185
- 8 Hartshorne, R. S., Jepson, B. N., Clarke, T. A., Field, S. J., Fredrickson, J., Zachara, J., Shi, L., Butt, J. N. and Richardson, D. J. (2007) Characterization of *Shewanella oneidensis* MtrC: a cell-surface decaheme cytochrome involved in respiratory electron transport to extracellular electron acceptors. *Journal of Biological Inorganic Chemistry*. **12**, 1083-1094
- 9 Shi, L., Chen, B. W., Wang, Z. M., Elias, D. A., Mayer, M. U., Gorby, Y. A., Ni, S., Lower, B. H., Kennedy, D. W., Wunschel, D. S., Mottaz, H. M., Marshall, M. J., Hill, E. A., Beliaev, A. S., Zachara, J. M., Fredrickson, J. K. and Squier, T. C. (2006) Isolation

- of a high-affinity functional protein complex between OmcA and MtrC: Two outer membrane decaheme c-type cytochromes of *Shewanella oneidensis* MR-1. *Journal of Bacteriology*. **188**, 4705-4714
- 10 Ross, D. E., Ruebush, S. S., Brantley, S. L., Hartshorne, R. S., Clarke, T. A., Richardson, D. J. and Tien, M. (2007) Characterization of protein-protein interactions involved in iron reduction by *Shewanella oneidensis* MR-1. *Applied and Environmental Microbiology*. **73**, 5797-5808
 - 11 Zhang, H., Tang, X., Munske, G. R., Zakharova, N., Yang, L., Zheng, C., Wolff, M. A., Tolic, N., Anderson, G. A., Shi, L., Marshall, M. J., Fredrickson, J. K. and Bruce, J. E. (2008) In vivo identification of the outer membrane protein omcA-mtrC interaction network in *Shewanella oneidensis* MR-1 cells using novel hydrophobic chemical cross-linkers. *Journal of Proteome Research*. **7**, 1712-1720
 - 12 Myers, J. M. and Myers, C. R. (1998) Isolation and sequence of omcA, a gene encoding a decaheme outer membrane cytochrome c of *Shewanella putrefaciens* MR-1, and detection of omcA homologs in other strains of *S-putrefaciens*. *Biochimica Et Biophysica Acta-Biomembranes*. **1373**, 237-251
 - 13 Cao, B., Shi, L. A., Brown, R. N., Xiong, Y. J., Fredrickson, J. K., Romine, M. F., Marshall, M. J., Lipton, M. S. and Beyenal, H. (2011) Extracellular polymeric substances from *Shewanella* sp HRCR-1 biofilms: characterization by infrared spectroscopy and proteomics. *Environmental Microbiology*. **13**, 1018-1031
 - 14 Smith, D. M. A. and Rosso, K. M. (2014) Possible Dynamically Gated Conductance along Heme Wires in Bacterial Multiheme Cytochromes. *Journal of Physical Chemistry B*. **118**, 8505-8512
 - 15 Lower, B. H., Lins, R. D., Oestreich, Z., Straatsma, T. P., Hochella, M. F., Shi, L. A. and Lower, S. K. (2008) In vitro evolution of a peptide with a hematite binding motif that may constitute a natural metal-oxide binding archetype. *Environmental Science & Technology*. **42**, 3821-3827
 - 16 Beliaev, A. S., Thompson, D. K., Khare, T., Lim, H., Brandt, C. C., Li, G., Murray, A. E., Heidelberg, J. F., Giometti, C. S., Yates, J., 3rd, Nealson, K. H., Tiedje, J. M. and Zhou, J. (2002) Gene and protein expression profiles of *Shewanella oneidensis* during anaerobic growth with different electron acceptors. *Omics : a journal of integrative biology*. **6**, 39-60
 - 17 Ruebush, S. S., Brantley, S. L. and Tien, M. (2006) Reduction of soluble and insoluble iron forms by membrane fractions of *Shewanella oneidensis* grown under aerobic and anaerobic conditions. *Applied and Environmental Microbiology*. **72**, 2925-2935
 - 18 Beliaev, A. S., Klingeman, D. M., Klappenbach, J. A., Wu, L., Romine, M. F., Tiedje, J. A., Nealson, K. H., Fredrickson, J. K. and Zhou, J. (2005) Global transcriptome analysis of *Shewanella oneidensis* MR-1 exposed to different terminal electron acceptors. *Journal of Bacteriology*. **187**, 7138-7145
 - 19 Stukalov, O., Korenevsky, A., Beveridge, T. J. and Dutcher, J. R. (2008) Use of atomic force microscopy and transmission electron microscopy for correlative studies of bacterial capsules. *Applied and Environmental Microbiology*. **74**, 5457-5465
 - 20 Fang, L., Cai, P., Li, P., Wu, H., Liang, W., Rong, X., Chen, W. and Huang, Q. (2010) Microcalorimetric and potentiometric titration studies on the adsorption of copper by *P. putida* and *B. thuringiensis* and their composites with minerals. *Journal of Hazardous Materials*. **181**, 1031-1038
 - 21 Freeman, C., Chapman, P. J., Gilman, K., Lock, M. A., Reynolds, B. and Wheeler, H. S. (1995) ION-EXCHANGE MECHANISMS AND THE ENTRAPMENT OF NUTRIENTS BY RIVER BIOFILMS. *Hydrobiologia*. **297**, 61-65

- 22 Albert, A. (1953) Quantitative studies of the avidity of naturally occurring substances for trace metals .3. Pteridines, riboflavin and purines. *Biochemical Journal*. **54**, 646-654
- 23 Romani, A. M., Fund, K., Artigas, J., Schwartz, T., Sabater, S. and Obst, U. (2008) Relevance of polymeric matrix enzymes during biofilm formation. *Microbial Ecology*. **56**, 427-436
- 24 Davey, M. E. and O'Toole, G. A. (2000) Microbial biofilms: from ecology to molecular genetics. *Microbiology and Molecular Biology Reviews*. **64**, 847-+
- 25 Teal, T. K., Lies, D. P., Wold, B. J. and Newman, D. K. (2006) Spatiometabolic stratification of *Shewanella oneidensis* biofilms. *Applied and Environmental Microbiology*. **72**, 7324-7330
- 26 Thormann, K. M., Saville, R. M., Shukla, S., Pelletier, D. A. and Spormann, A. M. (2004) Initial phases of biofilm formation in *Shewanella oneidensis* MR-1. *Journal of Bacteriology*. **186**, 8096-8104
- 27 O'Toole, G. A. (2003) To build a biofilm. *Journal of Bacteriology*. **185**, 2687-2689
- 28 De Vriendt, K., Theunissen, S., Carpentier, W., De Smet, L., Devreese, B. and Van Beeumen, J. (2005) Proteomics of *Shewanella oneidensis* MR-1 biofilm reveals differentially expressed proteins, including AggA and RibB. *Proteomics*. **5**, 1308-1316
- 29 Conrad, J. C. (2012) Physics of bacterial near-surface motility using flagella and type IV pili: implications for biofilm formation. *Research in Microbiology*. **163**, 619-629
- 30 Malvankar, N. S., Vargas, M., Nevin, K. P., Franks, A. E., Leang, C., Kim, B. C., Inoue, K., Mester, T., Covalla, S. F., Johnson, J. P., Rotello, V. M., Tuominen, M. T. and Lovley, D. R. (2011) Tunable metallic-like conductivity in microbial nanowire networks. *Nature Nanotechnology*. **6**, 573-579
- 31 An, D. D. and Parsek, M. R. (2007) The promise and peril of transcriptional profiling in biofilm communities. *Current Opinion in Microbiology*. **10**, 292-296
- 32 Stewart, P. S. and Franklin, M. J. (2008) Physiological heterogeneity in biofilms. *Nature Reviews Microbiology*. **6**, 199-210
- 33 Gonzalez, J. E. and Keshavan, N. D. (2006) Messing with bacterial quorum sensing. *Microbiology and Molecular Biology Reviews*. **70**, 859-+
- 34 Bodor, A., Elxnat, B., Thiel, V., Schulz, S. and Wagner-Dobler, I. (2008) Potential for luxS related signalling in marine bacteria and production of autoinducer-2 in the genus *Shewanella*. *Bmc Microbiology*. **8**
- 35 Plummer, P. J. (2012) LuxS and quorum-sensing in *Campylobacter*. *Frontiers in Cellular and Infection Microbiology*. **2**
- 36 Rajamani, S., Bauer, W. D., Robinson, J. B., Farrow, J. M., III, Pesci, E. C., Teplitski, M., Gao, M., Sayre, R. T. and Phillips, D. A. (2008) The Vitamin Riboflavin and Its Derivative Lumichrome Activate the LasR Bacterial Quorum-Sensing Receptor. *Molecular Plant-Microbe Interactions*. **21**, 1184-1192
- 37 Kalia, V. C. (2013) Quorum sensing inhibitors: An overview. *Biotechnology Advances*. **31**, 224-245
- 38 Okamoto, A., Hashimoto, K., Nealson, K. H. and Nakamura, R. (2013) Rate enhancement of bacterial extracellular electron transport involves bound flavin semiquinones. *Proceedings of the National Academy of Sciences of the United States of America*. **110**, 7856-7861
- 39 Lies, D. P., Hernandez, M. E., Kappler, A., Mielke, R. E., Gralnick, J. A. and Newman, D. K. (2005) *Shewanella oneidensis* MR-1 uses overlapping pathways for

- iron reduction at a distance and by direct contact under conditions relevant for biofilms. *Applied and Environmental Microbiology*. **71**, 4414-4426
- 40 von Canstein, H., Ogawa, J., Shimizu, S. and Lloyd, J. R. (2008) Secretion of flavins by *Shewanella* species and their role in extracellular electron transfer. *Applied and Environmental Microbiology*. **74**, 615-623
- 41 Marsili, E., Baron, D. B., Shikhare, I. D., Coursolle, D., Gralnick, J. A. and Bond, D. R. (2008) *Shewanella* Secretes flavins that mediate extracellular electron transfer. *Proceedings of the National Academy of Sciences of the United States of America*. **105**, 3968-3973
- 42 McLean, J. S., Pinchuk, G. E., Geydebrekht, O. V., Bilskis, C. L., Zakrajsek, B. A., Hill, E. A., Saffarini, D. A., Romine, M. F., Gorby, Y. A., Fredrickson, J. K. and Beliaev, A. S. (2008) Oxygen-dependent autoaggregation in *Shewanella oneidensis* MR-1. *Environmental Microbiology*. **10**, 1861-1876
- 43 Lower, B. H., Shi, L., Yongsunthon, R., Droubay, T. C., McCready, D. E. and Lower, S. K. (2007) Specific bonds between an iron oxide surface and outer membrane cytochromes MtrC and OmcA from *Shewanella oneidensis* MR-1. *Journal of Bacteriology*. **189**, 4944-4952
- 44 Eggleston, C. M., Voros, J., Shi, L., Lower, B. H., Droubay, T. C. and Colberg, P. J. S. (2008) Binding and direct electrochemistry of OmcA, an outer-membrane cytochrome from an iron reducing bacterium, with oxide electrodes: A candidate biofuel cell system. *Inorganica Chimica Acta*. **361**, 769-777
- 45 Xiong, Y. J., Shi, L., Chen, B. W., Mayer, M. U., Lower, B. H., Londer, Y., Bose, S., Hochella, M. F., Fredrickson, J. K. and Squier, T. C. (2006) High-affinity binding and direct electron transfer to solid metals by the *Shewanella oneidensis* MR-1 outer membrane c-type cytochrome OmcA. *Journal of the American Chemical Society*. **128**, 13978-13979
- 46 Meitl, L. A., Eggleston, C. M., Colberg, P. J. S., Khare, N., Reardon, C. L. and Shi, L. (2009) Electrochemical interaction of *Shewanella oneidensis* MR-1 and its outer membrane cytochromes OmcA and MtrC with hematite electrodes. *Geochimica Et Cosmochimica Acta*. **73**, 5292-5307
- 47 Mitchell, A. C., Peterson, L., Reardon, C. L., Reed, S. B., Culley, D. E., Romine, M. R. and Geesey, G. G. (2012) Role of outer membrane c-type cytochromes MtrC and OmcA in *Shewanella oneidensis* MR-1 cell production, accumulation, and detachment during respiration on hematite. *Geobiology*. **10**, 355-370

Materials & Methods

M.1 – SDS-PAGE experiments. Sodium dodecyl-sulphide (SDS) polyacrylamide gels were poured manually. After setting-up the glass casing, the Resolving gel was made and poured first. For duplicate 12% Resolving gels the following mixture was made, mixed thoroughly and poured immediately before setting:

- 3 mL H₂O
- 2.25 mL 1.5 M TRIS-HCl pH 8.8
- 45 µL 20% SDS solution
- 3.6 mL 30% polyacrylamide solution (37.5:1 acrylamide:bis)
- 90 µL 10% ammonium persulfate (APS) solution
- 9 µL tetramethylethylenediamine (TEMED).

Approximately 500 µL 50% (v/v) H₂O:propan-2-ol is applied to the top of freshly poured Resolving gel to induce flattening of the top of the Resolving gel as the H₂O:propan-2-ol mixture undergoes phase separation. After 25-30 minutes the Resolving gel sets and the H₂O:propan-2-ol mixture is poured off. Duplicate 4% Stacking gels are made of:

- 2.534 mL H₂O
- 0.44 mL 1.0 M TRIS-HCl pH 6.8
- 17.5 µL 20% SDS solution
- 0.47 mL 30% Acrylamide solution
- 35 µL 10% APS
- 3.5 µL TEMED.

The Stacking gel mixture was mixed thoroughly, poured immediately before setting on top of the Resolving gel and combs inserted to generate wells to subsequently pipette protein sample. After 25-30 minutes the Stacking gel is set and ready for use. A non-reducing 5× Sample Application Buffer is added to sample, consisting of 0.3 M Tris-HCl, 50% glycine, 1% SDS, 0.2% Bromophenol Blue.

Electrophoresis was run at 150 V, 25 mA for approximately 1 hour 20 minutes using 1 L Running buffer (25 mM TRIS-HCl, 192 mM glycine, 0.1% SDS) in a Bio-Rad Mini-PROTEAN Tetra Cell gel tank.

M1.1 – Gel Staining: Coomassie staining of polyacrylamide gels relies on the hydrophobic dye agent localizing to hydrophobic pockets within the protein present. Staining was done using InstantBlue solution (Expedeon). As such gels were incubated mixing with 20-30 mL Coomassie stain for 15 minutes, rinsed and imaged.

Silver staining relies on chemical treatment of the protein content within SDS polyacrylamide gels such that upon silver precipitation, silver preferentially binds to protein. Staining occurs with the gel constantly under mixing incubation at 4°C, starting with addition 50% methanol, 5% acetic acid solution for 20 minutes. This is replaced with 50% methanol for 10 minutes and the gel is then rinsed with H₂O for 10 minutes. The H₂O is replaced by a 1 minute 0.02 % Na₂S₂O₃ incubation, followed by 1 minute H₂O rinses and then 20 minute incubation in 0.1% AgNO₃ and a foil-wrapped gel tray to prevent photo-reductive Ag²⁺ precipitation. The AgNO₃ solution is replaced by a second set of 2 × H₂O rinses, and staining intensity is developed by addition of 20-30 mL batches of 2% Na₂CO₃, 0.04% formaldehyde solution for 30 seconds until desired stain intensity is achieved. This is replaced by a 2 × 5% acetic acid solution 3 minute soaks, followed by storage in 1% acetic acid and gel imaging.

“Haem” staining was performed using a peroxidase activity-staining technique. The gel is incubated mixing in 20 mL 0.25 M sodium acetate, pH 5.0 for 15 minutes, followed by addition of 20 mL 1% (w/v) 3,3',5,5'-tetramethylbenzidine (TMBD) in ethanol. After a continued mixing incubation for 10-15 minutes, 200 µL 30% H₂O₂ is added and the gel left to develop for 15-20 minutes before replacing the resultant solution with H₂O.

M.2 – Ultraviolet-visible Absorption Spectroscopy. Absorption spectra were measured from 800 – 200 nm at a scan rate of 120 nm min⁻¹ for high-resolution data and 600 nm min⁻¹ for

measuring $A_{410\text{nm}}$ and $A_{280\text{nm}}$ of FPLC fractions. Spectrum baseline was determined via recording spectra without cuvette, and then with a cuvette containing sample buffer. Quartz cuvettes with either 1.0 cm or 0.1 cm path lengths were used, unless 1.0 cm path length spectroscopic plastic cuvettes were used instead (Sarstedt AG & Co.).

M.2.1 – Oxidised and reduced protein spectra: A rubber seal was used to cap the cuvette, and the headspace purged with $\text{N}_{2(\text{g})}$ for 5-7 minutes to remove dissolved O_2 . Spectra is measured before and after N_2 -purging to ensure concentration has remained the same and sample has not changed/been damaged. Sample is then reduced or oxidised by titration with N_2 -purged the reductant 0.23 M $\text{Na}_2\text{S}_2\text{O}_4$ (i.e. 20 mg mL^{-1}) or the oxidant 60.7 mM $\text{K}_3[\text{Fe}(\text{CN})_6]$ (i.e. 20 mg mL^{-1}) respectively, with repeat measurements to check for sample equilibration.

M.2.2 – Protein Quantification: Where necessary, OmcA concentration was determined using OmcA's experimentally determined molar extinction coefficient, ϵ_λ (see Section M.2.3) and the Beer-Lambert law, i.e.:

$$\text{Concentration, mg mL}^{-1} = \frac{\text{Absorbance, } A}{\text{path length, } l \times \epsilon_\lambda} \times \text{molar mass, } M_r.$$

Due to low protein yield from purification, an estimated ϵ_λ of 1,100,000 $\text{M}^{-1} \text{cm}^{-1}$ (i.e. 110,000 $\text{M}^{-1} \text{cm}^{-1}$ per c-type haem [1]) was used to estimate UV-Vis quantification of OmcA_(wt).

M.2.3 – Pyridine Hemochrome Determination of Molar Extinction Co-efficients, ϵ_λ : Horse heart cytochrome c was used as a monohaem cytochrome c standard. Cytochrome in 50 mM HEPES, pH 7.0, 2 mM CaCl_2 is titrated into sample buffer such that $A_{410 \text{ nm}} \approx 1.0$, to a final volume of 2.5 mL. The sample then had 0.5 mL of 0.6 M NaOH, 0.68 mL of 12.2 mM pyridine and 0.32 mL Analytical H_2O . The sample is then split into two cuvettes, 1.7 mL each. Excess oxidant (i.e. 4 μL of 60.8 mM $\text{K}_3[\text{Fe}(\text{CN})_6]$) is added to one cuvette and excess reductant added to the other (i.e. 5 μL of 0.23 M $\text{Na}_2\text{S}_2\text{O}_4$).

Difference spectra (i.e. reduced spectrum minus oxidised spectrum) were analysed to determine extinction co-efficients. The oxidised cytochrome c UV-vis spectrum was thus measured and used to determine a ϵ_λ of known concentration for a single pyridine-ligated c-type haem:

$$[\text{Cyt } c] = \frac{\Delta A_{\text{Cyt } c, 550-535 \text{ nm}}}{\Delta \epsilon_{\text{Cyt } c, 550-535 \text{ nm}} \times l}$$

(where $[\text{Cyt } c]$ = horse heart cytochrome c concentration, $\Delta A_{550-535 \text{ nm}}$ = reduced $A_{550 \text{ nm}}$ minus oxidised $A_{535 \text{ nm}}$, $\Delta \epsilon_{550-535 \text{ nm}}$ = reduced $\epsilon_{550 \text{ nm}}$ minus oxidised $\epsilon_{535 \text{ nm}}$)

The number of c-type haems has been determined experimentally (i.e. the crystal structure of MtrF [2], eUndA [3], eOmcA [4] and primary structure of MtrC [5]), the pyridine-ligated haems of the analyte have a $\Delta \epsilon_{550-535 \text{ nm}}$ proportional to the number of c-type haems:

$$\epsilon_{\text{OmcA}, \lambda} = \frac{10 \times A_\lambda \times \Delta \epsilon_{\text{Cyt } c, 550-535 \text{ nm}}}{\Delta A_{\text{OmcA}, 550-535 \text{ nm}} \times l} = \frac{n \times A_\lambda}{[\text{OmcA}] \times l}$$

(where A_λ = Absorbance at wavelength λ , n = number of haems)

The UV-vis spectrum of an oxidised sample of the same concentration as the pyridine-ligated sample is then calibrated with the acquired ϵ_λ .

M.3 – Protein Purification.

Protein purification was performed using various Fast Purification Liquid Chromatography (FPLC) columns managed via ÄKTAprius plus and ÄKTAFPLC systems (GE Healthcare), unless manually run columns are specified. After each chromatography column, an SDS-PAGE gel was run as described in Section M.1 to determine the purity of eluted fractions to pool.

M.3.1 – *OmcA_(wt)* Purification: *Shewanella oneidensis* MR-1 cells were grown in a 100 mL starter Luria-Bertani (LB) media culture overnight at 30°C (200 rpm). This culture was used to inoculate 16 L of Luria-Bertani media (1 mL L⁻¹ inoculum) supplemented with 50 mM sodium-D,L-lactate and 20 mM iron (III) citrate. Cells were pelleted at 9,000 ×g, resuspended in 300 mL of 20 mM HEPES, pH 7.60, 100 mM NaCl and put through two subsequent French Press runs at 1000 psi. Debris was removed from the lysate by centrifugation at 15,000 ×g (4°C) for 15 minutes. Cell lysate supernatant then underwent two centrifugal wash steps in Buffer A (20mM HEPES, pH 7.60, 100 mM NaCl) at 205,076 ×g for 2 hours (at 4°C) and then solubilisation overnight in 540 mL Buffer B (Buffer A + 5% Triton X-100). EDTA-free, complete protease inhibitor cocktail (Roche Diagnostics GmbH, Germany) was added to the membrane-detergent suspension. The sample then underwent a centrifugation step (35 mins at 205,076 ×g, 4°C) to pellet insoluble debris. The solubilised *S. oneidensis* MR-1 membranes supernatant was then isolated for further purification.

OmcA_(wt) was purified from the solubilised *S. oneidensis* MR-1 membranes using Fast Protein Liquid Chromatography (FPLC) performed at 4°C (excluding manually-run detergent exchange performed at room temperature) using GE Healthcare AKTA systems. Throughout the purification, elution of protein was monitored by UV-absorption ($A_{280\text{nm}}$) by the aromatic residue component of peptide backbone. Elution of *OmcA_(wt)* amongst fractions collected was identified by peroxidase-haem staining, Coomassie staining and/or Silver staining of 12% (w/v) SDS-polyacrylamide gels. Where an issue with Coomassie-staining *OmcA_(wt)*/contaminants was experienced, *OmcA_(wt)* purity was identified by Silver and haem-staining duplicate SDS-PA gels. Final gels of this purification were loaded with 5 µg of protein (as determined by UV-visible $A_{410\text{nm}}$ as explained earlier). Each sample was centrifuged at 18,000 ×g for 10 mins (4°C) prior to loading protein onto FPLC columns.

Solubilised *S. oneidensis* MR-1 membrane supernatant was loaded onto a pre-equilibrated (Buffer C; 20mM HEPES, pH 7.60, 5% Triton X-100) 150 mL DEAE (diethylaminoethyl) Sepharose CL-6B. After 3 column volumes (CV) washes of column-bound sample with Buffer C run at 2 mL min⁻¹, the sample was eluted by running Buffer D (Buffer C + 1 M NaCl) at 1 mL min⁻¹ with a 0 – 50% linear gradient over 6 CV (900 mL). *OmcA_(wt)* eluted at 2 different NaCl concentrations. Both sets of fractions had the excess salt dialysed out overnight in Buffer E (Buffer A + 2% Triton X-100) and were further purified separately.

Both batches of samples were loaded (in separate runs) onto a Buffer E-equilibrated 60 mL Q-Sepharose column (at 1 mL min⁻¹) and run at 2mL min⁻¹ with a gradient of 10 – 30% Buffer F (Buffer E + 1 M NaCl) in 5% stepwise increments. Each gradient step was run for 3 CV and *OmcA_(wt)*-containing fractions were pooled. Excess NaCl was removed via “Amicon-exchange”, whereby 3 cycles of 10-fold sample concentration followed by 10-fold dilution with Buffer E using an Amicon pressure cell with a 30 kDa cut-off membrane.

Detergent exchange was then performed manually by binding the *OmcA_(wt)* sample to a Buffer E-equilibrated Q Sepharose cartridge (1 mL), washing the sample with 5-10 CV Buffer E and then 20 CV of Buffer G (Buffer A + 0.6% CHAPS). Protein was then eluted with ≈5 CV Buffer H (Buffer G + 1M NaCl) and excess NaCl removed via Amicon-exchange into Buffer G as described earlier.

The sample was then loaded onto a 1 mL Mono Q column in Buffer G, and after a 5.5 CV wash with Buffer G a linear gradient of 0-90% Buffer H applied over 10.5 CV at 0.2 mL min⁻¹. Excess NaCl was removed via Amicon-exchange into Buffer G to sample volume of 1 mL.

Finally, the sample was put through a Buffer G-equilibrated Sephadex G-25M PD10 column run under gravity-flow in an attempt to remove a low molecular weight co-purifying contaminant. The sample was then Amicon-exchanged into Buffer G as described earlier and

quantified by UV-visible spectroscopy as described earlier. Due to low protein yield from purification, an estimated ϵ_{λ} of $1,100,000 \text{ M}^{-1} \text{ cm}^{-1}$ was used to estimate UV-Vis quantification of OmcA_(wt).

M.3.2 – pOmcA Purification: pOmcA was purified from the periplasm of expression strain *Shewanella oneidensis* LS 330, which contains a pBAD/TOPO plasmid cloned with a recombinant form of the *omcA* open reading frame (locus SO_1779). The amino-terminus encoded in *omcA* containing a lipid-anchor sequence LXXC was replaced with the *mtrB* amino-terminus (cloning strategy described by [6]) to promote water solvation of expressed soluble OmcA (pOmcA). The starter culture of *S. oneidensis* LS 330 was grown in 100 mL of TB media (per litre: 12 g tryptone, 24 g yeast extract, 4 mL glycerol made up to 900 mL. Then post-autoclave addition of 100 mL filtered 10x phosphate buffer, per litre: 23.1 g KH_2PO_4 , 125.4 g K_2HPO_4) supplemented with $50 \mu\text{g mL}^{-1}$ kanamycin (TB+Kan₅₀) overnight (14 hours). The 12 L of TB+Kan₅₀ growth media was then inoculated with 5 mL overnight culture L⁻¹. Expression was induced with addition of 1 mM Arabinose when the O.D. = 0.6 (5-6 hours post-inoculation), and then cells were harvested by centrifugation at $7,000 \times g$ (for 15 mins, 4°C) 18 hours after inoculation. Cells were re-suspended in 15 mL of Buffer I (Buffer A + 150 mM NaCl, EDTA-free complete protease inhibitor cocktail (Roche Diagnostics GmbH, Germany), 0.05% CHAPS) per litre of initial cell culture volume. Cells were lysed by 2 rounds of French Press at 1,000 psi and insoluble debris removed by centrifugation at $15,500 \times g$ for 15 mins at 4°C. The supernatant went through an ultracentrifugation step at $150,000 \times g$ (for 1 hour at 4°C using a Beckman Ti-45 rotor), the supernatant of which was then loaded onto a Buffer I-primed, 5mL Nickel-Nitrilotriacetic acid (Ni-NTA) column through a 0.2 μm filter.

pOmcA was purified from the soluble fraction of lysed *S. oneidensis* LS 330 cells using Fast Protein Liquid Chromatography (FPLC) performed at 4°C (excluding manually-run Immobilised metal affinity column (IMAC i.e. Ni-NTA column) performed at room temperature) using GE Healthcare AKTA systems. Elution of OmcA amongst fractions collected was identified by peroxidase-haem staining, Coomassie staining and/or Silver staining of 12% (w/v) SDS-polyacrylamide gels. Where an issue with Coomassie-staining OmcA/contaminants was experienced, Silver- and haem-staining duplicate SDS-polyacrylamide gels identified OmcA purity. Ni-NTA-bound sample was sequentially washed with 4.5 CV of Buffer J (Buffer A + 300 mM NaCl, 0.05% CHAPS, 10% glycerol), Buffer K (Buffer J + 10 mM imidazole), and Buffer L (Buffer J + 40 mM imidazole). pOmcA was then eluted with Buffer M (Buffer J + 250 mM imidazole). Eluted sample was dialysed overnight (into Buffer J), concentrated to $\approx 1 \text{ mL}$ in an Amicon pressure cell with a 10 kDa cut-off membrane and then loaded (150 μL per run) onto a 16/60 Superdex 200 gel filtration column in Buffer N (20 mM TRIS, pH 7.8, 150 mM NaCl, 0.01% CHAPS). Gel filtration was run at 0.4 mL min^{-1} , and the pOmcA-containing fractions were pooled for each run. UV-visible spectra were measured for the various fractions for spectroscopic characterisation of the purity visible from duplicate SDS-PAGE gels. Seven independent gel filtration runs created separate pOmcA pools with $A_{410 \text{ nm}}:A_{280 \text{ nm}}$ ratio ≥ 6.0 .

All pOmcA was then pooled and Amicon-exchanged with a 10 kDa cut-off membrane into Buffer H as described previously. pOmcA was then quantified by UV-vis spectroscopy as described earlier (see Section M.2.2).

M.3.3 – eOmcA Purification: The spent growth-media of 100 g of *S. oneidensis* LS 330 cells (from a 7 L grow-up) that had been induced with 1 mM arabinose was concentrated ≈ 30 -fold using a Vivaflow 200 filtration cartridge with a 30 kDa cut-off membrane (Sartorius). The sample was then centrifuged at $8,000 \times g$ and then $18,000 \times g$ for 15 mins each (4°C), dialysed in 2 sequential batches of buffer A (20 mM HEPES, pH 7.60, 50 mM NaCl) and centrifuged again at $18,000 \times g$ for 15 mins (4°C) before being loaded onto a 150 mL diethylaminoethyl (DEAE) anion-exchange column equilibrated with buffer A. After a $3 \times$ column-volume (CV) wash of the sample-bound DEAE column (to achieve a steady baseline), a linear gradient of 0 –

50% [buffer B] (Buffer A + 1 M NaCl) was applied over 3 CV at 2 mL min⁻¹ and 10 mL fractions collected. UV-visible spectra were measured for the various fractions for spectroscopic characterisation of the purity visible from duplicate SDS-PAGE gels. Fractions with A_{410 nm}:A_{280 nm} ratio > 3.50 were then pooled and spun at 18,000 ×g for 10 mins (4°C).

The sample (80 mL pool) was dialysed in buffer C (20 mM HEPES, pH 7.60, 100 mM NaCl) overnight and then loaded onto a 90 mL Q-Sepharose anion exchange column primed with buffer C. After 2 CV buffer C wash, the sample was eluted with a 0-50% [buffer B] linear gradient over ≈6 CV at 1 mL min⁻¹ and 5 mL fractions collected. Selected fractions (A_{410nm}:A_{280nm} ratio > 4.50) were subsequently dialysed in buffer C and loaded onto the buffer C-equilibrated Q-Sepharose column. A ≈1.5 CV wash and linear gradient of 0-35% [buffer B] at 1 mL min⁻¹ was applied to elute the analyte into 4 mL fractions.

Selected fractions were pooled and concentrated to ≈2.2 mL, divided down to ≈0.75 mL aliquots and injected onto a Superdex 16/60 S-200. The gel filtration experiments were run at 0.10 mL min⁻¹ in 20 mM HEPES, pH 7.60, 100 mM NaCl. After 2 mL fractions were collected in the initial gel filtration run, fraction size was reduced to 1 mL.

Recombinant eOmca proteins eY³⁷⁴F, eT⁷²⁵G and eP⁷²⁶G were successfully purified using appropriate variations of the protocol described for eOmca.

M.4 – Electron Paramagnetic Resonance Spectroscopy. EPR experiments and data processing were performed in collaboration with Dr Andrew Gates, University of East Anglia, UK.

EPR samples were prepared by syringing 200 µL of protein into quartz EPR tubes that had been cleaned (i.e. HNO₃/H₂O and ethanol/H₂O washed). EPR sample path length was calibrated via sample height.

EPR spectra were recorded at 10 K ± 4 using a Bruker ER 200D X-band spectrometer connected to an ELEXYS control system (Bruker Analytische Messtechnik GmbH) with a variable temperature liquid helium cryostat (Oxford Instruments, U.K.).

M.4.1 – Potentiometric Titration: Sample poisoning at specific redox potentials was performed at room temperature (i.e. 293 K) in an anaerobic glovebox. The protein sample is transferred into a poisoning bulb (Fig. M.1) with redox mediator cocktail to buffer against potential bias of the sample protein (Table M.1). The protein sample was poised by titration with the reductant 0.23 M Na₂S₂O₄ or the oxidant 60.7 mM K₃[Fe(CN)₆]. Redox potential was measured using a calomel reference electrode and a platinum wire connected in series to a voltmeter (see Fig. M.1). After the protein reached a given target redox potential, the sample was extracted from the poisoning bulb, syringed into a quartz EPR tube, and the remaining sample underwent titration to the next target potential. Poised sample was frozen in N_{2(l)} within 60 seconds of sample equilibrating at a target potential, generating equimolar samples.

Table M.1 – *Redox Mediator cocktail contents.* Independent stock solutions of each mediator were prepared before combining to form a mediator cocktail stock solution. E_{m,7} = mid-point potential at pH 7.0.

Redox Mediator		Mediator Concentration (µM)	E _{m,7} (V)
Name	IUPAC Nomenclature		
DAD	2,3,5,6-tetramethyl-p-phenylenediamine	20	+0.276
PMS	phenazine methosulphate	20	+0.080
PES	phenazine ethosulphate	20	+0.055
ADQS*	anthraquinone-2,6-disulphonic acid	20	-0.185
AQS*	anthraquinone-2-sulphonic acid	20	-0.225
Benzyl viologen	1,1'-dibenzyl-4,4'-bipyridinium dichloride	15	-0.350
Methyl viologen	1,1'-dimethyl-4,4'-bipyridinium dichloride	15	-0.440

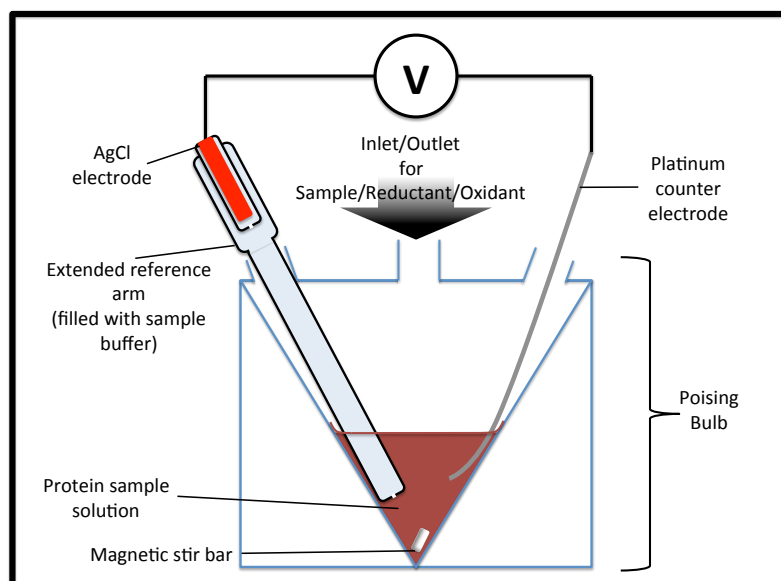
* = dissolved initially DMSO before final mix prepared.

Table M.2 – Sample-specific EPR spectrometer parameters.

Sample	Specific parameters/conditions				No. of Scans	Buffer*
	Frequency (GHz)	Temperature (K)	Power (mW)	Receiver Gain		
Analytical H ₂ O	9.688	10 ± 0.4	2.012	6.32 × 10 ⁵	3	N/A
1mM CuSO ₄ , 10 mM EDTA	9.688	21 ± 0.5	2.012	6.32 × 10 ⁴	1	N/A
pOmcA (155 μM; pH 7.60)	9.688	9.6 ± 0.4	2.012	6.32 × 10 ⁵	5	
OmcA _(wt) (25 μM; pH 7.60)	9.678	10 ± 0.5	2.012	6.32 × 10 ⁵	5	1
eOmcA (87 μM; pH 7.60)	9.688	10 ± 0.5	2.017	6.32 × 10 ⁵	5	
eOmcA (87 μM; pH 6.60)	9.683	10 ± 0.5	2.012	6.32 × 10 ⁵	5	2
eOmcA (87 μM; pH 5.60)	9.683	10 ± 0.25	2.012	6.32 × 10 ⁵	5	3
[#] 1mM CuSO ₄ , 10 mM EDTA	9.466	10 ± 0.1	2.012	6.32 × 10 ⁵	2	4
eOmcA (145 μM; pH 7.60)	9.688	7 ± 2	2.012	6.32 × 10 ⁵	3	
[#] eT ⁷²⁵ G (145 μM; pH 7.60)	9.464	10 ± 0.1	2.007	6.32 × 10 ⁴	2	1
eUndA (86 μM; pH 7.60)	9.688	7 ± 2	2.012	6.32 × 10 ⁵	3	

*Buffer: 20 mM buffer, 50 mM NaCl, 0.01% CHAPS, 1 % glycerol; 1 = HEPES, pH 7.60; 2 = PIPES, pH 6.60; 3 = MES, pH 5.60. Buffer 4 = 50 mM HEPES, pH 6.93. Parameters maintained constant are modulation amplitude = 10.00 Gauss, Sweep width = 3050 ± 6000 Gauss, Conversion and Time constant = 163.84 ms. [#] = Measured on a different Bruker ER 200D X-band spectrometer setup.

Fig. M.1. – *Poising protein at specific redox potentials.* Redox potential was measured using a calomel (AgCl) reference electrode interfacing the protein solution with a buffer-filled extended arm, and a platinum wire connected in series to a voltmeter to complete the circuit.



M.4.2 – Data Processing: For each spectra recorded, the Receiver Gain-induced “baseline-gradient” was determined by using WINEPR SimFonia (ver. 1.25, Bruker Analytische GmbH) and removed when subtraction with analytical grade H₂O spectrum did not remove the baseline gradient. The spectrum of H₂O was also used to remove cavity contributions from the sample spectra (see Fig. A2.10). Individual resonance species were simulated and scaled, also using WINEPR SimFonia (ver. 1.25, Bruker Analytische GmbH).

M.4.2.1 – Spin-Integration & Fitting the Nernst Equation: Resonance feature simulations were scaled and integrated to determine arbitrary spin intensity. The Field Strength spanned by integration was also recorded. The same procedure was repeated for each resonance feature simulated in each spectrum, and repeated for the spectrum of spin standard 1 mM CuSO₄:10 mM EDTA solution. Using the following formula, spin integration of the standard containing 1 mM spin was used to calibrate the spin concentration present in the protein samples:

$$I_n = \frac{I_o \times d^2 \times T \times 10^{\frac{dB}{20}}}{g_p^{av} \times l \times a}$$

(where I_n = normalised double integral, I_o = observed double integral, d = distance between integration start and end points [in Gauss], T = absolute temperature [K], dB = attenuator reading, l = path length sample height calibration, a = receiver gain)

$$\text{and } g_p^{av} = \frac{2}{3} \sqrt{\frac{g_1^2 + g_2^2 + g_3^2}{3}} + \frac{g_1 + g_2 + g_3}{9}$$

In combination with UV-Vis determination of protein concentration, spin quantity per protein molecule of each resonance feature was determined.

Mid-point potentials were determined by fitting signal intensities to an “oxidised derivation” of the Nernst equation (because oxidised ferric haem produces the signals being fitted):

$$E = E_m + \frac{RT}{nF} \ln \left(\frac{[\text{ox}]}{[\text{red}]} \right) \quad \dots \text{Eqn. M.2}$$

(where E = redox potential, E_m = mid-point redox potential, R = gas constant = $8.31446 \text{ V C K}^{-1} \text{ mol}^{-1}$, T = temperature (i.e. at poising, in Kelvin), n = number of electrons involved in molar redox process, F = Faraday constant = $9.64854 \times 10^4 \text{ C mol}^{-1}$, $[\text{ox}]$ = concentration of oxidized species, $[\text{red}]$ = concentration of reduced species)

$$\Rightarrow (E - E_m) \frac{nF}{RT} = \ln \left(\frac{[\text{ox}]}{[\text{red}]} \right)$$

$$\Rightarrow \frac{[\text{ox}]}{[\text{red}]} = \exp \left[(E - E_m) \frac{nF}{RT} \right] = \psi$$

(where \exp = Euler’s constant)

$$\Rightarrow [\text{ox}] = [\text{red}] \psi \quad \dots \text{Eqn. M.2a}$$

$$\text{If } [\text{ox}] + [\text{red}] = 1 \quad \Rightarrow [\text{red}] = 1 - [\text{ox}]$$

Using Eqn. M.2a,

$$\Rightarrow [\text{ox}] = (1 - [\text{ox}]) \psi \quad \Rightarrow [\text{ox}] = \psi - \psi [\text{ox}]$$

$$\Rightarrow [\text{ox}] + \psi [\text{ox}] = \psi \quad \Rightarrow [\text{ox}] (1 + \psi) = \psi$$

$$\Rightarrow [\text{ox}] = \frac{\psi}{(1 + \psi)} = \frac{\exp \left[(E - E_m) \frac{nF}{RT} \right]}{(1 + \exp \left[(E - E_m) \frac{nF}{RT} \right])} \quad \dots \text{Eqn. M.2b}$$

Signal intensities are scaled to 1.00 for Nernst fitting. If more than one species contributes to the signal being fitted, a constant is added such that:

$$[\text{ox}] = k \times (\xi_1 + \xi_2 + \dots + \xi_{\gamma-1} + \xi_\gamma) \quad \dots \text{Eqn. M.3}$$

(where $\frac{\exp \left[(E - E_m) \frac{nF}{RT} \right]}{1 + \exp \left[(E - E_m) \frac{nF}{RT} \right]} = \xi$; $k = \frac{1}{\gamma}$, γ = number of terms, based on number of contributing species).

M.5 – Magnetic Circular Dichroism (NIR-MCD). MCD experiments were performed in collaboration with Dr Myles Cheesman, University of East Anglia, UK.

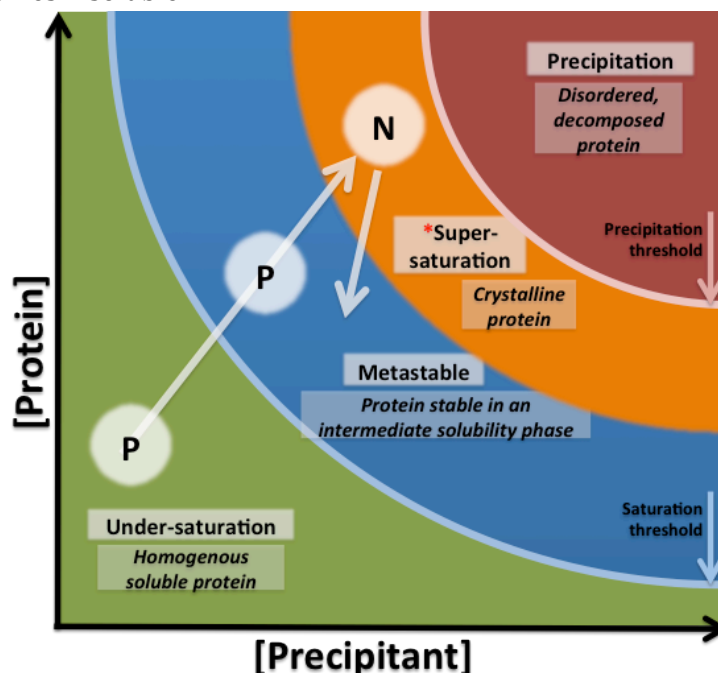
MCD was performed on air-oxidised pOmCA in deuterated-buffer 20 mM HEPES, pH 7.60, 0.1 M NaCl, at 293 K. The UV-vis spectrum in the absence of a magnetic field was measured to facilitate plotting $\Delta\epsilon$. The Circular Dichroism spectra of pOmCA in the UV-vis region with an applied magnetic field (i.e. $H = 8$ Tesla) were made using two cuvettes with different path lengths to obtain 10-fold amplification between spectra (i.e. 1.0 cm and 0.1 cm path length cuvettes). A Near-Infrared MCD spectrum was also measured (using a 1.0 cm path length cuvette). UV-vis measurements (800 – 200 nm) were made with a Jasco J810 spectropolarimeter. Near-Infrared MCD of pOmCA (2000 – 700 nm) was measured with a Jasco J730 spectropolarimeter.

M.6 – X-Ray Crystallography. Crystallography experiments were performed in collaboration with Dr Marcus Edwards, University of East Anglia, UK.

M.6.1 – Protein Crystallisation: Using a concentrated crystallisation cocktail, surface electrostatic charges and hydrophobic patches of eOmCA were altered via the cocktail's chemical constituents to promote crystallisation according to the phase diagram (Fig. M.2). Successful decrease of eOmCA solubility (stock protein concentration 6.7 mg mL^{-1}) lead to self-assembly of protein crystals using 0.1 M Tris/HEPES at pHs 7.5, 7.8 and 8.5 with 0.1 MgCl_2 and 16% PEG 20K as the precipitant. Further optimisations ultimately identified X-ray diffracting crystals formed in 0.1 M Bis-Tris Propane, pH 8.50, 0.1 M MgCl_2 and 15% PEG 20K.

Crystals of eY³⁷⁴F were formed in 0.1 M HEPES, pH 7.0, 0.1 M MgCl_2 , 14% PEG 20K. Crystals of eT⁷²⁵G were formed in 0.1 M Bis-Tris Propane, pH 8.0, 0.1 M MgCl_2 , 19% PEG 20K. Crystals of eP⁷²⁶G were formed in 0.1 M HEPES, pH 7.0, 0.1 M MgCl_2 , 12% PEG 20K. 20% DMSO was used as cryo-protectant as in eOmCA for all recombinant protein.

Fig. M.2 – A simplified phase diagram of protein crystallisation. Sample protein is purified (P) and exists in either the “Under-saturation” or “Metastable” phases. The process of crystallisation is to transition the purified protein to the Super-saturation phase where protein crystal nucleation (N) can occur (demarcated with red asterisk). Upon crystal nucleation, soluble protein concentration decreases and can reach re-enter the Metastable phase where crystal growth can continue. Seeding with crystals provides a crystallisation nucleus, which can enhance the rate of crystal growth via bypassing the nucleation process. However, once crystalline protein is obtained this does not guarantee that the crystals will diffract incident X-rays. Precipitation is produced by unfolded protein that becomes insoluble.



M6.2 – X-ray Diffraction Experiments: Exposure to brilliant X-rays used in protein crystallography generates free radicals that can cause severe damage to crystal structure and the constituent protein molecules. Cryogenics are employed to decrease the rate of free radical diffusion through the crystal. Protein crystals are thus vitrified using $N_2(l)$ (≈ 77 K) in the presence of cryo-protectant, a crystallisation cocktail additive that decreases the rate of ice formation [7]. The cryo-protectant found compatible with eOmCA crystals was 20% DMSO.

Crystals are mounted onto a goniostat that rotates the crystal (to the accuracy of a thousandth of a degree) during X-ray exposure. The electrical component of collimated (i.e. phase coherent), monochromatic X-rays generates electronic oscillations in the sample. This results in elastic scattering of incident X-rays, where the electrons are excited to oscillation and subsequently lose their energy by emitting X-rays of the same wavelength. Scattered X-rays parallel to the incident beam have the greatest intensity, and X-ray intensity decreases with increasing diffraction angle from the incident beam normal. The X-ray wavelength used for a “native” diffraction dataset of elastic scattering is within an order of magnitude of the protein molecule’s constituent atomic diameters (i.e. ≈ 1 Å).

The diffracted X-rays that can be used to build a structural model fulfil Bragg’s law:

$$n\lambda = 2d \sin \theta \quad \dots \text{Eqn. M.4}$$

(where n = wavelength-integer of molecule/unit cell spacing, λ = X-ray wavelength, d = distance between integer-spaced molecules, θ = angle ($^\circ$) of diffracted X-ray to incident X-ray)

In the scenario described in Eqn. M.4, phase-coherent diffracted X-rays from a protein with molecular equivalents organised in a periodic, translational manner undergo constructive

interference. The constructive interference amplifies the signal:noise ratio in an exponential manner, essentially the cause of greater signal:noise intensity from diffracting crystals compared to protein solutions in SAXS. Also amplified by diffracting crystals are any structural heterogeneities inherent in either the protein molecule (e.g. conformational variety) or the crystal's packing of protein in the unit lattice.

An electron density model is built by Fourier back-transformation of diffracted X-ray intensities. The intensity of the scattered X-rays provides information on the position of atoms within the protein crystals, which is a composite of structure factors. However elastic diffraction data alone is incomplete without phasing information. For the eOmCA structure model, the SAD dataset was put through density modification (using SHELX), which "... can be considered an extension of experimental phasing" [8]. After a structure model was built using COOT and Buccaneer, it was used as a search molecule in the native diffraction dataset with PHASER. Subsequent model refinement was done using COOT and Refmac.

For the eY³⁷⁴F, eT⁷²⁵G and eP⁷²⁶G diffraction datasets, molecular replacement with the determined eOmCA structure model was used to phase the native diffraction dataset via PHASER. Subsequent model refinement was done using COOT and Refmac.

M.7 – Analytical Gel Filtration Chromatography. All experiments were performed using a Superdex S-200 HR 30 (a bed volume of 24.0 mL) at a flow rate of 0.10 mL min⁻¹. The protein was re-constituted to a volume of 250 µL and injected into a 500 µL sample loop. The column was calibrated by determining the elution volumes of the following molecular weight standards: Ribonuclease (12.7 kDa), Conalbumin (75 kDa), Alcohol dehydrogenase (150 kDa) and Apoferritin (443 kDa). Column calibration was performed at both salt extremes (i.e. in both 20 mM HEPES, pH 7.60, 0.1 M NaCl and 0.1 M Bis-Tris Propane, pH 8.50, (no salt)) to assess the effect on protein elution volume; which was negligible (see Section 4.2). The elution volume of near-equimolar eOmCA (≈ 0.14 mM) was then determined in 50 mM BICINE, pH 8.50 with a range of NaCl and MgCl₂ concentrations, such that each salt concentration tested was performed as an independent gel filtration run. All analytical gel filtration experiments were performed on a single batch of eOmCA, eY³⁷⁴F and eMtrC respectively.

$$A_s = \frac{V_{e,10\%}(\text{trailing}) - V_e}{V_e - V_{e,10\%}(\text{leading})} \quad \dots \text{Eqn. M.5}$$

(V_e = elution volume, V_{e,10%}(trailing) and V_{e,10%}(leading) are the volumes at 10% peak height of the trailing and leading edge of the eOmCA elution peak respectively.)

M.8 – Analytical Ultracentrifugation (AUC). AUC experiments were performed in collaboration with Dr Thomas Clarke, University of East Anglia, UK.

The buoyant mass of a molecule is equal to its mass against the volume of solvent it displaces, given by:

$$M_b = M (1 - \bar{v}\rho) \quad \dots \text{Eqn. M.6}$$

(M_b = buoyant mass, M = "dry" mass of molecule, \bar{v} = partial specific volume of molecule in cm³ g⁻¹, ρ = solvent density in g mL⁻¹)

The sedimentation equilibrium experiment provides information on the size of buoyant molecule. The protein sample was loaded into the sample compartment of an AUC cell mounted into a An50Ti rotor, the other AUC cell compartment contains sample buffer (providing a baseline spectrum to subtract the sample). The concentration gradient generated by the centrifugal force was monitored in real-time by mounting specialist spectroscopic equipment into the Beckman Optima XL-I analytical ultracentrifuge. The concentration at a given point (x) along the concentration gradient is given by:

$$C_x = C_r \exp\left[\frac{M_b \omega^2}{RT} \left(\frac{x^2 - r^2}{2}\right)\right] \quad \dots \text{Eqn. M.7}$$

(C_x = concentration at point “x”, C_r = concentration at reference point “r” beneath sample meniscus, exp = Euler’s constant, ω = angular velocity in radians per second, R = gas constant, T = absolute temperature)

$$\Rightarrow \ln \Delta C \times \frac{2}{x^2 - r^2} = \frac{M_b \omega^2}{RT} \quad \dots \text{Eqn. M.8}$$

A global fit of the data obtained was performed using UltraScan 8.0 (<http://www.ultrascan.uthscsa.edu/>) to a least-squares model of non-interacting monomeric molecules in a solution of estimated viscosity. A graph which manipulates Eqn. M.8 produces a plot with a gradient directly proportional to the bouyant mass of the molecule. The molecular (i.e. M) weight can then be calculated. Absorbance, at wavelengths specified in Table M.3, was used to monitor eOmCA concentration as a function of radial displacement along the AUC cell.

Table M.3 – *AUC parameters for determination of OmCA molecular weight in solution.* All samples were run in 20mM HEPES, pH 7.6, 0.01% CHAPS, 50 mM NaCl, 1% glycerol (see Materials and Methods). pOmCA was run at 7000 and 10000 rpm. eOmCA was run at 8100, 12900 and 16200 rpm.

Protein	Estimated Molecular Weight (Da)	Protein Concentration (μ M)	Wavelength monitored (nm)
pOmCA	86,059	0.61	410
		3.05	450
eOmCA	86,059	0.87	410
		4.36	440
		8.71	440

M.9 – Small Angle X-ray Scattering (SAXS). The eMtrC was kindly obtained from Dr Marcus J. Edwards. Both the eMtrC and eOmCA samples were both dialysed into the sample buffers 50 mM BICINE, pH 8.50 with either 10 mM NaCl or 150 mM NaCl. Samples were then sent to the Oakridge National Laboratory, USA for SAXS data collection and processing.

M.10 – Analytical Gel Filtration Chromatography (AGFC). Retention of sample molecule within the AGFC column matrix is defined as K_{av} :

$$K_{av} = \frac{(V_e - V_o)}{(V_t - V_o)} \quad \dots \text{Eqn. M.9}$$

(V_e = elution volume of protein, V_o = column void volume, V_t = total bed volume)

A Superdex S-200 HR 10/30 analytical gel filtration column calibrated with proteins of known molecular weight provides the basis of extrapolating the molecular weight of a given protein. Molecular weight standards used are Ribonuclease A (12.7 kDa), Conalbumin (75 kDa), Alcohol dehydrogenase (150 kDa) and Apoferritin (443 kDa) at approximately 1 mg mL⁻¹. The column was calibrated at 0.10 mL min⁻¹ with independent runs of 250 μ L of each molecular weight standard in both 20 mM HEPES, pH 7.60, 0.1 M NaCl and 50 mM BICINE, pH 8.50 (no salt). Protein elution was monitored using $A_{280\text{nm}}$ profiles.

AGFC of eOmCA, eY³⁷⁴F and eMtrC was performed as with the molecular weight standards. Protein was exchanged into buffer, re-suspended to 250 μ L, injected into the same

500 µL injection loop and the calibrated Superdex S-200 column run at 0.10 mL min⁻¹. Protein elution was monitored using A_{280nm} profiles.

M.11 – Mineral Reduction Assay of nano-Hematite (α -Fe₂O₃, 30-43 nm diameter) via Ferrozine Assay determination of Ferrous Iron Concentration. The Mineral Reduction Assay (MRA) was performed in collaboration with Dr Dave Kennedy of the Pacific National Laboratory, USA. Several strains of *Shewanella oneidensis* (detailed in Table M.5) were cultured aerobically in 50 mL LB starter culture (overnight at 30°C, +Kan₅₀ for mutant cultures), which was used to inoculate a 50 mL M1 minimal media, 20 mM sodium D,L-lactate starter culture grown aerobically overnight at 30°C (see Table M.4).

Table M.4 – *2× M1 Minimal Media Recipe*: Recipe listed is for 1 L of 2× stock of M1 minimal media. 2× stock was made, autoclaved and used for either minimal media starter cultures or mineral reduction cultures.

2× M1 media constituents	2× Concentration (g L ⁻¹ or mL L ⁻¹)	2× Concentration (mM)	1× Concentration (mM)
PIPES (pH 7.0 w/NaOH)	18.14	60	30
NaH ₂ PO ₄	1.3	8.7	4.35
NH ₄ Cl	3	56.08	28
KCl	0.2	2.68	1.34
NaCl	3.5	60	30
Minerals (100x)*	20 mL	(below)	-
Vitamins (300x) [#]	6.6 mL	(below)	-
Fe(III)-NTA (100 mM)	0.2 mL	0.02	0.01
Na ₂ SeO ₄ (1 g/L)	2 mL	0.53	0.26

*Minerals (100×): NTA (1.5 g L⁻¹), MgSO₄ (3.0 g L⁻¹), MnSO₄•H₂O (0.5 g L⁻¹), NaCl (1.0 g L⁻¹), FeSO₄•7H₂O (0.1 g L⁻¹), CaCl₂•2H₂O (0.1 g L⁻¹), CoCl₂•6H₂O (0.1 g L⁻¹), ZnCl₂ (0.13 g L⁻¹), CuSO₄•5H₂O (0.01 g L⁻¹), AlK(SO₄)₂•12H₂O (0.01 g L⁻¹), H₃BO₃ (0.01 g L⁻¹), Na₂MoO₄ (0.025 g L⁻¹), NiCl₂•6H₂O (0.024 g L⁻¹), Na₂WO₄•2H₂O (0.025 g L⁻¹).

[#]Vitamins (300×): biotin (2.0 mg L⁻¹), folic acid (2.0 mg L⁻¹), pyridoxine HCl (10.0 mg L⁻¹), riboflavin (5.0 mg L⁻¹), thiamine (5.0 mg L⁻¹), nicotinic acid (5.0 mg L⁻¹), pantothenic acid (5.0 mg L⁻¹), B-12 (0.1 mg L⁻¹), p-aminobenzoic acid (5.0 mg L⁻¹), thiocetic acid (5.0 mg L⁻¹).

M1 media starter cultures were monitored for O.D._{600nm} and reconstituted with M1 minimal media (no lactate) to the target of O.D._{600nm} = 1.5 ($\approx 2 \times 10^9$ cells mL⁻¹, communication with Dr Dave Kennedy). The O.D._{600nm}-normalised cultures were used to inoculate 10 mL anaerobic M1 minimal media containing the mineral respiratory substrate hematite. The mineral reduction media was purged for 10 minutes prior to inoculation. The mineral reduction media contains M1 minimal media, the ferric mineral 4.67 mM α -Fe₂O₃ (i.e. 9.34 mM Fe³⁺, synthesised at PNL, USA) and 20 mM sodium D,L-lactate.

Mixed-extractions of 400 µL of culture were added to 400 µL of 1 M HCl for ferrozine assay of Fe²⁺ content. Extractions were performed 24, 48 and 120 hours post-inoculation in an anaerobic environment. Extraction-acid mixture is left for 1 hour in the dark at room temperature. The Fe-HCl sample is spun at 10,000 ×g for 5 mins and \approx 400 µL supernatant removed and preferentially kept dark for ferrozine assay.

The ferrozine assay was performed by addition of 100 µL Fe-HCl to 1 mL of 0.1% (w/v) ferrozine (i.e. monosodium 3-(2-pyridyl)-5,6-diphenyl-1,2,4-triazine-*p,p'*-disulfonic acid) in 50 mM HEPES buffer, pH 7.0. Hematite culture extractions were added directly to ferrozine with thorough mixing or diluted into 1mL 0.1 M HCl initially to obtain linear measurements. After 5

minutes incubation, $A_{562\text{ nm}}$ was measured, and Fe^{2+} concentration extrapolated from a calibration curve.

M.11.1 – Site-Directed Mutagenesis and Cloning of *omcA*: Cloning and site-directed mutagenesis was performed by Dr Liang Shi of Pacific National Laboratory, USA.

Table M.5 – 2× M1 Minimal Media Recipe: Recipe listed is for 1 L of 2× stock of M1 minimal media. 2× stock was made, autoclaved and used for either minimal media starter cultures or mineral reduction cultures.

Genotype	<i>in trans omcA</i> ⁺	eOmcA LS #	mOmcA LS #
MR-1 (i.e. wild-type)	N/A	N/A	N/A
	None (+empty pBAD202)		785
	<i>omcA</i>_(wt)⁺	330	786
	T⁷²⁵G	838	787
	P⁷²⁶V	821	788
<i>mtrC</i>⁻ <i>omcA</i>⁻	P⁷²⁶G	819	807
	T⁷²⁵G:S⁷²⁷G	820	823
	C⁷²⁷ins	839	808
	Y³⁷⁴F	822	844
	C⁵²⁷V	840	845

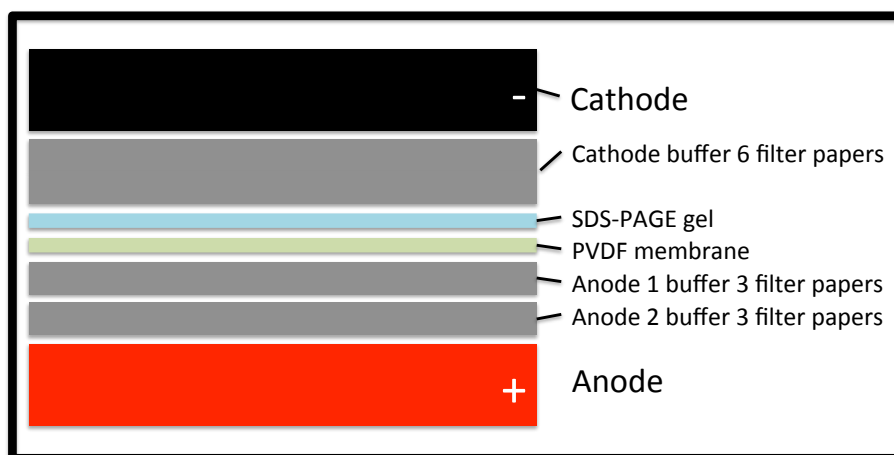
M.11.2 – Recombinant-OmcA Localisation Assay: *Shewanella oneidensis* strains LS 786 and 787 were grown in 50 mL overnight cultures to inoculate 1 L LB +Kan₅₀ cultures that were induced with 1 mM arabinose at O.D._{600nm} = 0.5 – 0.7. Cells were harvested at 8,000 ×g and re-suspended in 10 mL 0.1 M Tris-HCl, pH 7.4, 0.15 M NaCl, 1 mM CaCl₂, 1 μM MgCl₂. Samples were halved, and for each strain proteinase K added to one half to a final concentration of 17 μM, and the same volume of buffer added to the remaining sample half. Samples were then incubated at 37 °C for 25 minutes, then put on ice and complete protease inhibitor (Roche) added. Cells were then washed and reconstituted in the same buffer with the addition of complete protease inhibitor and 0.9 mM EDTA, whilst being maintained at 4 °C. Cells were then sonicated and incubated with DNase at 37 °C for 20 minutes before addition of SDS-PAGE loading buffer. Samples were then run on duplicate 12% SDS-polyacrylamide gels, where one was haem-stained and the other underwent western blotting.

M.11.2.1 – Western Blotting: Electrophoresis was used to transfer protein from SDS-PAGE gel to polyvinylidene fluoride (PVDF). Filter papers were soaked in the following buffers per PVDF membrane for 5 minutes: 6 filter papers in cathode buffer (25 mM Tris-HCl, pH 9.4, 40 mM ε-aminocaproic acid, 20% (v/v) methanol, 0.1% SDS), 3 filter papers in anode 1 buffer (0.3 M Tris-HCl, pH 10.4, 20% (v/v) methanol), and 3 filter papers in anode 2 buffer (25 mM Tris-HCl, pH 10.4, 20% (v/v) methanol). Meanwhile the PVDF membrane was soaked in 100 % methanol for 1 minute and the SDS-PAGE gel is soaked in anode 1 buffer for 1 minute. The

electrophoretic experiment was then setup as detailed in Fig. M.3 and run at 10 – 15 V, 85 mA for 1 hour.

The PVDF membrane was blocked with 5% milk powder in PBST buffer (8% (w/v) NaCl, 1.44% (w/v) Na_2HPO_4 , 0.2 % (w/v) KCl, 0.24% (w/v) KH_2PO_4 , 0.1% (v/v) TWEEN 20) for 15 minutes. Polyclonal anti-OmcA rabbit IgG (0.50 mg mL^{-1} average concentration, raised by Matt Marshall [9]) was added to a 1:10,000 dilution, and incubated with the membrane overnight at 4 °C. The membrane was washed 3× with PBST buffer and then 3× with PBS buffer (PBST buffer without Tween 20). The membrane was then blocked with 5% milk powder in PBST for 15 minutes, and then incubated with mouse anti-rabbit IgG with linked enzyme alkaline phosphatase for 1 hour. The membrane was again washed 3× with PBST buffer and then 3× with PBS buffer before addition of the substrate: 10 mL of 0.1 M Tris-HCl, pH 9.50, 0.1 M NaCl, 5 mM MgCl_2 with 33 μL BCIP (5-bromo-4-chloro-3-indolyl phosphate, Promega) and 66 μL NBT (nitro blue tetrazolium). The membrane was incubated with the substrate solution for 20 – 40 minutes for stain development.

Fig. M.3 – *Electrophoretic protein transfer from SDS-PAGE gel to PVDF membrane*. Filter papers, SDS-PAGE gel with electrophoretically separated proteins and PVDF membrane are soaked in the aforementioned buffers. Air bubbles are removed between layers before electrophoresis is performed.



References

- 1 Margoliash, E. and Frohwirt, N. (1959) Spectrum of horse-heart cytochrome-c. *Biochemical Journal*. **71**, 570-578
- 2 Clarke, T. A., Edwards, M. J., Gates, A. J., Hall, A., White, G. F., Bradley, J., Reardon, C. L., Shi, L., Beliaev, A. S., Marshall, M. J., Wang, Z., Watmough, N. J., Fredrickson, J. K., Zachara, J. M., Butt, J. N. and Richardson, D. J. (2011) Structure of a bacterial cell surface decaheme electron conduit. *Proceedings of the National Academy of Sciences of the United States of America*. **108**, 9384-9389
- 3 Edwards, M. J., Hall, A., Shi, L., Fredrickson, J. K., Zachara, J. M., Butt, J. N., Richardson, D. J. and Clarke, T. A. (2012) The Crystal Structure of the Extracellular 11-heme Cytochrome UndA Reveals a Conserved 10-heme Motif and Defined Binding Site for Soluble Iron Chelates. *Structure*. **20**, 1275-1284
- 4 Edwards, M. J., Baiden, N. A., Johs, A., Tomanicek, S. J., Liang, L., Shi, L., Fredrickson, J. K., Zachara, J. M., Gates, A. J., Butt, J. N., Richardson, D. J. and Clarke, T. A. (2014) The X-ray crystal structure of *Shewanella oneidensis* OmcA reveals new insight at the microbe-mineral interface. *Febs Letters*. **588**, 1886-1890

- 5 Myers, J. M. and Myers, C. R. (2001) Role for outer membrane cytochromes OmcA and OmcB of *Shewanella putrefaciens* MR-1 in reduction of manganese dioxide. *Applied and Environmental Microbiology*. **67**, 260-269
- 6 Eggleston, C. M., Voros, J., Shi, L., Lower, B. H., Droubay, T. C. and Colberg, P. J. S. (2008) Binding and direct electrochemistry of OmcA, an outer-membrane cytochrome from an iron reducing bacterium, with oxide electrodes: A candidate biofuel cell system. *Inorganica Chimica Acta*. **361**, 769-777
- 7 Garman, E. F. and Schneider, T. R. (1997) Macromolecular cryocrystallography. *Journal of Applied Crystallography*. **30**, 211-237
- 8 Rupp, B. (2010) *Biomolecular Crystallography: Principles, Practice, and Application to Structural Biology*. Garland Science
- 9 Marshall, M. J., Beliaev, A. S., Dohnalkova, A. C., Kennedy, D. W., Shi, L., Wang, Z. M., Boyanov, M. I., Lai, B., Kemner, K. M., McLean, J. S., Reed, S. B., Culley, D. E., Bailey, V. L., Simonson, C. J., Saffarini, D. A., Romine, M. F., Zachara, J. M. and Fredrickson, J. K. (2006) c-Type cytochrome-dependent formation of U(IV) nanoparticles by *Shewanella oneidensis*. *Plos Biology*. **4**, 1324-1333

Appendices

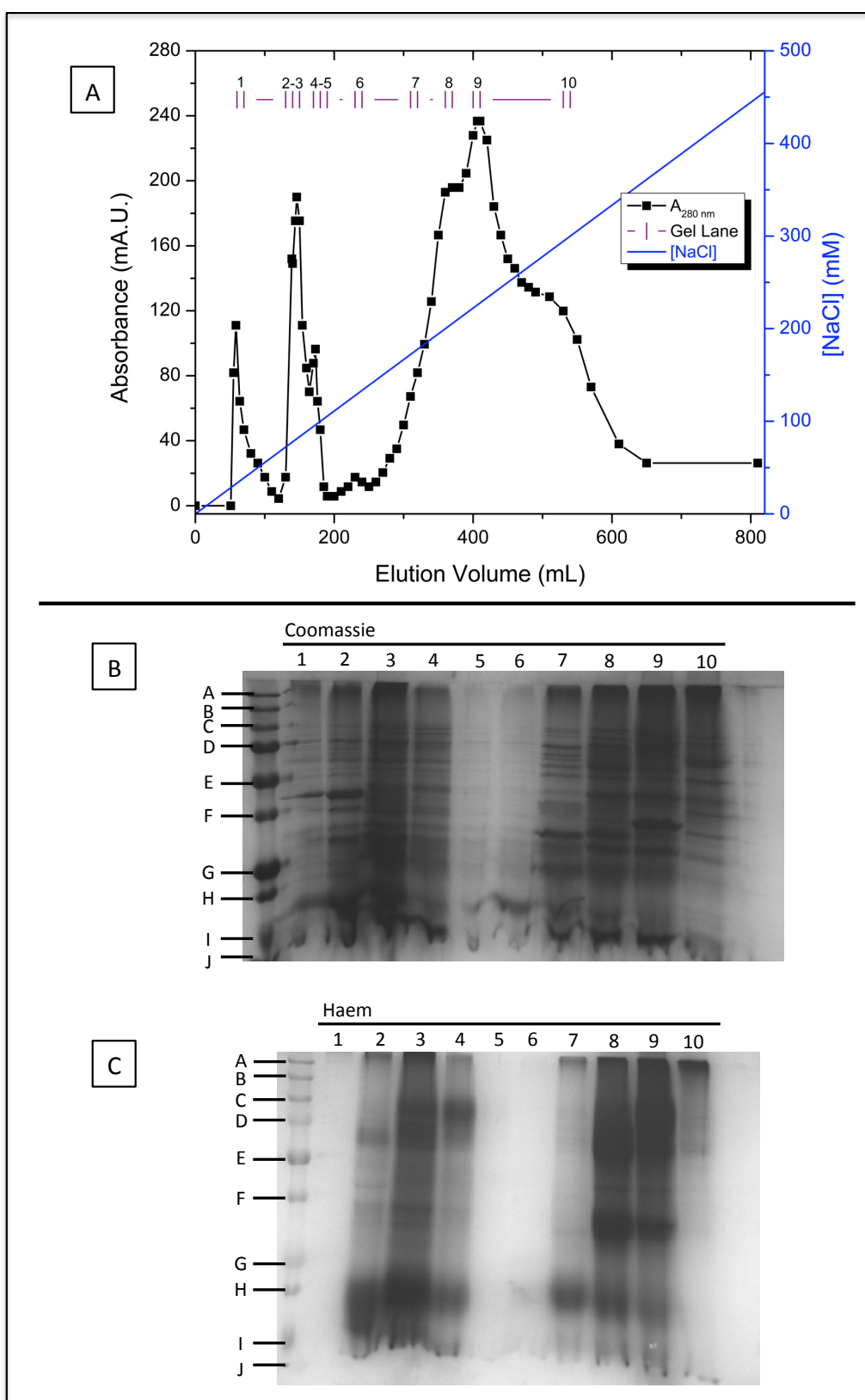


Fig. A2.1 – **OmcA_(wt) Purification.** (A) Chromatogram of protein elution from the diethylaminoethyl (DEAE) chromatography column via A_{280nm} detection. (B) Coomassie and (C) Haem-stained SDS-PAGE gels of fractionated eluent. Molecular weight markers are: A = 250 kDa, B = 150 kDa, C = 100 kDa, D = 75 kDa, E = 50 kDa, F = 37 kDa, G = 25 kDa, H = 15 kDa and I = 10 kDa.

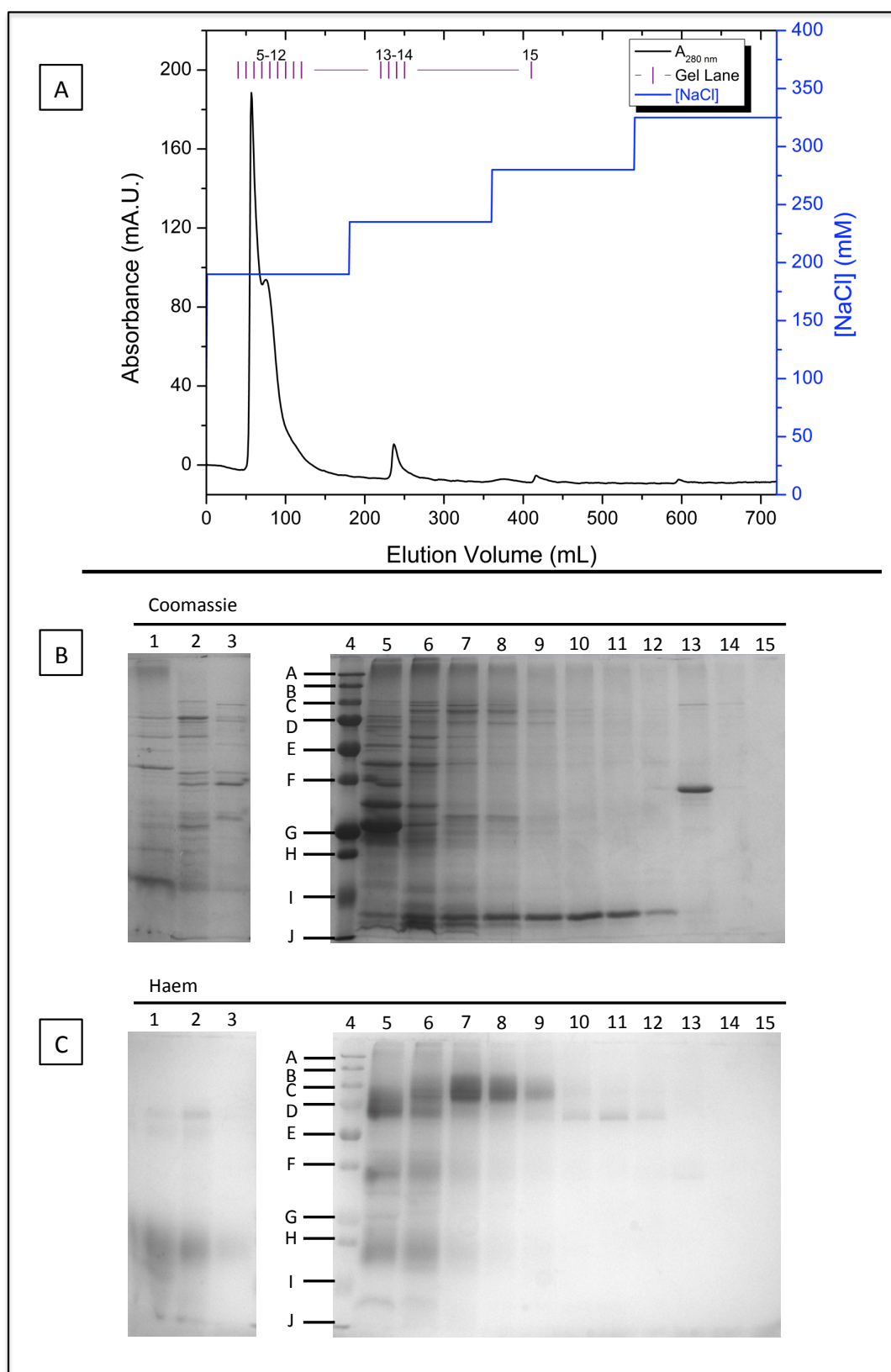


Fig. A2.2 – **OmcA_(wt) Purification.** (A) Chromatogram of protein elution from the Q-Sepharose chromatography column via $A_{280\text{nm}}$ detection. (B) Coomassie and (C) Haem-stained SDS-PAGE gels of fractionated eluent from Q-Sepharose columns. Molecular weight markers are: A = 250 kDa, B = 150 kDa, C = 100 kDa, D = 75 kDa, E = 50 kDa, F = 37 kDa, G = 25 kDa, H = 15 kDa and I = 10 kDa.

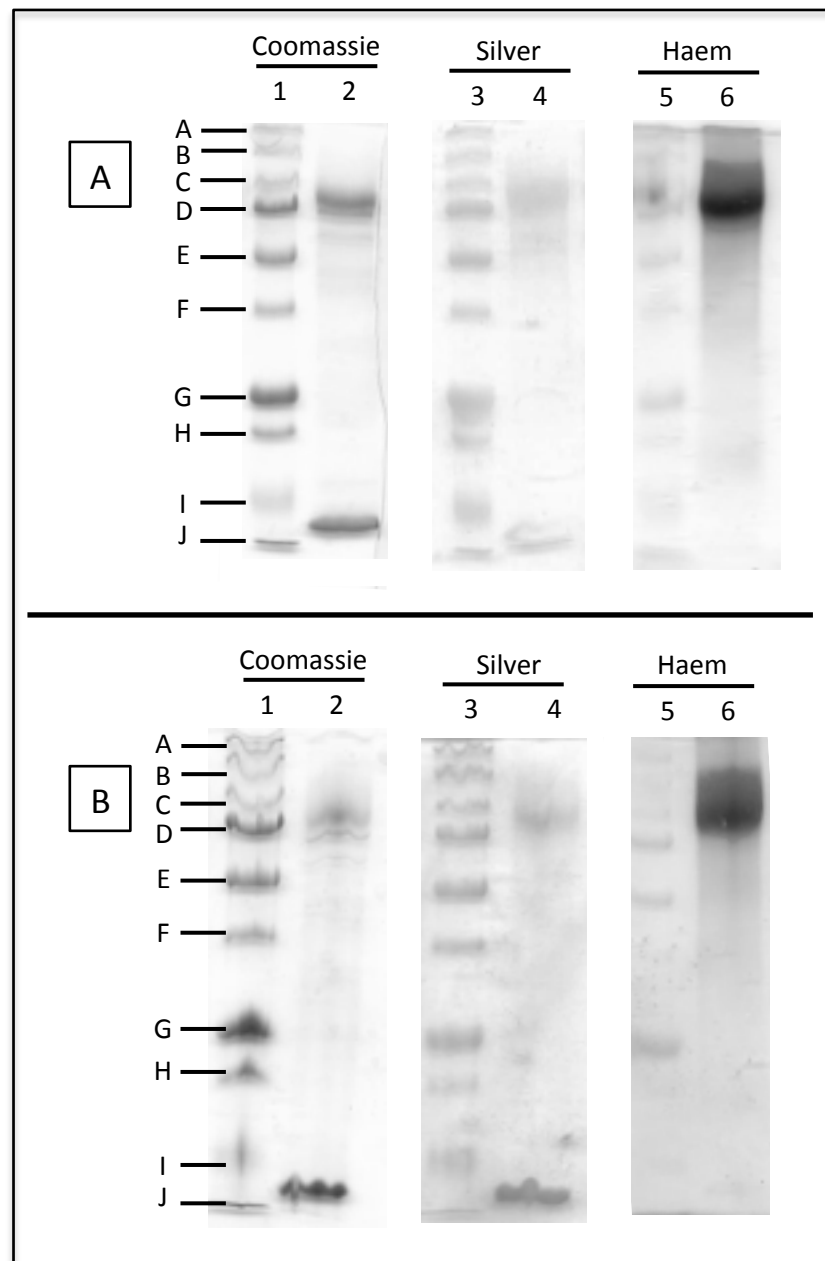


Fig. A2.3 – **OmcA_(wt) Purification.** Coomassie, Silver and Haem-stained SDS-PAGE gels of OmcA_(wt) pool after (A) Amicon-exchange and (B) elution from Sephadex G-25M PD10 desalting column. Molecular weight markers are: A = 250 kDa, B = 150 kDa, C = 100 kDa, D = 75 kDa, E = 50 kDa, F = 37 kDa, G = 25 kDa, H = 15 kDa and I = 10 kDa.

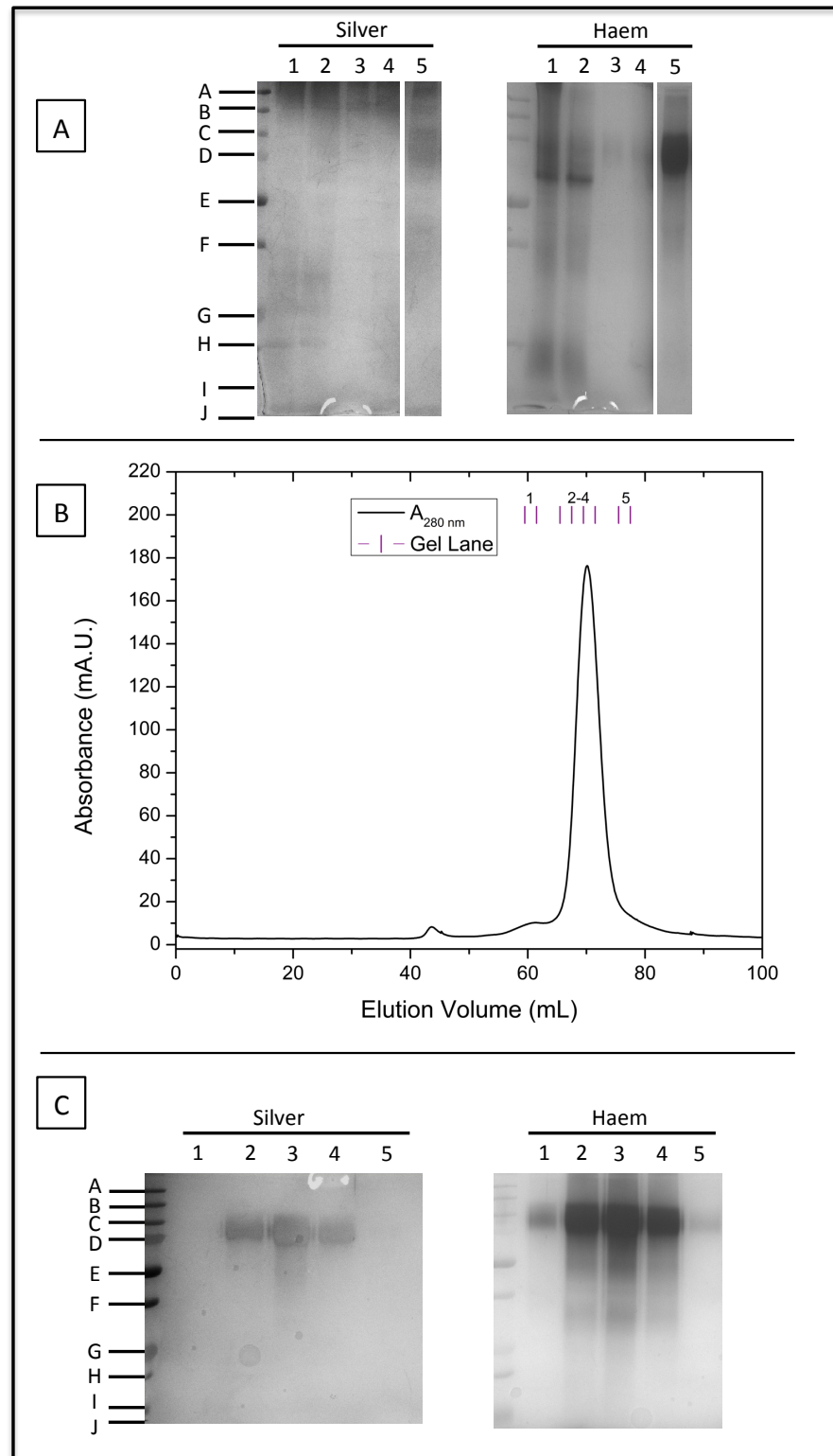


Fig. A2.4 – **pOmCA Purification.** (A) Silver and Haem-stained SDS-PAGE gels of pOmCA pool after cell lysate elution from a Ni^{2+} -charged IMAC column. Lanes: 1 = cell lysate washed with buffer containing no imidazole, 2 = 10 mM imidazole, 3 = 40 mM imidazole (1st wash), 4 = 40 mM imidazole (2nd wash) and 5 = 250 mM imidazole. (B) Representative chromatogram of pOmCA elutions from Superdex S-200 column, monitored via $A_{280\text{ nm}}$ detection. (C) Representative Silver and Haem-stained SDS-PAGE gels of fractionated eluent from Superdex S-200 columns. Molecular weight markers are: A = 250 kDa, B = 150 kDa, C = 100 kDa, D = 75 kDa, E = 50 kDa, F = 37 kDa, G = 25 kDa, H = 15 kDa and I = 10 kDa.

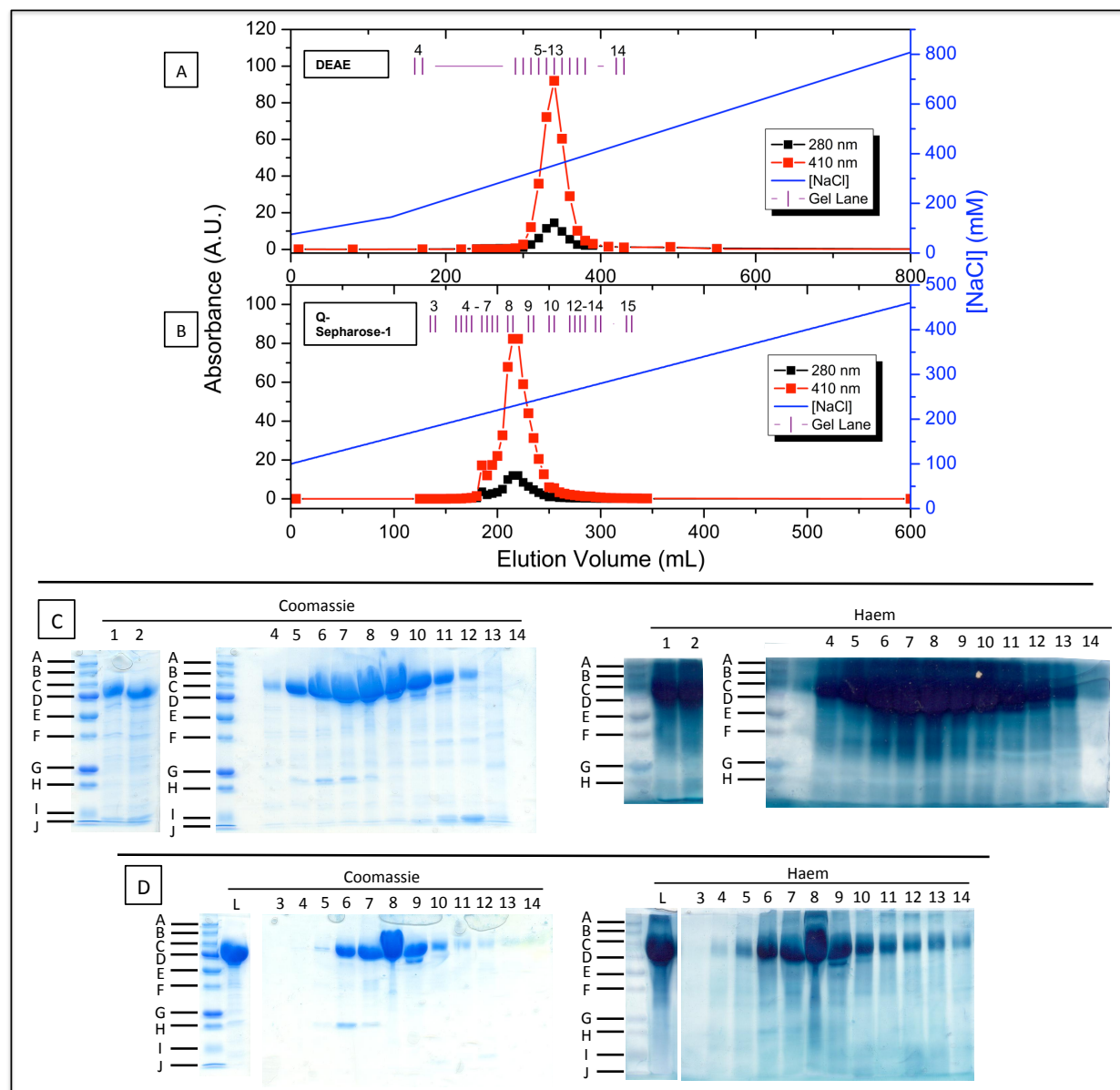


Fig. A2.5 - eOmcA Purification. (A) Chromatograms of eOmcA pool elution from the DEAE column. (B) Chromatograms of eOmcA pool elution from the Q-Sepharose column. (C) SDS-PAGE gels of eOmcA media (1) before and (2) after concentration with 30 kDa cut-off Sartorius cartridge, and eluted fractions from DEAE column (4-14). (D) SDS-PAGE gels of eOmcA elution from Q-Sepharose column. Lane L = sample loaded onto column. Molecular weight markers are: A = 250 kDa, B = 150 kDa, C = 100 kDa, D = 75 kDa, E = 50 kDa, F = 37 kDa, G = 25 kDa, H = 15 kDa and I = 10 kDa.

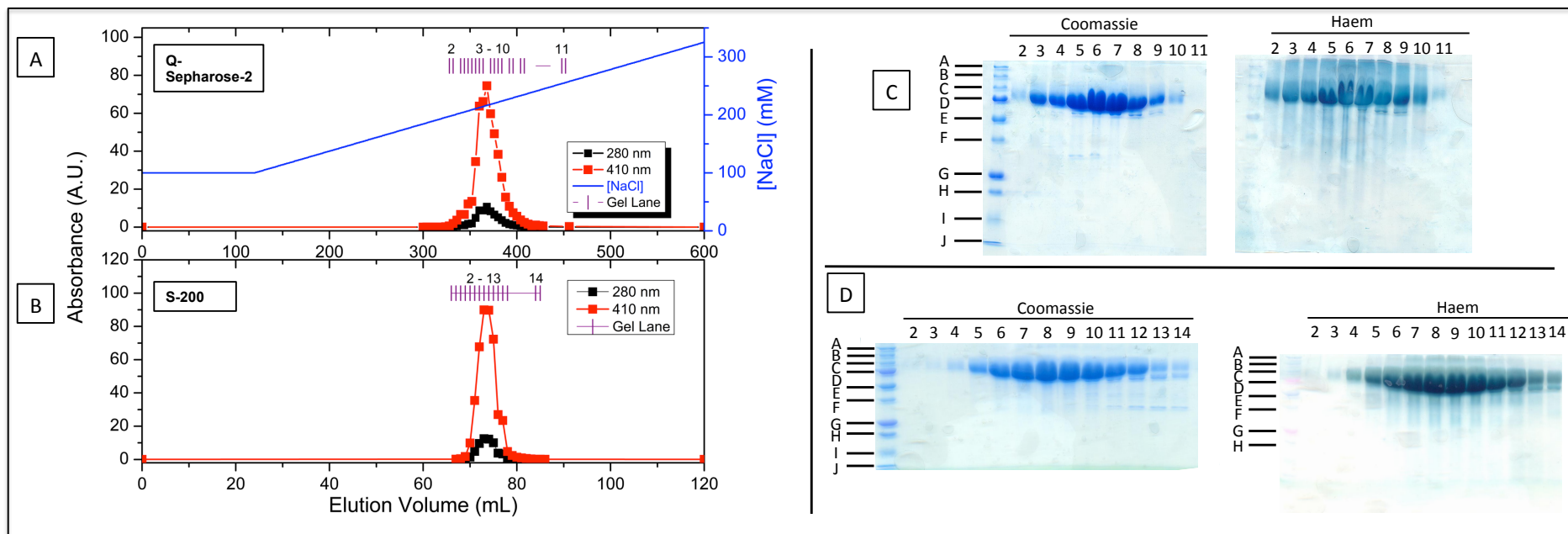


Fig. A2.6 – **eOmCA Purification.** (A) Chromatograms of eOmCA pool elution from the 2nd Q-Sepharose step. (B) Chromatograms of eOmCA pool elution from the Superdex S-200 16/60 column. (C) SDS-PAGE gels of eOmCA elution from the 2nd Q-Sepharose step. (D) SDS-PAGE gels of eOmCA elution from Superdex S-200 column. Molecular weight markers are: A = 250 kDa, B = 150 kDa, C = 100 kDa, D = 75 kDa, E = 50 kDa, F = 37 kDa, G = 25 kDa, H = 15 kDa and I = 10 kDa.

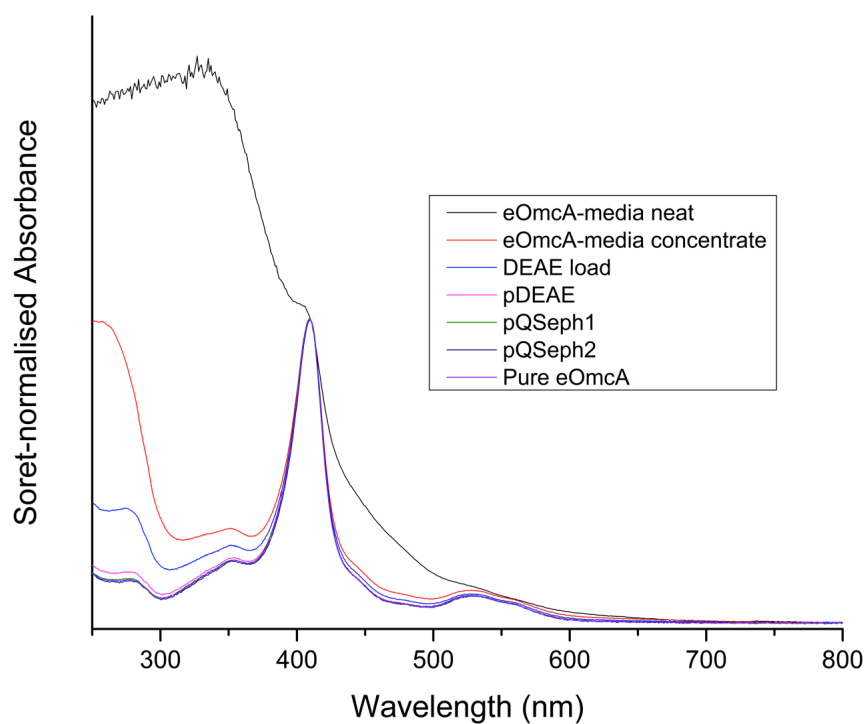


Fig. A2.7 – **Spectroscopic Monitoring of eOmcA pool haem:peptide ratio as a function of protein purity.**

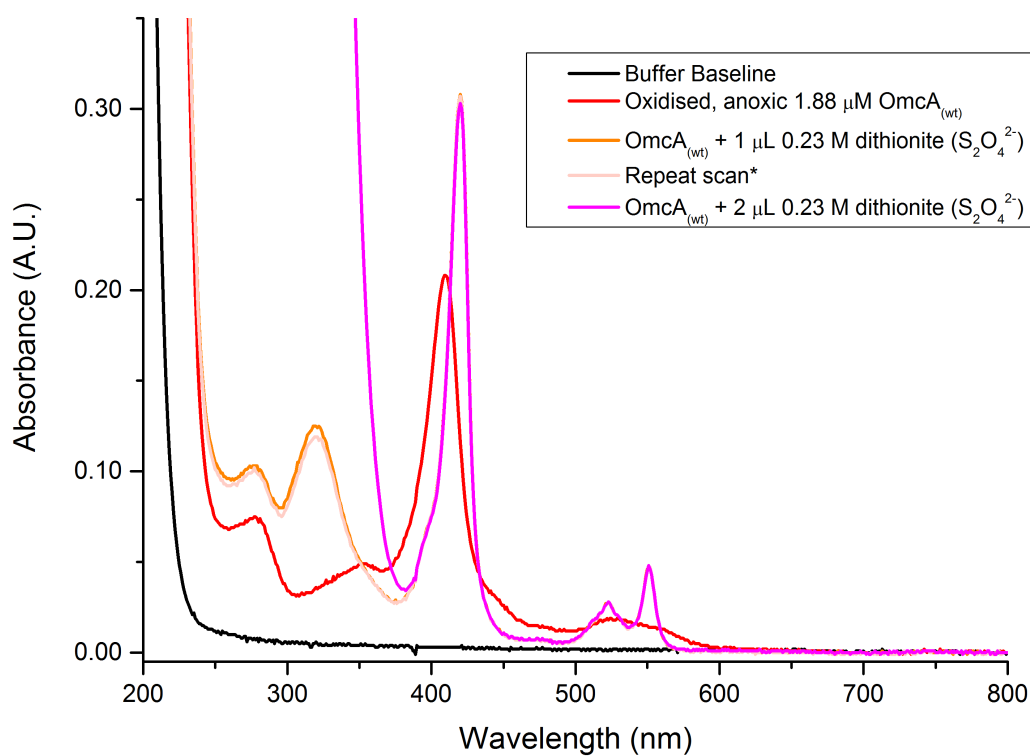


Fig. A2.8 – **Representative UV-Vis Spectra recorded to obtain oxidised and reduced protein spectra.**

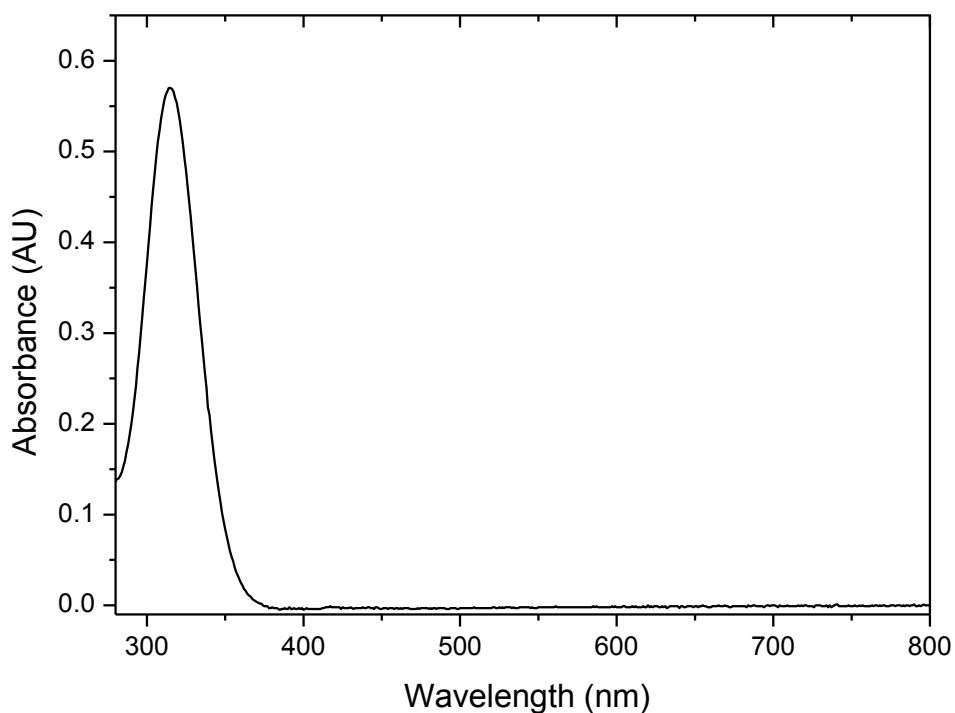


Fig. A2.9 – **Sodium Dithionite (i.e. $\text{Na}_2\text{S}_2\text{O}_4$) produces an Absorption Band at 314 nm.**

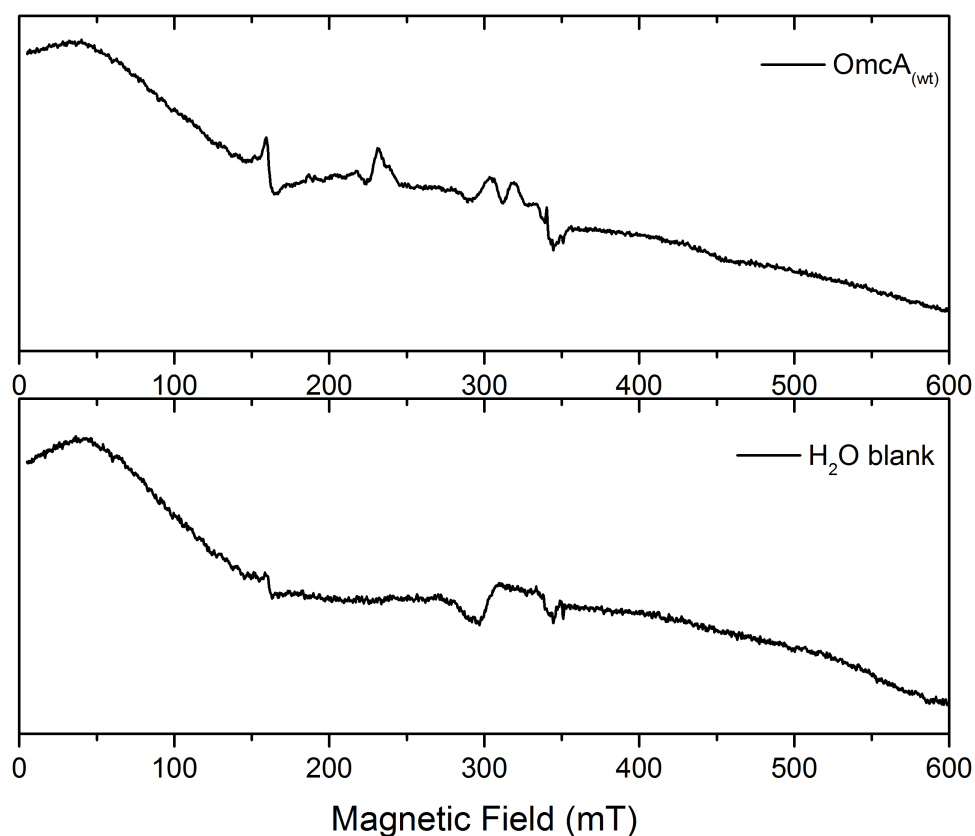


Fig. A2.10 – **Representative EPR spectrum as collected (upper panel) and Analytical Water blank spectrum (lower panel).** Spectral features observed in the H₂O blank spectrum are attributed to spectrometer resonator cavity impurities.

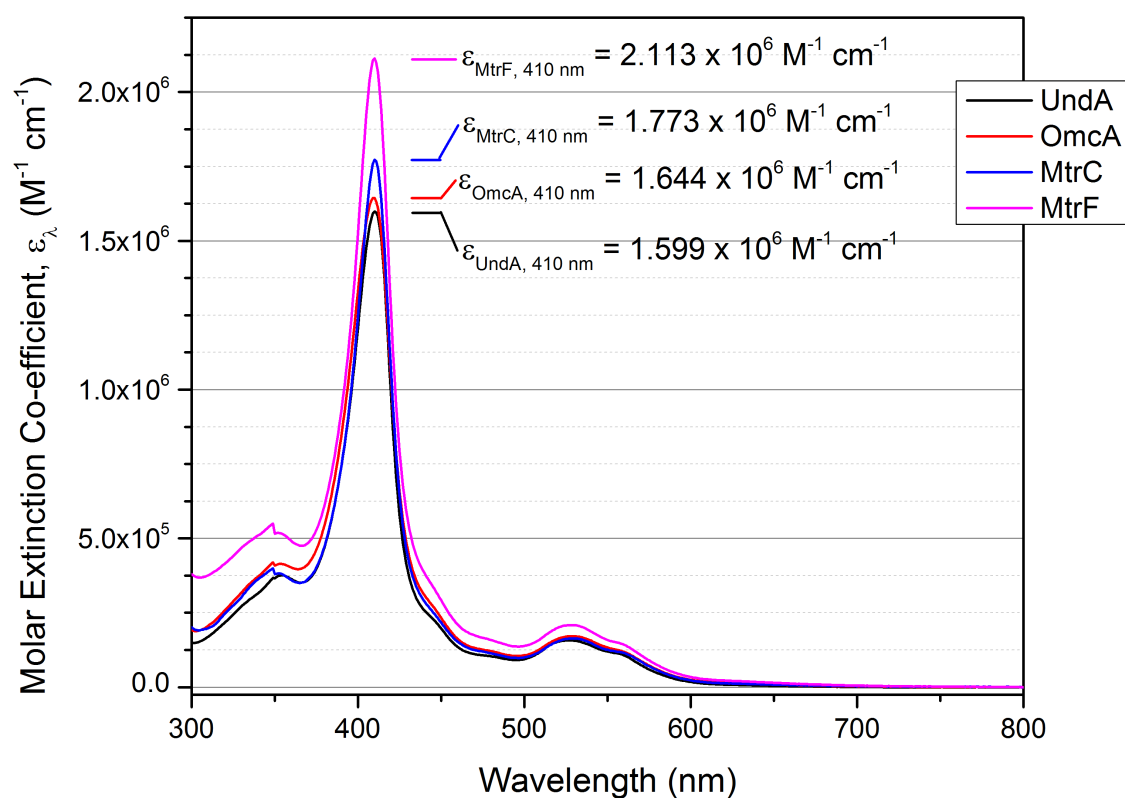


Fig. A2.11 – **Molar Extinction Coefficient Plots for eUndA, eOmcA, MtrF and eMtrC.** Molar extinction coefficients were determined four times for eOmcA (i.e. standard deviation = $30 \times 10^3 \text{ M}^{-1} \text{ cm}^{-1}$), twice for eUndA and MtrC, and once for MtrF.

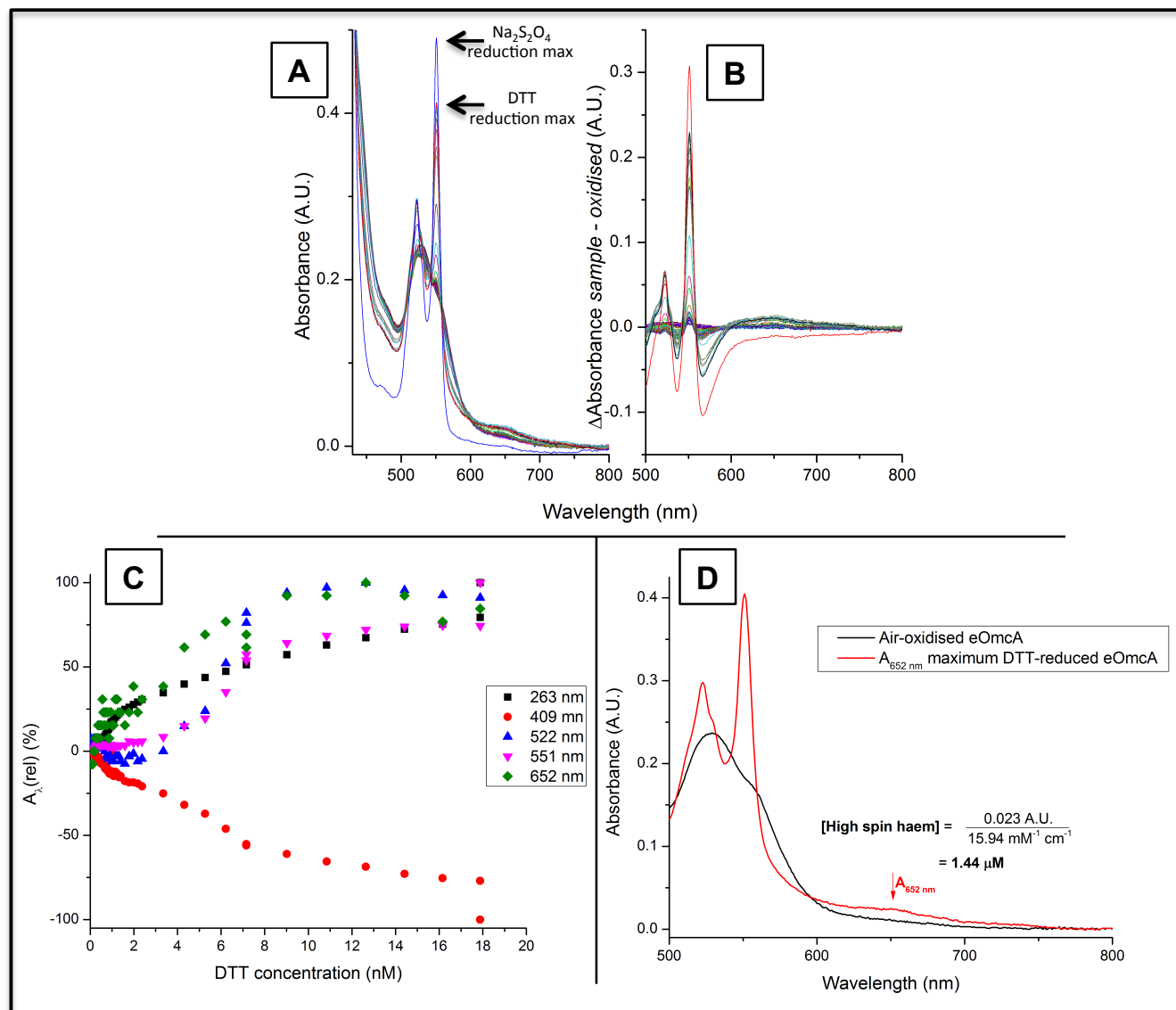


Fig. A4.1 – Spectroscopy of eOmcA reduction by DTT. (A) The spectra of the DTT titration of eOmcA. (B) The difference spectra (titrated minus oxidised) of the DTT titration of eOmcA. The “final” spectrum in both plots (blue in (A) and red in (B)) is the final (Na₂S₂O₄) reduction. (C) The plot of A_λ(rel) (term defined below) at specific wavelengths as a function of DTT concentration. Noteworthy is that A_{551 nm} and A_{652 nm} are produced by relatively slow reactions. (D) The oxidised and maximum A_{652 nm} spectra of eOmcA. There is a ≈ 1:1 ratio of [protein] and [high-spin haem]. There is a near 1:1 ratio of high-spin haem content (i.e. 1.4 μM) and [eOmcA] (i.e. 1.6 μM). Also apparent is that DTT reduction did not reduce all eOmcA’s haem content. DTT’s E_{m, 7.0} = -0.33 V vs S.H.E., which means reduction of eOmcA’s lower potential haems are unfavourable based on the potential difference (i.e. ΔE (DTT_{red}:haem) ≤ 0.00 V).

$$A_{\lambda}(\text{rel})\% = \frac{A_{\lambda}(x) - A_{\lambda}(\text{oxidised})}{A_{\lambda}(\text{max}) - A_{\lambda}(\text{oxidised})} \times 100\%$$